



**University of  
Nottingham**

UK | CHINA | MALAYSIA

**Aeronautical carbon fibre composites with high  
electrical conductivity and fracture toughness  
utilizing functionalized interleaves**

By

**Dongyuan Hu**

(MSc., BEng.)

A thesis submitted to the University of Nottingham Ningbo China  
for the degree of Doctor of Philosophy

September 2022

## Abstract

Carbon fibre reinforced polymers (CFRP) are extensively used in current advanced aircraft due to their light weight, high strength to weight ratio and good corrosion resistance. Future aeronautical CFRPs are likely to be highly integrated material systems with excellent mechanical properties and additional functionalities. This thesis focuses on the concept of structural-functional integration for CFRPs, by combining high fracture toughness and electrical conductivity with balanced mechanical properties.

Firstly, fracture toughness is significantly improved via interleaving the carbon-epoxy plies with a polyamide toughening layer. A high temperature rosin-sourced epoxy was formulated as the green matrix resin. The effects of interleaving on fracture toughness, impact resistance, toughening mechanisms and in-plane mechanical properties are investigated. The Mode I and Mode II interlaminar fracture toughness values were both significantly improved by interleaving along with the CAI residual strength with only a modest reduction in in-plane mechanical properties.

Proprietary electroless copper-nickel plated polyester veils were also evaluated as interleaves, forming a bi-continuous network in interlaminar regions, also improving the Mode I and Mode II interlaminar fracture toughness values. The resulting electrically conductive network yielded major

improvements in the through-thickness electrical conductivity of laminates and this was also dependent on compaction. A series-resistor model was applied to estimate the through-thickness electrical conductivity for a given conductive network. Compaction had a lower influence on flexural and interlaminar shear properties although a 20% decrease in interlaminar shear strength was noted for FIT specimens due to the low intra-ply shear resistance of interlayers.

## Acknowledgement

Firstly, my sincere gratitude goes to my main supervisors, Prof. Xiaosu Yi, Dr. Xiaoling Liu and Prof. Chris Rudd, who offered me the chance to study in the Advanced Composites Group of UNNC. Prof. Xiaosu Yi, a true master of composites, thank you for introducing me to the world of composites and teaching me the significant of enthusiasm, imagination and creativity in engineering and research explorations. Dr. Xiaoling Liu, thank you for your kind supports and encouragements. When my research got stuck, you always had ideas to keep me going forward. Prof. Chris Rudd, thank you for teaching me to enjoy the PhD life. Although you went to Singapore in my second year of PhD, you still support me with generous helps and guidance for my publications.

My thanks also go to my colleagues and friends, Minqiang Jiang, Ziqian Liu, Siqi Hao, Lizhe He, Peiyuan Lei, Lu Tong, Ningxin etc., for sharing both the happy and hard time in my PhD life. I also want to thank the staffs in composites team and FOSE technician team, Dr. Robert Pierce, Xiaoye Cong, Xin Wang, Saihua Li, Liangliang Zhu, Jane Zhang etc., who gave me the supports through my research projects.

Then I would like to thank my teammates in UNNC PGR basketball team, Jiangqi Wu, Hao Zhang, Vasyl, Jake, Dani, Alain, etc. Thanks for sharing the

happiness on the basketball court. I will remember the efforts we made to win the games.

My heartfelt appreciation goes to my parents, who have always supported and encouraged me to get over the challenges not only in the research but also in the daily life. Thanks to my family for their endless loves and cares for me.

Finally, I would like to acknowledge the UNNC, Technical Fibre Products Ltd, Ningbo Science and Technology Innovation Project, Ningbo HTZ project, Shanghai Aircraft Manufacturing Co. Ltd, Shanghai Key Laboratory of Spacecraft Mechanism and other funding bodies for the financial support during my studies.

# List of publications

## Journal papers

1. **Dongyuan Hu**, Xvfeng Zhang, Xiaoling Liu\*, Zhen Qin, Li Hu, Chris Rudd, and Xiaosu Yi\*, Study on Toughness Improvement of a Rosin-Sourced Epoxy Matrix Composite for Green Aerospace Application, Journal of Composites Science, Volume 4(4), 2020, 168, <https://doi.org/10.3390/jcs4040168>
2. **Dongyuan Hu**, Xiaosu Yi\*, Minqiang Jiang, Genghong Li, Xiaoye Cong, Xiaoling Liu\*, Chris Rudd, Development of highly electrically conductive composites for aeronautical applications utilizing bi-functional composite interleaves, Aerospace Science and Technology, Volume 98, 2020, 105669, <https://doi.org/10.1016/j.ast.2019.105669>.
3. **Dongyuan Hu**, Xiaoling Liu\*, Weiping Liu, Guocai Li, Chris Rudd, Xiaosu Yi\*, The effects of compaction and interleaving on through-thickness electrical resistance and in-plane mechanical properties for CFRP laminates, Composites Science and Technology, Volume 223, 2022, 109441, <https://doi.org/10.1016/j.compscitech.2022.109441>.
4. Lu Tong, **Dongyuan Hu**, Lu Chao, Xiaoling Liu\*, Chunhong Wang\*, Xiaosu Yi\*, Development of hybrid breathing materials for sustainable composite manufacturing, Journal of Cleaner Production, Volume 321, 2021, 129028, <https://doi.org/10.1016/j.jclepro.2021.129028>.

# Table of Content

<b>Abstract .....</b>	<b>i</b>
<b>Acknowledgement .....</b>	<b>iii</b>
<b>List of publications .....</b>	<b>v</b>
<b>Table of Content.....</b>	<b>vi</b>
<b>List of Figures .....</b>	<b>xii</b>
<b>List of Tables.....</b>	<b>xx</b>
<b>Abbreviations.....</b>	<b>xxii</b>
<b>Symbols.....</b>	<b>xxv</b>
<b>Chapter 1: Introduction .....</b>	<b>1</b>
1.1 Background .....	1
1.1.1 Toughening of CFRPs .....	2
1.1.2 Electrical conductivity of CFRPs in aircraft design.....	3
1.2 Aims and objectives .....	6
1.3 Thesis structure.....	8
1.4 Reference.....	9
<b>Chapter 2: Literature review.....</b>	<b>12</b>
2.1 Interlaminar fracture toughness of CFRP laminates.....	12
2.1.1 Mode I and Mode II interlaminar fracture toughness.....	13

2.1.2 Impact and after-impact properties of CFRP laminates .....	15
2.2 CFRP toughening technology.....	20
2.2.1 Matrix toughening technology .....	20
2.2.1.1 Rubber and thermoplastic fillers .....	20
2.2.1.2 Nano fillers .....	24
2.2.2 Interleaving toughening technology .....	27
2.2.2.1 Microparticles and nanoparticles .....	27
2.2.2.2 Films and veils .....	29
2.3 Electrical properties of aeronautical CFRP laminates .....	39
2.3.1 Anisotropic electrical conductivity .....	39
2.3.2 Relationship between electrical conductivity and functionalities ...	40
2.3.2.1 Heating of carbon fibre .....	40
2.3.2.2 Self-sensing .....	41
2.3.3 Integration of CFRP laminates in aircraft .....	43
2.3.4 Methods for improving electrical conductivity of CFRP laminates..	45
2.3.4.1 Resin Modification .....	45
2.3.4.2 Carbon fibre surface modification.....	48
2.3.4.3 Interleaving.....	51
2.4 Conclusions.....	57
2.5 References .....	58



## Chapter 3: Study of toughness improvement of green epoxy matrix

<b>carbon fibre composites .....</b>	<b>75</b>
3.1 Abstract .....	78
3.2 Introduction.....	79
3.3 Material and methods.....	81
3.3.1 Materials .....	81
3.3.2 Fabrication of composite laminates .....	86
3.3.3 Preparation of test specimens .....	87
3.3.4 Determination of interlaminar fracture toughness .....	89
3.3.5 Drop-weight Impact and Compression after Impact test .....	91
3.3.6 Mechanical tests .....	91
3.3.7 Scanning electron microscopy .....	94
3.4 Results and discussion.....	94
3.4.1 Interlaminar fracture toughness .....	94
3.4.2 Toughening mechanisms.....	97
3.4.3 Drop-weight impact and residual compression after impact strength .....	102
3.4.4 In-plane mechanical properties.....	105
3.5 Conclusion.....	108
3.6 References.....	109

<b>Chapter 4: Development of carbon fibre epoxy composites with high electrical conductivity and fracture toughness utilizing bi-functional composite interleaves .....</b>	<b>114</b>
4.1 Abstract .....	117
4.2 Introduction.....	117
4.3 Materials and methods .....	123
4.3.1 Materials .....	123
4.3.2 Fabrication of composite laminates .....	124
4.3.2.1 Manufacturing .....	124
4.3.2.2 Fracture toughness specimens .....	126
4.3.2.3 Electrical conductivity specimens .....	127
4.3.3 Determination of interlaminar fracture toughness .....	129
4.3.4 Determination of volume electrical conductivity .....	131
4.3.5 Scanning Electron Microscopy.....	134
4.4 Results and discussion.....	134
4.4.1 Interlaminar fracture toughness of laminates .....	134
4.4.2 Morphology and toughening mechanisms .....	138
4.4.3 Volume electrical conductivity .....	143
4.5 Conclusion.....	146
4.6 References .....	147

<b>Chapter 5: The effects of compaction and interleaving on through-</b>	
<b>thickness electrical resistance and in-plane mechanical properties for</b>	
<b>CFRP laminates.....</b>	<b>151</b>
5.1 Abstract.....	154
5.2 Introduction.....	155
5.3 Material and methods.....	159
5.3.1 Materials .....	159
5.3.2 Design and fabrication of test specimens .....	160
5.3.2.1 Design of the dry carbon fibre specimens .....	160
5.3.2.2 Design of the cured CFRP specimens .....	160
5.3.3 Manufacturing .....	162
5.3.4 Test of compaction - through thickness electrical properties of dry	
cross-ply carbon fibre fabrics.....	162
5.3.5 Determination of through - thickness resistivity of cured CFRP	
laminates .....	164
5.3.6 Determination of mechanical properties of CFRP specimens.....	165
5.4 Results and discussion.....	166
5.4.1 Compaction - through thickness electrical properties of dry cross-ply	
carbon fibre fabrics .....	166
5.4.2 Through-thickness electrical resistivity of cured cross-ply CFRP	
laminates .....	172

5.4.3 Mechanical properties.....	179
5.5 Conclusion.....	182
5.6 References.....	184
<b>Chapter 6: Conclusions and future work .....</b>	<b>188</b>
6.1 Overall summary .....	188
6.2 Future works.....	189
6.2.1 Functionalized interleaves .....	189
6.2.2 Development of a hybrid inner network.....	190

# List of Figures

Figure 1-1. Material composition of advanced aircraft. (a) Boeing 787 and (b) Airbus A350XWB [1,2]. .....	1
Figure 1-2. Schematics of electrical installation in aircraft and ENS system. (a) electrical installation, (b) ENS in fuselage [20]. .....	5
Figure 2-1. Three fundamental rupture modes [1]. .....	12
Figure 2-2. Solid object (a) without crack and (b) with a crack subjected to the external force [3]. .....	14
Figure 2-3. Schematic of barely visible impact damage in CFRP laminates [4]. .....	16
Figure 2-4. Normalised residual compressive strength against (a) impact energy and (b) total damage area. ....	18
Figure 2-5. C-scan and sectional microscope image for test laminates under low-velocity impact. (a) 3D woven composite, (b) NCF and (c) UD prepreg laminates [7]. .....	19
Figure 2-6. SEM of the fracture surface in rubber-modified epoxy [8]. .....	21
Figure 2-7. SEM from the stress-whitened area of fractured specimens [9]. ..	21
Figure 2-8. Schematic diagram of toughening mechanisms proposed for thermoplastic-modified epoxies: (1) crack pinning, (2) particle bridging, (3) crack path deflection, (4) particle yielding, (5) particle-yielding- induced shear banding, and (6) microcracking [12]. .....	22

Figure 2-9. Microstructures of the s epoxy/PES system. (a) Particulate microstructure second phase of thermoplastic-rich particles in continuous epoxy-rich matrix. (b) Particulate and co-continuous microstructures. (c) Co-continuous microstructure - where both the PES-rich and the epoxy-rich phases are continuous in nature. (d) Phase-inverted microstructure - second phase of epoxy- rich particles in a continuous PES-rich phase [17].....23

Figure 2-10. SEM image of fracture surface of  $G_{IIC}$  test for CFRP filled with silica nanoparticles. The white arrow indicates the direction of crack propagation [36]. .....25

Figure 2-11. SEM photographs of fracture surfaces of DCB specimen at different magnifications: the blank laminate (a, b), and PPO (10–50  $\mu\text{m}$ )-interleaved laminates with 10 wt % particle loading (c–f) [45]. .....28

Figure 2-12. Cross-sectional SEM images of interlayers with different PES film thickness: (A) 0  $\mu\text{m}$ ; (B) 18.4  $\mu\text{m}$ ; (C) 40.5  $\mu\text{m}$ ; (D) 54.1  $\mu\text{m}$ ; and (E) 97.5  $\mu\text{m}$  [54]. .....30

Figure 2-13. SEM images of Mode I fracture surfaces: (a) unidirectional with epoxy system, (b) unidirectional with vinyl ester system, (c) PE veil interleaved with epoxy system, and (d) carbon veil interleaved with epoxy system[57]. .....31

Figure 2-14. Interlaminar morphology of Ex-situ specimens (the thermoplastic phase was chemically etched) [64]. .....32

Figure 2-15. Percentage increase in Mode I and Mode II fracture toughness. (a) areal density and (b) coverage of the interleave [70]. .....34

Figure 2-16. CNT-enhanced nonwoven carbon tissue (NWCT) fabrication [71]. .....35

Figure 2-17. SEM micrographs of the fracture surfaces with CNT interleaves. (a) Mode I, (b) Mode II [74].	36
Figure 2-18. Schematic of current injection experimental setup [107].	42
Figure 2-19. Electrical Structure Network (ESN) in A350XWB. (a) Schematic of system installation, (b) ESN set-up in fuselage and (b) metallic connectors of ENS [114].	45
Figure 2-20. SEM images for the specimens with 6.3 vol% GO. (a) interlaminar region and (b) fibre surface view [120].	47
Figure 2-21. Micro-voids in the (a) 0 wt% CNF, (b) 0.5 wt% CNF, (c) 1 wt% CNF, and (d) 1.5 wt% CNF composite specimens [123].	48
Figure 2-22. SEM morphologies of Cu-CNT coated carbon fibre [124].	49
Figure 2-23. SEM images of (a) CNT growth and (b) GNPs-coated on CNT growth [127].	50
Figure 2-24. SEM images of nylon veil after surface-loading with AgNWs [137].	53
Figure 2-25. SEM images of (a,b) plan view of the paper, (c,d) cross section of the plant fibre, and (e) cross section of paper embedded in epoxy resin [138].	54
Figure 3-1. Viscosity-temperature curves of the resin system.	82
Figure 3-2. Dynamic mechanical test curves of the rosin-sourced epoxy cast bar.	83
Figure 3-3. SEM images of polyamide nonwoven veil. (a,b) smooth side, (c,d) rough side.	85

Figure 3-4. Sectional image of polyamide veil (four layers). .....	85
Figure 3-5. Schematic diagram of manufacturing set-up. ....	86
Figure 3-6. Curing procedure of the composite laminates. ....	87
Figure 3-7. Results of Mode I toughness test. (a) Typical DCB load- displacement curve, (b) Mode I interlaminar toughness.....	95
Figure 3-8. Typical R-curve for Mode I toughness test. ....	96
Figure 3-9. Results of Mode II toughness test. (a) ENF load-displacement curve, (b) Mode II interlaminar toughness.....	97
Figure 3-10. Plane view of fracture surfaces of NVIC <sup>-ILT</sup> . (a) Mode I, (b) Mode II.....	98
Figure 3-11. Failure mode of NVIC <sup>-ILT</sup> in DCB test. (a) side view, (b) through open mouth.....	99
Figure 3-12. SEM images of fracture surface. (a and b) lower surface, (c and d) upper surface.....	99
Figure 3-13. Optical observation of crack growth mode. (a) Mode I, (b) Mode II.....	101
Figure 3-14. SEM images of Mode II fracture surface. (a,b) Lower surface, (c,d) upper surface.....	101
Figure 3-15. Time histories of the applied force during impact test.....	102
Figure 3-16. Results of residual compression strength test. (a) Load- displacement curve, (b) residual compressive after impact strength.....	104



Figure 3-17. Sectional observation near impact head area. (a) Control <sup>-CAI</sup> , (b) NVIC <sup>-CAI</sup> . .....	105
Figure 3-18. Load-displacement curves of in-plane mechanical test. (a) tensile, (b) flexural, (c) compressive and (d) interlaminar shear. ....	107
Figure 4-1. Electrical installation principle of ENS applied to CFRP fuselage. [1].....	120
Figure 4-2. Images of the copper-nickel plated polyester veil (CNPV). (a) Plane view of CNPV by SEM, (b) Plane view of CNPV by optical microscopy, (c) Section view of CNPV by SEM (d) EDS at the cross section of CNPV fibres .....	124
Figure 4-3. Schematic diagrams of manufacturing set-up.....	125
Figure 4-4. Curing procedure of CFRP specimens .....	126
Figure 4-5. Schematic diagram of FIT composite laminates for toughness study. ....	127
Figure 4-6. Schematic diagram of FIT <sup>e</sup> composite laminates for electrical conductivity study.....	128
Figure 4-7. Cured composite laminates. (a)FIT <sup>e2</sup> , (b) Control <sup>e</sup> .....	128
Figure 4-8. Diagram of test specimens for interlaminar fracture toughness study. (a) DCB specimen, (b) ENF specimen. ....	131
Figure 4-9. Diagram of test specimens and electrical resistance measurement. (a) through-thickness direction, (b) in-plane direction. ....	133
Figure 4-10. Mode I interlaminar fracture toughness for test specimens. ....	135

Figure 4-11. Typical DCB Load-displacement curves .....	135
Figure 4-12. Typical R-curves for Mode I test .....	136
Figure 4-13. Mode II interlaminar fracture toughness for test specimens. ...	137
Figure 4-14. Typical Load-displacement curves for Mode II test.....	137
Figure 4-15. Typical side view of FIT <sup>t</sup> specimens for Mode I interlaminar fracture test. (a) Interlayer structure during Mode I test, (b) SEM image at crack region .....	139
Figure 4-16. Plane view of FIT <sup>t</sup> fracture surface after Mode I interlaminar fracture test. (a) Overall observation (b) SEM image .....	140
Figure 4-17. Typical side view of FIT <sup>t</sup> specimens regarding to Mode II interlaminar fracture test. (a) Failure state of FIT <sup>t</sup> during Mode II test, (b) SEM images at crack region.....	141
Figure 4-18. Plane view of FIT <sup>t</sup> fracture surface after Mode II interlaminar fracture test. (a) Overall observation of upper fracture surface (b) SEM image at upper fracture surface, (c) Overall observation of lower fracture surface, (d) SEM image at lower fracture.....	142
Figure 4-19. Through-thickness electrical conductivity of test specimens (TTEC) .....	144
Figure 4-20. In-plane electrical conductivity of test specimens .....	144
Figure 4-21. Typical cross section of FIT <sup>e</sup> specimens under optical microscope .....	146
Figure 5-1. SEM image of nickel-plated polyester fibre veil .....	160

Figure 5-2. Schematic diagrams of experimental set-up. (a) compression moulding, (b) Real-time compaction-through thickness resistance recording. .... 164

Figure 5-3. Effects of compaction on different dry cross-stacked carbon fibre fabrics. (a) Compressive load-thickness curves, (b)  $R_{tt}$ -thickness curves, (c) Relationship between  $R_{tt}$  and compressive load, (d) Relationship between  $\rho_{tt}$  and  $V_{CF}$ . .... 168

Figure 5-4. Relationship between  $R_{tt}$  and number of plies. (a) Control<sup>D</sup>, (b) FIT<sup>D</sup> and (c) NPV<sup>D</sup>..... 170

Figure 5-5. (a) Resistance of single dry ply ( $k$ ) and (b) interfacial contact resistance ( $R_0$ ) as a function of load. .... 171

Figure 5-6. Through-thickness electrical resistivity ( $\rho_{tt}$ ) versus carbon fibre volume fraction ( $V_{CF}$ ) for dry cross-stacked specimens (solid lines) and cured cross-ply specimens (scatters)..... 173

Figure 5-7. The relationship between resin content ( $w_{resin}$ ) and carbon fibre volume fraction ( $V_{CF}$ )..... 174

Figure 5-8. Schematic illustration regarding the effects of electrical functionalized interleaves on through thickness conductive contacts, at low and high compaction. (a) Control<sup>E</sup> and (b) FIT<sup>E</sup> ..... 175

Figure 5-9. Sectional microscope observation for test specimens. (a) Control<sup>E</sup>, (b) FIT<sup>E</sup> ..... 177

Figure 5-10. The effects of the number of NPV layers on  $\rho_{tt}$ ..... 178

Figure 5-11. Longitudinal flexural properties of test specimens. (a) Load-displacement curves, (b) flexural strength and modulus ..... 180

Figure 5-12. Interlaminar shear properties of test specimens (a) Load-displacement curves, (b) ILSS ..... 181

Figure 5-13. Sectional microscope images of FIT<sup>M</sup>-58.4% specimen after interlaminar shear test ..... 182

Figure 6-1. The three main studies of this thesis. .... 188

## List of Tables

Table 1-1. Summary of different techniques to improve the electrical conductivity for carbon fibre-epoxy laminates. ....	6
Table 2-1. Summary of Matrix Toughening Technology for CFRP laminates	26
Table 2-2. Summary of Interleaving Toughening Technology for CFRP laminates .....	37
Table 2-3. Different techniques for improving the electrical conductivity of CFRP laminates.....	55
Table 3-1. Physical and chemical properties of the resin system.....	82
Table 3-2. Technical data of SYT49S, 12K, T700-grade carbon fibre.....	84
Table 3-3. Physical property of high temperature rosin-sourced epoxy /UN-SYT49S prepreg. ....	84
Table 3-4. Characteristics of specimens for interlaminar toughness study. ...	88
Table 3-5. Characteristics of specimens for CAI study. ....	88
Table 3-6. Characteristic of specimens for mechanical properties study. ....	89
Table 3-7. Characteristics of impact damage area.....	103
Table 3-8. In-plane mechanical properties of test specimens. ....	106
Table 4-1. Electrical conductivity of composite specimens studied.....	121
Table 4-2. Characteristics of test specimens for toughness study .....	127

Table 4-3. Characteristics of test specimens for electrical conductivity study .....	129
Table 5-1. Summary of different techniques to improve the through-thickness electrical conductivity for carbon fibre-epoxy laminates. ....	158
Table 5-2. Characteristics of specimens for through thickness electrical conductivity (TTEC) study.....	161
Table 5-3. Characteristics of specimens for mechanical properties study ...	162

## Abbreviations

2D	Two Dimensional
3D	Three Dimensional
5H	5-Harness Satin Weave
ABC	Acrylonitrile Butadiene Styrene
AgNP	Sliver Nanoparticle
AgNW	Sliver Nanowire
ASTM	American Society for Testing and Materials
BIM	Bismaleimides
BMC	Bulk Moulding Compound
BOZ	Benzoxazine
CAI	Compression After Impact
CF	Carbon Fibre
CFRC	Carbon Fibre Reinforced Polymer Matrix Composite
CFRP	Carbon Fibre Reinforced Polymer
CLC	Combined Loading Compression
CNF	Carbon Nanofibre
CNT	Carbon Nanotube
CRN	Current Return Network
CSR	Core-Shell Rubber
CTBN	Carboxyl Terminated Butadiene Nitrile Rubber
DCB	Double Cantilever Beam
DMC	Dough Moulding Compound
DWCNT	Double-Wall Carbon Nanotubes
EMI	Electromagnetic Interference
ENF	End Notch Flexure

EP	Epoxy
ESIS	European Structural Integrity Society
ESN	Electrical Structure Network
FCCVD	Floating Catalyst Chemical Vapor Deposition
FIT	Functionalized Interleave Technology
GNP	Graphene Nanoplatelet
GO	Graphene Oxide
IFT	Interlaminar Fracture Toughness
ILSS	Interlaminar Shear Strength
ITT	Interleaving Toughening Technology
LSP	Lightning Strike Protection
MBN	Metallic Bonding Network
MBT	Modified Beam Theory
MWCNT	Multi-Wall Carbon Nanotubes
NCF	Non-Crimp- Fabrics
NV	Non-Woven Veil
PA	Polyamide
PAI	Polyamideimides
PAN	Polyacrylonitrile
PC	Polycarbonate
PCL	Polycaprolactone
PE	Polyester
PEEK	Polyetherether Ketone
PEI	Polyetherimide
PEK-C	Polyaryletherketone Cardo
PES	Polyether Sulfone
PET	Polyethylene-Terephthalate



PI	Polyimide
PP	Polypropylene
PPO	Poly (Phenylene Oxide)
PPS	Polyphenylene Sulfide
PSF	Polysulfone
PVB	Polyvinyl Butyral
PVC	Polyvinyl Chloride
PVDF	Polyvinylidene Fluoride
RAM	Maleopimaric Acid
rEGOs	Reduced Exfoliated Graphene Oxides
RTM	Resin Transfer Moulding
SEM	Scanning Electron Microscopy
SWCNT	Single-Wall Carbon Nanotubes
TrGO	Thermally Reduced Graphene Oxide
TTEC	Through-Thickness Electrical Conductivity
UD	Unidirectional
UPR	Unsaturated Polyester
VARTM	Vacuum Assisted Resin Transfer Moulding
VGCF	Vapor Grown Carbon Fibre

# Symbols

$V_{CF}$	Carbon Fibre Volume Fraction
$F^{cu}$	Compressive Modulus
$E_c$	Compressive Strength
$T_m$	Crystalline Melting Point
$U_t$	Drop-Weight Absorbed Energy
$E_B$	Flexural Modulus
$\sigma_f$	Flexural Strength
$T_g$	Glass Transition Temperature
$\sigma_{xy}$	In-Plane Electrical Conductivity
$G_{Ic}$	Mode I Interlaminar Fracture Toughness
$G_{IIc}$	Mode II Interlaminar Fracture Toughness
$\omega_{resin}$	Resin Content
$F^{sbs}$	Short-Beam Strength
$U$	Strain Energy
$G_c$	Strain Energy Release Rate
$K_c$	Stress Intensity Factor
$S$	Surface Energy
$E^{chord}$	Tensile Modulus
$F^{tu}$	Tensile Strength
$\rho_{tt}$	Through-Thickness Electric Resistivity
$\sigma_z$	Through-Thickness Electrical Conductivity
$R_{tt}$	Through-Thickness Electrical Resistance

# Chapter 1: Introduction

## 1.1 Background

Carbon fibre reinforced polymer matrix composites (CFRPs) have increasingly replaced light alloys in civil airframes. The obvious weight savings, and services life extension provide life cycle cost benefits for fleet operators. As shown in Figure 1-1, the use of composites materials in Boeing 787 Dreamline aircraft has reached 50% of the total aircraft structural weight. The Fuselage, main wing box and stabilizer boxes are designed with carbon fibre epoxy laminates. Similarly, the Airbus A350 XBW has improved the composites content to 53% with CFRP fuselage skin panels, rear fuselage and fin [1,2].

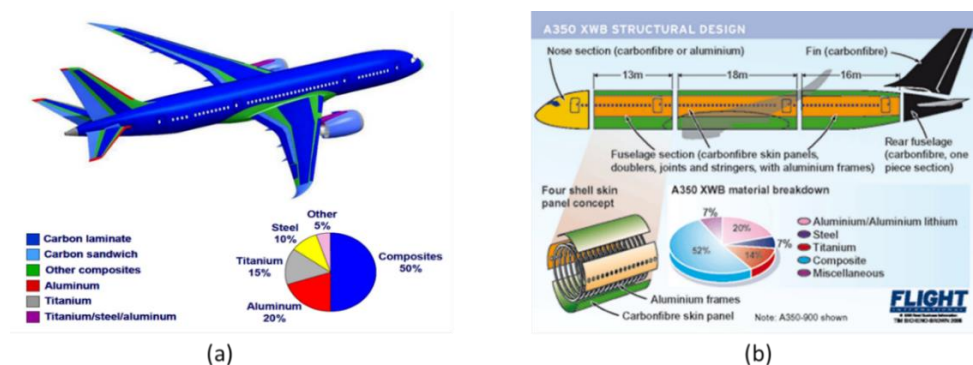


Figure 1-1. Material composition of advanced aircraft. (a) Boeing 787 and (b) Airbus A350XBW [1,2].

Advanced aircraft also require a complex electrical system with implied weight reductions and high levels of reliability. Here CFRP structures introduce some

complexities including significant anisotropic material properties with classical shortcomings in out-of-plane properties especially fracture toughness and through-thickness electrical conductivity.

### ***1.1.1 Toughening of CFRPs***

Engineering resins such as epoxy provide high cross-link density, leading to many desirable engineering properties such as high modulus, high strength, and chemical resistance. However, the same characteristics also causes the low ductility and poor fracture toughness for the cured epoxies [3]. Due to the anisotropic mechanical and thermal properties between the carbon fibre plies, a concentration of interlaminar stresses is found near the edges of laminates and adjacent to any defects. Delamination is typically severe at free edges, cracks, joints, and impact sites [4]. These may be mitigated by using a toughened epoxy matrix. Elastomeric components are typically introduced into the epoxy to form a bi-continuous granular structure, via reaction induced phase separation, phase inversion and phase coarsening [5]. Typical toughening agents include Carboxyl-terminated butadiene-acrylonitrile (CTBN) and amine-terminated butadiene-acrylonitrile (ATBN) as reactive liquid rubbers, as well as Polyether sulfone (PES), Polyetherimide (PEI) and Polymethyl methacrylate (PMMA) as thermoplastics [6–11]. However, the toughening agents may influence the thermal properties adversely and likely

increase the viscosity of the resin matrix, complicating processing and fibre wetting [12].

Interleaving as a toughening approach was first studied in aeronautical composites structures as arrester strips to prevent fatigue crack propagation and damage control [13]. After decades of investigation, Interleaf Toughening Technology (ITT) has become an established approach for CFRP laminates. Generally, ITT involves the insertion of interply layers in the form of particles, fibres, and films. Unlike rubber-toughened resins, the ITT barely modifies the interlaminar structures of laminates, hence viscosity and fibre wetting problems are resolved. Incorporation of reactive thermoplastics such as PES, PEI and PSF interleaves can significantly enhance the fracture toughness of CFRP [14–17]. Typically, the interleaves undergo phase separation process during curing, forming bi-continuous structures between adjacent plies. However, the complex phase morphology is dependent on the thermodynamic and kinetics conditions the thermoplastic interleaves and thermosetting epoxy matrix. Therefore, these toughening methods are specific to the matched resin formulations.

### ***1.1.2 Electrical conductivity of CFRPs in aircraft design***

The operation of any electrical equipment requires positive and negative conductors to form an electrical loop. Grounding is also required for the safety

and stability of the system. Metallic aircraft rely on the fuselage and wings to act a part of electrical return network on the aircraft [18]. Clearly CFRP laminates are highly anisotropic and offer higher resistivity than that of aircraft alloys. Both factors can impact on electrical functionality [19]. Lightning Strike Protection (LSP), Electromagnetic Interference (EMI) and Electromagnetic Shielding (EMS) are similarly affected. Currently, the industrial solution is to introduce metallic conductors to improve grounding as shown in Figure 1-2. For example, an Electrical Structure Network (ESN) is distributed throughout the fuselage to offer the electrical and environmental conditions required for the correct functioning of aircraft systems. Metallic Bonding Network (MBN) components are thus assembled on the wings, belly fairing and tail cone to provide the failure current return path, equipment bonding and lightning strike protection [20]. Clearly these metallic conductors offset some of the lightweight advantages of CFRP structures.

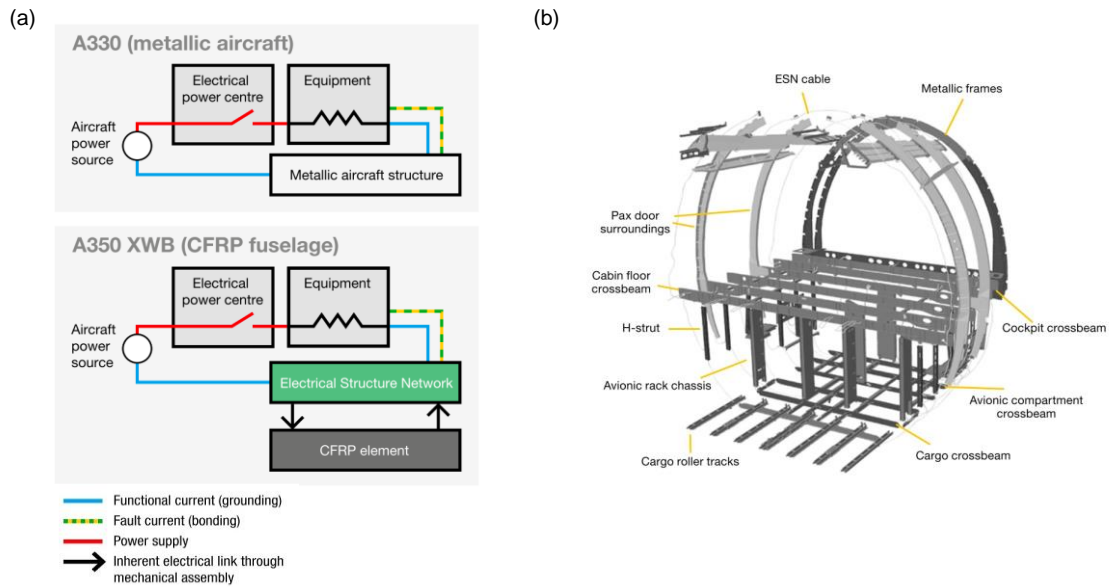


**Figure 1-2. Schematics of electrical installation in aircraft and ENS system. (a) electrical installation, (b) ENS in fuselage [20].**

Improving the electrical conductivity of CFRPs remains a major challenge for the next generation of aerospace composites. The traditional method is to blend conductive fillers into the insulating resin matrix. Fillers include nano-scale materials such as carbon nanotubes (CNTs), graphene and silver nanowires in an attempt to simultaneously improve the electrical conductivity and mechanical properties. However, the filler content must reach or exceed the percolation threshold in order to form continuous paths and high loadings, will again increase viscosity and inhibit fibre wetting, resulting in weak interfacial bonding and poor dispersion. Table 1-1 summarizes some recent attempts to use various additives to improve the electrical conductivity. It

clearly remains a significant challenge to achieve high electrical conductivity without sacrificing some aspects of mechanical performance.

**Table 1-1. Summary of different techniques to improve the electrical conductivity for carbon fibre-epoxy laminates.**

Specimens	Electrical conductivity (S/m)		Fibre Volume Fraction $V_{CF}$ (%)
	Through-thickness	In-plane	
Filled with 2 wt% SWNTs (0/90) [21]	1.8	14285	-
3 wt% CB-CC (UD) [22]	55.6	X-1961 Y-91	65.4
Interleaved with 2 vol% GNP (0/90) [23]	15.5	16667	56.7
Interleaved co-polyimide veils with 10 wt% CNT (UD) [24]	3.2	X-2600 Y-8.6	57
1 wt% CNTs on carbon fibre surface (0/90) [25]	1	-	-
0.4 wt% DWCNT [26]	0.53	X-6300 Y-0.018	67
6.8 vol% GO [27]	18	X-22000 Y-70	57

## 1.2 Aims and objectives

The current project aims to prepare a multifunctional CFRP laminates with high electrical conductivity and high fracture toughness, while minimising

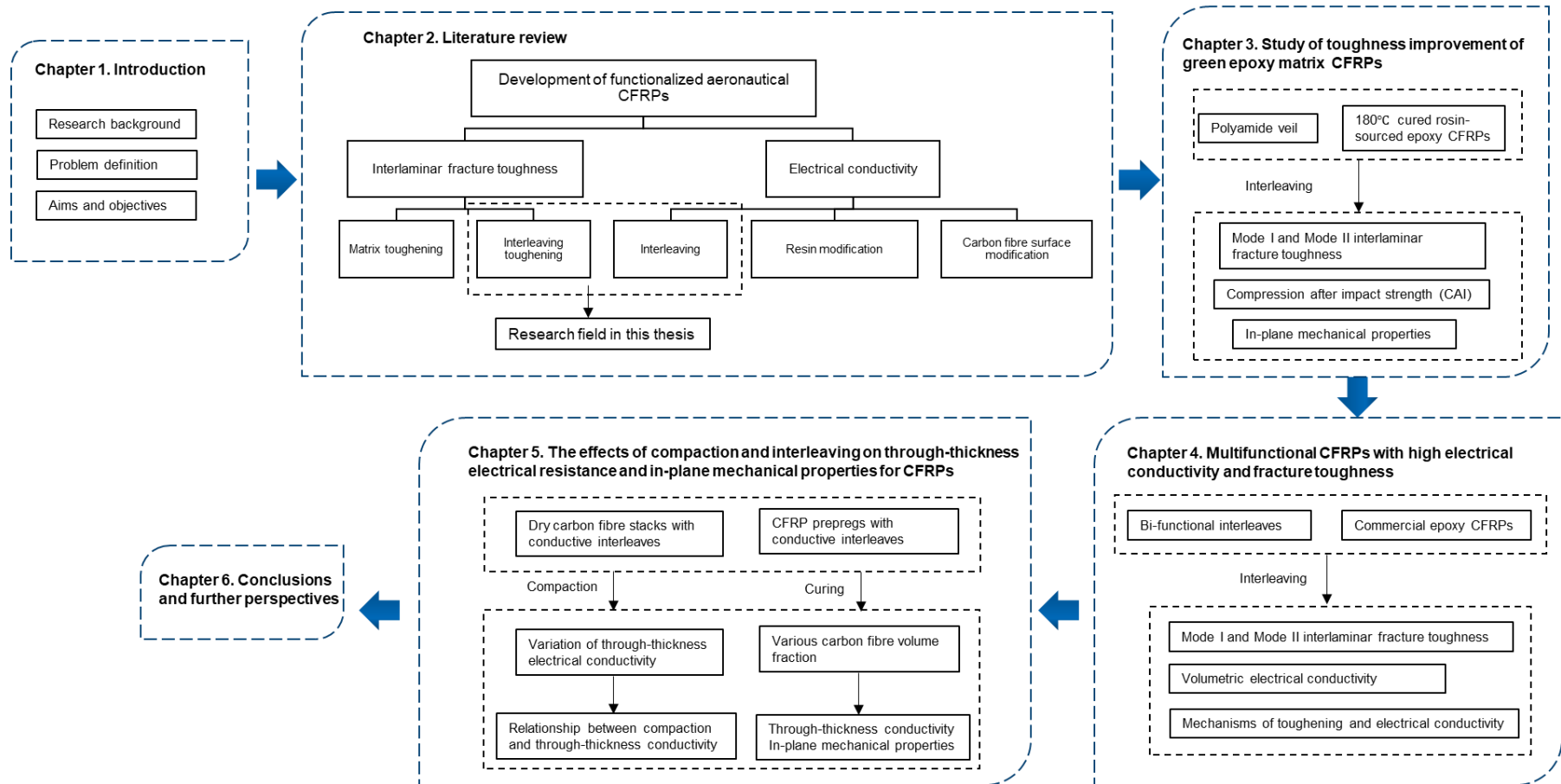


adverse impacts on static mechanical properties. The proposed innovation is based on advanced interleaf elements.

The main objectives are:

1. To identify a toughening interleaf that can overcome the technical limitation of the phase transformation toughening method and investigate its influence on Mode I and Mode II interlaminar fracture toughness, compression after impact strength and in-plane mechanical properties.
2. Evolving a bi-functional composite interleaf to simultaneously improve toughness and through-thickness electrical conductivity and to characterise the arising electrical and mechanical performance in CFRP laminates.

# 1.3 Thesis structure



## 1.4 Reference

- [1] A. Lefeuvre, S. Garnier, L. Jacquemin, B. Pillain, G. Sonnemann, Anticipating in-use stocks of carbon fiber reinforced polymers and related waste flows generated by the commercial aeronautical sector until 2050, *Resour. Conserv. Recycl.* 125 (2017) 264–272. doi:10.1016/j.resconrec.2017.06.023.
- [2] M. Maria, Advanced composite materials of the future in aerospace industry, *Incas Bull.* 5 (2013) 139–150. doi:10.13111/2066-8201.2013.5.3.14.
- [3] J. Chen, Toughening Epoxy Polymers and Carbon Fibre Composites with Core-Shell Particles, Block Copolymers and Silica Nanoparticles, Imperial College London, 2013. <http://hdl.handle.net/10044/1/14261>.
- [4] K. Shivakumar, R. Panduranga, Interleaved polymer matrix composites - A review, *Collect. Tech. Pap. - AIAA/ASME/ASCE/AHS/ASC Struct. Struct. Dyn. Mater. Conf.* (2013) 1–13.
- [5] N.G. Ozdemir, T. Zhang, I. Aspin, F. Scarpa, H. Hadavinia, Y. Song, Toughening of carbon fibre reinforced polymer composites with rubber nanoparticles for advanced industrial applications, *Express Polym. Lett.* 10 (2016) 394–407. doi:10.3144/expresspolymlett.2016.37.
- [6] Z. Chen, J. Tian, J. Guo, Q. Liu, N. Jia, Effect of Polyetherimide on Toughening T700 / Epoxy Composite Materials 2, *Aerosp. Mater. Technol.* 46 (2016) 37–39.
- [7] J. Yao, K. Niu, Y. Niu, T. Zhang, Toughening efficiency and mechanism of carbon fibre epoxy matrix composites by PEK-C, *Compos. Struct.* 229 (2019) 111431. doi:10.1016/j.compstruct.2019.111431.
- [8] J.L. Tsai, B.H. Huang, Y.L. Cheng, Enhancing fracture toughness of glass/epoxy composites by using rubber particles together with silica nanoparticles, *J. Compos. Mater.* 43 (2009) 3107–3123. doi:10.1177/0021998309345299.
- [9] T. Inoue, Reaction-induced phase decomposition in polymer blends, *Prog. Polym. Sci.* 20 (1995) 119–153. doi:10.1016/0079-6700(94)00032-W.

- [10] W. Gan, Y. Yu, M. Wang, Q. Tao, S. Li, Viscoelastic effects on the phase separation in thermoplastics-modified epoxy resin, *Macromolecules*. 36 (2003) 7746–7751.  
doi:10.1021/ma034649a.
- [11] B. Guo, D. Jia, Effects of epoxy content on dynamic mechanical behaviour of PEI-toughened dicyanate-novolac epoxy blends, *Polym. Int.* 53 (2004) 1378–1381.  
doi:10.1002/pi.1548.
- [12] S. Sprenger, M.H. Kothmann, V. Altstaedt, Carbon fiber-reinforced composites using an epoxy resin matrix modified with reactive liquid rubber and silica nanoparticles, *Compos. Sci. Technol.* 105 (2014) 86–95. doi:10.1016/j.compscitech.2014.10.003.
- [13] J.G. Goree, Preliminary Investigation of Crack Arrest in Composite Laminates Containing Buffer Strips, NASA CR-3000, 1978.
- [14] C. Cheng, C. Zhang, J. Zhou, M. Jiang, Z. Sun, S. Zhou, Y. Liu, Z. Chen, L. Xu, H. Zhang, M. Yu, Improving the interlaminar toughness of the carbon fiber/epoxy composites via interleaved with polyethersulfone porous films, *Compos. Sci. Technol.* 183 (2019).  
doi:10.1016/j.compscitech.2019.107827.
- [15] Q. Cheng, Z. Fang, Y. Xu, X.S. Yi, Improvement of the impact damage resistance of BMI/graphite laminates by the ex-situ method, *High Perform. Polym.* 18 (2006) 907–917.  
doi:10.1177/0954008306068296.
- [16] G. Li, P. Li, C. Zhang, Y. Yu, H. Liu, S. Zhang, X. Jia, X. Yang, Z. Xue, S. Ryu, Inhomogeneous toughening of carbon fiber/epoxy composite using electrospun polysulfone nanofibrous membranes by in situ phase separation, *Compos. Sci. Technol.* 68 (2008) 987–994. doi:10.1016/j.compscitech.2007.07.010.
- [17] D. Quan, D. Yue, Y. Ma, G. Zhao, R. Alderliesten, On the mix-mode fracture of carbon fibre/epoxy composites interleaved with various thermoplastic veils, *Compos. Commun.* 33 (2022) 101230. doi:10.1016/j.coco.2022.101230.
- [18] C.E. Jones, P.J. Norman, G.M. Burt, C. Hill, G. Allegri, J.M. Yon, I. Hamerton, R.S. Trask, A Route to Sustainable Aviation: A Roadmap for the Realization of Aircraft Components with

Electrical and Structural Multifunctionality, *IEEE Trans. Transp. Electrification*. 7 (2021) 3032–3049. doi:10.1109/TTE.2021.3078118.

[19] C.E. Jones, P.J. Norman, M. Szykiel, R. Pena Alzola, G.M. Burt, S.J. Galloway, L.F. Kawashita, S.R. Hallett, Electrical and Thermal Effects of Fault Currents in Aircraft Electrical Power Systems with Composite Aerostructures, *IEEE Trans. Transp. Electrification*. 4 (2018) 660–670. doi:10.1109/TTE.2018.2833838.

[20] H.S. Kim, H.T. Hahn, Graphite fiber composites interlayered with single-walled carbon nanotubes, *J. Compos. Mater.* 45 (2011) 1109–1120. doi:10.1177/0021998311402726.

[21] D. Zhang, L. Ye, S. Deng, J. Zhang, Y. Tang, Y. Chen, CF / EP composite laminates with carbon black and copper chloride for improved electrical conductivity and interlaminar fracture toughness, *Compos. Sci. Technol.* 72 (2012) 412–420. doi:10.1016/j.compscitech.2011.12.002.

[22] H.S. Kim, Hahn, Graphite Nanoplatelets Interlayered Carbon/Epoxy Composites, *AIAA J.* 47 (2009) 2779–2784. doi:10.2514/1.39522.

[23] K. Dydek, A. Boczkowska, P. Latko-Duralek, M. Wilk, K. Padykuła, R. Kozera, Effect of the areal weight of CNT-doped veils on CFRP electrical properties, *J. Compos. Mater.* 54 (2020) 2677–2685. doi:10.1177/0021998320902227.

[24] Y. Lin, M. Gigliotti, M.C. Lafarie-frenot, J. Bai, D. Marchand, D. Mellier, Experimental study to assess the effect of carbon nanotube addition on the through-thickness electrical conductivity of CFRP laminates for aircraft applications \*, *Compos. Part B*. 76 (2015) 31–37. doi:10.1016/j.compositesb.2015.02.015.

## Chapter 2: Literature review

### 2.1 Interlaminar fracture toughness of CFRP laminates

Delamination resistance is quantified by interlaminar fracture toughness, which is one of the important linear-elastic fracture mechanic parameters for CFRPs. The interlaminar fracture toughness is defined as the critical strain energy release rate, which is expressed as the amount of energy released in delamination propagation per unit length. Figure 2-1 shows the modes of crack propagation caused by corresponding loadings [1]. The crack opening mode (Mode I) is caused by the normal stresses perpendicular to the crack plane, resulting in the delamination surfaces separating. The crack sliding mode (Mode II) is due to shear stress parallel to the crack plane, causing the surfaces to slide over each other without relative crack opening. The tearing or anti-plane shear mode (Mode III) is caused by the out-of-plane shear stress, resulting in the crack propagation perpendicular to the delamination surfaces. Any of these fracture modes or mixed modes can initiate the delamination of CFRP laminates.

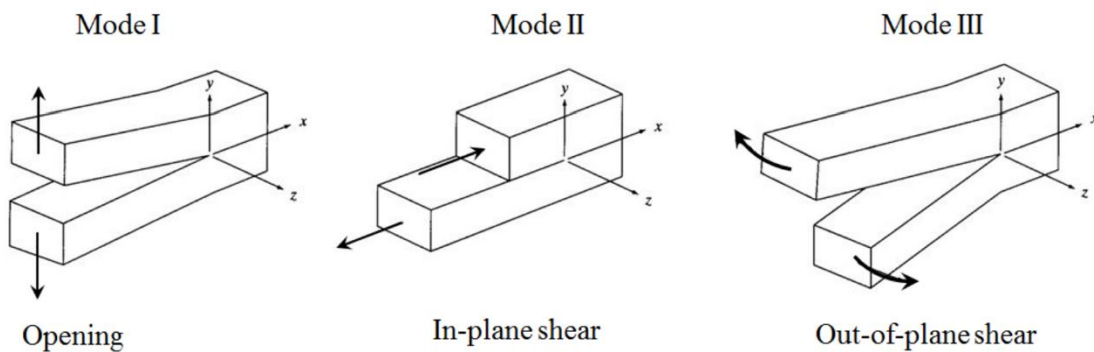


Figure 2-1. Three fundamental rupture modes [1].

### **2.1.1 Mode I and Mode II interlaminar fracture toughness**

Mode I and Mode II delamination likely more critical than Mode III because the latter is generally higher than that of other two modes [2]. Mode I and Mode II interlaminar fracture toughness of CFRP laminates have been successfully characterized via the linear-elastic fracture mechanics. For isotropic and brittle metallic materials, interlaminar fracture toughness is characterized by the stress intensity factor ( $K_C$ ), which is related to the stress distribution at the crack tip. However, crack growth in CFRP laminates is more complex due to the possibility of multiple failure events. Thus, the interlaminar fracture toughness of CFRP laminates is commonly expressed as strain energy release rate ( $G_C$ ). For Mode I and Mode II interlaminar fracture toughness, the relative strain energy release rate can be determined using a compliance method, as follows:

$$G_I \text{ or } G_{II} = \frac{1}{w} \frac{dU}{da} \quad (2-1)$$

Where U is the total elastic energy in the specimen, w is the width of specimen, a is the crack length. In practice, the crack propagation in CFRP laminates could be stable or unstable. According to [3], the stability of crack could be considered using the energy balance criteria, as shown in Figure 2-2.

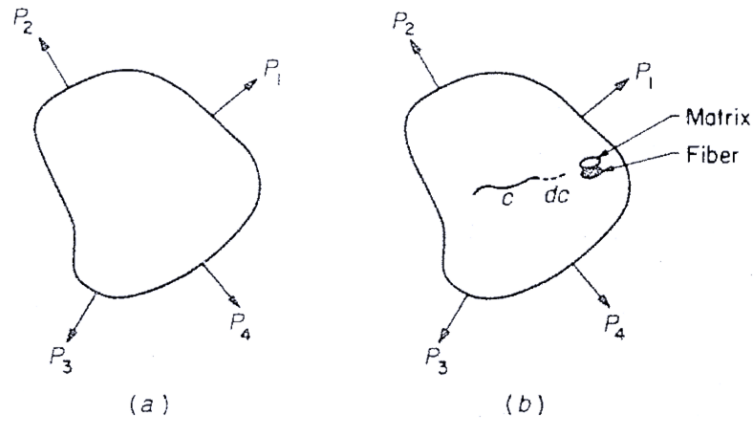


Figure 2-2. Solid object (a) without crack and (b)with a crack subjected to the external force [3].

The difference in energy is attributed to the new surface energy  $S$  introduced by crack propagation and the decreased strain energy  $U$ . The total energy of the cracked body system  $U_2$  can be expressed as:

$$U_2 = U_1 + S - U \quad (2-2)$$

Where  $U_1$  is the total energy of no cracked body system. Stable crack propagation is considered as the additional energy entering the body by increasing loading:

$$\frac{\partial U_2}{\partial c} > 0 \quad (2-3)$$

Further, the relationship between strain energy released and surface energy increased during stable crack propagation can be obtained by substitution 2-2 into 2-3:



$$\frac{\partial U}{\partial c} < \frac{\partial S}{\partial c} \quad (2-4)$$

Unstable crack propagation is considered as the total energy  $U_2$  decreased or constant:

$$\frac{\partial U_2}{\partial c} \leq 0 \quad (2-5)$$

And the strain energy release rate is greater than the surface energy increase rate:

$$\frac{\partial U}{\partial c} \geq \frac{\partial S}{\partial c} \quad (2-6)$$

Mode I and Mode II interlaminar fracture toughness test methods are prescribed by ISO and ASTM. These methods are generally exclusive for unidirectional beam type CFRP laminates, with the crack growth along with the fibre direction. The double cantilever beam (DCB) test and end notched flexure (ENF) test are popular methods to determine the Mode I and Mode II interlaminar fracture toughness, respectively.

### ***2.1.2 Impact and after-impact properties of CFRP laminates***

Impact events are expected service time for CFRP aero-structures, which may range from the drop of hand tools to high-speed impact from bird-strike, hail or ballistic projectiles. Low-energy impact may pose a greater threat because it can induce the blind delamination with less detectable surface damage. During the low energy impact,

the delamination is mainly driven by the Mode II interlaminar shear stresses, resulting from the bending of the laminated structure.

Figure 2-3 indicates typical damage modes for CFRP laminates [4]. Impact resistance is the capacity to absorb and dissipate impact energy. The absorption of energy may be via material deformation or new surface creation. In the brittle materials, for example ceramics and epoxies, the energy absorbed by deformation and creation of new fracture surfaces is small thus the fracture toughness of such materials is relatively low.

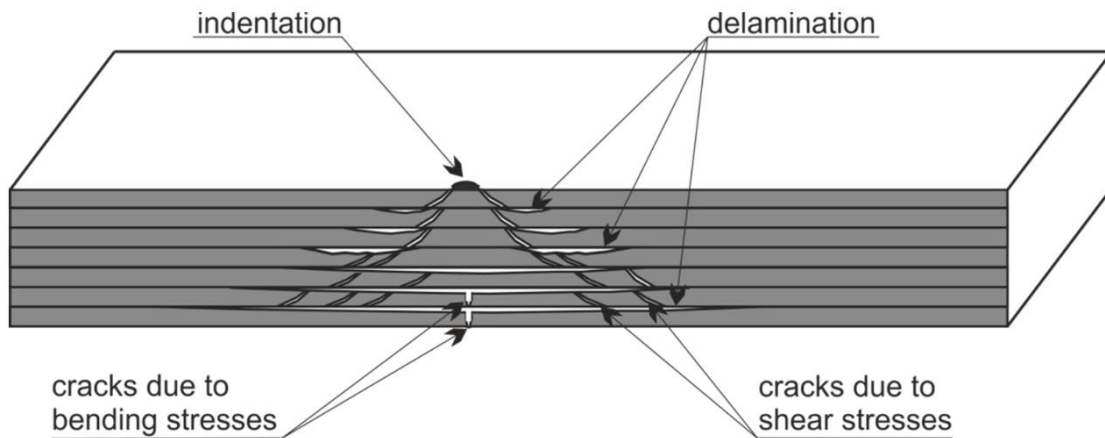


**Figure 2-3. Schematic of barely visible impact damage in CFRP laminates [4].**

The drop-weight impact test is commonly used to assess low speed impact resistance CFRP laminates. The absorbed energy is calculated as follows:

$$U_t = \frac{W}{2g} (u_1^2 - u_2^2) \quad (2-7)$$

Where, W is the weight of the drop head,  $u_1/u_2$  is the velocity of the drop head just before/after impact and g is the gravity acceleration. The contact force versus time data

is continuously recorded during the impact process, as well as the dent depth after impact. ASTM D7136 is a widely used test standard.

Damage resistance is the property that enables a material to withstand damage development under external loading. Meanwhile, the ability of the damaged structure to resist catastrophic failure is termed *damage tolerance*. The latter is a key property of CFRP laminates such that they may continue to carry loads safely with sub-surface delamination after the low-energy impact events. Impact tolerance is often characterised by the residual tensile strength and residual compressive strength after impact (CAI).

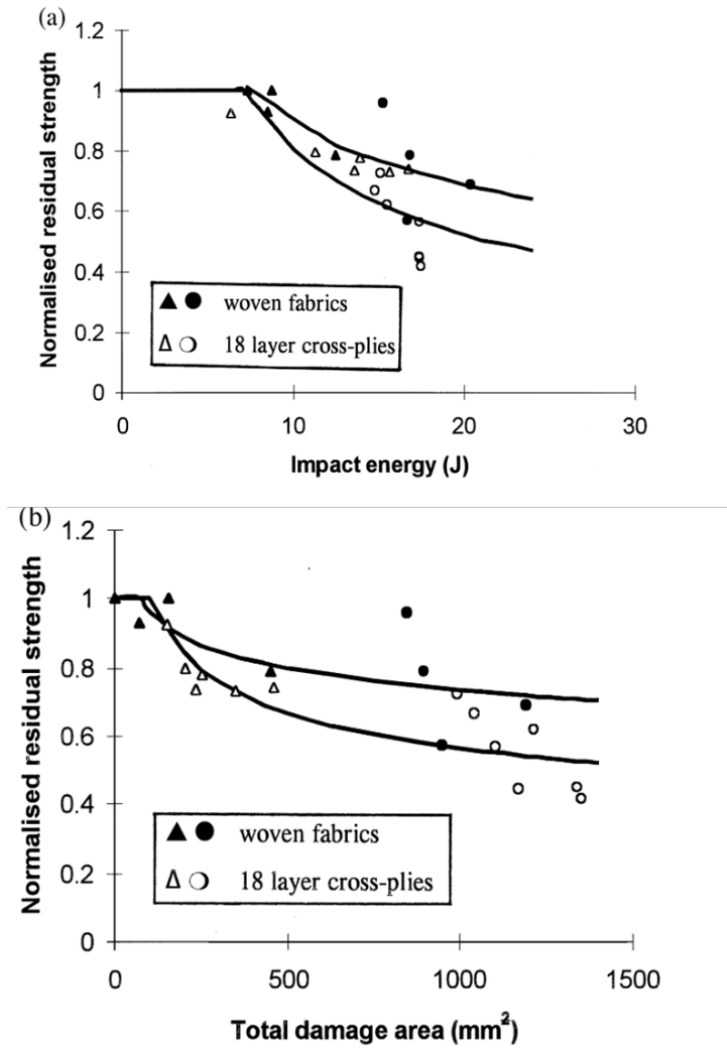


**Figure 2-4. Normalised residual compressive strength against (a) impact energy and (b) total damage area.**

Cartie and Irving[5] highlighted the key role of resin toughness in controlling impact resistance of CFRP laminates. There was no such improvement when using high strength and high modulus carbon fibres. Kim and Sham [6] compared CAI strength of woven and cross-ply CFRP laminates as a function of impact energy and total damage area. As shown in Figure 2-4, the woven-fabric laminates show proportionately higher CAI strength than cross-ply laminates. However, the woven-fabric laminates also

exhibited a lower maximum impact load. Delamination growth was mainly driven by the Mode II rather than Mode I mechanisms under low-velocity impact. Chen and Hodgkinson [7] compared the impact tolerance of unidirectional prepreg laminates (UD), Non-Crimp-Fabrics (NCF), two dimensional (2D) fabrics and three dimensional (3D) fabric laminates. The best impact tolerance at low-velocity impact was found in the 3D woven fabric laminates whilst the NCF composites had superior impact resistance under high-velocity impact. The laminated specimens achieved the best in-plane mechanical properties. Figure 2-5 shows the C-scan and sectional microscope image for test laminates under low-velocity impact.

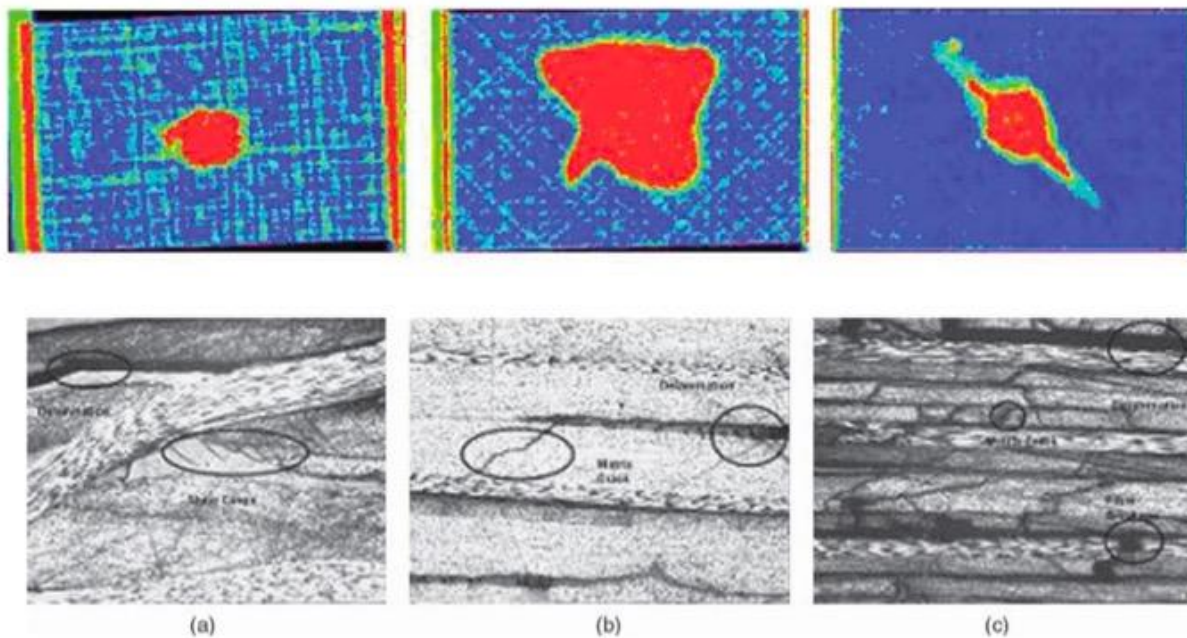


**Figure 2-5. C-scan and sectional microscope image for test laminates under low-velocity impact. (a) 3D woven composite, (b) NCF and (c) UD prepreg laminates [7].**

## **2.2 CFRP toughening technology**

The brittleness of the epoxy matrix drives the low fracture toughness of the CFRP laminates. The fracture toughness of typical epoxy resin is below  $100\text{J/m}^2$  yielding mode I and II interlaminar fracture toughness of epoxy based CFRP laminates of around  $200\text{ J/m}^2$  and  $700\text{ J/m}^2$ , respectively. The main toughening approaches for CFRP laminates involve either matrix toughening or interleaving toughening technology.

### ***2.2.1 Matrix toughening technology***

#### ***2.2.1.1 Rubber and thermoplastic fillers***

The simplest approach is to disperse a second phase toughening fillers into the matrix to improve its fracture toughness. The toughening mechanisms involve plastic shear yielding and localized cavitation near the crack tip. Kinloch et.al [8] explored the microstructure and fracture behaviour of a carboxyl terminated butadiene nitrile rubber (CTBN)-modified epoxy. The stress intensity factor  $K_c$  for rubber-modified epoxy was significantly higher than that of neat epoxy. Figure 2-6 shows the fracture surface of rubber-modified epoxy, exhibiting multiple rubber particle cavities, together with clear plastic shear flow of resin matrix. Pearson and Yee [9] also studied epoxies modified via CTBN liquid rubbers and found improvements in fracture toughness for rubber-modified blends. Figure 2-7 shows the plastic deformation and particle-particle interaction. Further, Quan and Ivankovic [10] investigated core-shell rubber (CSR) nanoparticle modified epoxies. The fracture toughness was significantly improved from  $343\text{J/m}^2$  to  $2671\text{J/m}^2$  for epoxy with 30% volume fraction of CSR nanoparticles.

Although rubber particles bring effective toughening results for epoxies, they significantly reduce the glass transition temperature, Young's modulus and strength and increase viscosity due to the inherent properties of the rubber [11].

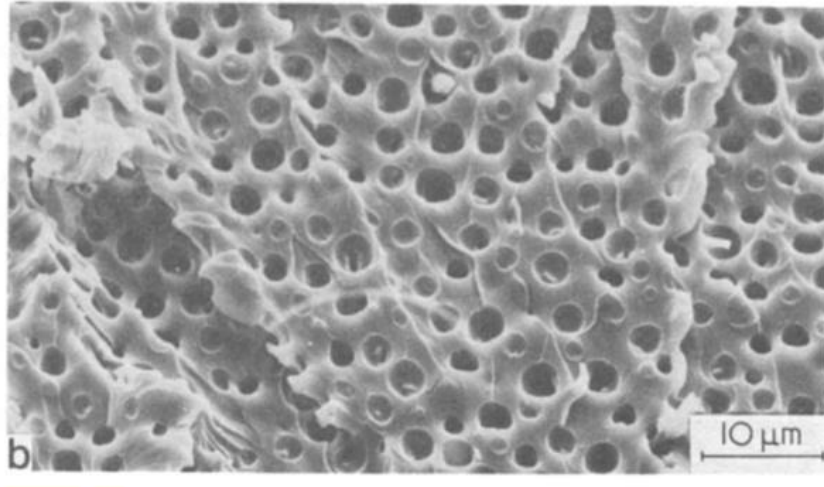


Figure 2-6. SEM of the fracture surface in rubber-modified epoxy [8].

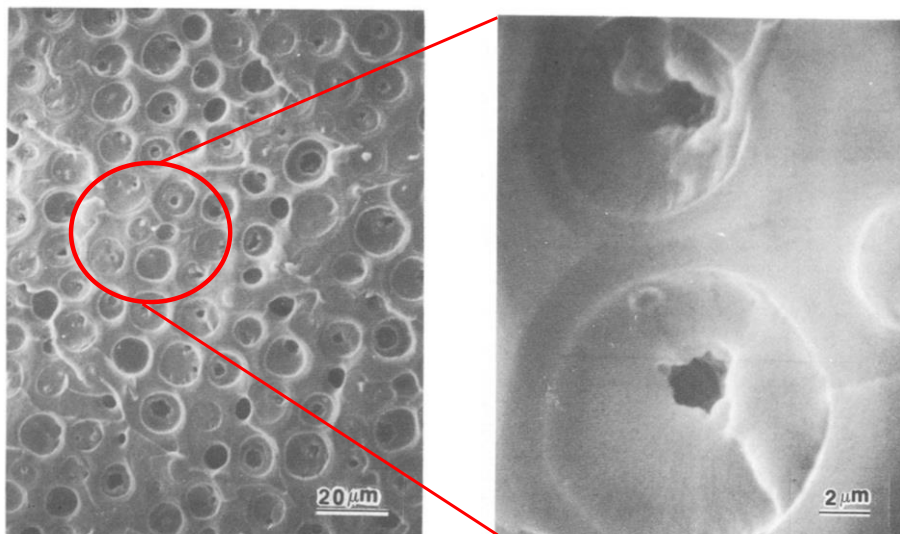
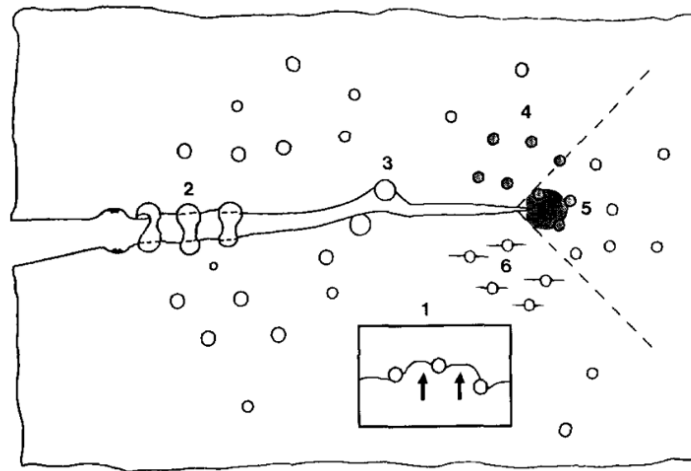


Figure 2-7. SEM from the stress-whitened area of fractured specimens [9].

High-performance thermoplastic particles provide an alternative toughening agent, whilst mitigating the impact on thermal and static mechanical properties. The toughening mechanisms involve crack pinning, crack deflection, particle bridging, particle yielding, particle yielding-induced shear band and branching induced microcracking, as shown in Figure 2-8 [12].



**Figure 2-8. Schematic diagram of toughening mechanisms proposed for thermoplastic-modified epoxies: (1) crack pinning, (2) particle bridging, (3) crack path deflection, (4) particle yielding, (5) particle-yielding- induced shear banding, and (6) microcracking [12].**

A two-phase structure is critical to improve fracture toughness and this may include particulate dispersion, co-continuous and phase inversion, and reaction induced phase separation. The co-continuous phase or phase inversion morphology is the most successful [13,14]. Girard-Reydet et.al [15] studied epoxy modified with PEI. The precure temperature significantly affected the viscosity of the blend system and the extent of the phase separation process and thus the final morphologies which also changed with the PEI content. At 10 wt% the PEI particles were dispersed in the epoxy



rich phase but 20 wt% PEI yielded a co-continuous or invert structures and this improved the fracture toughness significantly. Nobuyuki et. al [16] investigated the epoxy modified with 15 wt% PES and produced useful toughening effects which were highly susceptible to the heating rate during curing. Figure 2-9 shows the phase morphology of epoxy/PES blends from the investigation of Kinloch et al. [17].

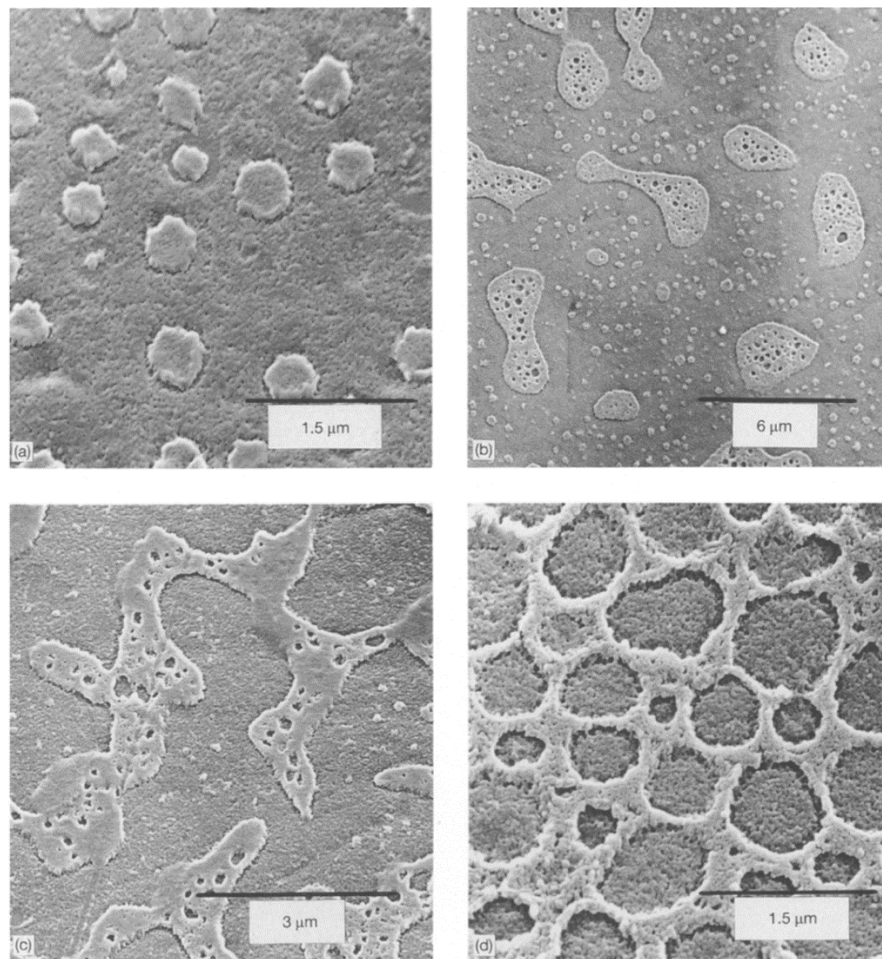


**Figure 2-9. Microstructures of the epoxy/PES system. (a) Particulate microstructure second phase of thermoplastic-rich particles in continuous epoxy-rich matrix. (b) Particulate and co-continuous microstructures. (c) Co-continuous microstructure - where both the PES-rich and the epoxy-rich phases are continuous in nature. (d) Phase-inverted microstructure - second phase of epoxy-rich particles in a continuous PES-rich phase [17].**

The toughening investigation for other thermoplastic resin such as polysulfone (PSF), PEEK and polyaryletherketone cardo (PEK-C) have been extensively reported [18–21]. However, the reported toughness improvement for CFRP do not generally extend to interlaminar fracture toughness [22]. Since the interlaminar resin rich region is constrained by the fibre plies, this in turn constrains the crack propagation zone in comparison to bulk polymer blends [23]. In addition, high loading of thermoplastic is required to achieve the co-continuous or phase inversion morphology, resulting the significantly increased viscosity and manufacturing challenges with strong influences of the thermodynamic and kinetic conditions on final toughness [24,25].

### *2.2.1.2 Nano fillers*

Carbon-based nanoparticles such as graphene nanoplatelets (GNPs), carbon nanotubes (CNTs) and graphene oxides (GOs) have all been studied in this context. Potential toughening mechanisms include nanotube pull-out, debonding, microcracks, crack pinning and crack deflection[26]. Zaman et al. [27] investigated GNP modified epoxy resin, increasing  $K_c$  and  $G_c$  by 57% and 106% respectively, at 2.5 wt% loading. Mannov et al. [28] used thermally reduced graphene oxide (TrGO) to improve CAI strength of CFRPs and GFRPs by 19% and 55% respectively at 0.3 wt% loading. Kostopoulos et al. [29] added 0.5 wt% multi-wall carbon nanotubes (MWCNTs) to epoxy matrix, improving CAI strength and modulus by 12-15% without significant change in delamination area and absorbed energy. Other nanoparticles such as nanoclays, nanosilica and nanorubbers are also extensively studied [30–33]. Carolan et al. [34] found that CSR and silica nanoparticles significantly improved the fracture

energy of epoxy. Siddiqui et al.[35] showed that nanoclay shows useful toughening efficiency with 7 wt% increasing CFRP  $G_{Ic}$  by approximately 100% . The flexural strength decreased with the nanoclay content, but 26% increase in flexural modulus was achieved at 3 wt% addition. One of main problems with nano-particles is their agglomeration as shown in Figure 2-10 [36] and potential increase in matrix viscosity.

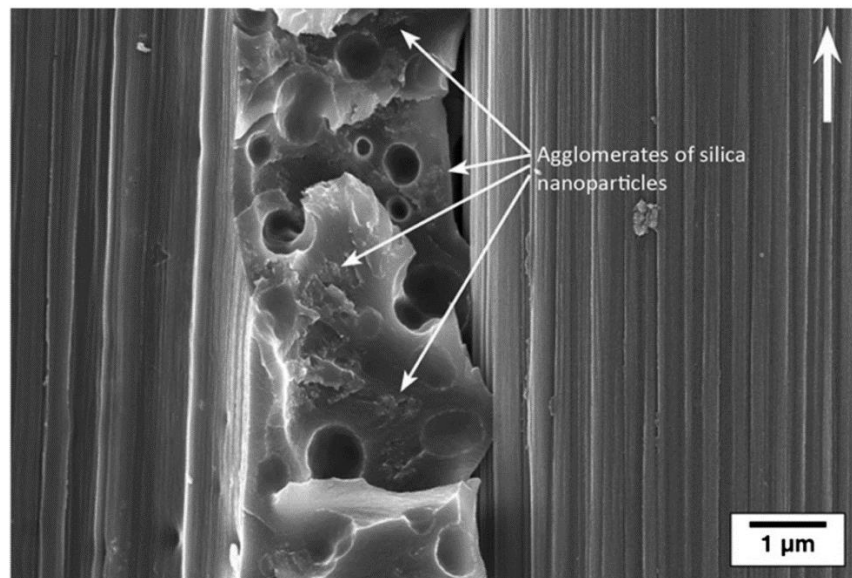


**Figure 2-10. SEM image of fracture surface of  $G_{Ic}$  test for CFRP filled with silica nanoparticles. The white arrow indicates the direction of crack propagation [36].**

**Table 2-1. Summary of recent Matrix Toughening Technology for CFRP laminates**

<b>Matrix Toughening Technology</b>										
Fibre and Resin	Carbon Fibre Volume Fraction (V <sub>CF</sub> %)	Toughening Particles	Particle Loading	Fracture Toughness (J/m <sup>2</sup> )				CAI (MPa)		Notes
				G <sub>IC</sub>		G <sub>IIC</sub>		Initial	Modified	
				Initial	Modified	Initial	Modified			
1. UD carbon fibre fabric epoxy[18]	-	PEK-C	0.33 mg/cm <sup>2</sup>	102	168					Flexural strength was not compromised
2. UD carbon fibre epoxy[28]	58.7	TrGO	0.3 and 0.5 wt%					147	175	-
3. UD carbon fibre epoxy[29]	58	MWCNT	0.5 wt%					160	180	Less improvement under low-velocity impact
4. Biaxial textile fabric carbon fibre epoxy[34]	-	Silica nanoparticles and CSR	0 to 16 wt%	1246	1851					Toughening efficiency of silica nanoparticles is not that outstanding
5. Plain woven carbon fibre epoxy[35]	-	Nano organoclay	0, 3, 5 and 7 wt%	210	430					Flexural strength decreased with nanoclay content, but 26% increase at 3 wt%
6. Cross ply carbon fibre epoxy[37]	-	MWCNT doped nylon micro-particle	7 wt%	400	600	2100	2600			Thermal activated self-healing functionality
7. Twill carbon fibre fabric epoxy[38]	52	CNBR-NP and NBR-NP	20 phr	372	1305	1090	2000			24% decrease in ILSS
8. UD carbon fibre epoxy[39]	-	Layered silicates	9 wt%	240	325	730	1050			Larger particles are favorable for mode I; smaller particles show better performance in mode II.
9. UD carbon fibre fabric epoxy[40]	-	Silica nanoparticle	10 and 20 wt%	238	666	969	750			Decrease in ILSS

## ***2.2.2 Interleaving toughening technology***

Addition of selective materials in the interlaminar region can potentially improve the interlaminar fracture toughness, delamination resistance and impact tolerance. Such an approach is termed interleaf toughening technology (ITT) [41]. The interleaves may take the form of particles, films, or veils which reduce the delamination progression through various mechanisms including crack bridging, crack deflection, microcrack and plastic deformation [42]. Comparing to the matrix modification toughening method, this approach has little impact on the manufacturing process and does not change the inherent properties of fibres and matrix.

### ***2.2.2.1 Microparticles and nanoparticles***

The micron-scale thermoplastic particles such as PES and PA have been used successfully to improve interlaminar toughness. The toughening mechanisms resemble those of thermoplastic modified thermoset resins. Woo and Mao. [43] used PEI particles with different areal weight as interleaf materials to evaluate the Mode I and Mode II interlaminar fracture toughness of CFRP laminates. The PEI particles were initially melted and dissolved into the epoxy matrix and then phase separation occurred at the interlaminar region during curing. The Mode I fracture toughness ( $G_{Ic}$ ) and Mode II fracture toughness ( $G_{IIc}$ ) were increased from 165 J/m<sup>2</sup> to 540 J/m<sup>2</sup> and 290 J/m<sup>2</sup> to 1300 J/m<sup>2</sup> respectively under 39g/m<sup>2</sup> particle loading. Groleau et al. [23] used PA particles to improve  $G_{IIc}$  of interleaved CFRP laminates by 83%. Liu et al. [44] used PES and PA microparticle interleaves to increase  $G_{Ic}$  in CFRP by around 130%. Huang et al. [45] reported 65% and 40% improvement in  $G_{Ic}$  using 10 wt% PPO particle loading.

Figure 2-11 shows the SEM images of Mode I fracture surface, where crack pinning, crack deflection, and strong interfacial bonding between resin matrix and PPO particles can be observed.

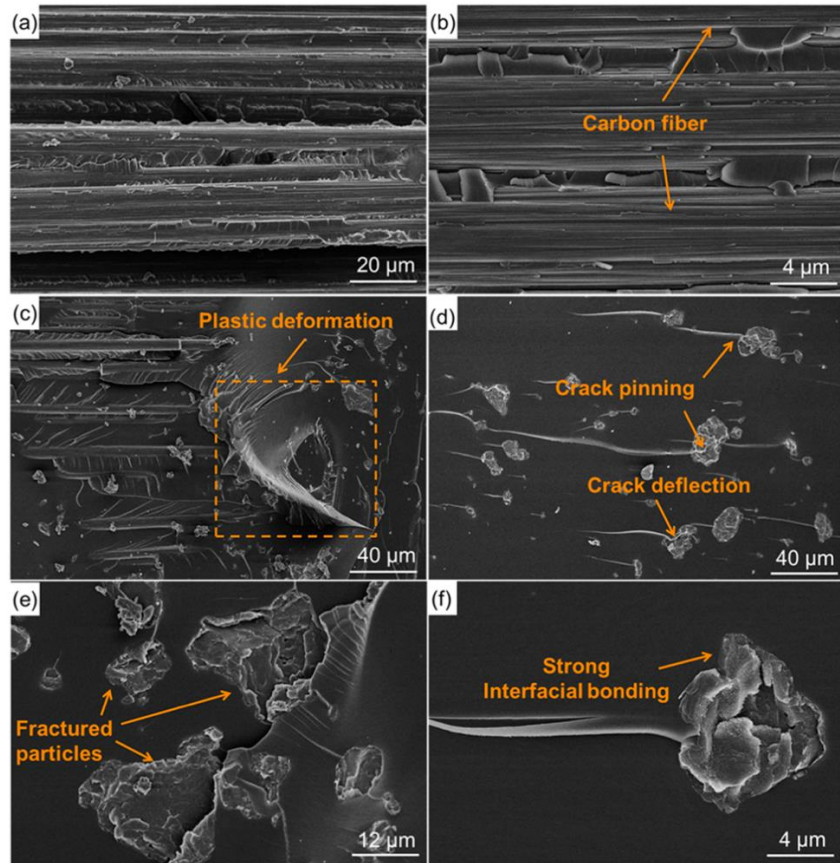


**Figure 2-11. SEM photographs of fracture surfaces of DCB specimen at different magnifications: the blank laminate (a, b), and PPO (10–50 μm)-interleaved laminates with 10 wt % particle loading (c–f) [45].**

Nanoparticle-based interleaves have also been reported [46–49]. Ning et al. [50] used GO interleaves to increase CFRP Mode I interlaminar fracture toughness by 170% for at 2g/m<sup>2</sup> loading. Chaudhry et al. [51] used MWCNTs to improve  $G_{Ic}$  in woven laminates by 32% at 1g/m<sup>2</sup> loading. Li et al.[52] used vapor grown carbon fibre (VGCF) powder

interleaves to improve  $G_{Ic}$  value by 95% at 20g/m<sup>2</sup> VGCF loading. It should be emphasised that all of these lab scale experiments remain to be optimized for industrial scale-up.

### *2.2.2.2 Films and veils*

#### 2.2.2.2.1.1 Microscale

Textiles, non-wovens or film interleaves offer the advantages of convenience in handling and even distribution of polymer. Aksoy and Carlsson [53] investigated the Mode II fracture toughness of graphite/epoxy laminates with thermoset and thermoplastic films. The main toughening mechanism was attributed to the shear-yielding of the material around the crack tips and enlargement of the crack tip zone. Thermoplastic films were superior based on their high yield strength and strain to failure. Cheng et al.[54] fabricated porous PES films as interleaves. As shown in Figure 2-12, a co-continuous or phase inversion morphology developed during curing. A 97.5  $\mu\text{m}$  PES film improved  $G_{Ic}$  and  $G_{IIc}$  by 61.5% and 55.1% respectively. However, it was also noted that such films may also inhibit resin flow and interply adhesion strength [42].

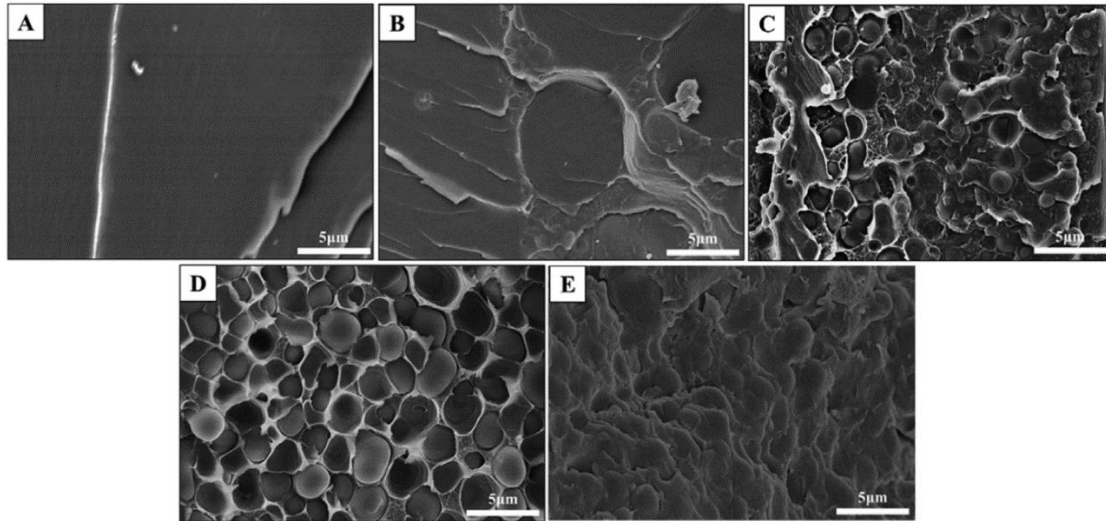


**Figure 2-12. Cross-sectional SEM images of interlayers with different PES film thickness: (A) 0  $\mu\text{m}$ ; (B) 18.4  $\mu\text{m}$ ; (C) 40.5  $\mu\text{m}$ ; (D) 54.1  $\mu\text{m}$ ; and (E) 97.5  $\mu\text{m}$  [54].**

Microfibre nonwoven veils can be dry laid, wet laid or spun laid [55]. Comparing to films, such veils generally have higher porosity and absorbency, lighter weight and lower cost. Tsotsis [42] used various types of polymer veils including polyamide, polyester, and blended all of were melt-bonded onto carbon fibre fabrics before laminating. The veils yielded significant toughening to CFRP laminates with very little cost addition. Kuwata and Hogg [56,57] used carbon fibre veils, polyester veils, polyamide veils and carbon/polyester hybrid veils non-woven veils to study Mode I and Mode II interlaminar fracture toughness for CFRP. Figure 2-13 shows the Mode I fracture surface of test specimens. The polyester veils provide the highest improvement of 50% in  $G_{Ic}$  for unidirectional laminates which was mainly attributed to the fibre bridging. However, the Mode I crack propagation for the carbon and polyamide interleaved laminates are unstable so that significant low  $G_{Ic}$  values were obtained. The carbon and polyamide interleaves were only marginally effective. Ramirez et al. [58] investigated the Mode I



and Mode II effects using PEEK and PPS nonwoven veils, linking Mode I interlaminar fracture toughness to the coverage of the veil. Quan et al. [59] investigated toughening using PET, PPS and PA-12 veils on CFRP. The PET and PPS veils provided more effective toughening for UD laminates while the PA veils worked better with NCF and 5HS laminates.

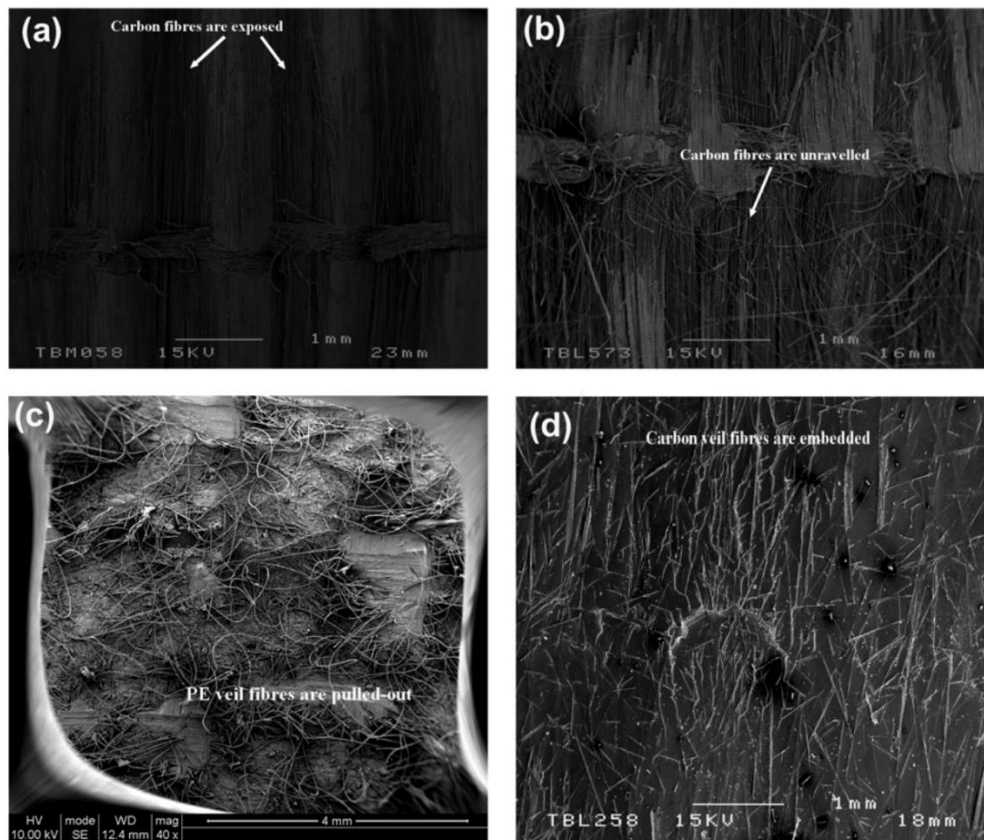


**Figure 2-13. SEM images of Mode I fracture surfaces: (a) unidirectional with epoxy system, (b) unidirectional with vinyl ester system, (c) PE veil interleaved with epoxy system, and (d) carbon veil interleaved with epoxy system[57].**

Referring to above methods, the interleaves are infiltrated with the resin matrix to form the toughening layers in interlaminar regions, which can be described as in-situ

toughening. For current aerostructures, a CAI value between 250 MPa and 300MPa, is a reasonable upper limit. Yi et al. [60] have proposed the concept of ex-situ toughening, which interleaves selective thermoplastics such as PEK-C in structural CFRP laminates. Different from the traditional in-situ toughening, the co-continuous or phase inversion morphology is not only formed at interlaminar regions, but also slightly penetrates the thermosetting carbon plies, as shown in Figure 2-14. The ex-situ concept has been successfully demonstrated for high toughness structural CFRP laminates with epoxy, BMI, benzoxazine (BOZ) and PI matrix, via autoclave RTM. The ex-situ CFRP laminates significantly improve the out-of-plane properties such as interlaminar fracture toughness, impact resistance and tolerance without sacrificing the in-plane properties [61–64]. The CAI value was improved to 345 MPa for ex-situ laminates with PEK-C interleaves, comparing to the reference laminates at 267 MPa.

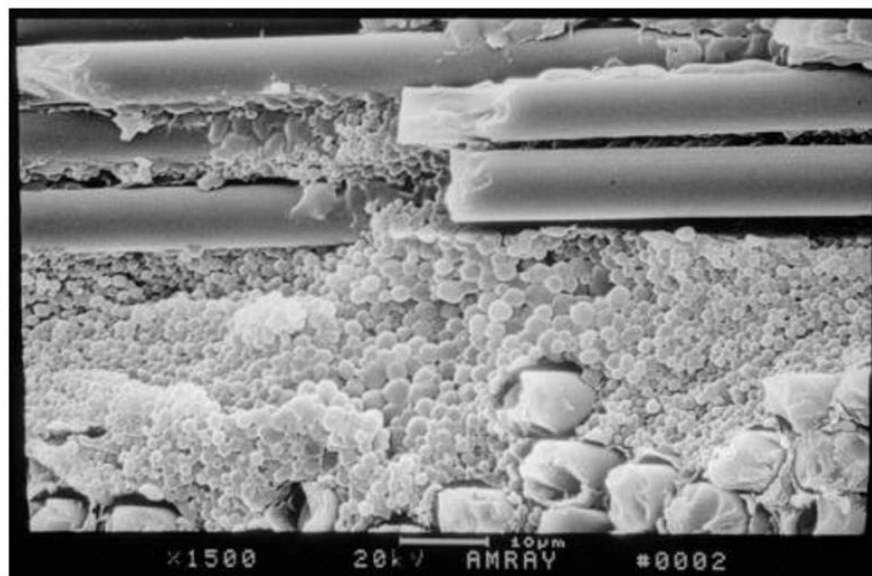


**Figure 2-14. Interlaminar morphology of Ex-situ specimens (the thermoplastic phase was chemically etched) [64].**

#### 2.2.2.2.1.2 Nanoscale

With the development of advanced nanotechnology, the CNTs and polymer nanofibre veils are available and suitable for interleaving due to their unique properties. The nanofibers are generally less than 1  $\mu\text{m}$  in diameter with an aspect ratio  $>100$  [65]. The nanofibres can be produced by template synthesis, melt blowing, drawing or electrospinning. Electrospinning is common due to its simplicity and low-cost. Beckermann and Pickering [66] used nanofiber veil interleaves from PA66, polycaprolactone (PCL), polyvinyl butyral (PVB), PES and polyamideimides (PAI). The optimal  $4.5\text{g}/\text{m}^2$  PA66 veil increased  $G_{Ic}$  and  $G_{IIc}$  by 150% and 70%, respectively. Zhang et al. [67] directly deposited the electrospun PCL, poly (vinylidene fluoride) (PVDF) and PAN nanofibres onto the carbon fibre fabric before the resin impregnation and curing. Only the PCL interleaved laminates show a toughness improvement. Magniez et al. [68] used PVDF to toughen carbon fibre epoxy laminates, with 60% improvement in Mode II toughness and 20% reduction in Mode I toughness. However, Saghafi et al. [69] reported 36% improvement of Mode I toughness by achieved by interleaving with PVDF nanofibres. Vallack and Sampson [70] compared the  $G_{Ic}$  and  $G_{IIc}$  data of composites interleaved with microfibre and electrospun nanofibre veils. Figure 2-15 shows the percentage change in  $G_{Ic}$  and  $G_{IIc}$  against the areal density and mean coverage of the veil, where all nanofibre interleaved composites are identified by triangular markers. Obviously, the electrospun nanofibre veils have much higher coverage but only provide modest improvement in fracture toughness, in comparison with microfibre veils. They suggested that these high coverage nanofibre veils act more like continuous films. The

small pore size and high coverage of electrospun veils inhibit the resin infusion into the veils, resulting in rapid crack propagation with less deflection.

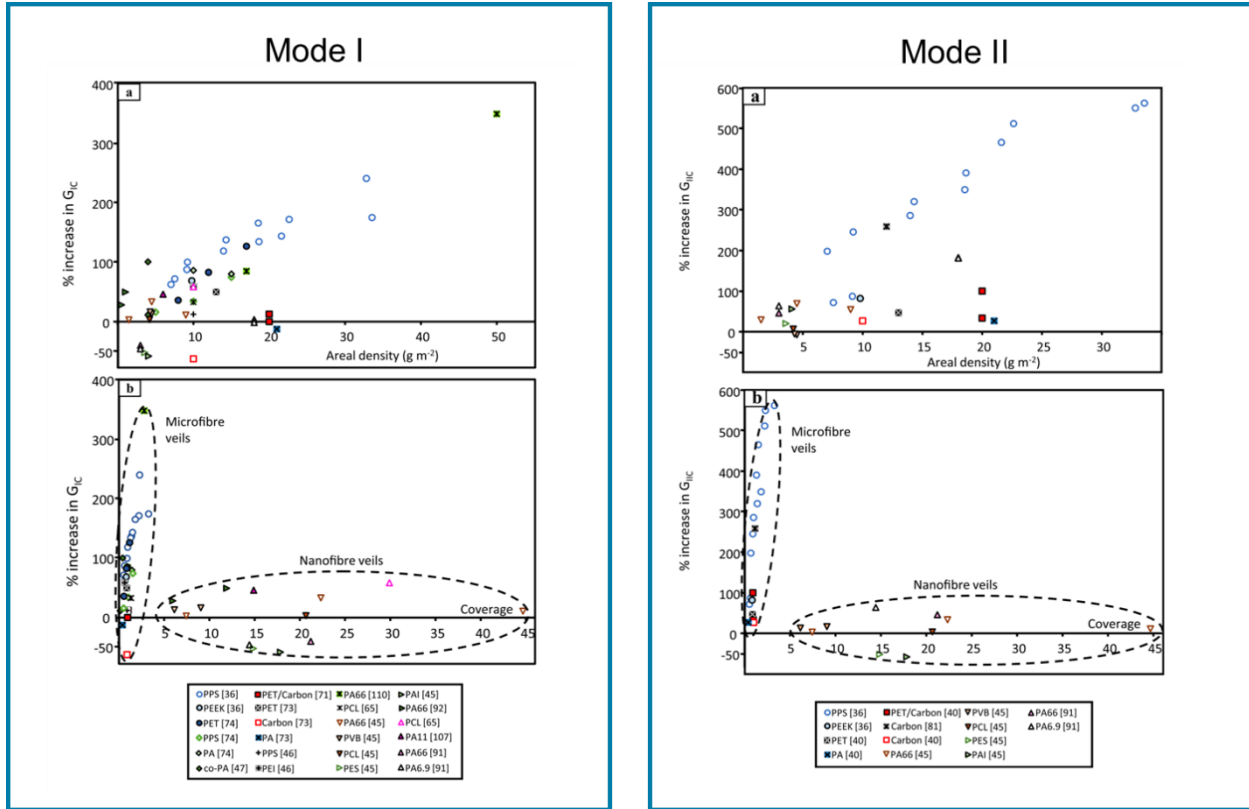


**Figure 2-15. Percentage increase in Mode I and Mode II fracture toughness. (a) areal density and (b) coverage of the interleave [70].**

Carbon nanotubes are the tube-like lattices, which include single-wall carbon nanotubes (SWCNTs) and multi-wall carbon nanotubes (MWCNTs). The latter have been incorporated into veil style interleaves to enhance the toughness of CFRPs. Lee et al. [71] used carbon fibre nonwoven coated with MWCNTs to improve Mode I and Mode II toughness by 30% and 250% (Figure 2-16). Quan et al. [72] found that CFRP interleaved with MWCNT doped PET veil reduced  $G_{Ic}$  and  $G_{IIc}$  as the MWCNTs restrain the fibre bridging of PEI veils. Rodríguez-González and Rubio-González [73] directly

sprayed different concentration of MWCNTs onto the prepreg surfaces with 16% and 17% improvement of  $G_{Ic}$  and  $G_{IIc}$  under 0.05 wt% and evidence of improved interfacial bonding. Ou et al. [74] applied floating catalyst chemical vapor deposition (FCCVD) to manufacture the CNT veils from the gas phase (Figure 2-17) yielding a slight increase (12%) of Mode II toughness but significant decrease (71%) of Mode I toughness attributed to the dense veil acting like a defect. Interleaving extra resin films can improve the infiltration of the veils and the interlaminar properties, where the  $G_{IIc}$  value of specimens with fully wetted CNT veils was increased by 88%. Hamer et al. [75] used electrospun PA66 nanofibre veil with MWCNTs as interleaves to produce carbon/epoxy laminates. Song et al. [76] also prepared hybrid CNT/PA66 nanofibre veils to toughen CFRP, where the CNTs were coated on the PA66 nanofibre surfaces. Both studies indicate the significant improvement in fracture toughness of CFRP laminates by interleaving the hybrid veils.

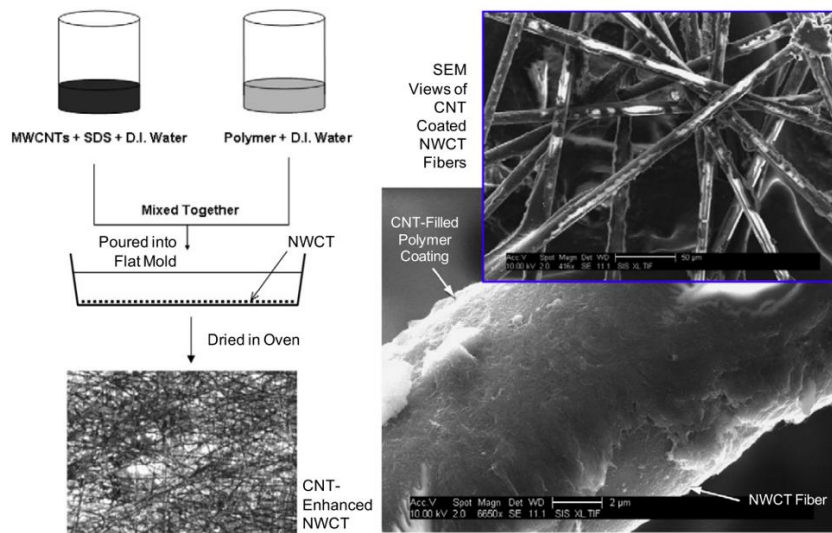
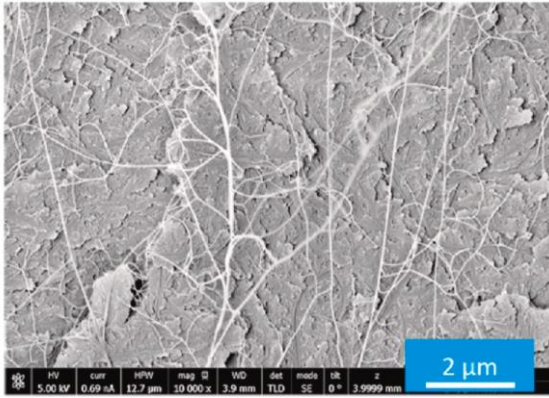
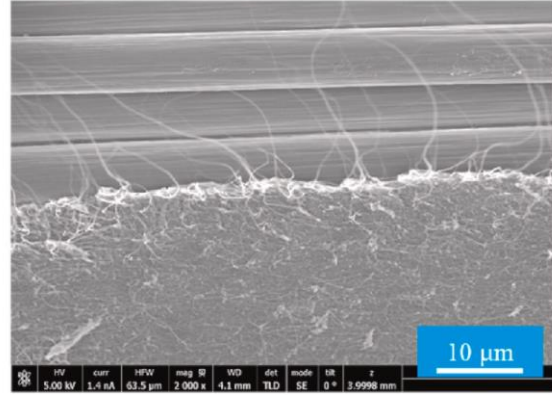


Figure 2-16. CNT-enhanced nonwoven carbon tissue (NWCT) fabrication [71].



(a)



(b)

**Figure 2-17. SEM micrographs of the fracture surfaces with CNT interleaves. (a) Mode I, (b) Mode II [74].**

**Table 2-2. Summary of recent Interleaving Toughening Technology for CFRP laminates**

<b>Interleaving Toughening Technology</b>										
Fibre and Resin	Carbon Fibre Volume Fraction ( $V_{CF}$ %)	Interleaf Materials	Content	Fracture Toughness ( $J/m^2$ )				CAI (MPa)		Notes
				$G_{IC}$		$G_{IIC}$		Initial	Modified	
				Initial	Modified	Initial	Modified			
1. UD carbon fibre fabric epoxy[43]	62	PEI particle	8.2-39.1 $g/m^2$	190	530	290	1300			Fracture toughness increased with PEI content
2. Carbon fibre fabric epoxy[23]	54	Nylon-12 particle	40 vol% interplay concentration			1400	2500			-
3. UD carbon fibre epoxy[44]	-	PES and PA particles	PES 20 wt% PA 15 wt%	700	2200			120	275	Less improvement under low-velocity impact
4. Plain-weave carbon fibre fabric epoxy[34]	-	PPO particle	5, 10 and 15 wt%	131	216	768	1073			The smallest PPO particles (10–50 $\mu m$ ) with 10 wt % particle loading yields maximum enhancements
5. UD carbon fibre epoxy [50]	-	GO	0-3 $g/m^2$	413	859					Numerical simulations to predict the interfacial tensile strengths
7. UD carbon fibre epoxy [46]	-	Aligned CNT	1 vol%	370	530	350	1100			-
8. 2/2 twill carbon fibre fabric epoxy [51]	-	MWCNT	0-4 $g/m^2$	700	950					The most optimum amount of CNT loading (1.0 $g/m^2$ )
9. UD carbon fibre epoxy[52]	-	VGCF powder	0-30 $g/m^2$	489	616					Increase in flexural properties
10. Plain woven carbon fibre fabric epoxy[54]	48%	PES film	20-100 $\mu m$	375	600	1700	2700			Uniform distribution and outstanding solubility of PES inhibit the big decline in mechanical properties of composites.

11. Plain woven carbon fibre fabric epoxy[77]	43%	PES fibre web	7.3-28.3 g/m <sup>2</sup>	380	740	1600	2650	160	230	Decrease in impact and mechanical properties for 28.3 g/m <sup>2</sup> PES web
12. UD carbon fibre fabric epoxy[42]	-	PA, PE, and blended veils	4.24 g/m <sup>2</sup>					133	PA-211 PE-119 BD-141	-
13. UD carbon fibre fabric epoxy[56,57]	-	Carbon, PE, PA, and hybrid veils	10-20 g/m <sup>2</sup>	850		1400				-
14. UD carbon fibre fabric epoxy[58]	-	PEEK and PPS veils	11 g/m <sup>2</sup> , 7 g/m <sup>2</sup>	310	PEEK-500 PPS-520	1000			PEEK-4100 PPS-3000	Interlaminar toughness increased with veil coverage to a plateau
15. UD carbon fibre fabric BMI[62]	60	PEK-C film	17.5 wt%					180	254	Ex-situ concept
16. 2/2 twill carbon fibre fabric epoxy[68]	-	PVDF nanofibre	5 wt%	1020	800	1750	2600			Significant decrease in interlaminar toughness for PVDF nanofilm
17. Plain weave carbon fibre fabric epoxy[78]	-	Aramid nanofibre	0-0.6g/m <sup>2</sup>	350	640					Denser ANF interlayers resulted in further decrease in Mode I toughness
18. UD carbon fibre epoxy[79]	-	Nylon 66 nanofibre	30-80 μm	620	680					Significant decrease in Mode I toughness for thick interleaf



## 2.3 Electrical properties of aeronautical CFRP laminates

### 2.3.1 Anisotropic electrical conductivity

Carbon fibres consist of extremely stable hexagonal plane grids and the delocalized electron cloud between the planes[80]. The free electrons in the electron cloud provide the good electrical conductivity of carbon fibres, with values ranging from  $5.9 \times 10^4$  S/m to  $1.42 \times 10^5$  S/m [81]. It is reported that higher carbonization temperature during manufacturing contributes to higher carbon content and larger crystallites orientated in fibre direction, resulting in the increase of electrical conductivity [82–86]. However, the traditional resin matrix is electrically insulating due to the lack of free electrons. For example, the electrical conductivity of epoxy is around  $7.34 \times 10^{-11}$  S/m to  $1.25 \times 10^{-13}$  S/m [87]. Obviously, the only path for the direct current flowing through the CFRPs via the carbon fibres.

In practice, CFRPs are stacked in different lay-up sequences to meet structural requirements. Thus, the electrical conductivity is highly anisotropic, where the in-plane electrical conductivity is likely to be significantly higher than that in through-thickness direction due to the in-plane alignment of carbon fibres. The through-thickness conductive path is governed by the random fibre-fibre contacts between plies. Thus, the electrical conductivity of CFRP laminates depends on fibre type, fibre orientation, degree of curing and fibre volume fraction. In general, for prepreg based CFRP, the longitudinal electrical conductivity is of the order  $10^3$  S/m to  $10^4$  S/m, while the through-thickness value is typically  $10^{-4}$  S/m to 1 S/m [88–90].

### ***2.3.2 Relationship between electrical conductivity and functionalities***

For CFRP laminates, the electrical properties can be used for secondary functions, particularly the heating and self-sensing. Several investigations will be described and discussed as follow.

#### ***2.3.2.1 Heating of carbon fibre***

Yarlagadda et al. [91] indicated three possible heating mechanisms for CFRP laminates: a) fibre Joule heating, junction heating with b) dielectric hysteresis and c) fibre contact resistance. Athanasopoulos and Kostopoulos [92] describe Joule heating of the dry carbon fibre preform based on stacking sequence. Their simulations agreed well with thermal camera results under given electric potential fields. Hayes et al. [93] studied the curing of a 65×25 cm CFRP laminate by directly connecting the carbon fibres to the electric current, in which the in-plane resistance of the plain weave carbon fibre prepreg is utilized and the copper foils were used as electrodes. The best heat distribution was obtained when the copper electrodes contacted all inner plies. Induction heating can also be used to cure thermoset CFRPs [94]. Although it is mainly applicable to small scale components due to the size of induction coils [95,96].

The Joule heat or induction heating is suitable for welding and bonding applications [97,98]. Frauenhofer et al. [99] investigated the mechanical properties of adherents and adhesives bonded by inductive curing. The results show that the heat penetration depth for CFRP is significantly high compared to the metals, providing the high potential for assembly and repair operations. However, thermal of the matrix caused by the inductive

heat may reduce mechanical strength of the bonds. Park et al. [100] studied self-healing of CFRP laminates with thermally mendable polymer, bis-maleimide tetrafuran (2MEP4F), as the matrix. The carbon fibres were electrically heated to activate Diels-Alder reaction of the matrix so that the pre-cracked specimens were repaired.

### *2.3.2.2 Self-sensing*

For CFRP laminates, the basic principle of self-sensing depends on the electrical resistance changes of carbon fibres under various loadings or damages.

Todoroki et al. [101] measured the electric resistance change of CFRP laminates for delamination detection. Delamination cracks were detected by measuring the resistance change in fibre direction. The through-thickness conductivity exhibited significant effects on delamination detection. Angelidis et al. [102] investigated the effect of mechanical strain on electrical resistance response of unidirectional and multidirectional CFRP laminates. The changes in local current and resistance were detected under mechanical strain points. Sevkati et al. [103] measured the electrical resistance of CFRP laminates under tensile loading. With the strain increasing, the electrical resistance of CFRP laminates increases with a decreasing rate at beginning, then decreases, and finally shows the exponential increase to the breakage points. Hart and Zhupanska [104] developed predictive finite element models to characterize the anisotropic electrical resistivities and electrical response of CFRP laminates, which leads to a non-destructive damage sensing technique. Schueler et al. [105] and Han et al. [106] also studied the electrical conductivity and surface potential distributions of CFRP laminates to detect delamination location, combining with finite element analysis. Besides the direct

measurement of electrical resistance, Grammatikos et al. [107] developed a non-destructive technique based on current stimulated thermography. As shown in Figure 2-18, Joule heating enabled the thermal camera to characterize impact damages with different energy levels.

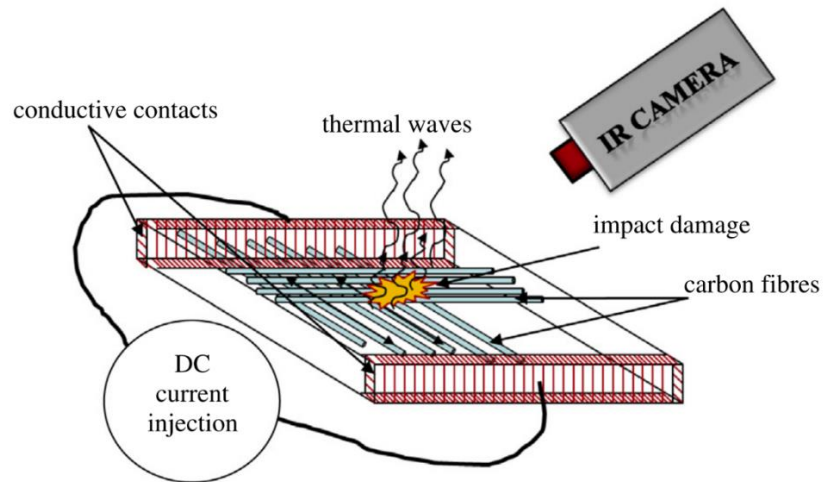


**Figure 2-18. Schematic of current injection experimental setup [107].**

The reliability and sensitivity of self-sensing for CFRP laminates can be improved by using an electrically conductive resin matrix. Conductive nanoparticles can penetrate the inner insulated regions as in-situ sensors, providing high sensitivity to reflect the micro cracks. Vavouliotis et al. [108] dispersed MWCNTs into an epoxy matrix to prepared the electrically conductive CFRP laminates which increase the electrical conductivity by several orders of magnitude but not significantly change the electrical response under load. Grammatikos and Paipetis [109] monitored the electrical resistance of CNTs filled CFRP laminates to characterize their strain rate and structural integrity. Their results show that the addition of CNTs significantly increase the sensitivity of the electrical resistance measurement, where notable changes can be detected under very small deformation.

### ***2.3.3 Integration of CFRP laminates in aircraft***

Comparing to the conventional metallic aircraft structures, the high anisotropic electrical resistance, particularly the low through-thickness electrical conductivity of CFRP laminates presents significant differences in electrical and environmental performance such as lightning strike protection, electromagnetic shielding, and functional current path.

Previously, the metallic fuselage provided the functions of signal/fault current return and voltage reference for all electrical equipment [110]. It is also a high conductive shielding cage to reflect electromagnetic waves. Under lightning strike, the high electrical and thermal conductivity of metallic structures can quickly dissipate the large lightning current and heat so that subsequently eliminate the damage. However, the relatively

low electrical conductivity of CFRP structures introduces risks of Joule heating, thermal damage and inadequate electromagnetic interference shielding[111]. Lightning strike protection is a particular concern for aircraft safety with CFRP. Unprotected structures are vulnerable to local vaporization, burning, and explosion under direct strike[112,113].

Current industrial practice is to augment CFRP aerostructures with discrete metallic conductors to deliver an overall electrically conductive network. For example, an Electrical Structure Network (ESN) is constructed in the pressurized fuselage of Airbus A350 XWB aircraft to provide for the correct functioning of aircraft systems. Besides, a Metallic Bonding Network (MBN) is used on the wings, tail cone, empennage, and belly fairing of the aircraft to offer the failure return path, equipment bonding, lightning strike protection and electrostatic discharge protection [114]. Figure 2-19 shows the schematics of ENS and MBN and the electrical installation for CFRP fuselage. The Boeing 787 aircraft utilizes a Current Return Network (CRN) to serve the same functions [115]. Obviously, the lightweight advantages of CFRP structures are partially compromised by constructing these heavier metal networks, which also increases the design and maintenance cost.

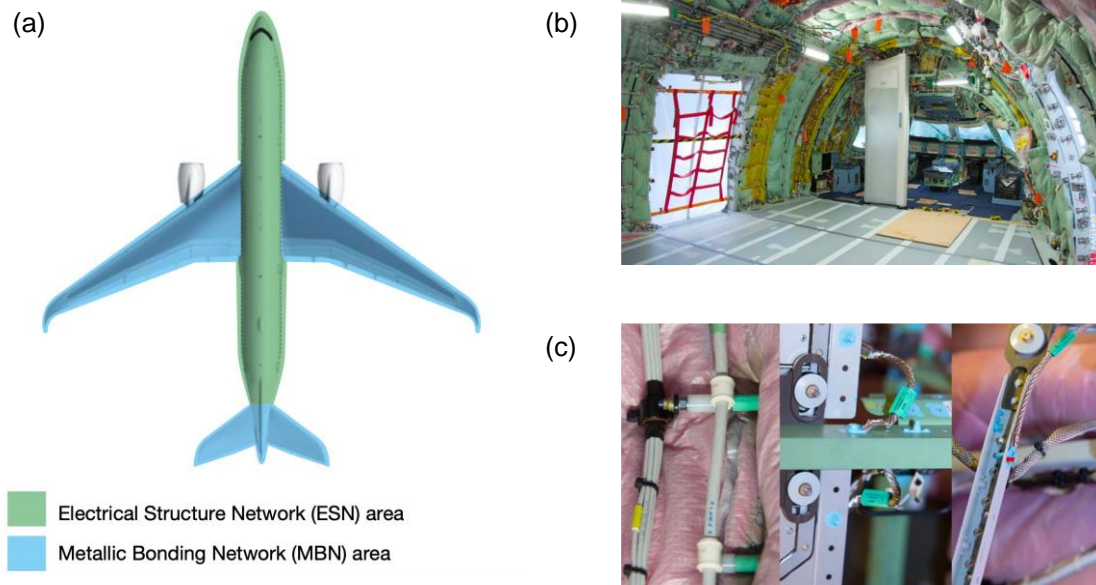


**Figure 2-19. Electrical Structure Network (ESN) in A350XWB. (a) Schematic of system installation, (b) ESN set-up in fuselage and (c) metallic connectors of ENS [114].**

### ***2.3.4 Methods for improving electrical conductivity of CFRP laminates***

Many different methods have been investigated to increase the electrical conductivity of CFRP laminates, in which the improvement of through-thickness conductivity is particularly critical. Overall, the methods could be divided into three categories; resin matrix modification, carbon fibre surface modification and interleaving.

#### ***2.3.4.1 Resin Modification***

In general, the resin modification methods are referring to the dispersion or mixing the conductive fillers into the resin matrix. The mechanism follows percolation theory, where dramatic increase of conductivity can be achieved when the filler content passes the percolation threshold to form a continuous path [116]. Nano-scale fillers such as CNTs, GOs, GNPs, silver nanowires (AgNWs), and silver nanoparticles (AgNPs) all have

potential to simultaneously improve the electrical and mechanical properties of CFRP laminates. Sawi et al. [117] mixed double-wall carbon nanotubes (DWCNTs) into the epoxy to produce the CFRP laminates. The percolation threshold was round 0.04 wt% of CNT at which the through-thickness conductivity is increased from 0.0066 S/m to 0.53 S/m. Li et al. [118] introduced 5 wt% GNP into the epoxy matrix causing the through-thickness conductivity of CFRP to increase from 0.02 S/m to 0.6 S/m, with only a slight increase for in-plane conductivity. The flexural modulus and interlaminar shear strength were increased by 15% and 18%, respectively. Kandare et al. [119] synergistically dispersed GNPs, AgNPs and AgNWs into epoxy . The arising CFRP results showed maximum improvement in through-thickness electrical conductivity (0.3 S/m) and minimal decrease of mechanical properties at 0.95 vol% of GNP and 0.05 vol% of AgNWs. However, significant decrease in compressive and tensile strength was observed by adding 0.05 vol% of AgNWs individually. Senis et al. [120] mixed commercial GO into epoxy increasing through-thickness electrical conductivity from 5.43 S/m to 18 S/m (Figure 2-20).



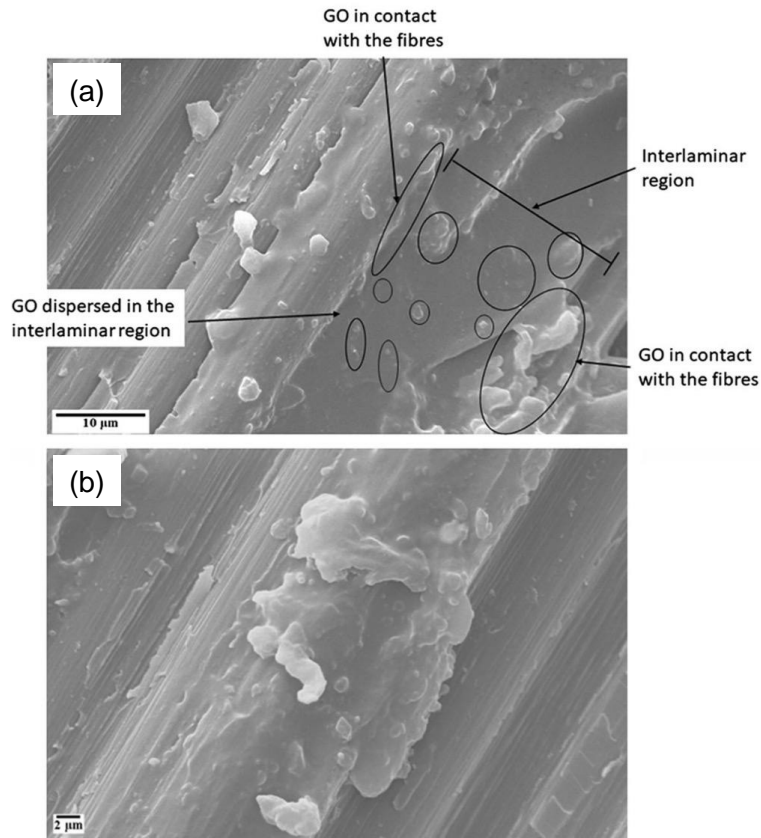


**Figure 2-20. SEM images for the specimens with 6.3 vol% GO. (a) interlaminar region and (b) fibre surface view [120].**

However, the addition of conductive fillers also caused several issues. They have a high tendency to agglomerate in the resin matrix, together with the filtering effects and the increase of resin viscosity leading to uneven dispersion and voids [121,122]. Figure 2-21 shows the typical observation of the carbon nanofibre (CNF) filled composite laminates where more voids are formed by increasing the CNF concentration (VARTM), where more voids are formed by increasing the CNF concentration [123]. Thus, it is also important to investigate the better methods to incorporate the conductive materials into resin matrix.

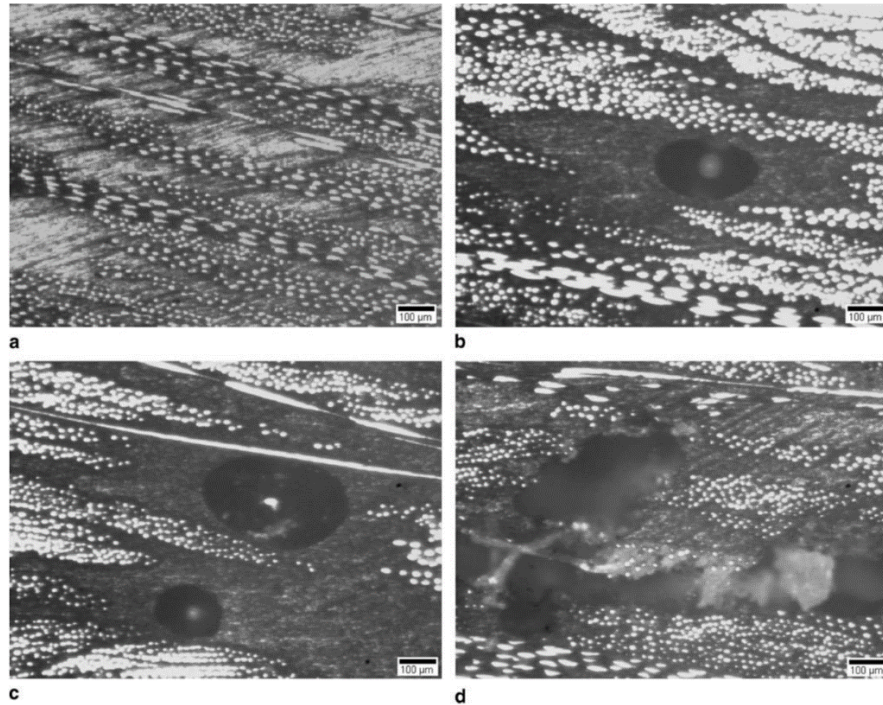


**Figure 2-21. Micro-voids in the (a) 0 wt% CNF, (b) 0.5 wt% CNF, (c) 1 wt% CNF, and (d) 1.5 wt% CNF composite specimens [123].**

#### *2.3.4.2 Carbon fibre surface modification*

Concerning the wetting, viscosity and agglomeration problems in conductive particle filled CFRPs, surface conductive modification methods have been proposed to increase the electrical conductivity and mechanical properties of CFRPs in which the conductive nanoparticles are uniformly deposited onto the fibre surfaces. These surface additives not only increase the interfacial interaction between fibre and resin matrix but also create more effective conductive paths between adjacent fibres.

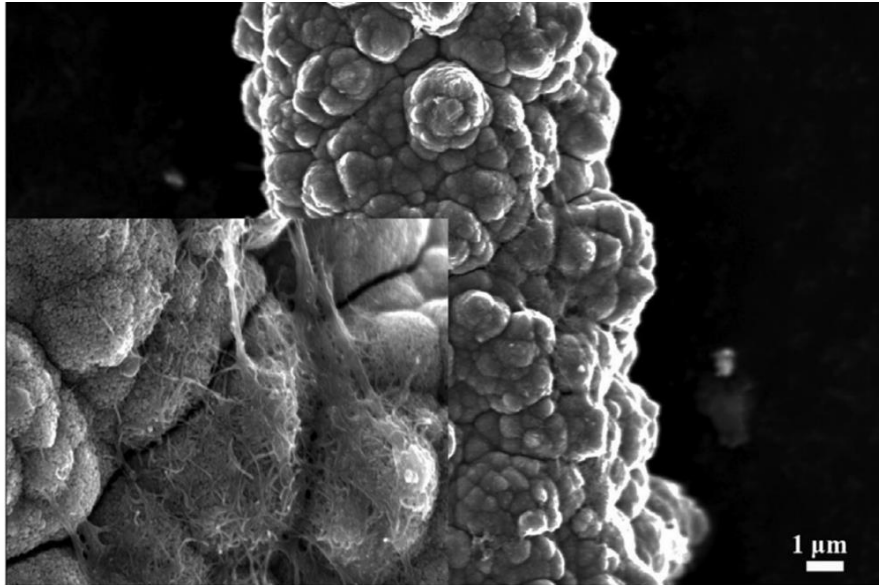


**Figure 2-22. SEM morphologies of Cu-CNT coated carbon fibre [124].**

Yan et al. [124] used electrophoretic techniques to coat CNTs and copper onto the surface of carbon fibres. Figure 2-22 shows the modified carbon fibres, where the copper particles and CNTs are highly compacted to form continuous structures. The in-plane and the through-thickness electrical conductivity were improved from 28.3 S/m to 211.6 S/m and 0.0065 S/m to 0.186 S/m, respectively. The interlaminar shear strength is also increased from 43.5 MPa to 58.5 MPa. Qin et al. [125] reported that the through-thickness electrical conductivity of CFRP laminates can be improved from 2.5 S/m to 7 S/m by coating GNPs onto the surface of carbon fibres along with 82% and 19% improvement in transverse flexural strength and interlaminar shear strength. Pozegic et al. [126] grew CNTs on the surface of carbon fibres causing the through-thickness electrical conductivity to increase from 0.18 S/m to 0.88 S/m. Duongthipthewa et al. [127] grew CNTs on the surface of nickel-coated carbon fibres thus the longitudinal and through-thickness electrical conductivity increased from 3000 S/m to 9000 S/m and 5

S/m to 84 S/m (Figure 2-23). Besides, the interlaminar shear strength, flexural strength, and impact toughness were improved by 45%, 19% and 71%, respectively.

Bhanuprakash et al. [128] coated carbon fibres with reduced exfoliated graphene oxides (rEGOs), TrGOs and original GO using electrophoretic deposition. Significant improvement in  $G_{IC}$ , interlaminar shear strength and through-thickness electrical conductivity were achieved, because of the strong mechanical and chemical bonding between coated GOs and epoxy resin matrix as well as the increase of conductive paths between fibres.

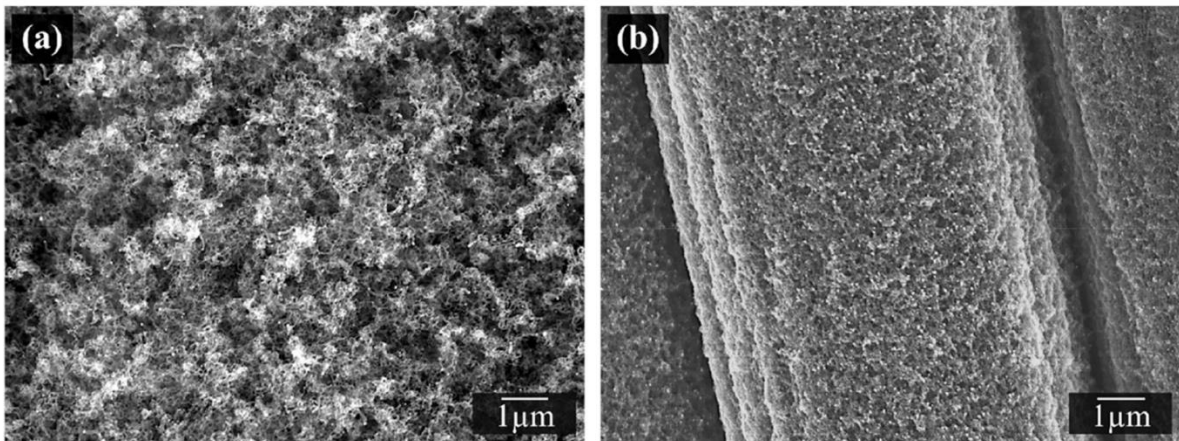


**Figure 2-23. SEM images of (a) CNT growth and (b) GNPs-coated on CNT growth [127].**

In general, coating methods remain limited by the numbers of conductive paths because the surface additives cannot significantly close the distance of resin rich regions between the carbon fibres. Although a good interface between epoxy and CNT layers has been reported, the wettability of coated carbon fibres depends on the types of surface additives and polymer matrix, which may cause adverse effects on other properties (for example in compression).

### *2.3.4.3 Interleaving*

Because the low through-thickness electrical conductivity of CFRP laminates is mainly attributed to the insulating resin rich regions, using high conductive interleaves is a logical way to further increase the electrical conductivity. The formation of a volumetric conductive network through the contacts between interleaves and carbon fibres is the key point for conductivity improvement.

Carbon based veils are one of the important conductive interleaves due to their excellent inherent electrical and mechanical properties. Xu et al. [129] interleaved CNT film between each carbon fibre ply, causing the through-thickness electrical conductivity to improve from 3000 S/m to 8000 S/m and 0.7 S/m to 2 S/m for specimen with 1.09 wt% of CNT films, respectively. Xu et al. [130] later used carbon fibre nonwoven veils as interleaves to increase the through-thickness and in-plane electrical conductivity of interleaved specimens from 1.5 S/m to 2.7 S/m and 500 S/m to 1000 S/m. The Mode I and Mode II interlaminar fracture toughness also both increased by around 100%. Zhao et al. [131] used carbon fibre veils as interleaves to prepare the carbon/ bismaleimide composite laminates. The through-thickness electrical conductivity improved from 0.43 S/m to 27.9 S/m. The carbon fibre interleaves also improved lightning strike protection, where both damage depth and residual strength were enhanced. Kumar et al. [132] manufactured MWCNT buckypapers as interleaves to improve through-thickness electrical conductivity from 10 S/m to 52 S/m. These were also effective against simulated lightning strike. Despite the improvement in electrical properties, significant decreases in mechanical properties were detected.

Latko-Duralek et al. [133] doped 3.5 wt% of MWCNTs into the copolyamide nonwoven veils as the conductive interleaves increasing the CFRP through-thickness electrical conductivity by 2 orders of magnitude. However, the interlaminar shear strength was decreased from 63.5 MPa to 54 MPa due to a discontinuity in the nonwoven layers, local agglomeration of the polymer, and the presence of pores and voids at interlayers. Barjasteh et al. [134] used a graphene/graphite particle coated polyamide 12 conductive nonwoven veils as interleaves to simultaneously increase the interlaminar fracture toughness and electrical conductivity of CFRP laminates. The through-thickness electrical conductivity was significantly increased from  $1 \times 10^{-8}$  S/m to  $2.5 \times 10^{-3}$  S/m. In addition, the Mode I and Mode II fracture toughness also improved up to 42% and 141%, respectively. Li et al. [135] produced plasma-treated conductive interleaves from MWCNTs doped PA12 films. The through-thickness and transverse electrical conductivity were improved by 21-fold and 2-fold, respectively. Considerable improvement of Mode I fracture toughness was also achieved due to the strong interfacial adhesion after plasma treatment.

Guo and Yi [136] used the reactive PEK-C film as the carrier interleaves to provide high fracture toughness for CFRP laminates. AgNWs were loaded at the surface of film to give the electrical conductivity. The AgNWs loaded PEK-C films improved the Mode I and Mode II fracture toughness from 306 J/m<sup>2</sup> to 396 J/m<sup>2</sup> and 718 J/m<sup>2</sup> to 1576 J/m<sup>2</sup>, respectively. However, the through-thickness electrical conductivity decreased from 12.2 S/m to 1.5 S/m due to insulating PEK-C films and the low AgNWs loading. Guo and Yi [137] later boosted the through-thickness electrical conductivity from 12 S/m to

138 S/m using the PA veils with surface-loaded AgNWs, as shown in Figure 2-24. The Mode I and Mode II fracture toughness were also improved by 118% and 227%, respectively. The same authors later [138] investigated AgNWs loaded plant-fibre paper as interleaves on fracture toughness and electrical conductivity of CFRP laminates, as shown in Figure 2-25. With 0.95 g/m<sup>2</sup> loading of AgNWs, the surface resistivity of conductive paper increased to 2.3 Ω/sq. The through-thickness electrical conductivity 4.7 S/m to 17.9 S/m. However, significant reduction of interlaminar fracture toughness was detected because of the weak interfacial bonding strength between paper and epoxy resin.

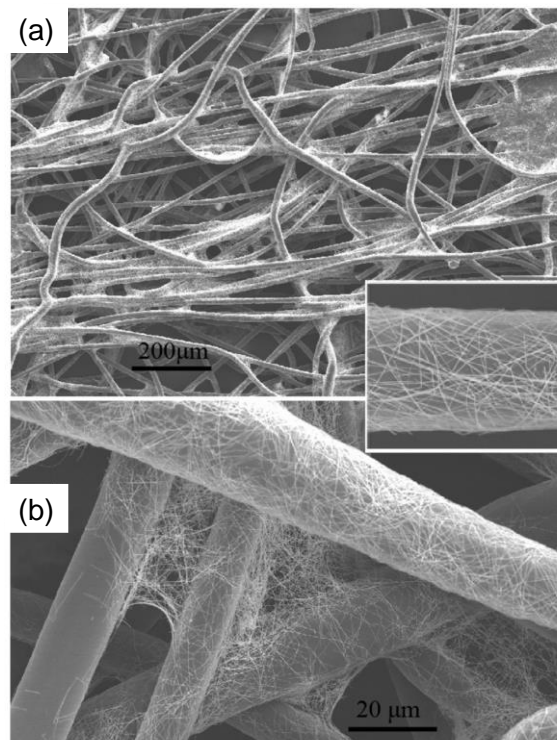


**Figure 2-24. SEM images of nylon veil after surface-loading with AgNWs [137].**

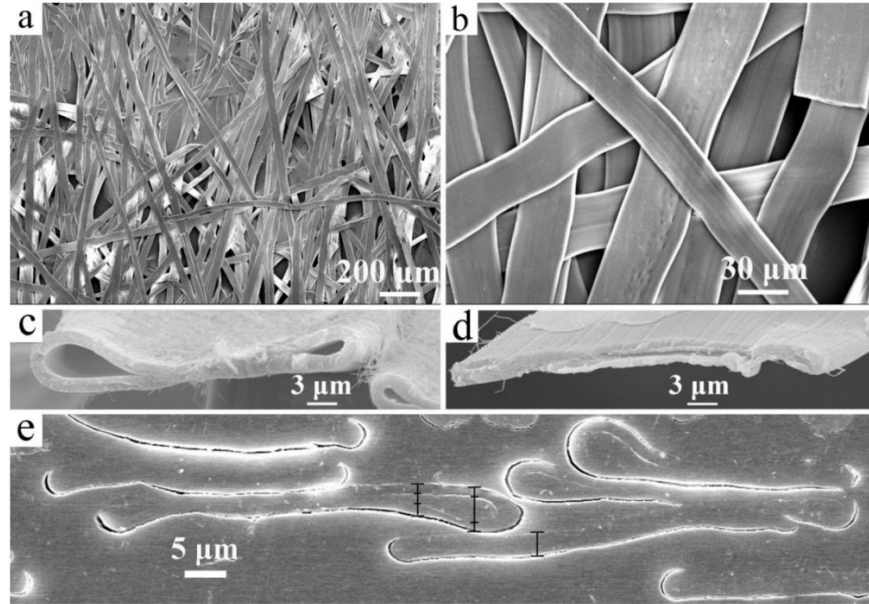


Figure 2-25. SEM images of (a,b) plan view of the paper, (c,d) cross section of the plant fibre, and (e) cross section of paper embedded in epoxy resin [138]



**Table 2-3. Different techniques for improving the electrical conductivity of CFRP laminates**

<b>Resin modification</b>								
Fibre and Resin	Carbon Fibre Volume Fraction ( $V_{CF}$ %)	Conductive Materials	Content	Initial electrical conductivity (S/m)		Improved electrical conductivity (S/m)		Notes
				In-plane	Through-thickness	In-plane	Through-thickness	
1. UD carbon fibre fabric epoxy[117]	66	MWCNT	0.4 wt%	X-2500 Y-0.53	$6.6 \times 10^{-3}$	X-2900 Y-1.2	0.063	Non-linear relationship between temperature and electrical conductivity
2. Carbon fibre fabric epoxy[118]	-	GNP	2 and 5 wt%	~100	~0.02	~120	0.6	Slight increase in flexural properties and ILSS
3. Plain woven carbon fibre epoxy [119]	45	GNP, AgNW and AgNP	Up to 1 vol%		0.077		0.3	Significant decrease in compressive and tensile properties with 0.05 vol% AgNWs
4. UD carbon fibre fabric epoxy[120]	57	GO	0-6.3 vol%	X- $2.2 \times 10^4$ Y-56.1	5.43	Y-69	18	Improvement in ILSS with GO addition
<b>Carbon fibre surface modification</b>								
6. UD carbon fibre fabric epoxy[124]	56	CNT and copper	~15 wt%	28.3	$6.5 \times 10^{-3}$	211.6	0.186	Improvement in ILSS, slightly decrease in tensile strength
7. UD carbon fibre epoxy[125]	65	GNP	3 wt% of solution		2.5		6.9	Increase in flexural properties and ILSS
8. Plain weave Carbon fibre epoxy[126]	40	CNT	4.27 vol%	1000	0.18	2600	0.88	Improvement in thermal conductivity
9. Plain weave Carbon fibre epoxy[127]	58	Nickle, CNT and GNP	Nickle:10-40 nm CNT: $5 \times 10^{10}$ tubes/cm <sup>2</sup> GNP: 0-0.2 wt%	X-3000	8	X-9000	80	Increase in flexural strength and ILSS

10. UD carbon fibre fabric epoxy[128]	-	GOs	0.25 mg/ml in solvent	1900	14	2230	32	Significant improvement in flexural properties and ILSS, less effect on Mode I toughness
<b>Interleaving</b>								
11. UD carbon fibre fabric epoxy[129]	-	CNT film	0.22, 0.65 and 1.09 wt%	3000	0.7	8000	2	Insufficient wetting of resin in thick CNT film
12. Woven carbon fibre fabric epoxy[130]	60	CF non-woven veil	7.8 g/cm <sup>2</sup>	500	1.5	1000	2.7	99% and 100% improvement in Mode I and Mode II toughness
13. UD carbon fibre epoxy[131]	56	Conductive CF veil	8-60 g/m <sup>2</sup>		0.43		27.9	Less effect on flexural strength and ILSS, significant improvement in LSP
14. Plain woven carbon fibre fabric epoxy[132]	55	MWCNT doped buckypaper	0.15 mm	1000	10	7394	52	Decreased the mechanical properties, but effectively improved LSP
15. Carbon fibre epoxy[133]	54	MWCNT doped PA nonwovens	CNT: 3.5 wt% Nonwoven: 30g/m <sup>2</sup>	260	2x10 <sup>-5</sup>	450	2x10 <sup>-3</sup>	Decreased ILSS
16. UD carbon fibre fabric epoxy[134]	54	Graphene/graphite-PA12 nonwovens	6 and 12 g/m <sup>2</sup>		1 10 <sup>-8</sup>		2.5x10 <sup>-3</sup>	Improved Mode I and Mode II toughness
17. UD carbon fibre epoxy[136]	-	AgNWs loaded PEK-C film	AgNW: 0.75 g/m <sup>2</sup>	X-25000 Y-21.4	12.2	X-25000 Y-1492.5	1.5	Improved Mode I and Mode II toughness
18. UD carbon fibre epoxy[137]	45	AgNWs loaded nylon nonwoven	AgNW: 1.5 g/m <sup>2</sup>	X-25000 Y-21.4	12.2	X-25000 Y-2564	138.5	Significantly improved in Mode I and Mode II toughness
19. UD carbon fibre fabric epoxy[138]	55	AgNWs loaded plant paper	AgNW: 0.95 g/m <sup>2</sup>	X-6000 Y-9.7	4.7	X-6000 Y-1670	18	~70% decrease in Mode I and Mode II toughness

## 2.4 Conclusions

Critical considerations for the development of functionalized aeronautical CFRPs are emphasized in terms of toughness and electrical conductivity properties. The necessary insights of toughening and electrical conductivity concepts have been studied, combining with the detail reviews of multiple improvement techniques.

It is possible to simultaneously improve the electrical conductivity and toughness of CFRP laminates. The main issues of using resin modification techniques are the increase of resin viscosity and uneven dispersion of functional fillers. The carbon fibre surface treatment yields some increase in electrical and mechanical properties of CFRP laminates, whereas the surface coatings of carbon fibres do not significantly reduce the resin rich regions between each carbon fibre ply, resulting in the limitation of the conductivity improvement. Interleaving techniques show relative advantages including simple incorporation with laminated system, less influence on raw material components, and focusing on the critical interlaminar regions. However, the mechanical properties of interleaved CFRP laminates may be limited by the selection of interleaves. For example, a weak interaction between interleaves and resin matrix can significantly reduce the interlaminar shear strength and toughness. Nanofibre veils do not generally show the expected efficiency of improvement in toughness and electrical properties of CFRP laminates compared with the micro-fibre veils. The current studies show that the highest through-thickness electrical conductivity has been increased to 138 S/m using a PA veil loaded with AgNWs. However, AgNWs are expensive, and a large number of

organic solvents are used in preparation, resulting in environmental challenges and difficulties for large-scale applications.

## 2.5 References

- [1] D.S. Kammer, Slip Fronts at Frictional Interfaces: A Numerical and Theoretical Study, ETH Zurich, 2014. doi:10.5075/epfl-thesis-6492.
- [2] J.M. Hodgkinson, Mechanical Testing of Advanced Fibre Composites, Woodhead Publishing Limited, Cambridge, 2000. doi:10.1201/9781439822791.
- [3] B.D. Agarwal, L.J. Broutman, K. Chandrashekhara, Analysis and Performance of Fiber Composites, Third, Wiley & Sons, 2002. doi:10.1016/0921-5093(92)90189-8.
- [4] A. Wronkowicz-Katunin, A. Katunin, K. Dragan, Reconstruction of barely visible impact damage in composite structures based on non-destructive evaluation results, Sensors (Switzerland). 19 (2019). doi:10.3390/s19214629.
- [5] D.D.R. Cartié, P.E. Irving, Effect of resin and fibre properties on impact and compression after impact performance of CFRP, Compos. - Part A Appl. Sci. Manuf. 33 (2002) 483–493. doi:10.1016/S1359-835X(01)00141-5.
- [6] J.K. Kim, M.L. Sham, Impact and delamination failure of woven-fabric composites, Compos. Sci. Technol. 60 (2000) 745–761. doi:10.1016/S0266-3538(99)00166-9.
- [7] F. Chen, J.M. Hodgkinson, Impact behaviour of composites with different fibre architecture, Proc. Inst. Mech. Eng. Part G J. Aerosp. Eng. 223 (2009) 1009–1017. doi:10.1243/09544100JAERO451.
- [8] A.J. Kinloch, S.J. Shaw, D.A. Tod, D.L. Hunston, Deformation and fracture behaviour of a rubber-toughened epoxy: 1. Microstructure and fracture studies, Polymer (Guildf). 24 (1983) 1341–1354. doi:10.1016/0032-3861(83)90070-8.
- [9] R.A. Pearson, A.F. Yee, Toughening mechanisms in elastomer-modified epoxies Microscopy studies, J. Mater. Sci. 21 (1986) 2475–2488.

- [10] D. Quan, A. Ivankovic, Effect of core-shell rubber (CSR) nano-particles on mechanical properties and fracture toughness of an epoxy polymer, *Polymer (Guildf)*. 66 (2015) 16–28. doi:10.1016/j.polymer.2015.04.002.
- [11] J. Wang, Z. Xue, Y. Li, G. Li, Y. Wang, W.H. Zhong, X. Yang, Synergistically effects of copolymer and core-shell particles for toughening epoxy, *Polymer (Guildf)*. 140 (2018) 39–46. doi:10.1016/j.polymer.2018.02.031.
- [12] R.A. Pearson, A.F. Yee, Toughening mechanisms in thermoplastic-modified epoxies: 1. Modification using poly(phenylene oxide), *Polymer (Guildf)*. 34 (1993) 3658–3670. doi:10.1016/0032-3861(93)90051-B.
- [13] K. Tangthana-umrung, H. Mahmood, X. Zhang, M. Gresil, Enhancing interlaminar fracture toughness of woven carbon fibre/epoxy composites with engineering thermoplastic and carbon-based nanomaterials, *Compos. Struct.* 282 (2022) 115073. doi:10.1016/j.compstruct.2021.115073.
- [14] W. Gan, Y. Yu, M. Wang, Q. Tao, S. Li, Viscoelastic effects on the phase separation in thermoplastics-modified epoxy resin, *Macromolecules*. 36 (2003) 7746–7751. doi:10.1021/ma034649a.
- [15] E. Girard-Reydet, V. Vicard, J.P. Pascault, H. Sautereau, Polyetherimide-modified epoxy networks: Influence of cure conditions on morphology and mechanical properties, *J. Appl. Polym. Sci.* 65 (1997) 2433–2445. doi:10.1002/(SICI)1097-4628(19970919)65:12<2433::AID-APP15>3.0.CO;2-1.
- [16] D.L. and T.O. Nobuyuki ODAGIRI, Hajime KISHI, A Study of Resin Fracture Toughness Robustness: Comparison of Particle-toughened Thermosetting Resin and Micro Phase-separated Thermosetting Resin, *Mater. Syst.* 37 (2020) 29–35.
- [17] A.J. Kinloch, M.L. Yuen, S.D. Jenkins, Thermoplastic-toughened epoxy polymers, *J. Mater. Sci.* 29 (1994) 3781–3790. doi:10.1007/BF00357349.
- [18] J. Yao, K. Niu, Y. Niu, T. Zhang, Toughening efficiency and mechanism of carbon fibre epoxy matrix composites by PEK-C, *Compos. Struct.* 229 (2019) 111431. doi:10.1016/j.compstruct.2019.111431.

- [19] L. Karthikeyan, D. Mathew, T.M. Robert, Poly(ether ether ketone)-bischromenes: Synthesis, characterization, and influence on thermal, mechanical, and thermo mechanical properties of epoxy resin, *Polym. Adv. Technol.* 30 (2019) 1061–1071. doi:10.1002/pat.4539.
- [20] B. Francis, S. Thomas, J. Jose, R. Ramaswamy, V. Lakshmana Rao, Hydroxyl terminated poly(ether ether ketone) with pendent methyl group toughened epoxy resin: Miscibility, morphology and mechanical properties, *Polymer (Guildf)*. 46 (2005) 12372–12385. doi:10.1016/j.polymer.2005.10.103.
- [21] N.G. Yun, Y.G. Won, S.C. Kim, Toughening of epoxy composite by dispersing polysulfone particle to form morphology spectrum, *Polym. Bull.* 52 (2004) 365–372. doi:10.1007/s00289-004-0293-x.
- [22] B. Vieille, V.M. Casado, C. Bouvet, About the impact behavior of woven-ply carbon fiber-reinforced thermoplastic- and thermosetting-composites: A comparative study, *Compos. Struct.* 101 (2013) 9–21. doi:10.1016/j.compstruct.2013.01.025.
- [23] M.R. Groleau, Y.B. Shi, A.F. Yee, J.L. Bertram, H.J. Sue, P.C. Yang, Mode II fracture of composites interlayered with nylon particles, *Compos. Sci. Technol.* 56 (1996) 1223–1240. doi:10.1016/S0266-3538(96)00080-2.
- [24] J. Cui, Y. Yu, S. Li, Studies on the phase separation of polyetherimide-modified epoxy, *Macromol. Chem. Phys.* 199 (1998) 1645–1649.
- [25] J. Zhang, Q. Guo, B.L. Fox, Study on thermoplastic-modified multifunctional epoxies : Influence of heating rate on cure behaviour and phase separation, *Compos. Sci. Technol.* 69 (2009) 1172–1179. doi:10.1016/j.compscitech.2009.02.016.
- [26] K. Liu, C.W. Macosko, Can nanoparticle toughen fiber-reinforced thermosetting polymers?, *J. Mater. Sci.* 54 (2018) 4471–4483. doi:10.1007/s10853-018-03195-9.
- [27] I. Zaman, T.T. Phan, H.C. Kuan, Q. Meng, L.T. Bao La, L. Luong, O. Youssf, J. Ma, Epoxy/graphene platelets nanocomposites with two levels of interface strength, *Polymer (Guildf)*. 52 (2011) 1603–1611. doi:10.1016/j.polymer.2011.02.003.

- [28] E. Mannov, H. Schmutzler, S. Chandrasekaran, C. Viets, S. Buschhorn, F. Tölle, R. Mülhaupt, K. Schulte, Improvement of compressive strength after impact in fibre reinforced polymer composites by matrix modification with thermally reduced graphene oxide, *Compos. Sci. Technol.* 87 (2013) 36–41. doi:10.1016/j.compscitech.2013.07.019.
- [29] V. Kostopoulos, A. Baltopoulos, P. Karapappas, A. Vavouliotis, A. Paipetis, Impact and after-impact properties of carbon fibre reinforced composites enhanced with multi-wall carbon nanotubes, *Compos. Sci. Technol.* 70 (2010) 553–563. doi:10.1016/j.compscitech.2009.11.023.
- [30] Y. Zeng, H.Y. Liu, Y.W. Mai, X.S. Du, Improving interlaminar fracture toughness of carbon fibre/epoxy laminates by incorporation of nano-particles, *Compos. Part B Eng.* 43 (2012) 90–94. doi:10.1016/j.compositesb.2011.04.036.
- [31] J.L. Tsai, B.H. Huang, Y.L. Cheng, Enhancing fracture toughness of glass/epoxy composites by using rubber particles together with silica nanoparticles, *J. Compos. Mater.* 43 (2009) 3107–3123. doi:10.1177/0021998309345299.
- [32] T. Liu, W.C. Tjiu, Y. Tong, C. He, S.S. Goh, T.S. Chung, Morphology and fracture behavior of intercalated epoxy/clay nanocomposites, *J. Appl. Polym. Sci.* 94 (2004) 1236–1244. doi:10.1002/app.21033.
- [33] Y. Tang, L. Ye, Z. Zhang, K. Friedrich, Interlaminar fracture toughness and CAI strength of fibre-reinforced composites with nanoparticles - A review, *Compos. Sci. Technol.* 86 (2013) 26–37. doi:10.1016/j.compscitech.2013.06.021.
- [34] D. Carolan, A. Ivankovic, A.J. Kinloch, S. Sprenger, A.C. Taylor, Toughened carbon fibre-reinforced polymer composites with nanoparticle-modified epoxy matrices, *J. Mater. Sci.* 52 (2017) 1767–1788. doi:10.1007/s10853-016-0468-5.
- [35] N.A. Siddiqui, R.S.C. Woo, J.K. Kim, C.C.K. Leung, A. Munir, Mode I interlaminar fracture behavior and mechanical properties of CFRPs with nanoclay-filled epoxy matrix, *Compos. Part A Appl. Sci. Manuf.* 38 (2007) 449–460. doi:10.1016/j.compositesa.2006.03.001.
- [36] S. Sprenger, M.H. Kothmann, V. Altstaedt, Carbon fiber-reinforced composites using an epoxy resin matrix modified with reactive liquid rubber and silica nanoparticles, *Compos. Sci. Technol.* 105 (2014) 86–95. doi:10.1016/j.compscitech.2014.10.003.

- [37] V. Kostopoulos, A. Kotrotsos, P. Tsokanas, S. Tsantzalīs, Toughening and healing of composites by CNTs reinforced copolymer nylon micro-particles, *Mater. Res. Express*. 5 (2018). doi:10.1088/2053-1591/aaabfb.
- [38] N.G. Ozdemir, T. Zhang, I. Aspin, F. Scarpa, H. Hadavinia, Y. Song, Toughening of carbon fibre reinforced polymer composites with rubber nanoparticles for advanced industrial applications, *Express Polym. Lett.* 10 (2016) 394–407. doi:10.3144/expresspolymlett.2016.37.
- [39] J. Hutschreuther, R. Kunz, J. Brey, V. Altstädt, Influence of particle size on toughening mechanisms of layered silicates in CFRP, *Materials (Basel)*. 13 (2020). doi:10.3390/ma13102396.
- [40] Y. Tang, L. Ye, D. Zhang, S. Deng, Characterization of transverse tensile, interlaminar shear and interlaminar fracture in CF/EP laminates with 10 wt% and 20 wt% silica nanoparticles in matrix resins, *Compos. Part A Appl. Sci. Manuf.* 42 (2011) 1943–1950. doi:10.1016/j.compositesa.2011.08.019.
- [41] G. de Souza, J.R. Tarpani, Interleaving CFRP and GFRP with a Thermoplastic Ionomer: The Effect on Bending Properties, *Appl. Compos. Mater.* 28 (2021) 559–572. doi:10.1007/s10443-021-09874-2.
- [42] T.K. Tsotsis, Interlayer toughening of composite materials, *Polym. Compos.* 30 (2009) 70–86. doi:10.1002/pc.20535.
- [43] E.M. Woo, K.L. Mao, Evaluation of Interlaminar-Toughened Poly(EtherImid e)-Modified Epoxy/Carbon Fier Composite, *Polym. Compos.* 17 (1996) 799–805.
- [44] D. Liu, G. Li, B. Li, Y. Luan, H. Ling, X. Yang, In-situ toughened CFRP composites by shear-calender orientation and fiber-bundle filtration of PA microparticles at prepreg interlayer, *Compos. Part A Appl. Sci. Manuf.* 84 (2016) 165–174. doi:10.1016/j.compositesa.2016.01.015.
- [45] Y. Huang, W. Liu, Q. Jiang, Y. Wei, Y. Qiu, Interlaminar Fracture Toughness of Carbon-Fiber-Reinforced Epoxy Composites Toughened by Poly(phenylene oxide) Particles, *ACS Appl. Polym. Mater.* 2 (2020) 3114–3121. doi:10.1021/acsapm.0c00285.



- [46] E.J. Garcia, B.L. Wardle, A. John Hart, Joining prepreg composite interfaces with aligned carbon nanotubes, *Compos. Part A Appl. Sci. Manuf.* 39 (2008) 1065–1070.  
doi:10.1016/j.compositesa.2008.03.011.
- [47] J. Jia, X. Du, C. Chen, X. Sun, Y.W. Mai, J.K. Kim, 3D network graphene interlayer for excellent interlaminar toughness and strength in fiber reinforced composites, *Carbon N. Y.* 95 (2015) 978–986. doi:10.1016/j.carbon.2015.09.001.
- [48] M. Arai, Y. Noro, K. ichi Sugimoto, M. Endo, Mode I and mode II interlaminar fracture toughness of CFRP laminates toughened by carbon nanofiber interlayer, *Compos. Sci. Technol.* 68 (2008) 516–525. doi:10.1016/j.compscitech.2007.06.007.
- [49] M.H.R. Jen, Y.C. Tseng, C.H. Wu, Manufacturing and mechanical response of nanocomposite laminates, *Compos. Sci. Technol.* 65 (2005) 775–779.  
doi:10.1016/j.compscitech.2004.10.010.
- [50] H. Ning, J. Li, N. Hu, C. Yan, Y. Liu, L. Wu, F. Liu, J. Zhang, Interlaminar mechanical properties of carbon fiber reinforced plastic laminates modified with graphene oxide interleaf, *Carbon N. Y.* 91 (2015) 224–233. doi:10.1016/j.carbon.2015.04.054.
- [51] M.S. Chaudhry, A. Czekanski, Z.H. Zhu, Characterization of carbon nanotube enhanced interlaminar fracture toughness of woven carbon fiber reinforced polymer composites, *Int. J. Mech. Sci.* 131–132 (2017) 480–489. doi:10.1016/j.ijmecsci.2017.06.016.
- [52] Y. Li, N. Hori, M. Arai, N. Hu, Y. Liu, H. Fukunaga, Improvement of interlaminar mechanical properties of CFRP laminates using VGCF, *Compos. Part A Appl. Sci. Manuf.* 40 (2009) 2004–2012. doi:10.1016/j.compositesa.2009.09.002.
- [53] A. Aksoy, L.A. Carlsson, Interlaminar shear fracture of interleaved graphite/epoxy composites, *Compos. Sci. Technol.* 43 (1992) 55–69. doi:10.1016/0266-3538(92)90133-N.
- [54] C. Cheng, C. Zhang, J. Zhou, M. Jiang, Z. Sun, S. Zhou, Y. Liu, Z. Chen, L. Xu, H. Zhang, M. Yu, Improving the interlaminar toughness of the carbon fiber/epoxy composites via interleaved with polyethersulfone porous films, *Compos. Sci. Technol.* 183 (2019).  
doi:10.1016/j.compscitech.2019.107827.

- [55] A. Wilson, The formation of dry, wet, spunlaid and other types of nonwovens, *Appl. Nonwovens Tech. Text.* (2010) 3–17. doi:10.1016/B978-1-84569-437-1.50001-X.
- [56] M. Kuwata, P.J. Hogg, Interlaminar toughness of interleaved CFRP using non-woven veils: Part 2. Mode-II testing, *Compos. Part A Appl. Sci. Manuf.* 42 (2011) 1560–1570. doi:10.1016/j.compositesa.2011.07.017.
- [57] M. Kuwata, P.J. Hogg, Interlaminar toughness of interleaved CFRP using non-woven veils: Part 1. Mode-I testing, *Compos. Part A Appl. Sci. Manuf.* 42 (2011) 1551–1559. doi:10.1016/j.compositesa.2011.07.016.
- [58] V.A. Ramirez, P.J. Hogg, W.W. Sampson, The influence of the nonwoven veil architectures on interlaminar fracture toughness of interleaved composites, *Compos. Sci. Technol.* 110 (2015) 103–110. doi:10.1016/j.compscitech.2015.01.016.
- [59] D. Quan, F. Bologna, G. Scarselli, A. Ivankovic, N. Murphy, Interlaminar fracture toughness of aerospace-grade carbon fibre reinforced plastics interleaved with thermoplastic veils, *Compos. Part A Appl. Sci. Manuf.* 128 (2020) 105642. doi:10.1016/j.compositesa.2019.105642.
- [60] G. Gardiner, *Aerocomposites: The move to multifunctionality*, *Compos. World.* (2015) 42–48.
- [61] L. Wei, X. Ya-Hong, Y. Xiao-Su, A. Xue-Feng, Preliminary study on resin transfer molding of highly-toughened graphite laminates by ex-situ method, *J. Mater. Sci.* 39 (2004) 2263–2266. doi:10.1023/B:JMISC.0000017803.00661.e7.
- [62] Q. Cheng, Z. Fang, Y. Xu, X.S. Yi, Improvement of the impact damage resistance of BMI/graphite laminates by the ex-situ method, *High Perform. Polym.* 18 (2006) 907–917. doi:10.1177/0954008306068296.
- [63] X.S. Yi, Research, development and enhancement of high-performance polymer matrix composites for aerospace in China, *ICCM Int. Conf. Compos. Mater.* (2009) 1–12.
- [64] X.S. Yi, X. An, Developments of high-performance composites by innovative ex situ concept for aerospace application, *J. Thermoplast. Compos. Mater.* 22 (2009) 29–49. doi:10.1177/0892705708091605.

- [65] X. Wang, T. Lin, *Needleless Electrospinning of Nanofibers: Technology and Applications*, First edit, Jenny Stanford Publishing, New York, 2013. doi:<https://doi.org/10.1201/b15489>.
- [66] G.W. Beckermann, K.L. Pickering, Mode I and Mode II interlaminar fracture toughness of composite laminates interleaved with electrospun nanofibre veils, *Compos. PART A*. 72 (2015) 11–21. doi:[10.1016/j.compositesa.2015.01.028](https://doi.org/10.1016/j.compositesa.2015.01.028).
- [67] J. Zhang, T. Yang, T. Lin, C.H. Wang, Phase morphology of nanofibre interlayers: Critical factor for toughening carbon/epoxy composites, *Compos. Sci. Technol.* 72 (2012) 256–262. doi:[10.1016/j.compscitech.2011.11.010](https://doi.org/10.1016/j.compscitech.2011.11.010).
- [68] K. Magniez, C. De Lavigne, B.L. Fox, The effects of molecular weight and polymorphism on the fracture and thermo-mechanical properties of a carbon-fibre composite modified by electrospun poly (vinylidene fluoride) membranes, *Polymer (Guildf)*. 51 (2010) 2585–2596. doi:[10.1016/j.polymer.2010.04.021](https://doi.org/10.1016/j.polymer.2010.04.021).
- [69] H. Saghafi, T. Brugo, G. Minak, A. Zucchelli, The effect of PVDF nanofibers on mode-I fracture toughness of composite materials, *Compos. Part B Eng.* 72 (2015) 213–216. doi:[10.1016/j.compositesb.2014.12.015](https://doi.org/10.1016/j.compositesb.2014.12.015).
- [70] N. Vallack, W.W. Sampson, Materials systems for interleave toughening in polymer composites, *J. Mater. Sci.* 57 (2022) 6129–6156. doi:[10.1007/s10853-022-06988-1](https://doi.org/10.1007/s10853-022-06988-1).
- [71] S.H. Lee, H. Kim, S. Hang, S.K. Cheong, Interlaminar fracture toughness of composite laminates with CNT-enhanced nonwoven carbon tissue interleave, *Compos. Sci. Technol.* 73 (2012) 1–8. doi:[10.1016/j.compscitech.2012.09.011](https://doi.org/10.1016/j.compscitech.2012.09.011).
- [72] D. Quan, C. Mischo, X. Li, G. Scarselli, A. Ivanković, N. Murphy, Improving the electrical conductivity and fracture toughness of carbon fibre/epoxy composites by interleaving MWCNT-doped thermoplastic veils, *Compos. Sci. Technol.* 182 (2019). doi:[10.1016/j.compscitech.2019.107775](https://doi.org/10.1016/j.compscitech.2019.107775).
- [73] J.A. Rodríguez-González, C. Rubio-González, Influence of sprayed multi-walled carbon nanotubes on mode I and mode II interlaminar fracture toughness of carbon fiber/epoxy composites, *Adv. Compos. Mater.* 28 (2019) 19–36. doi:[10.1080/09243046.2018.1458510](https://doi.org/10.1080/09243046.2018.1458510).

- [74] Y. Ou, C. González, J.J. Vilatela, Understanding interlaminar toughening of unidirectional CFRP laminates with carbon nanotube veils, *Compos. Part B Eng.* 201 (2020). doi:10.1016/j.compositesb.2020.108372.
- [75] S. Hamer, H. Leibovich, A. Green, R. Avrahami, E. Zussman, A. Siegmann, D. Sherman, Mode I and Mode II fracture energy of MWCNT reinforced nanofibrilmats interleaved carbon/epoxy laminates, *Compos. Sci. Technol.* 90 (2014) 48–56. doi:10.1016/j.compscitech.2013.10.013.
- [76] Y. Song, N. Zheng, X. Dong, J. Gao, Flexible Carboxylated CNT/PA66 Nanofibrous Mat Interleaved Carbon Fiber/Epoxy Laminates with Improved Interlaminar Fracture Toughness and Flexural Properties, *Ind. Eng. Chem. Res.* 59 (2020) 1151–1158. doi:10.1021/acs.iecr.9b05854.
- [77] C. Cheng, Z. Chen, Z. Huang, C. Zhang, R. Tusiime, J. Zhou, Z. Sun, Y. Liu, M. Yu, H. Zhang, Simultaneously improving mode I and mode II fracture toughness of the carbon fiber/epoxy composite laminates via interleaved with uniformly aligned PES fiber webs, *Compos. Part A Appl. Sci. Manuf.* 129 (2020) 105696. doi:10.1016/j.compositesa.2019.105696.
- [78] J. Nasser, L. Zhang, H. Sodano, Aramid nanofiber interlayer for improved interlaminar properties of carbon fiber/epoxy composites, *Compos. Part B Eng.* 197 (2020) 108130. doi:10.1016/j.compositesb.2020.108130.
- [79] M.T. Aljarrah, N.R. Abdelal, Improvement of the mode I interlaminar fracture toughness of carbon fiber composite reinforced with electrospun nylon nanofiber, *Compos. Part B Eng.* 165 (2019) 379–385. doi:10.1016/j.compositesb.2019.01.065.
- [80] N. Forintos, T. Czigany, Multifunctional application of carbon fiber reinforced polymer composites: Electrical properties of the reinforcing carbon fibers – A short review, *Compos. Part B Eng.* 162 (2019) 331–343. doi:10.1016/j.compositesb.2018.10.098.
- [81] B.A. Newcomb, H.G. Chae, *The properties of carbon fiber*, Second, Elsevier Ltd., 2018.
- [82] X. Qin, Y. Lu, H. Xiao, Y. Wen, T. Yu, A comparison of the effect of graphitization on microstructures and properties of polyacrylonitrile and mesophase pitch-based carbon fibers, *Carbon N. Y.* 50 (2012) 4459–4469. doi:10.1016/j.carbon.2012.05.024.

- [83] Y. Huang, R.J. Young, Effect of fibre microstructure upon the modulus of PAN- and pitch-based carbon fibres, *Carbon N. Y.* 33 (1995) 97–107. doi:10.1016/0008-6223(94)00109-D.
- [84] D.. Edie, The effect of processing on the structure and properties of carbon fibers, *Carbon N. Y.* 36 (1998) 345–362. doi:https://doi.org/10.1016/S0008-6223(97)00185-1.
- [85] F.G. Emmerich, Young's modulus, thermal conductivity, electrical resistivity and coefficient of thermal expansion of mesophase pitch-based carbon fibers, *Carbon N. Y.* 79 (2014) 274–293. doi:10.1016/j.carbon.2014.07.068.
- [86] D.-H. Cho, S.-B. Yoon, C.-W. Cho, J.-K. Park, Effect of additional heat-treatment temperature on chemical, microstructural, mechanical, and electrical properties of commercial PAN-based carbon fibers, *Carbon Lett.* 12 (2011) 223–228. doi:10.5714/cl.2011.12.4.223.
- [87] C. Thiagarajan, Smart Characterisation of damage in carbon fibre reinforced composites under static and fatigue loading conditions by means of electrical resistivity measurements, Cranfield University, 1996.
- [88] S.C. Brown, C. Robert, V. Koutsos, D. Ray, Methods of modifying through-thickness electrical conductivity of CFRP for use in structural health monitoring, and its effect on mechanical properties – A review, *Compos. Part A Appl. Sci. Manuf.* 133 (2020) 105885. doi:10.1016/j.compositesa.2020.105885.
- [89] L. Ye, Functionalized interleaf technology in carbon-fibre-reinforced composites for aircraft, *Natl. Sci. Rev.* 1 (2014) 7–8. doi:10.1093/nsr/nwt007.
- [90] S. Das, T. Yokozeki, A brief review of modified conductive carbon/glass fibre reinforced composites for structural applications: Lightning strike protection, electromagnetic shielding, and strain sensing, *Compos. Part C Open Access.* 5 (2021). doi:10.1016/j.jcomc.2021.100162.
- [91] H. Kim, S. Yarlagadda, J.W. Gillespie, N.B. Shevchenko, B.K. Fink, A study on the induction heating of carbon fiber reinforced thermoplastic composites, *Adv. Compos. Mater.* 11 (2002) 71–80. doi:10.1163/156855102753613309.

- [92] N. Athanasopoulos, V. Kostopoulos, Resistive heating of multidirectional and unidirectional dry carbon fibre preforms, *Compos. Sci. Technol.* 72 (2012) 1273–1282.  
doi:10.1016/j.compscitech.2012.04.018.
- [93] S.A. Hayes, A.D. Lafferty, G. Altinkurt, P.R. Wilson, M. Collinson, P. Duchene, Direct electrical cure of carbon fiber composites, *Adv. Manuf. Polym. Compos. Sci.* 1 (2015) 112–119.  
doi:10.1179/2055035915Y.0000000001.
- [94] D. Abliz, Y. Duan, L. Steuernagel, L. Xie, D. Li, G. Ziegmann, Curing methods for advanced polymer composites -A review, *Polym. Polym. Compos.* 21 (2013) 341–348.  
doi:10.1177/096739111302100602.
- [95] K.J. Miller, K.N. Collier, H.B. Soll-Morris, R. Swaminathan, M.E. McHenry, Induction heating of FeCo nanoparticles for rapid rf curing of epoxy composites, *J. Appl. Phys.* 105 (2009) 1–4.  
doi:10.1063/1.3073833.
- [96] S. Ye, N.B. Cramer, B.E. Stevens, R.L. Sani, C.N. Bowman, Induction curing of thiol-acrylate and thiol-ene composite systems, *Macromolecules.* 44 (2011) 4988–4996.  
doi:10.1021/ma200098e.
- [97] S. Pappadà, A. Salomi, J. Montanaro, A. Passaro, A. Caruso, A. Maffezzoli, Fabrication of a thermoplastic matrix composite stiffened panel by induction welding, *Aerosp. Sci. Technol.* 43 (2015) 314–320. doi:10.1016/j.ast.2015.03.013.
- [98] S.H. Mcknight, S.T. Holmes, J.W. Gillespie, C.L.T. Lambing, J.M. Marinelli, Scaling issues in resistance-welded thermoplastic composite joints, *Adv. Polym. Technol.* 16 (1997) 279–295.  
doi:10.1002/(SICI)1098-2329(199711)16:4<279::AID-ADV3>3.0.CO;2-S.
- [99] M. Frauenhofer, H. Kunz, K. Dilger, Fast curing of adhesives in the field of CFRP, *J. Adhes.* 88 (2012) 406–417. doi:10.1080/00218464.2012.660386.
- [100] J.S. Park, T. Darlington, A.F. Starr, K. Takahashi, J. Riendeau, H. Thomas Hahn, Multiple healing effect of thermally activated self-healing composites based on Diels-Alder reaction, *Compos. Sci. Technol.* 70 (2010) 2154–2159. doi:10.1016/j.compscitech.2010.08.017.

- [101] A. Todoroki, M. Tanaka, Y. Shimamura, Measurement of orthotropic electric conductance of CFRP laminates and analysis of the effect on delamination monitoring with an electric resistance change method, *Compos. Sci. Technol.* 62 (2002) 619–628. doi:10.1016/S0266-3538(02)00019-2.
- [102] N. Angelidis, C.Y. Wei, P.E. Irving, The electrical resistance response of continuous carbon fibre composite laminates to mechanical strain, *Compos. Part A Appl. Sci. Manuf.* 35 (2004) 1135–1147. doi:10.1016/j.compositesa.2004.03.020.
- [103] E. Sevkat, J. Li, B. Liaw, F. Delale, A statistical model of electrical resistance of carbon fiber reinforced composites under tensile loading, *Compos. Sci. Technol.* 68 (2008) 2214–2219. doi:10.1016/j.compscitech.2008.04.011.
- [104] R.J. Hart, O.I. Zhupanska, The role of electrical anisotropy and effective conducting thickness in understanding and interpreting static resistance measurements in CFRP composite laminates, *J. Compos. Mater.* 54 (2020) 867–882. doi:10.1177/0021998319870860.
- [105] R. Schueler, S.P. Joshi, K. Schulte, Damage detection in CFRP by electrical conductivity mapping, *Compos. Sci. Technol.* 61 (2001) 921–930. doi:10.1016/S0266-3538(00)00178-0.
- [106] C. Han, B. Sun, B. Gu, Electric conductivity and surface potential distributions in carbon fiber reinforced composites with different ply orientations, *Text. Res. J.* 92 (2022) 1147–1160. doi:10.1177/00405175211048160.
- [107] S.A. Grammatikos, E.Z. Kordatos, T.E. Matikas, C. David, A.S. Paipetis, Current injection phase thermography for low-velocity impact damage identification in composite laminates, *Mater. Des.* 55 (2014) 429–441. doi:10.1016/j.matdes.2013.09.019.
- [108] A. Vavouliotis, A. Paipetis, V. Kostopoulos, On the fatigue life prediction of CFRP laminates using the Electrical Resistance Change method, *Compos. Sci. Technol.* 71 (2011) 630–642. doi:10.1016/j.compscitech.2011.01.003.
- [109] S.A. Grammatikos, A.S. Paipetis, On the electrical properties of multi scale reinforced composites for damage accumulation monitoring, *Compos. Part B Eng.* 43 (2012) 2687–2696. doi:10.1016/j.compositesb.2012.01.077.

- [110] A. Piche, R. Perraud, C. Lochot, Modeling of large avionic structures in electrical network simulations, Proc. 2012 ESA Work. Aerosp. EMC 2012. (2012) 1–5.
- [111] X. Luo, D.D.L. Chung, Electromagnetic interference shielding using continuous carbon-fiber carbon-matrix and polymer-matrix composites, Compos. Part B Eng. 30 (1999) 227–231. doi:10.1016/S1359-8368(98)00065-1.
- [112] C. Karch, C. Metzner, Lightning protection of carbon fibre reinforced plastics - An Overview, 2016 33rd Int. Conf. Light. Prot. ICLP 2016. (2016). doi:10.1109/ICLP.2016.7791441.
- [113] K. Yousefpour, Novel considerations for lightning strike damage mitigation of Carbon Fiber Reinforced Polymer Matrix ( CFRP ) composite laminates, Mississippi State University, 2021.
- [114] C. Lochot, D. Slomianowski, A 350 XWB Electrical structure network, Airbus Tech. Mag. (2014) 20–25.
- [115] S.M. Braden, M.J. Doherty, S.M. Scott, Current return network, 2011.
- [116] G. Wasselynck, D. Trichet, J. Fouladgar, Determination of the electrical conductivity tensor of a CFRP composite using a 3-D percolation model, IEEE Trans. Magn. 49 (2013) 1825–1828. doi:10.1109/TMAG.2013.2241039.
- [117] I. El Sawi, P.A. Olivier, P. Demont, H. Bougherara, Processing and electrical characterization of a unidirectional CFRP composite filled with double walled carbon nanotubes, Compos. Sci. Technol. 73 (2012) 19–26. doi:10.1016/j.compscitech.2012.08.016.
- [118] Y. Li, H. Zhang, Z. Huang, E. Bilotti, T. Peijs, Graphite Nanoplatelet Modified Epoxy Resin for Carbon Fibre Reinforced Plastics with Enhanced Properties, J. Nanomater. 2017 (2017). doi:10.1155/2017/5194872.
- [119] E. Kandare, A.A. Khatibi, S. Yoo, R. Wang, J. Ma, P. Olivier, N. Gleizes, C.H. Wang, Improving the through-thickness thermal and electrical conductivity of carbon fibre/epoxy laminates by exploiting synergy between graphene and silver nano-inclusions, Compos. Part A Appl. Sci. Manuf. 69 (2015) 72–82. doi:10.1016/j.compositesa.2014.10.024.



- [120] E.C. Senis, I.O. Golosnoy, J.M. Dulieu-Barton, O.T. Thomsen, Enhancement of the electrical and thermal properties of unidirectional carbon fibre/epoxy laminates through the addition of graphene oxide, *J. Mater. Sci.* 54 (2019) 8955–8970. doi:10.1007/s10853-019-03522-8.
- [121] W. Xin, F. Sarasini, J. Tirillò, I. Bavasso, F. Sbardella, L. Lampani, I.M. De Rosa, Impact and post-impact properties of multiscale carbon fiber composites interleaved with carbon nanotube sheets, *Compos. Part B Eng.* 183 (2020). doi:10.1016/j.compositesb.2019.107711.
- [122] M. Burkov, A. Eremin, Hybrid CFRP/SWCNT Composites with Enhanced Electrical Conductivity and Mechanical Properties, *J. Mater. Eng. Perform.* 27 (2018) 5984–5991. doi:10.1007/s11665-018-3695-x.
- [123] R. Sadeghian, S. Gangireddy, B. Minaie, K.T. Hsiao, Manufacturing carbon nanofibers toughened polyester/glass fiber composites using vacuum assisted resin transfer molding for enhancing the mode-I delamination resistance, *Compos. Part A Appl. Sci. Manuf.* 37 (2006) 1787–1795. doi:10.1016/j.compositesa.2005.09.010.
- [124] F. Yan, L. Liu, M. Li, M. Zhang, L. Shang, L. Xiao, Y. Ao, One-step electrodeposition of Cu/CNT/CF multiscale reinforcement with substantially improved thermal/electrical conductivity and interfacial properties of epoxy composites, *Compos. Part A Appl. Sci. Manuf.* 125 (2019) 105530. doi:10.1016/j.compositesa.2019.105530.
- [125] W. Qin, F. Vautard, L.T. Drzal, J. Yu, Mechanical and electrical properties of carbon fiber composites with incorporation of graphene nanoplatelets at the fiber-matrix interphase, *Compos. Part B Eng.* 69 (2015) 335–341. doi:10.1016/j.compositesb.2014.10.014.
- [126] T.R. Pozegic, J. V. Anguita, I. Hamerton, K.D.G.I. Jayawardena, J.S. Chen, V. Stolojan, P. Balocchi, R. Walsh, S.R.P. Silva, Multi-Functional Carbon Fibre Composites using Carbon Nanotubes as an Alternative to Polymer Sizing, *Sci. Rep.* 6 (2016) 1–11. doi:10.1038/srep37334.
- [127] A. Duongthiphewa, Y. Su, L. Zhou, Electrical conductivity and mechanical property improvement by low-temperature carbon nanotube growth on carbon fiber fabric with nanofiller incorporation, *Compos. Part B Eng.* 182 (2020) 107581. doi:10.1016/j.compositesb.2019.107581.

- [128] L. Bhanuprakash, S. Parasuram, S. Varghese, Experimental investigation on graphene oxides coated carbon fibre/epoxy hybrid composites: Mechanical and electrical properties, *Compos. Sci. Technol.* 179 (2019) 134–144. doi:10.1016/j.compscitech.2019.04.034.
- [129] H. Xu, X. Tong, Y. Zhang, Q. Li, W. Lu, Mechanical and electrical properties of laminated composites containing continuous carbon nanotube film interleaves, *Compos. Sci. Technol.* 127 (2016) 113–118. doi:10.1016/j.compscitech.2016.02.032.
- [130] F. Xu, B. Yang, L. Feng, D. Huang, M. Xia, Improved interlaminar fracture toughness and electrical conductivity of CFRPs with non-woven carbon tissue interleaves composed of fibers with different lengths, *Polymers (Basel)*. 12 (2020) 1–12. doi:10.3390/POLYM12040803.
- [131] Z.J. Zhao, G.J. Xian, J.G. Yu, J. Wang, J.F. Tong, J.H. Wei, C.C. Wang, P. Moreira, X.S. Yi, Development of electrically conductive structural BMI based CFRPs for lightning strike protection, *Compos. Sci. Technol.* 167 (2018) 555–562. doi:10.1016/j.compscitech.2018.08.026.
- [132] V. Kumar, S. Sharma, A. Pathak, B.P. Singh, S.R. Dhakate, T. Yokozeki, T. Okada, T. Ogasawara, Interleaved MWCNT buckypaper between CFRP laminates to improve through-thickness electrical conductivity and reducing lightning strike damage, *Compos. Struct.* 210 (2019) 581–589. doi:10.1016/j.compstruct.2018.11.088.
- [133] P. Latko-Duralek, K. Dydek, P. Bolimowski, E. Golonko, P. Duralek, R. Kozera, A. Boczkowska, Nonwoven fabrics with carbon nanotubes used as interleaves in CFRP, *IOP Conf. Ser. Mater. Sci. Eng.* 406 (2018). doi:10.1088/1757-899X/406/1/012033.
- [134] E. Barjasteh, C. Sutanto, T. Reddy, J. Vinh, A graphene/graphite-based conductive polyamide 12 interlayer for increasing the fracture toughness and conductivity of carbon-fiber composites, *J. Compos. Mater.* 51 (2017) 2879–2887. doi:10.1177/0021998317705707.
- [135] W. Li, D. Xiang, L. Wang, E. Harkin-Jones, C. Zhao, B. Wang, Y. Li, Simultaneous enhancement of electrical conductivity and interlaminar fracture toughness of carbon fiber/epoxy composites using plasma-treated conductive thermoplastic film interleaves, *RSC Adv.* 8 (2018) 26910–26921. doi:10.1039/c8ra05366a.

- [136] M. Guo, X. Yi, The production of tough, electrically conductive carbon fiber composite laminates for use in airframes, *Carbon N. Y.* 58 (2013) 241–244.  
doi:10.1016/j.carbon.2013.02.052.
- [137] M. Guo, X. Yi, G. Liu, L. Liu, Simultaneously increasing the electrical conductivity and fracture toughness of carbon-fiber composites by using silver nanowires-loaded interleaves, *Compos. Sci. Technol.* 97 (2014) 27–33. doi:10.1016/j.compscitech.2014.03.020.
- [138] M. Guo, X. Yi, Effect of paper or silver nanowires-loaded paper interleaves on the electrical conductivity and interlaminar fracture toughness of composites, *Aerospace.* 5 (2018) 1–15. doi:10.3390/aerospace5030077.
- [139] W.X. Wang, Y. Takao, T. Matsubara, H.S. Kim, Improvement of the interlaminar fracture toughness of composite laminates by whisker reinforced interlamination, *Compos. Sci. Technol.* 62 (2002) 767–774. doi:10.1016/S0266-3538(02)00052-0.
- [140] Z. Wu, X. Yi, A. Wilkinson, Interlaminar fracture toughness of carbon fibre / RTM6-2 composites toughened with thermoplastic-coated fabric reinforcement, *Compos. Part B.* 130 (2017) 192–199. doi:10.1016/j.compositesb.2017.08.003.
- [141] G.W. Beckermann, K.L. Pickering, Mode I and Mode II interlaminar fracture toughness of composite laminates interleaved with electrospun nanofiber veils, *Compos. Part A Appl. Sci. Manuf.* 72 (2015) 11–21.
- [142] J.W. Kim, J.S. Lee, Influence of interleaved films on the mechanical properties of carbon fiber fabric/polypropylene thermoplastic composites, *Materials (Basel).* 9 (2016). doi:10.3390/ma9050344.
- [143] L. Daelemans, S. Van Der Heijden, I. De Baere, H. Rahier, W. Van Paepegem, K. De Clerck, Improved fatigue delamination behaviour of composite laminates with electrospun thermoplastic nanofibrous interleaves using the Central Cut-Ply method, *Compos. Part A.* (2016). doi:10.1016/j.compositesa.2016.12.004.
- [144] M. Guo, X. Yi, C. Rudd, X. Liu, Preparation of highly electrically conductive carbon-fiber composites with high interlaminar fracture toughness by using silver-plated interleaves, *Compos. Sci. Technol.* 176 (2019) 29–36. doi:10.1016/j.compscitech.2019.03.014.

[145] X. Yi, M. Guo, G. Liu, W. Zhao, L. Liu, H. Cui, Composite conductive sheet, fabricating method and application thereof, EP.2687364B1, 2015.

## **Chapter 3: Study of toughness improvement of green epoxy matrix carbon fibre composites**

Status: this chapter has been published in Journal of composites science

Authors: Dongyuan Hu, Xvfeng Zhang, Xiaoling Liu, Zhen Qin, Li Hu, Chris Rudd and Xiaosu Yi

As the first step of this research, a proof-of-concept study of toughness improvement for a green epoxy based CFRP is presented in this chapter. A brief introduction on green composites and toughening approaches is first given to emphasize the motivation.

Considering the technical limitation of the reaction induced phase transformation toughening method, a proprietary polyamide non-woven veil was used as the interleaf to toughen a green epoxy based CFRP to physically form the interpenetrated network at interlaminar region. The tests regarding the interlaminar fracture toughness, CAI were implemented to demonstrate the toughening efficiency. In addition, the effect of interleaving on in-plane mechanical properties were also considered. Discussions on toughening mechanism and mechanical properties of the interleaved green composite system are presented, with the comparison of a commercial petroleum-sourced counterpart.

Article

# Study on Toughness Improvement of a Rosin-Sourced Epoxy Matrix Composite for Green Aerospace Application <sup>†</sup>

Dongyuan Hu <sup>1</sup>, Xvfeng Zhang <sup>2</sup>, Xiaoling Liu <sup>1,\*</sup>, Zhen Qin <sup>3</sup>, Li Hu <sup>3</sup>, Chris Rudd <sup>4</sup>  
and Xiaosu Yi <sup>1,2,\*</sup>

<sup>1</sup> Advanced Materials and Composites Department, University of Nottingham Ningbo China, 199 Taikang East Road, Ningbo 315000, China; dongyuan.hu2@nottingham.edu.cn

<sup>2</sup> AVIC Composite Co. Ltd., High-tech Park, Shunyi District, Beijing 101300, China; 010xufeng@sina.com

<sup>3</sup> Shanghai Key Laboratory of Spacecraft Mechanism, 3888 Yuanjiang Road, Minhang District, Shanghai 201109, China; qinzhen981621@163.com (Z.Q.); rocketeer\_hu@outlook.com (L.H.)

<sup>4</sup> College of Science and Engineering, James Cook University, 149 Sims Drive, Singapore 387380, Singapore; chris.rudd@jcu.edu.au

\* Correspondence: xiaoling.liu@nottingham.edu.cn (X.L.); xiaosu.yi@nottingham.edu.cn (X.Y.)

<sup>†</sup> Dedicated to Prof. Dr.-Ing. Ortwin Hahn for his 80th birthday. Xiaosu Yi and his research team.

Received: 19 October 2020; Accepted: 5 November 2020; Published: 10 November 2020



**Abstract:** A high temperature epoxy resin was formulated by using a rosin-sourced anhydride-type curing agent, i.e., maleopimaric acid (RAM), and a two-component epoxy consisting of an E51-type epoxy and a solid phenolic epoxy to form a bio-sourced green matrix resin. The glass transition temperature of the final resin was 238 °C. Carbon fiber composite prepreg and was manufactured and laminated into composite specimens. Interleaving Toughening Technology (ITT) was applied to the laminates by using Polyamide interleaf veils. The interlaminar fracture toughness and compression after impact (CAI) strength were investigated and showed that the opening Mode I interlaminar fracture toughness GIC and the Mode II interlaminar fracture toughness GIIC of the specimens with interleaves were significantly improved from 227.51 J/m<sup>2</sup> to 509.22 J/m<sup>2</sup> and 1064.3 J/m<sup>2</sup> to 1510.8 J/m<sup>2</sup>, respectively. Correspondingly, the drop-weight impact test shows that the interleaves reduced the impact damage area from 20.9% to 11.3% of the total area, and the CAI residual strength was increased from 144 MPa to 191 MPa. Meanwhile, mechanical tests showed that the in-plane properties of the interleaved laminates were slightly reduced due to carbon fiber volume fraction reduction. In conclusion, the high glass transition temperature, fracture toughness and CAI behaviour make the green resin matrix composite a potential candidate for aerospace applications.

**Keywords:** rosin-sourced epoxy resin; interleaving toughening; glass transition temperature; toughness; CAI; in-plane mechanical properties

## 1. Introduction

Carbon fiber reinforced polymer matrix composites (CFRCs), mostly the thermosetting epoxy matrix composites, have been widely used in the aerospace industry because of their performance advantages such as light weight, high specific stiffness and strength, and fatigue and corrosion resistance. However, it is well known that all of the epoxies used today in aerospace are petroleum-sourced, i.e., they are all originated from non-sustainable fossil resource. Facing the world-wide challenge in environment, resources and sustainability, the aerospace industry has to adapt to the global need to decrease its environmental impact and greenhouse gas emissions, especially for commercial air transport [1]. Additionally, living on a planet with limited resources, another important sustainability

**Blank page**

### 3.1 Abstract

A high temperature epoxy resin was formulated by using a rosin-sourced anhydride-type curing agent, i.e., maleopimaric acid (RAM), and a two-component epoxy consisting of an E51-type epoxy and a solid phenolic epoxy to form a bio-sourced green matrix resin. The glass transition temperature of the final resin was 238 °C. Carbon fiber composite prepreg and was manufactured and laminated into composite specimens. Interleaving Toughening Technology (ITT) was applied to the laminates by using Polyamide interleaf veils. The interlaminar fracture toughness and compression after impact (CAI) strength were investigated and showed that the opening Mode I interlaminar fracture toughness  $G_{Ic}$  and the Mode II interlaminar fracture toughness  $G_{IIc}$  of the specimens with interleaves were significantly improved from 227.51 J/m<sup>2</sup> to 509.22 J/m<sup>2</sup> and 1064.3 J/m<sup>2</sup> to 1510.8 J/m<sup>2</sup>, respectively. Correspondingly, the drop-weight impact test shows that the interleaves reduced the impact damage area from 20.9% to 11.3% of the total area, and the CAI residual strength was increased from 144 MPa to 191 MPa. Meanwhile, mechanical tests showed that the in-plane properties of the interleaved laminates were slightly reduced due to carbon fibre volume fraction reduction. In conclusion, the high glass transition temperature, fracture toughness and CAI behaviour make the green resin matrix composite a potential candidate for aerospace applications.

Keywords: rosin-sourced epoxy resin; interleaving toughening; glass transition temperature; toughness; CAI; in-plane mechanical properties



## 3.2 Introduction

Carbon fibre reinforced polymer matrix composites (CFRPs) have been widely used in the aerospace industry because of their performance advantages such as light weight, high specific stiffness and strength, and fatigue and corrosion resistance. However, it is well known that all of the epoxies used today in aerospace are petroleum-sourced, i.e., they are all originated from non-sustainable fossil resource. Facing the world-wide challenge in environment, resources and sustainability, the aerospace industry has to adapt to the global need to decrease its environmental impact and greenhouse gas emissions, especially for commercial air transport [1]. Additionally, living on a planet with limited resources, another important sustainability goal is hence to reduce the consumption of non-renewable materials. Today's aviation industry is thus looking for bio-sourced materials for green aviation and green manufacturing as green alternatives [2].

Starting in 2016, European and Chinese scientists and engineers were working together in the ECO-COMPASS project to develop aeronautical composites with a reduced environmental footprint [3]. One of the objectives of ECO-COMPASS was to provide a preliminary assessment of a bio-sourced epoxy matrix composite and its usability in aviation [4]. This was an intermediate temperature epoxy cured with a rosin-anhydride-type curing agent with around 30% bio-content [5]. It was noticed that the glass transition temperature, i.e.,  $T_g$ , of the rosin-sourced epoxy matrix composites reinforced with glass fibre was about 191–193°C, which was much higher than conventional epoxy composites (typically c.110°C). The higher  $T_g$  is possibly attributed to the bulky fused

ring structure of the rosin-anhydride curing agent, imposing a considerable restriction on the segmental mobility between the cross-links [6]. Obviously, the higher glass transition temperature is beneficial for structural composites used in aviation.

However, as is well-known, compared with amine cured epoxies, anhydride cured epoxies generally show higher rigidity, lower curing shrinkage and more sustainability, but more brittleness [7–9]. The aerostructures from CFRCs are typically required to be resistant against impact delamination and damage, which is generally related with interlaminar fracture toughness and compression after impact strength, thus epoxy matrix composite laminates generally need to be toughened. Traditionally, epoxy matrix CFRC laminates are toughened by introducing thermoplastic components into the thermosetting matrix resin to form a bi-continuous granular structure in a manner of reaction-induced phase separation and phase coarsening [10–16]. However, such a complex phase structuring is highly dependent on the thermodynamic and kinetic conditions of the two polymer components, i.e., the thermoplastic toughness modifier and thermosetting epoxy matrix, making the toughening usually restrictive [17,18].

Thermosetting polymer matrix CFRC laminates can also be toughened by interleaving non-woven textile veils to construct an interpenetrating thermoplastic network in the interlaminar region [19–26]. One of the major benefits of the so-called interleaving toughening technology (ITT) is its independence of the thermodynamic and kinetics of the polymer phases. It is also demonstrated that CFRC laminates of high electrical conductivity and high toughness can be simultaneously achieved by electrically functionalizing the interleaving material [27–29].

In the present paper, a similar rosin-anhydride sourced curing agent and a high-temperature epoxy matrix resin cured with the agent was developed and reported. Carbon fibre reinforced composite laminates (CFRCs) using the high-temperature epoxy matrix were then toughened by interleaving a specially designed polyamide veil. The in-plane mechanical properties and out-of-plane properties were tested in terms of Mode I and II interlaminar fracture toughness and Compression After Impact (CAI) strength, as well as tensile, flexural, compression and interlaminar shear strength etc. The toughening mechanism was studied by microstructure observation. It was finally found that the rosin-sourced epoxy matrix CFRC could provide higher  $T_g$ , higher toughness, higher CAI and promising mechanical properties for use in aviation.

### **3.3 Material and methods**

#### **3.3.1 Materials**

Similar to the intermediate temperature epoxy resin, a high temperature epoxy matrix resin was formulated using a rosin-sourced anhydride curing agent, i.e., maleopimaric acid, and a two-component epoxy consisting of an E51-type epoxy and a solid phenolic epoxy to form a bio-sourced green matrix resin. The bio-content of the final epoxy system was about 40% by weight. For the composites with 57% carbon fibre volume fraction, the overall green content was around 12%. The maleopimaric acid was initially developed by the Ningbo Institute of Materials Technology and Engineering, Chinese Academy of Sciences [30], and was provided for the study. The physical and chemical properties of the resin system are listed in Table 3-1.

**Table 3-1. Physical and chemical properties of the resin system**

Density, g/cm <sup>2</sup>	Gel Time at 120°C, s	Peak Exothermic Temperature (T <sub>p</sub> ) under 10 °C/min Heating Rate, °C
1.18	500	164

The apparent viscosity was performed on a cone plate viscometer (CAP2000+, Brookfield, Middleborough, MA, USA) with 6th rotation spider at a rotation rate of 300 RPM and a shear rate of 1000 s<sup>-1</sup>. Figure 3-1 shows the curves of viscosity-temperature. In the temperature range of 90–150°C the viscosity is just below 2000 mPa·s, which is suitable for glue film infiltrating the firmer. In the range of 60–70°C, the viscosity is in the range of 20,000–10,000 mPa·s, which is very good fit for adhesive film preparation.

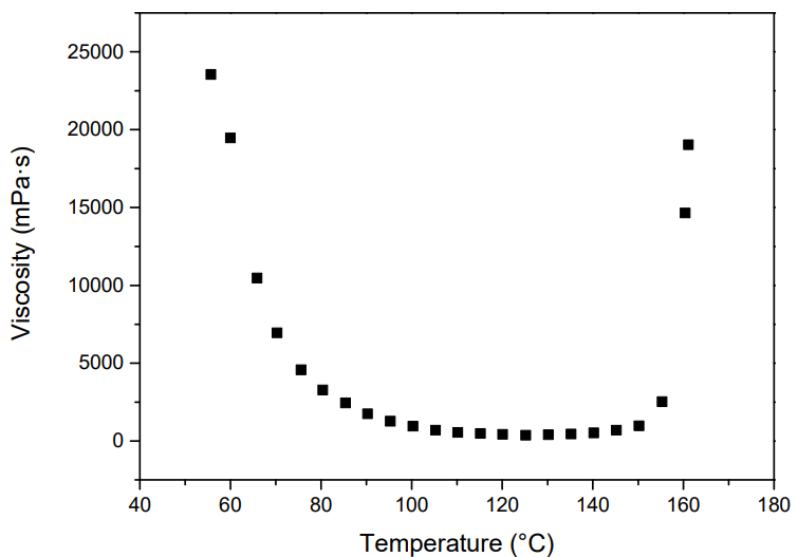


**Figure 3-1. Viscosity-temperature curves of the resin system.**

The high temperature epoxy resin was then cured at 180°C for 3 hr to produce a cast bar for dynamic mechanical analysis (DMA242E, Netzsch Instruments, German). The rectangular bar of 50 mm×10.2 mm×3.1 mm was placed on a three-point bending clamp, and tested at an oscillation frequency of 2 Hz, amplitude of 10 μm, and a heating rate of 3°C min<sup>-1</sup>. As shown in Figure 3-2, the cast bar specimen shows a single peak at 238°C, indicating its glass transition temperature, T<sub>g</sub>.

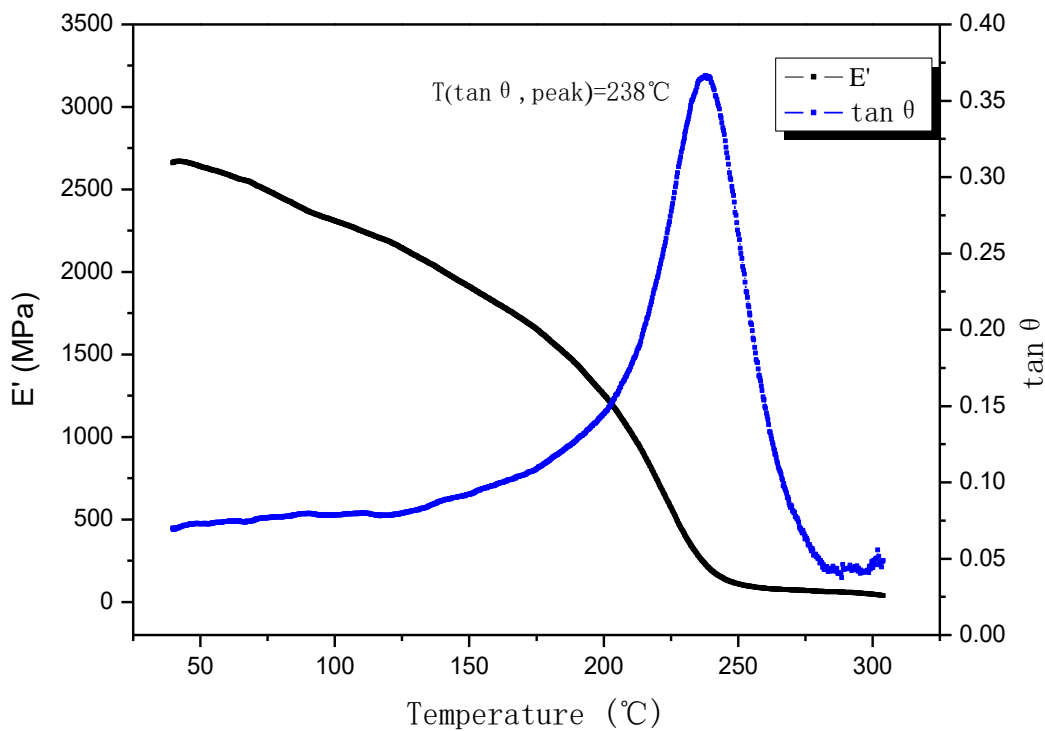


**Figure 3-2. Dynamic mechanical test curves of the rosin-sourced epoxy cast bar.**

A commercial T700-grade carbon fibre SYT49S was chosen as reinforcement material for production of the green composites, Table 3-2, supplier Jiangsu Tianniao Hi-Tech Co., Ltd. The prepreg produced (Table 3-3) shows a resin weight fraction of 37.2 wt% and an areal density of 223.4 g/m<sup>2</sup>. The nominal thickness of the prepreg was 0.14 mm.

**Table 3-2. Technical data of SYT49S, 12K, T700-grade carbon fibre**

Strength, MPa	Modulus, GPa	Elongation at break, %	Linear density, g/km	Density, g/cm <sup>3</sup>	Diameter, $\mu\text{m}$
4900	230	2.1	800	1.79	7

**Table 3-3. Physical property of high temperature rosin-sourced epoxy /UN-SYT49S prepreg**

Area density, g/m <sup>2</sup>	Resin content, wt%	Areal weight, g/m <sup>2</sup>	Volatile content, wt%
140	37.2	223.4	0.85

A proprietary polyamide non-woven veil (NV) was used as the interleaf material, provided by N<sup>2</sup>IC New Materials Co. Ltd, Ningbo, China. The nominal thickness and areal weight were 60  $\mu\text{m}$  and 26.4 g/m<sup>2</sup>, respectively. The average diameter of the polyamide fibre was around 14  $\mu\text{m}$ . Figure 2 shows the upper and lower surface SEM images of the nonwoven used. As seen, the polyamide fibres are randomly entangled and fusion-bonded to form a porous network structure. The bonded nodes are found on both surfaces. The diameter of bonded nodes was approximately 0.45 mm with 0.9–1.5 mm nodal spacing. Due to the fusion bonding, the polyamide fibres at the node regions are sunken and parallel to the plane of the veil. In addition, many granular particles are found on one surface. The diameter of the particles was 30–100  $\mu\text{m}$  and the space between each of them was around 0.7 mm. Some particles coalesced as shown in Figure 3-3. Figure 3-4 shows the sectional optical microscope image for a four-layer sample of the NVs casted in epoxy resin. The fusion-bonded nodes and the particles can be easily distinguished.

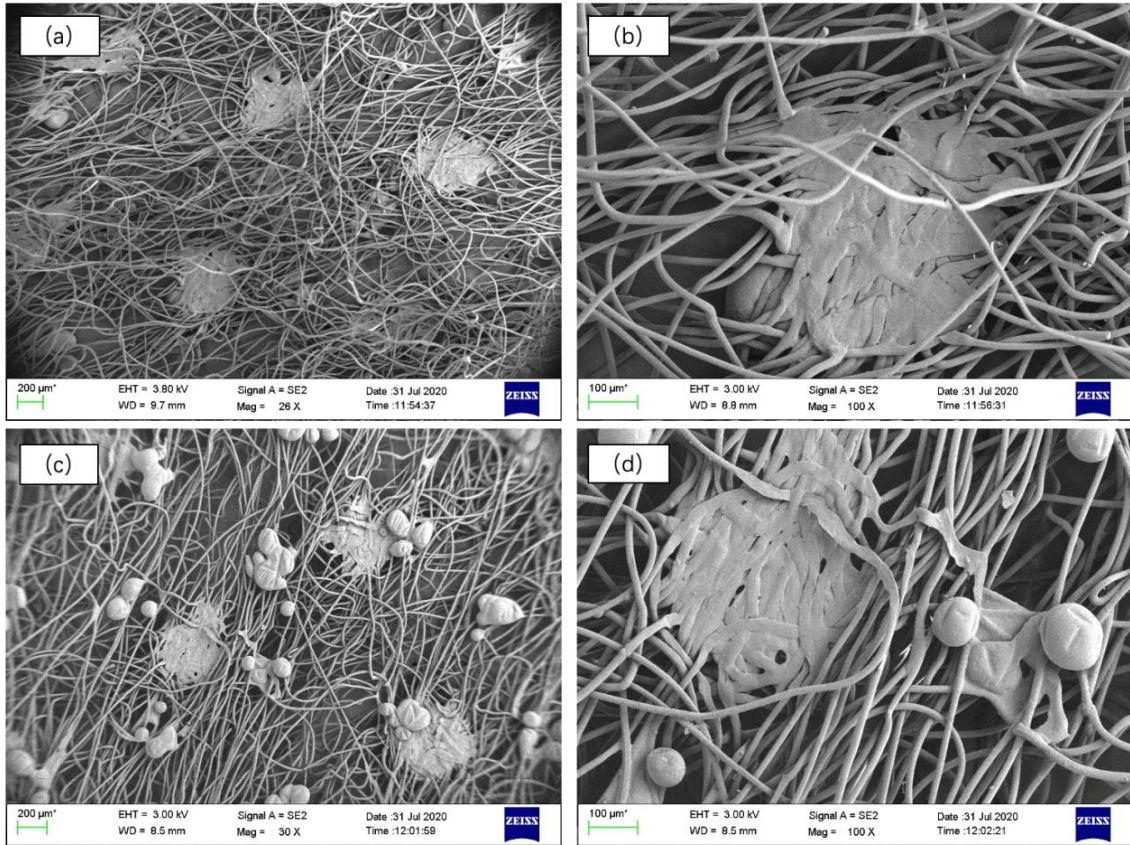


Figure 3-3. SEM images of polyamide nonwoven veil. (a,b) smooth side, (c,d) rough side.

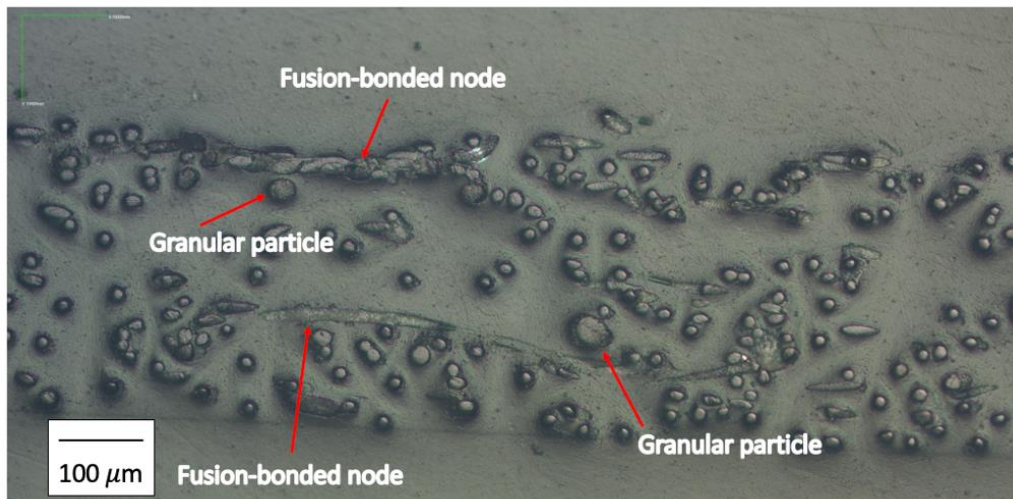


Figure 3-4. Sectional image of polyamide veil (four layers).

### 3.3.2 Fabrication of composite laminates

Vacuum bag assisted compression moulding was used to manufacture the composite laminates. The prepregs were cut into 295 mm × 295 mm plies. Then the laminate performs were placed on the tool plate. Figure 3-5 shows a schematic of the manufacturing set-up. A rigid hollow steel mould with a 300 mm × 300 mm inner area was used to fix the boundary of the specimens. A thick glass fibre reinforced PTFE film was placed on the top of performs to transfer the load from the hot platen to the laminate performs. The laminate performs were degassed in a vacuum bag under room temperature. After the pressure reached 0.09 MPa, the preforms were transferred to the hot press. Figure 3-6 illustrates the parameters of the curing procedure. Cured composite laminates were removed from the press and cooled to room temperature with a vacuum applied throughout the cycle.

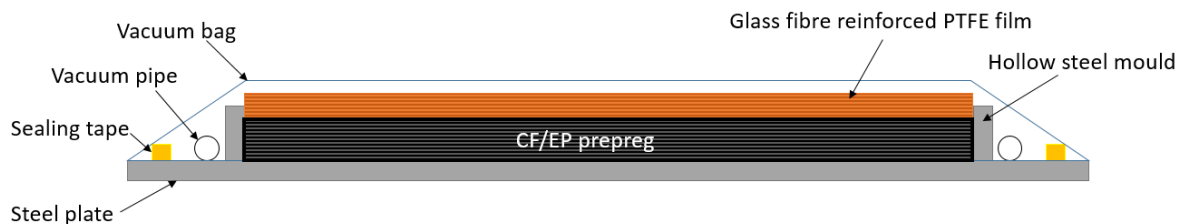


Figure 3-5. Schematic diagram of manufacturing set-up.



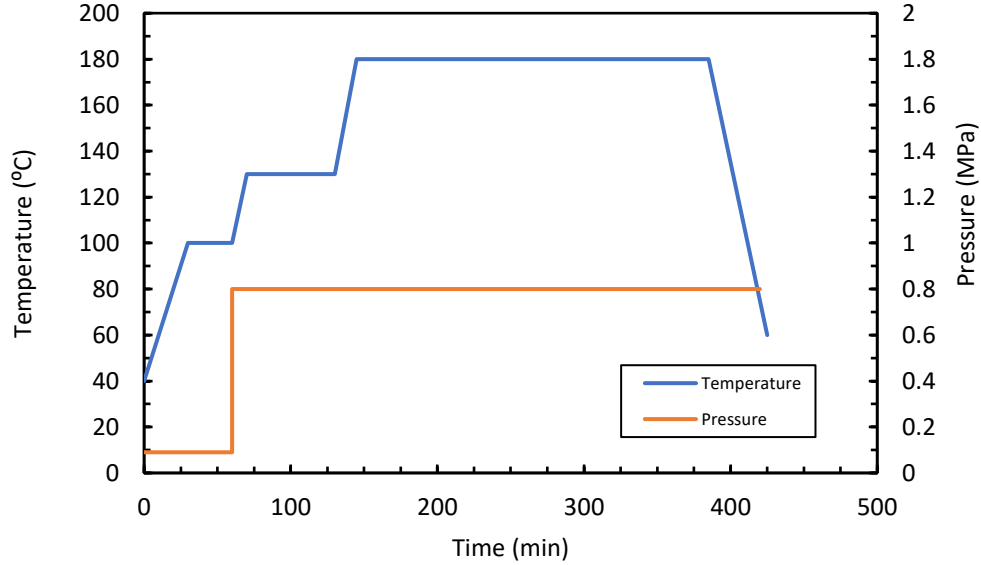


Figure 3-6. Curing procedure of the composite laminates.

### 3.3.3 Preparation of test specimens

Table 3-4 shows characteristics of test specimens for interlaminar fracture toughness study. 24 plies of the rosin-sourced epoxy matrix composites reinforced with unidirectional SYT49S carbon fibres were hand-stacked at 0° orientation for Mode I and II interlaminar fracture toughness test, respectively. At the central layer, a 10 µm thick release film (100 mm×300 mm) was placed at one end to simulate an initial crack for the control specimens, designed as Control<sup>-IFT</sup>. For the interleaved specimens, the nonwoven veils were additionally placed between each carbon fibre ply, designed as NVIC<sup>-IFT</sup>.

**Table 3-4. Characteristics of specimens for interlaminar toughness study**

Specimen	Lay-up	Thickness (mm)	Veil mass fraction (wt %)	Fibre volume fraction ( $V_{CF}$ %)
Control <sup>-IFT</sup>	[0] <sub>24</sub>	3.3±0.02	-	56.7±0.32
NVIC <sup>-IFT</sup>		3.9±0.01	12.31±0.15%	48.1±0.18

For drop-weight impact and compression after impact (CAI) study, the stacking sequence of laminate was [+45/0/-45/90]<sub>4s</sub>. The laminate specimens were fully interleaved with the nonwoven veils between each carbon fibre ply, and one top of the specimens as the impact side was also covered with a nonwoven veil layer, designed as NVIC<sup>-CAI</sup>. Table 3-5 shows the characteristics of the test specimens for CAI study.

**Table 3-5. Characteristics of specimens for CAI study**

Specimen	Lay-up	Thickness (mm)	Veil mass fraction (wt%)	Fibre volume fraction ( $V_{CF}$ %)
Control <sup>-CAI</sup>	[+0/-/90] <sub>4s</sub>	4.38±0.02	-	57.04±0.05
NVIC <sup>-CAI</sup>		4.86±0.02	12.44±0.38	51.48±0.21

For mechanical properties study, laminate specimens with different stacking sequence were used to match the requirement of ASTM standards. The nonwoven veils were also placed between each carbon fibre ply to manufacture the NVIC specimens. The characteristics of all test specimens are shown in Table 3-6. For interleaving the NVs, it should be noted that the rough side (with granular particles) is the downside.

**Table 3-6. Characteristic of specimens for mechanical properties study**

Specimens	Lay-up	Thickness (mm)	Veil mass fraction (wt%)	Fibre volume fraction ( $V_{CF}$ %)	Test
Control <sup>T</sup>	[0] <sub>5</sub>	0.7±0.01	-	55.56±0.8	Tensile test
NVIC <sup>T</sup>		0.81±0.01	11.24±0.1	48.28±0.53	
Control <sup>FS</sup>	[0] <sub>20</sub>	2.69±0.01	-	58.1±0.32	Flexural and Interlaminar shear strength test
NVIC <sup>FS</sup>		3.09±0.01	11.9±0.06	50.7±0.13	
Control <sup>C</sup>	[0/90] <sub>6</sub>	1.6±0.01	-	58.44±0.37	Compression (CLC) test
NVIC <sup>C</sup>		1.78±0.02	13.08±0.07	52.67±0.58	

### **3.3.4 Determination of interlaminar fracture toughness**

The interlaminar fracture toughness was determined by Mode I and Mode II tests, according to ASTM D5228 and ASTM D7905 [31,32], respectively. Tests were conducted on an MTS E42 universal test machine with a 5 KN load cell. The Double Cantilever Beam (DCB) specimen was prepared for Mode I toughness test with dimensions: width  $b = 25$  mm, length  $L = 180$  mm. In order to measure the delamination length during test, white water-based marking fluid was coated on one edge of the specimen. A 1 mm vertical scale was used for first 5 mm from the insert end and a 5 mm vertical scale was used for the remaining 45 mm. The crosshead rate was set as 1 mm/min for loading procedure and 10 mm/min for the unloading procedure. The Mode-I energy release rate,  $G_{Ic}$  was obtained through modified beam theory (MBT) with the following governing Equation (3-1):

$$G_{Ic} = \frac{3P\delta}{2b(a + |\Delta|)} \quad (3-1)$$

where P is the load,  $\delta$  is the corresponding loading displacement, b is the specimen width, a is the delamination length and  $|\Delta|$  is a function of delamination length obtained by generating a least squares plot of the  $C^{1/3}$ . The initiation value  $G_{Ic-ini}$  was calculated from the load point where the delamination began, and the propagation value  $G_{Ic-prop}$  was calculated from each record point during delamination process.

The 3-point End Notch Flexure (ENF) test specimens were prepared for Mode II toughness test. In pre-cracked region, three vertical compliance calibration lines were marked as 20, 30, and 40 mm from the tip of insert.

Specimens were loaded under 0.5 mm/min crosshead rate with 100 mm span length. The unloading crosshead rate was set as 1 mm/min. The Mode-II interlaminar fracture toughness was determined by following equation (3-2):

$$G_{IIc} = G_Q = \frac{3mP_{Max}^2 a_0^2}{2B} \quad (3-2)$$

where  $G_Q$  is the candidate toughness,  $P_{MAX}$  is the maximum force from fracture test,  $a_0$  is the initial crack length (30 mm), B is the specimen width and m is the slope CC coefficient which was obtained through linear least squares linear regression analysis.

### **3.3.5 Drop-weight Impact and Compression after Impact test**

According to ASTM D7136 [33], the drop-weight impact test was conducted using Instron CEAST 9340 drop tower system to determine the damage resistance of CFRP laminates. Three Control<sup>-CAI</sup> specimens and three NVIC<sup>-CAI</sup> specimens were tested. The dimensions of the test specimen were width  $b = 100$  mm, length  $L = 150$  mm. Test specimens were fixed by toggle clamp on the fixture base. The specified ratio of impact energy to specimen thickness was set as 6.7 J/mm. The induced damage area was measured by C-Scan, using a MISTRAS UPK-T36 immersion system with a 5 MHz transducer. Subsequently, one Control<sup>-CAI</sup> and one NVIC<sup>-CAI</sup> specimen was cut near the impact point to obtain the sectional delamination images. The compression test was carried out according to ASTM D7137 [34] for the rest of the specimens. Tests were conducted on an Instron hydraulic test machine with a 25 KN load cell. The loading rate was set as 1.25 mm/min. Specimens were loaded until failure and the CAI strength was calculated.

### **3.3.6 Mechanical tests**

The mechanical tests included flexure, interlaminar shear strength, compression and tensile fracture. For each experiment, five control specimens and five NVIC specimens were tested. The flexural strength and elasticity bending modulus ( $0^\circ$ ) was determined under a 3-point bending followed by ASTM D790 [35]. The dimensions of the test specimen were width  $b = 12.7$  mm, length  $L = 125$  mm. The span-thickness ratio was

1:32 (span length = 96 mm) and the crosshead rate is set as 1 mm/min. The flexural strength and modulus were calculated by Equations (3-3) and (3-4), respectively.

$$\sigma_f = \frac{3PL}{2bd^2} \quad (3-3)$$

$$E_B = \frac{L^3m}{4bd^3} \quad (3-4)$$

where  $\sigma_f$  is the flexural strength,  $E_B$  is the elasticity bending modulus, P is the peak load, L is the support span (96 mm), b is the width of specimen, d is the depth of specimen and m is the slope of tangent to the initial straight-line portion of load-displacement curve.

The interlaminar shear strength ( $0^\circ$ ) was determined by the short beam test according to ASTM D2344 [36]. The dimensions of the specimens were 6 mm in width and 18 mm in length. A span-thickness ratio is 1:4. Test specimens were loaded under 1 mm/min crosshead rate. The interlaminar shear strength is obtained as a short-beam strength as Equation (3-5).

$$F^{sbs} = 0.75 \times \frac{P_m}{bh} \quad (3-5)$$

where  $F^{sbs}$  is the short-beam strength,  $P_m$  is the maximum load, b is the specimen width and h is the specimen thickness.

The compression test followed ASTM D6641 [37] using a combined loading compression (CLC) test fixture. The dimensions of the specimen are 12 mm in width and 140 mm in length. The gauge length was 13 mm where the two strain gauges are bonded on both surfaces. The loading rate was set as 1.3 mm/min. The laminate compressive strength and modulus were obtained by Equations (3-6) and (3-7), respectively.

$$F^{cu} = \frac{P_f}{wh} \quad (3-6)$$

$$E_c = \frac{P_2 - P_1}{(\varepsilon_{x2} - \varepsilon_{x1})wh} \quad (3-7)$$

where  $F^{cu}$  is the compressive strength,  $E_c$  is the compressive modulus,  $\nu_{xy}^c$  is the compressive Poisson's ratio,  $P_f$  is the peak load to failure,  $\varepsilon_{x2}/\varepsilon_{x1}$  is the actual strain nearest upper/lower end of strain range used,  $P_2/P_1$  is the load at  $\varepsilon_{x2}/\varepsilon_{x1}$ ,  $w$  is the specimen width and  $h$  is the specimen length.

The tensile test (0°) followed ASTM D3039 [38]. The dimensions of specimens were 15 mm in width and 250 mm in length. Two strain gages were bonded at the central position to obtain the strain. Aluminium tabs with 1.5 mm thickness, 56 mm length and 15 mm width were bonded by an epoxy adhesive. The crosshead rate was set as 2 mm/min. Tensile strength and modulus are determined as follows (Equations (3-8) and (3-9)):

$$F^{tu} = \frac{P_{max}}{A} \quad (3-8)$$

$$E^{chord} = \frac{\Delta\sigma}{\Delta\varepsilon} \quad (3-9)$$

where,  $F^{tu}$  is the tensile strength,  $E^{chord}$  is the elasticity tensile chord modulus,  $P_{max}$  is the maximum load,  $A$  is the cross-section area of specimen,  $\Delta\sigma/\Delta\varepsilon$  is the difference between applied stress/strain.

### **3.3.7 Scanning electron microscopy**

Scanning Electron Microscopy (SEM) was conducted using a Zeiss Sigma VP SEM to investigate the microstructure. Test specimens were coated with a 4  $\mu\text{m}$  thick gold layer through Leica EM SCD 500 Gold sputter before SEM observation.

## **3.4 Results and discussion**

### **3.4.1 Interlaminar fracture toughness**

The typical Mode I load-displacement curves are shown in Figure 3-7a. Both test groups show a linear increase before cracking occurred. Compared with Control<sup>-IFT</sup>, higher loads and further displacements for NVIC<sup>-IFT</sup> specimens were obtained to initiate the crack. During the crack propagation, the NVIC<sup>-IFT</sup> specimens showed an obvious non-linear growth until the peak load was achieved. The maximum loads of NVIC<sup>-IFT</sup> were almost twice those of Control<sup>-IFT</sup>. As a result, the average Mode I interlaminar fracture



toughness  $G_{IC-ini}$  and  $G_{IC-prop}$  of  $NVIC^{-IFT}$  increased from 116.2 J/m<sup>2</sup> to 241.4 J/m<sup>2</sup> and 227.51 J/m<sup>2</sup> to 509.22 J/m<sup>2</sup> respectively (Figure 3-7b). The typical R-curves show that the  $G_{IC-prop}$  values of  $NVIC^{-IFT}$  were higher than that of control at each recorded point (Figure 3-8). The  $G_{IC}$  value increased with the growth of delamination length, especially for the  $NVIC^{-IFT}$ . Besides, relatively larger variation for  $NVIC$  specimens was detected. This might be caused by the complex interfacial failure process and the veil structure under Mode I delamination.

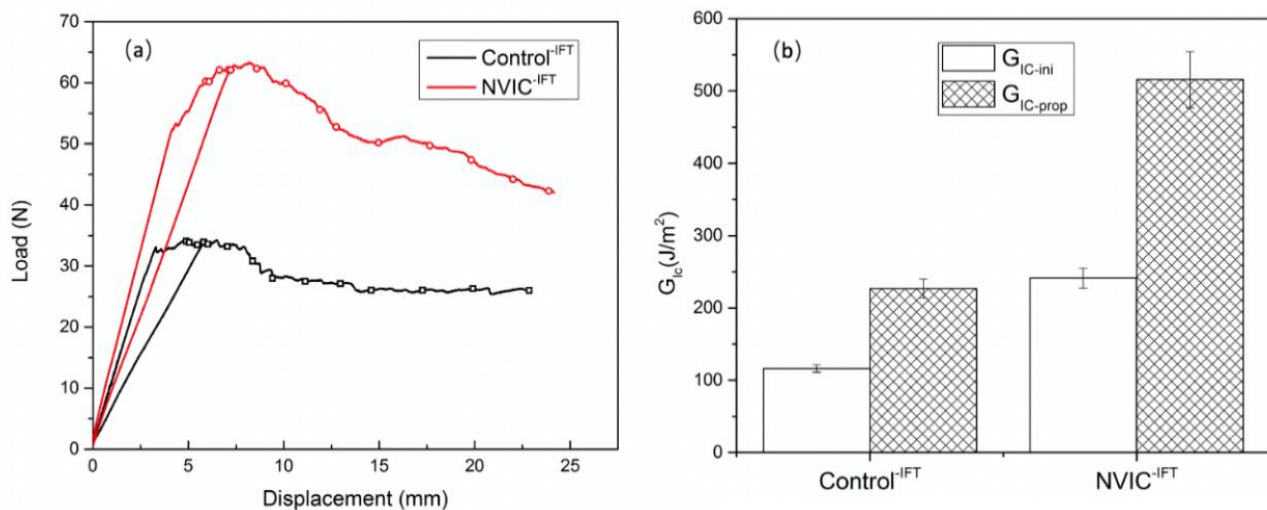


**Figure 3-7. Results of Mode I toughness test. (a) Typical DCB load-displacement curve, (b) Mode I interlaminar toughness.**

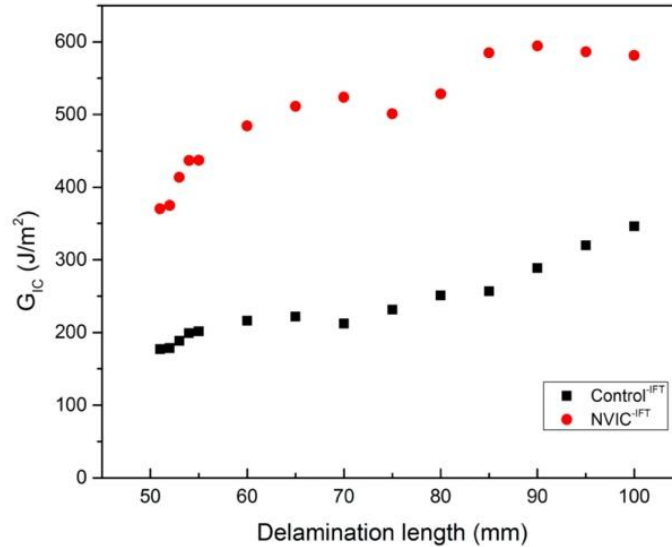


**Figure 3-8. Typical R-curve for Mode I toughness test.**

Figure 3-9a shows the Mode II load-displacement curves. Because the nonwoven veils are added between each carbon fibre ply, the slope of linear region of NVIC<sup>IFT</sup> specimens is slightly higher than that of Control<sup>IFT</sup>. The Control<sup>IFT</sup> showed linear elastic behaviour up to 820 N peak load at 2.98 mm displacement, after which it drops sharply to 418 N accompanied by a sudden fracture. In contrast, the NVIC<sup>IFT</sup> demonstrated a quasi-ductile fracture at 3.25 mm with 1038 N peak load. Then the load dropped slowly and silently to 812 N. The existence of nonwoven veils interlayers not only delayed the initiation of Mode II cracks but also increased the fracture energy for further crack growth. The average  $G_{IIc}$  values of NVIC<sup>IFT</sup> were improved from 1064.3 J/m<sup>2</sup> to 1510.8 J/m<sup>2</sup> (Figure 3-9b). The discussion of Mode I and II toughening mechanisms will be provided in following section.

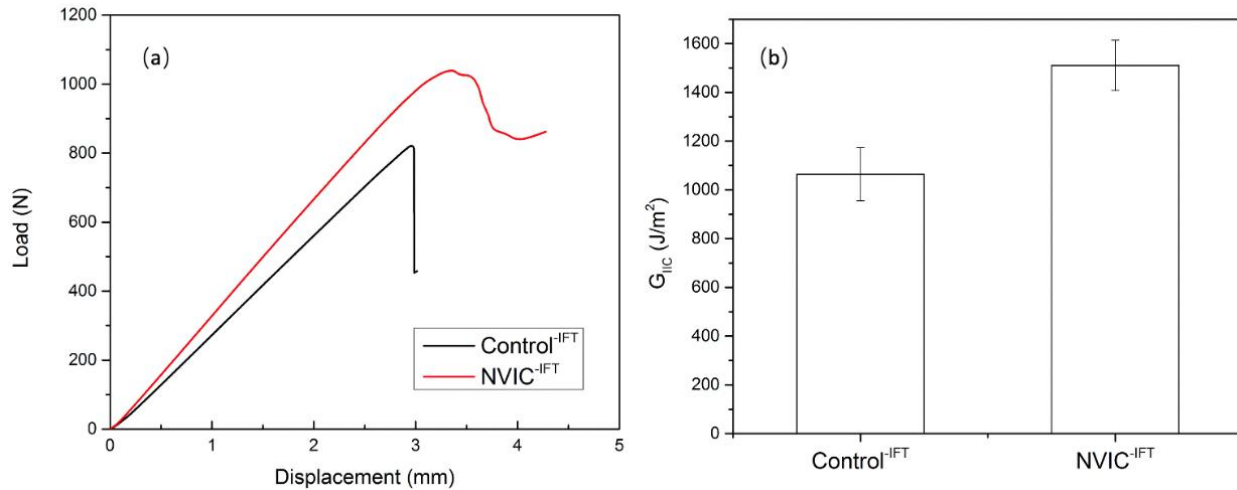


**Figure 3-9. Results of Mode II toughness test. (a) ENF load-displacement curve, (b) Mode II interlaminar toughness.**

### **3.4.2 Toughening mechanisms**

According to the plane and side observation at delamination area (Figure 3-10a and Figure 3-13a), the Mode I delamination clearly occurs inside the polyamide/epoxy interlayer. It indicates that the Mode I delamination is dominated by the cohesive failure of the interlayer. Figure 3-11 shows the polyamide fibre failure of NVIC<sup>-IFT</sup> during a Mode I toughness test. For both sides, the polyamide fibres are gradually pulled out from the interlayer because of the interpenetrating network formed by epoxy matrix and non-woven veils, i.e., the polyamide fibre directions change from parallel to perpendicular to the carbon fibre plies. This process includes the fibre debonding, bridge and breakage, which leads to the fracture energy consumption. The SEM images of Mode I fracture surfaces are shown in Figure 3-12. Large numbers of fibre pull-out and breakage are evident at both sides of the fracture surfaces. The fusion-bond nodes are split, which also indicates that the cohesive strength of the fusion-bond node is

lower than the bond strength between polyamide fibres and the epoxy matrix. In addition, the granular particles cannot be found either, but instead are regular distributed holes on the lower fracture surface (Figure 3-12a, b). Compared with the smooth fracture surface near these holes, the surfaces of the holes are rougher. Polyamide fibres, which are initially contacted with the granular particles, are pulled-out or broken and covered by the rough particles. Similar areas can also be found on the upper fracture surface (Figure 3-12c, d). It is considered that the granules have been split during the delamination process. The current study cannot demonstrate whether these particles have negative effects on Mode I toughness improvement. We will explore this in further investigations.

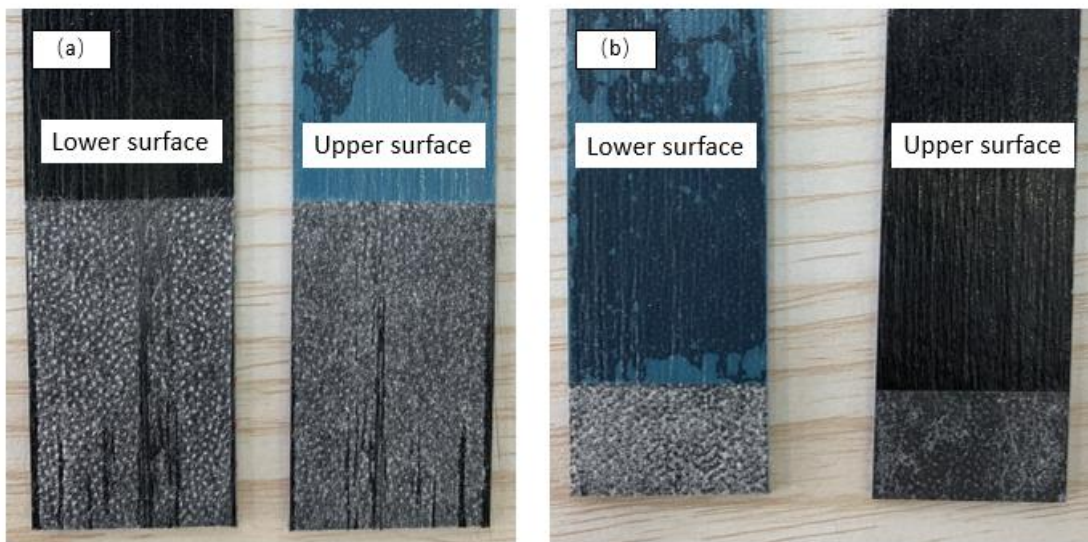


**Figure 3-10. Plane view of fracture surfaces of NVIC<sup>-ILT</sup>. (a) Mode I, (b) Mode II.**

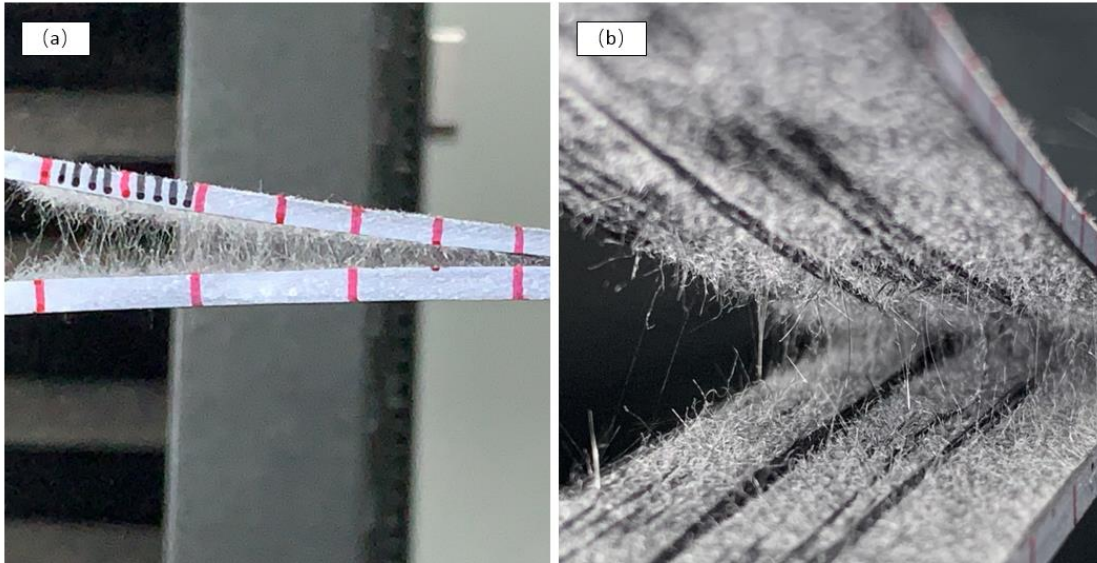


Figure 3-11. Failure mode of NVIC<sup>-ILT</sup> in DCB test. (a) side view, (b) through open mouth.

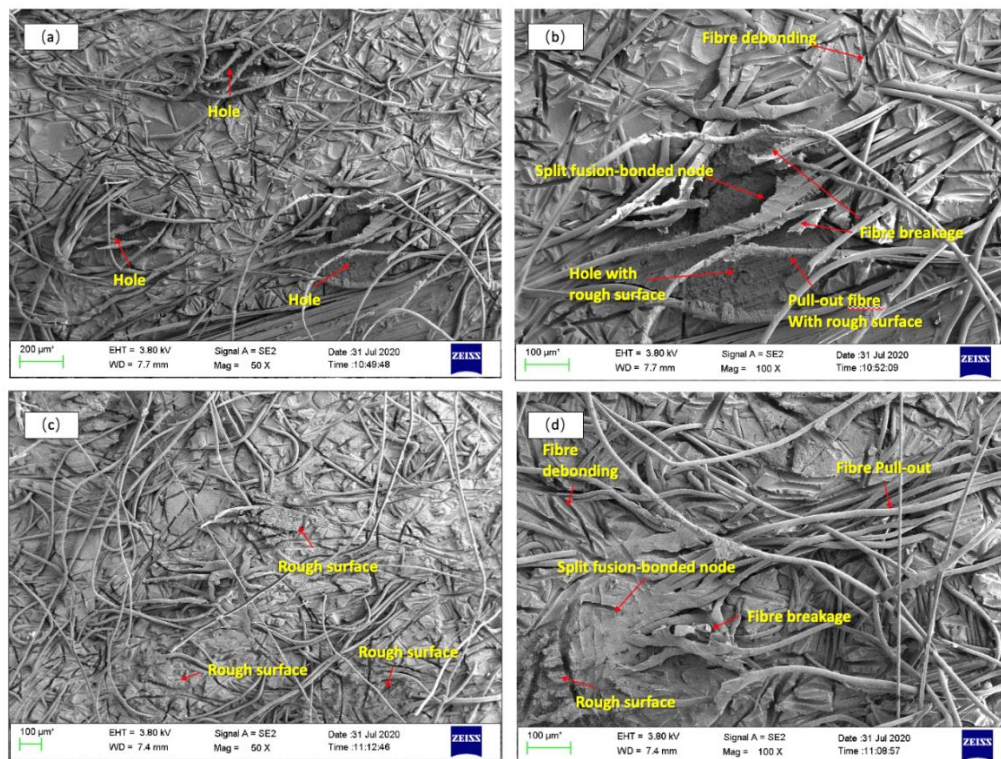


Figure 3-12. SEM images of fracture surface. (a and b) lower surface, (c and d) upper surface.

Figure 3-10b shows two Mode II fracture surfaces. The density of polyamide fibres on the lower surface is much higher than that of the upper surface. A closer section image at the crack region (Figure 3-13b) shows fractures at the CF/veils interface as well as the interlayer. SEM images of Mode II fracture surface show (carbon) fibre interface failure and polyamide fibre pull-out at both surfaces (Figure 3-14). Taking a closer inspection, complete fusion-bond nodes can be recognized, which are partly embedded into the lower fracture surface. Around the nodes, fibre pull-out and broken polyamide fibres resemble exposed plant roots. Granules cannot be found on the fracture surface and are probably concealed under the carbon fibre interface. Partially rough areas can be found near the exposed fusion-bonded nodes, which indicate that these particles were split during the Mode II delamination process. Thus, it is suggested that the cohesive failure occurs at the fusion-bond nodes and granules nearby, while the adhesive failure takes place at the polyamide/epoxy interpenetrating region. The Mode II delamination mostly occurs at the interface between the interlayer and CF ply with a small part transferred in the interlayer, i.e., the interlaminar shear strength of the interlayer is comparatively higher than the interfacial shear strength between the carbon fibre layer and the interlayer. Cracks propagate along the upper CF/veils interface and are reflected at the fusion-bonded nodes, with micro-interfacial failure, fibre pull-out and breakage are the major mechanisms for Mode II toughness improvement.

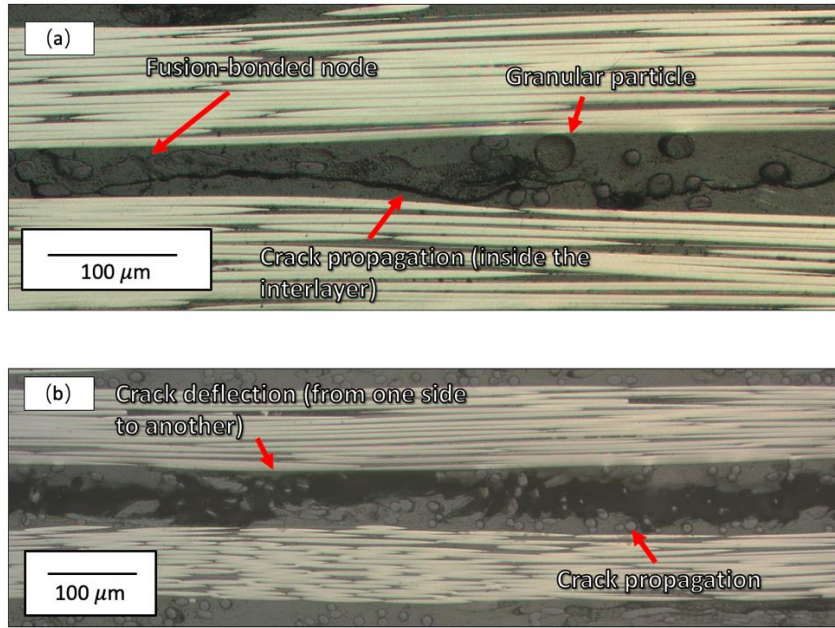


Figure 3-13. Optical observation of crack growth mode. (a) Mode I, (b) Mode II.

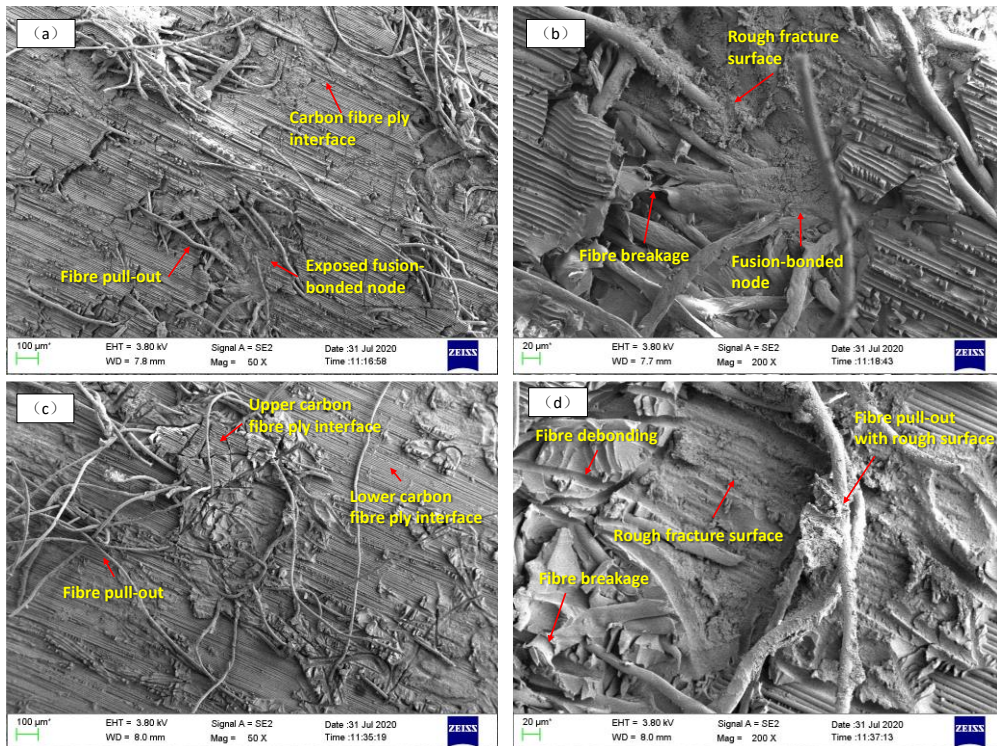


Figure 3-14. SEM images of Mode II fracture surface. (a,b) Lower surface, (c,d) upper surface.

### 3.4.3 Drop-weight impact and residual compression after impact strength

The typical time histories of applied force during impact test are presented in Figure 3-15. The ratio of impact energy to specimen thickness is set as 6.7 J/mm. Both curves show the peak force was generated around 2 ms. The peak impact force acting on NVIC<sup>CAI</sup> is around 2000 N higher than that of Control<sup>CAI</sup>. Table 3-7 shows the typical ultrasonic images of impacted specimens by using UTwin software. According to the images, the delamination area of Control<sup>CAI</sup> was around 20.9%. In contrast, the NVIC<sup>CAI</sup> showed a significant improvement of impact resistance, as the delamination area was reduced to 11.33%.

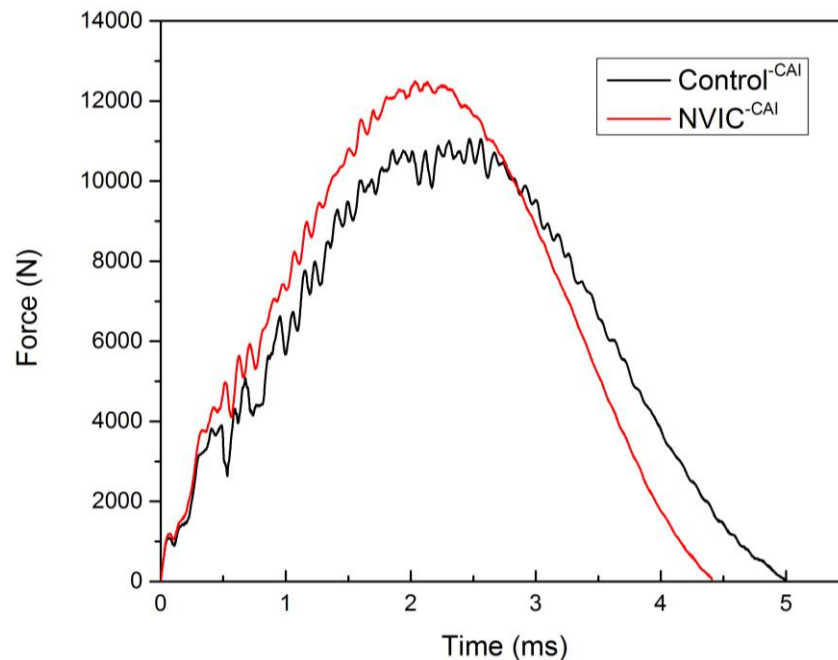


Figure 3-15. Time histories of the applied force during impact test.



**Table 3-7. Characteristics of impact damage area**

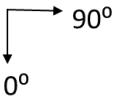
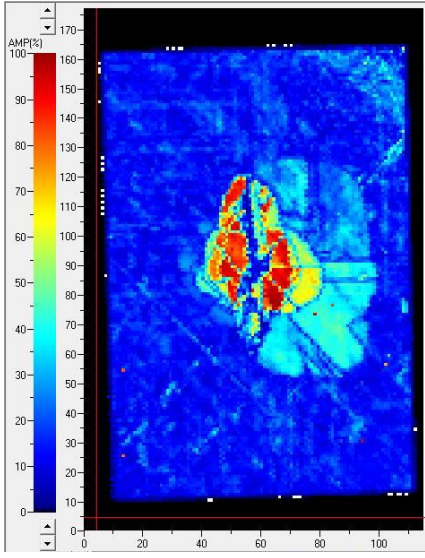
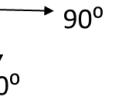
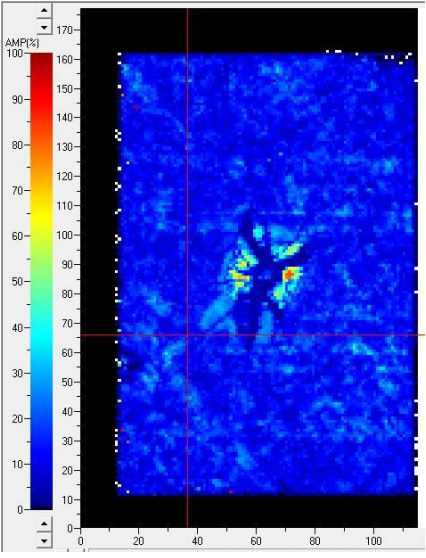
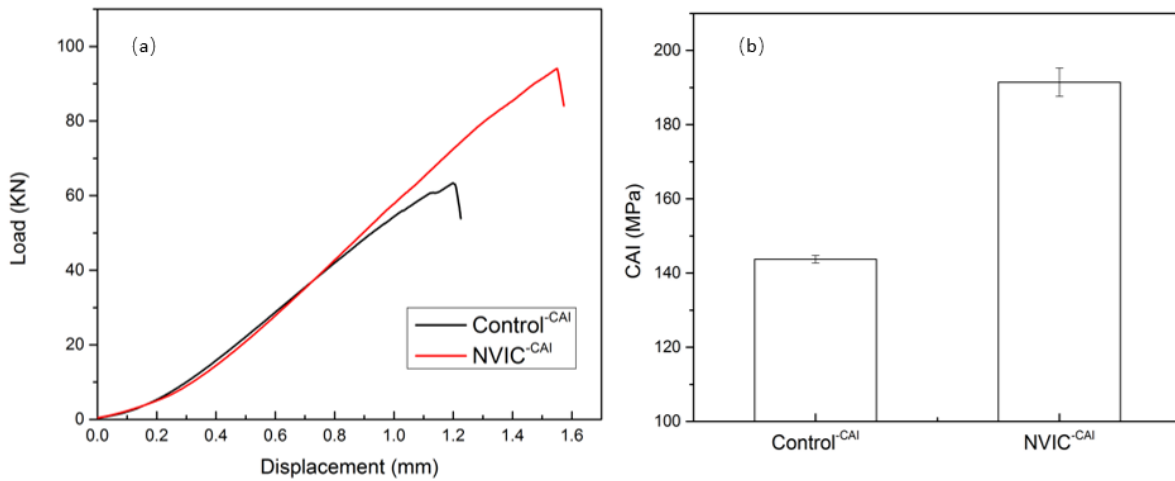
Impact energy (J).	Control <sup>CAI</sup>	NVIC <sup>CAI</sup>
6.7 J/mm	<div style="text-align: center;">  </div> <div style="text-align: center;">  </div> <p style="text-align: center;">Damage area: 3201.1 mm<sup>2</sup> (20.9%)</p>	<div style="text-align: center;">  </div> <div style="text-align: center;">  </div> <p style="text-align: center;">Damage area: 1713.82 mm<sup>2</sup> (11.33%)</p>

Figure 3-16a shows the compressive load-displacement curve for impacted specimens. The Control<sup>CAI</sup> fails under 61.77 KN with 1.21 mm crosshead displacement. Compared with the control specimen, the failure load of NVIC<sup>CAI</sup> increased from 61.77 KN to 92.64 KN with further crosshead displacement (1.55 mm). Although the thickness of NVIC laminate was increased from 4.4 mm to 4.8 mm (Table 3-5), the CAI strength of NVIC<sup>CAI</sup> remained significantly improved from 143.7 MPa to 191.4 MPa, which was approximately 36% higher than Control<sup>CAI</sup> (Figure 3-16b).



**Figure 3-16. Results of residual compression strength test. (a)Load-displacement curve, (b) residual compressive after impact strength.**

Figure 3-17 shows microscope images of the damaged section near the impact point. For Control<sup>-CAI</sup>, many interlaminar delaminations were found, with the 45° diagonal cracks passing through the carbon fibre layers (Figure 3-16a). For NVIC<sup>-CAI</sup>, the impact also caused many 45° diagonal cracks inside the carbon fibre plies. However, closer inspection of the interlayer regions reveals that the delamination mostly happened in the interlayer with the cracks randomly deflecting from one interlayer/lamina interface to another (Figure 3-16b). As mentioned in section 1.4.1 and 1.4.2, the increase of CAI strength of NVIC<sup>-CAI</sup> is significant.

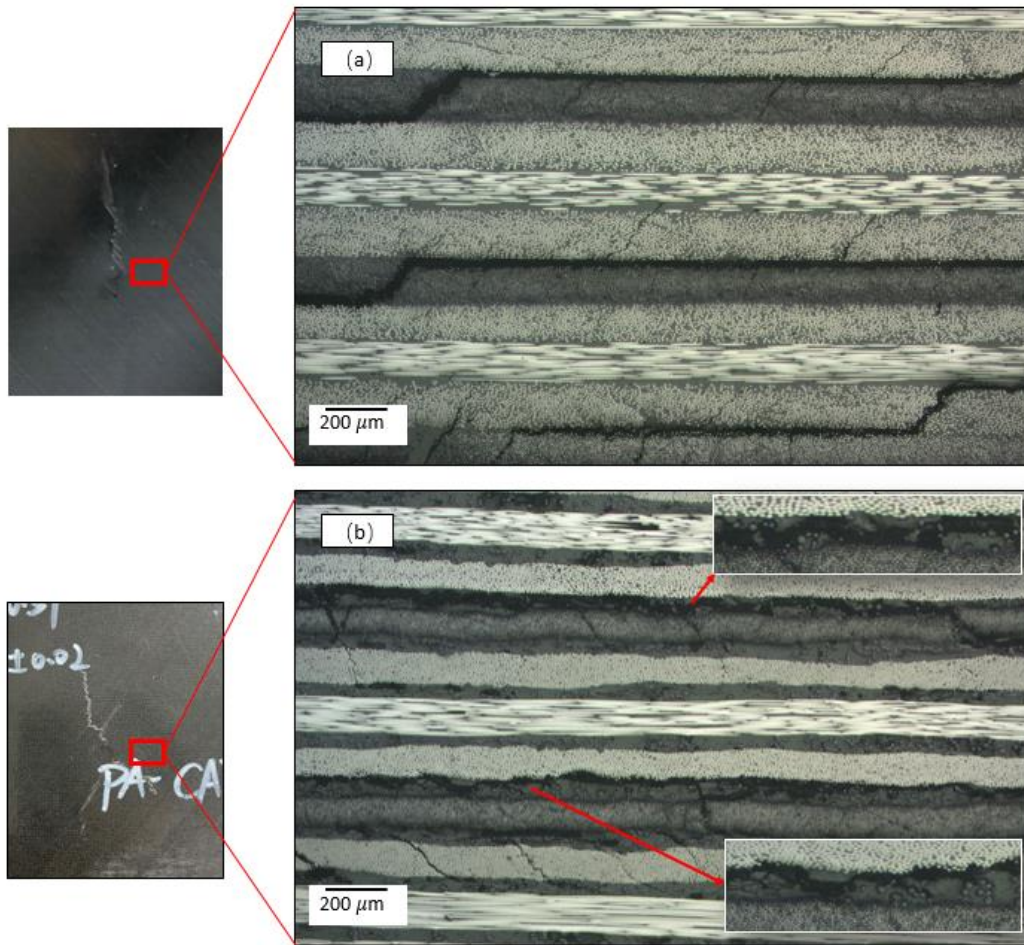


Figure 3-17. Sectional observation near impact head area. (a) Control<sup>-CAI</sup>, (b) NVIC<sup>-CAI</sup>.

### 3.4.4 In-plane mechanical properties

The in-plane mechanical properties of test specimens are listed in Table 3-8, compared with the state-of-art counterparts as reference [39]. It should be noted that the compression strength and modulus of reference is in the 0° fibre direction, which is generally higher than that of test specimens in this paper (0/90°). The overall mechanical properties of the green composites are comparable to the commercial petroleum-sourced products in the aerospace application

**Table 3-8. In-plane mechanical properties of test specimens**

Mechanical property	UNI T	Commercial Product (LY556/T700 Toray 12K, $V_{CF} = 65\%$ , UD) [39]	Control	NVIC
Flexural strength 0°	MPa	1396.96	1187.3±46.4	1049.2±39
Flexural modulus 0°	GPa	104.16	104±2.8	93±1.4
Interlaminar shear strength	MPa	57.83	73±0.2	66.2±1
Tensile strength 0°	MPa	1235.7	2121.9±77.2	1821.6±47.9
Tensile modulus 0°	GPa	134.58	130.1±2.8	115.6±11.1
Compression strength [0/90] <sub>ns</sub>	MPa	674.7 (0°)	469.3±22.8	428.6±26
Compression modulus [0/90] <sub>ns</sub>	GPa	153.73 (0°)	66.8±5.1	55.1±2.2

For green composite specimens, in the 0° tensile test, because the tensile properties of CFRP laminates are generally controlled by the fibre properties, similar load-displacement curves are obtained for all test specimens (Figure 3-18a). With increasing strain, the curves start to zigzag due to the fibre/matrix debonding and the transverse matrix cracking. All specimens failed under similar peak loads (around 21 KN), with a brittle-explosive failure mode. However, because the polyamide veils increase the total thickness of composite laminates, this reduced the carbon fibre volume fraction and the tensile strength and modulus of NVIC was reduced by 14.2% and 11.1%, respectively.

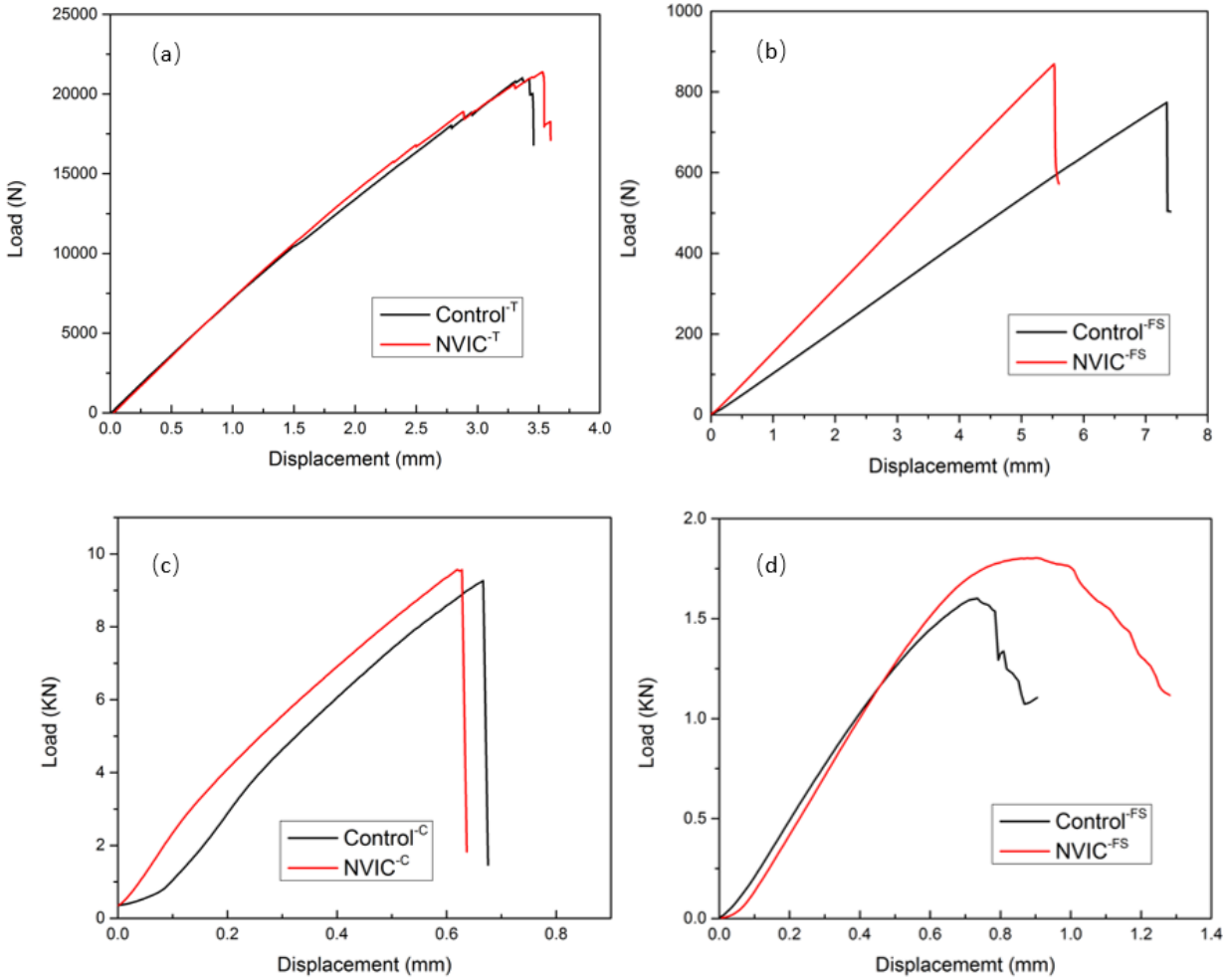


**Figure 3-18. Load-displacement curves of in-plane mechanical test. (a) tensile, (b) flexural, (c) compressive and (d) interlaminar shear.**

In the flexural test, the final failure took place on the compression surface. The load-displacement curves (Figure 3-18b) indicate that the test specimens exhibit a linear elastic behaviour. Compared with the Control<sup>FS</sup>, the NVIC<sup>FS</sup> showed a relatively higher slope and failure load at shorter crosshead displacement. Figure 3-18c shows the typical failure mode from the compressive test. The final failure occurred within the gauge section, including delamination, fibre fracture and matrix cracking. The typical load-displacement curves showed no dramatic difference between the two test groups.

The interlaminar shear strength (ILSS) is one of the limiting design characteristics for composite laminates because of the anisotropic and relatively low mechanical properties in thickness direction. The final failure occurred at the one edge of the test specimen. Compared with the Control<sup>FS</sup>, the peak load of NVIC<sup>FS</sup> was slightly improved (from 1.6 to 1.77 KN) with an obvious ductile stage (Figure 3-18d). However, the calculated ILSS of NVIC<sup>FS</sup> was still reduced from 73.03 MPa to 66.23 MPa (9.3% decrease) due to the increase of cross section area. The overall decrease of in-plane mechanical properties with the addition of non-woven veils was attributed to the reduction of carbon fibre volume fraction of the toughened laminates. It should be noted that the compromise between toughness and mechanical properties is likely to be affected by the polyamide veil itself, i.e., areal weight and fibre architecture. In order to control the loss of mechanical properties, the content of the polyamide veil might be reduced, whilst retaining some toughness improvement. Our further investigations to explore these relations remain ongoing

### **3.5 Conclusion**

We investigated the use of heat-bonded polyamide non-wovens as toughening interleaves in a green composite. Testing revealed useful improvements in toughness and CAI arising from changes in fracture mechanics with the incorporation of interleaves. Extensive study from fracture surfaces has yielded important information about crack propagation and the roles of the different features in the non-woven mat in controlling this.

It is shown that the mechanical properties of the green composite system showed generally comparable performance with its commercial petroleum-sourced counterpart. Whilst the toughening effect was significant and demonstrable for the interleaved green composite, we also determined some reduction in static, in-plane properties due to the higher polymer ratio when interleaves were used. It is likely that some of this reduction could be mitigated by changing the stacking sequence and/or reducing the areal weight of the interleaves. Industrial application potential for a high temperature, toughened, “green composite” should be significant.

### 3.6 References

- [1] M. Darecki, C. Edelstenne, T. Enders, E. Fernandez, P. Hartman, J.-P. Herteman, M. Kerkloh, I. King, P. Ky, M. Mathieu, G. Orsi, G. Schotman, C. Smith, J.-D. Wörner, Flightpath 2050 Europe’s Vision for Aviation, 2011. doi:10.2777/50266.
- [2] X. Liu, X. Yi, J. Zhu, Bio-based epoxies and composites as environmentally friendly alternative materials., in: Q. Guo (Ed.), *Thermosets Struct. Prop. Appl.*, 2nd ed., Elsevier, 2018: pp. 621–637. doi:10.1016/B978-0-08-101021-1.00019-8.
- [3] X. Yi, K. Tserpes, Special issue “ECO-COMPASS: Ecological and multifunctional composites for application in aircraft interior and secondary structures,” *Aerospace*. 6 (2019) 6–8. doi:10.3390/aerospace6020017.
- [4] J. Bachmann, X. Yi, H. Gong, X. Martinez, G. Bugeda, S. Oller, K. Tserpes, E. Ramon, C. Paris, P. Moreira, Z. Fang, Y. Li, Y. Liu, X. Liu, G. Xian, J. Tong, J. Wei, X. Zhang, J. Zhu, S. Ma, T. Yu, Outlook on ecologically improved composites for aviation interior and secondary structures, *CEAS Aeronaut. J.* 9 (2018) 533–543. doi:10.1007/s13272-018-0298-z.
- [5] X. Yi, X. Zhang, J. Tong, G. Xian, *BIO-COMPOSITES: Development of Bio-Composites for Green Aviation and Ground Vehicles*, Sampe J. (2018) 16–26.

- [6] X.F. Zhang, Y.Q.Q.G. Wu, J.H. Wei, J.F. Tong, X.S. Yi, Curing kinetics and mechanical properties of bio-based composite using rosin-sourced anhydrides as curing agent for hot-melt prepreg, *Sci. China Technol. Sci.* 60 (2017) 1318–1331. doi:10.1007/s11431-016-9029-y.
- [7] S. Kumar, S.K. Samal, S. Mohanty, S.K. Nayak, Study of curing kinetics of anhydride cured petroleum-based (DGEBA) epoxy resin and renewable resource based epoxidized soybean oil (ESO) systems catalyzed by 2-methylimidazole, *Thermochim. Acta.* 654 (2017) 112–120. doi:10.1016/j.tca.2017.05.016.
- [8] F. Hu, S.K. Yadav, J.J. La Scala, J.M. Sadler, G.R. Palmese, Preparation and Characterization of Fully Furan-Based Renewable Thermosetting Epoxy-Amine Systems, *Macromol. Chem. Phys.* 216 (2015) 1441–1446. doi:10.1002/macp.201500142.
- [9] A. Marotta, N. Faggio, V. Ambrogi, P. Cerruti, G. Gentile, A. Mija, Curing Behavior and Properties of Sustainable Furan-Based Epoxy/Anhydride Resins, *Biomacromolecules.* 20 (2019) 3831–3841. doi:10.1021/acs.biomac.9b00919.
- [10] D.W.Y. Wong, L. Lin, P.T. McGrail, T. Peijs, P.J. Hogg, Improved fracture toughness of carbon fibre/epoxy composite laminates using dissolvable thermoplastic fibres, *Compos. Part A Appl. Sci. Manuf.* 41 (2010) 759–767. doi:10.1016/j.compositesa.2010.02.008.
- [11] P. Van Velthem, W. Ballout, D. Daoust, M. Sclavons, F. Cordenier, E. Henry, D. Dumont, V. Destoop, T. Pardoën, C. Bailly, A Influence of thermoplastic diffusion on morphology gradient and on delamination toughness of RTM-manufactured composites, *Compos. PART A.* 72 (2015) 175–183. doi:10.1016/j.compositesa.2015.02.012.
- [12] D.J. Hourston, J.M. Lane, The toughening of epoxy resins with thermoplastics: 1. Trifunctional epoxy resin-polyetherimide blends, *Polymer (Guildf).* 33 (1992) 1379–1383. doi:10.1016/0032-3861(92)90110-l.
- [13] N.G. Yun, Y.G. Won, S.C. Kim, Toughening of epoxy composite by dispersing polysulfone particle to form morphology spectrum, *Polym. Bull.* 52 (2004) 365–372. doi:10.1007/s00289-004-0293-x.



- [14] Z. Sun, L. Xu, Z. Chen, Y. Wang, R. Tusiime, C. Cheng, S. Zhou, Y. Liu, M. Yu, H. Zhang, Enhancing the mechanical and thermal properties of epoxy resin via blending with thermoplastic polysulfone, *Polymers (Basel)*. 11 (2019). doi:10.3390/polym11030461.
- [15] H. Chen, C. Su, T. Huang, T. Li, Investigation of the relationship between morphology and tribological properties of an epoxy resin based on tetraglycidyl 4,4'-diaminodiphenylmethane modified with polyetherimide oligomers, *J. Appl. Polym. Sci.* 131 (2014) n/a-n/a. doi:10.1002/app.39863.
- [16] Z. Wu, X.S. Yi, A. Wilkinson, Interlaminar fracture toughness of carbon fibre/RTM6-2 composites toughened with thermoplastic-coated fabric reinforcement, *Compos. Part B Eng.* 130 (2017) 192–199. doi:10.1016/j.compositesb.2017.08.003.
- [17] J. Zhang, Q. Guo, B.L. Fox, Study on thermoplastic-modified multifunctional epoxies : Influence of heating rate on cure behaviour and phase separation, *Compos. Sci. Technol.* 69 (2009) 1172–1179. doi:10.1016/j.compscitech.2009.02.016.
- [18] W. Gan, Y. Yu, M. Wang, Q. Tao, S. Li, Viscoelastic effects on the phase separation in thermoplastics-modified epoxy resin, *Macromolecules*. 36 (2003) 7746–7751. doi:10.1021/ma034649a.
- [19] M.T. Aljarrah, N.R. Abdelal, Improvement of the mode I interlaminar fracture toughness of carbon fiber composite reinforced with electrospun nylon nanofiber, *Compos. Part B Eng.* 165 (2019) 379–385. doi:10.1016/j.compositesb.2019.01.065.
- [20] N. Zheng, Y. Huang, H.Y. Liu, J. Gao, Y.W. Mai, Improvement of interlaminar fracture toughness in carbon fiber/epoxy composites with carbon nanotubes/polysulfone interleaves, *Compos. Sci. Technol.* 140 (2017) 8–15. doi:10.1016/j.compscitech.2016.12.017.
- [21] H. Zhou, X. Du, H.Y. Liu, H. Zhou, Y. Zhang, Y.W. Mai, Delamination toughening of carbon fiber/epoxy laminates by hierarchical carbon nanotube-short carbon fiber interleaves, *Compos. Sci. Technol.* 140 (2017) 46–53. doi:10.1016/j.compscitech.2016.12.018.
- [22] P.J. Hogg, Toughening of thermosetting composites with thermoplastic fibres, *Mater. Sci. Eng. A*. 412 (2005) 97–103. doi:10.1016/j.msea.2005.08.028.

- [23] F. Xu, B. Yang, L. Feng, D. Huang, M. Xia, Improved interlaminar fracture toughness and electrical conductivity of CFRPs with non-woven carbon tissue interleaves composed of fibers with different lengths, *Polymers (Basel)*. 12 (2020) 1–12. doi:10.3390/POLYM12040803.
- [24] V.A. Ramirez, P.J. Hogg, W.W. Sampson, The influence of the nonwoven veil architectures on interlaminar fracture toughness of interleaved composites, *Compos. Sci. Technol.* 110 (2015) 103–110. doi:10.1016/j.compscitech.2015.01.016.
- [25] Q. Cheng, Z. Fang, X. Yi, X. An, B. Tang, Y. Xu, “ Ex Situ ” Concept for Toughening the RTMable BMI Matrix Composites , Part I : Improving the Interlaminar Fracture Toughness, *J. Appl. Polym. Sci.* 109 (2008). doi:10.1002/app.
- [26] J. Nasser, L. Zhang, H. Sodano, Aramid nanofiber interlayer for improved interlaminar properties of carbon fiber/epoxy composites, *Compos. Part B Eng.* 197 (2020). doi:10.1016/j.compositesb.2020.108130.
- [27] X. Yi, M. Guo, G. Liu, W. Zhao, L. Liu, H. Cui, Composite conductive sheet, fabricating method and application thereof, EP.2687364B1, 2015.
- [28] D. Hu, X. Yi, M. Jiang, G. Li, X. Cong, X. Liu, C. Rudd, Development of highly electrically conductive composites for aeronautical applications utilizing bi-functional composite interleaves, *Aerosp. Sci. Technol.* 98 (2020) 105669. doi:10.1016/j.ast.2019.105669.
- [29] M. Guo, X. Yi, C. Rudd, X. Liu, Preparation of highly electrically conductive carbon- fi ber composites with high interlaminar fracture toughness by using silver-plated interleaves, *Compos. Sci. Technol.* 176 (2019) 29–36. doi:10.1016/j.compscitech.2019.03.014.
- [30] X. Liu, W. Xin, J. Zhang, Rosin-based acid anhydrides as alternatives to petrochemical curing agents, *Green Chem.* 11 (2009) 1018–1025. doi:10.1039/b903955d.
- [31] ASTM D5528-01 Standard Test Method for Mode I Interlaminar Fracture Toughness of Unidirectional Fiber-Reinforced Polymer Matrix Composites, ASTM Int. (n.d.).
- [32] ASTM D7905 Standard Test Method for Mode II Interlaminar Fracture Toughness of Unidirectional Fiber-Reinforced Polymer Matrix Composites, ASTM Int. (n.d.).

[33] ASTM D7136/D7136M - 12 Standard Test Method for Measuring the Damage Resistance of a Fiber-Reinforced Polymer Matrix Composite to a Drop-Weight Impact Event, ASTM Int. (n.d.).

[34] ASTM D7137 / D7137M - 17 Standard test method for compressive residual strength properties of damaged polymer matrix composite plates, ASTM Int. (n.d.). [www.astm.org](http://www.astm.org).

[35] ASTM D790 - 17 Standard Test Methods for Flexural Properties of Unreinforced and Reinforced Plastics and Electrical Insulating Materials, ASTM Int. (n.d.).

[36] ASTM D2344 / D2344M - 16 Standard test method for short-beam strength of polymer matrix composite materials and their laminates, ASTM Int. (n.d.).

[37] ASTM D6641 / D6641M - 16e1 Standard Test Method for Compressive Properties of Polymer Matrix Composite Materials Using a Combined Loading Compression ( CLC ) Test Fixture, ASTM Int. (n.d.).

[38] ASTM D3039 / D3039M - 17 Standard Test Method for Tensile Properties of Polymer Matrix Composite Materials, ASTM Int. (n.d.).

[39] C. Venkateshwar Reddy, P. Ramesh Babu, R. Ramnarayanan, D. Das, Mechanical Characterization of Unidirectional Carbon and Glass/Epoxy Reinforced Composites for High Strength Applications, Mater. Today Proc. 4 (2017) 3166–3172.

doi:10.1016/j.matpr.2017.02.201.

## **Chapter 4: Development of carbon fibre epoxy composites with high electrical conductivity and fracture toughness utilizing bi-functional composite interleaves**

Status: This chapter has been published in Aerospace Science and Technology

Authors: Dongyuan Hu, Xiaosu Yi, Minqiang Jiang, Genghong Li, Xiaoye Cong, Xiaoling Liu, Chris Rudd

In chapter 3, a high toughness green epoxy based CFRP with promising mechanical properties was prepared by interleaving a special designed polyamide non-woven veil. The non-woven veils were well wetted by the epoxy matrix to form an interpenetrating network as interlayers, which is the key for interlaminar fracture toughness and CAI improvement. In addition, interleaving the veils did not change the inherent state of carbon fibre layers, the in-plane properties of toughened CFRPs were well reserved.

Following the positive results in chapter 3, the next issue is how to simultaneously improve the fracture toughness and electrical conductivity for aeronautical CFRPs. Here, a proprietary electroless copper-nickel plated polyester non-woven veil was selected as the interleaf material to produce the multifunctional CFRPs. The tests of interlaminar toughness and electrical conductivity were performed. Then the discussion and conclusion in terms of the significant improvement in toughness and electrical conductivity are presented.



## Development of highly electrically conductive composites for aeronautical applications utilizing bi-functional composite interleaves



Dongyuan Hu<sup>a</sup>, Xiaosu Yi<sup>a,b,\*</sup>, Minqiang Jiang<sup>a</sup>, Genghong Li<sup>a</sup>, Xiaoye Cong<sup>a</sup>, Xiaoling Liu<sup>a,\*</sup>, Chris Rudd<sup>c</sup>

<sup>a</sup> Faculty of Science and Engineering, The University of Nottingham Ningbo China, 199 Taikang East Road, Ningbo, 315100, China

<sup>b</sup> National Key Laboratory of Advanced Composites, AVIC Composite Technology Center, Beijing, 101300, China

<sup>c</sup> James Cook University, Singapore, 149 Sims Drive, 387380, Singapore

### ARTICLE INFO

#### Article history:

Received 18 September 2019

Received in revised form 13 December 2019

Accepted 23 December 2019

Available online 3 January 2020

#### Keywords:

Interlaminar fracture toughness

Electrical conductivity

Functionalized Interlayer Technology

Bi-functionality

### ABSTRACT

With the wide application of composite materials in modern aerospace industry, multifunctional carbon fibre composites are likely to play an important role in next generation aircraft. Here, carbon fibre reinforced epoxy composites were produced by using Functionalized Interleaf Technology (FIT). The electroless copper-nickel plated polyester veils (CNPV) were used as the interleaves to replace the initial resin-rich interlaminar regions with functional interlayers. The latter shows useful toughening efficiency, in which the  $G_{IC}$  and  $G_{IIC}$  values for interleaved specimens increased by 59% and 31%, respectively. At the same time, the in-plane ( $\sigma_{xy}$ ) and through-thickness ( $\sigma_z$ ) electrical conductivities were also improved from 74.12 S/cm to 1079.6 S/cm and  $1.5 \times 10^{-3}$  S/cm to 5.29 S/cm, respectively. Moreover, it is found that the effective electric contact area at electrodes was increased by incorporating additional functionalized veils. Therefore, the interleaf material can be characterized by its bi-functionality as it provides both toughening efficiency in the interlaminar region and the ability to form an electrically conductive path crossing the resin-rich interlaminar layer, perpendicular to the laminate plane.

© 2020 Elsevier Masson SAS. All rights reserved.

### 1. Introduction

The increasingly use of carbon fibre reinforced polymers (CFRPs) for aircraft structures presents several advantages in terms of weight and maintenance but leads to differences in the electrical functioning of aircraft systems, compared to a metallic aircraft structure. To achieve similar electrical, environmental and mechanical performance of aircraft structures made of different materials, typically metals and CFRPs, a highly distributed conductive network, known as the Electrical Structure Network (ESN) is necessarily constructed and installed to offer the electrical and environmental conditions required for the correct functioning of aircraft systems (Fig. 1). ESN is a metallic redundant and passive network made of thousands of structural metallic elements, mechanical elements and specific ESN components [1]. Because of the inherent electrical connection between the ESN and CFRP structures and skins, the aircraft designer has to ensure the aircraft structural integrity, i.e. loss of mechanical properties in the CFRPs due to the joule effect (i.e. Ohmic heating). Obviously, if

CFRP aerostructures were multifunctional, i.e. if they possessed high electrical conductivities similar to metals while maintaining their excellent mechanical properties, the joule effect of the CFRPs would be eliminated. Moreover, it would be easier for the aircraft designer not only to install the electrical system, but also to handle the issues like Electromagnetic Interference (EMI), Electromagnetic Shielding (EMS) and Lightning Strike Protection (LSP) of the composites fuselage aircraft [2,3]. Therefore, research and development of structurally electrically conductive CFRPs is an attractive goal. However, achieving highly electrically conductivity of the state-of-the-art CFRPs without sacrificing structural performance via, e.g. interlaminar fracture toughness remains a technical challenge.

Aerostructures from CFRPs are typically laminated material system consisting of a number of carbon fibre plies, resulting in a significant anisotropy in electrical and mechanical properties, where the out-plane properties are particularly critical. These include the through-thickness electrical conductivity (TTEC), the interlaminar fracture toughness and Compression After Impact strength (CAI) [4–7]. Many methods have been studied for improving the overall toughness and electrical conductivities without paying special attention to the anisotropy of the laminate. One such way to enhance electrical conductivity is to blend conductive fillers into the matrix

\* Corresponding authors.

E-mail addresses: Xiaosu.yi@nottingham.edu.cn (X. Yi),

Xiaoling.liu@nottingham.edu.cn (X. Liu).

<https://doi.org/10.1016/j.aescte.2019.105669>

1270-9638/© 2020 Elsevier Masson SAS. All rights reserved.

**Blank page**

## 4.1 Abstract

With the wide application of composite materials in modern aerospace industry, multifunctional carbon fibre composites are likely to play an important role in next generation aircraft. Here, carbon fibre reinforced epoxy composites were produced by using Functionalized Interleaf Technology (FIT). The electroless copper-nickel plated polyester veils (CNPV) were used as the interleaves to replace the initial resin-rich interlaminar regions with functional interlayers. The latter shows useful toughening efficiency, in which the  $G_{Ic}$  and  $G_{IIc}$  values for interleaved specimens increased by 59% and 31%, respectively. At the same time, the in-plane ( $\sigma_{xy}$ ) and through-thickness ( $\sigma_z$ ) electrical conductivities were also improved from 74.12 S/cm to 1079.6 S/cm and  $1.5 \times 10^{-3}$  S/cm to 5.29 S/cm, respectively. Moreover, it is found that the effective electric contact area at electrodes was increased by incorporating additional functionalized veils. Therefore, the interleaf material can be characterized by its bi-functionality as it provides both toughening efficiency in the interlaminar region and the ability to form an electrically conductive path crossing the resin-rich interlaminar layer, perpendicular to the laminate plane.

Key words: Interlaminar fracture toughness; Electrical conductivity; Functionalized Interlayer Technology; Bi-functionality

## 4.2 Introduction

The increasingly use of carbon fibre reinforced polymers (CFRPs) for aircraft structures presents several advantages in terms of weight and maintenance but leads to

differences in the electrical functioning of aircraft systems, compared to a metallic aircraft structure. To achieve similar electrical, environmental and mechanical performance of aircraft structures made of different materials, typically metals and CFRPs, a highly distributed conductive network, known as the Electrical Structure Network (ESN) is necessarily constructed and installed to offer the electrical and environmental conditions required for the correct functioning of aircraft systems (Figure 4-1). ESN is a metallic redundant and passive network made of thousands of structural metallic elements, mechanical elements and specific ESN components [1]. Because of the inherent electrical connection between the ESN and CFRP structures and skins, the aircraft designer has to ensure the aircraft structural integrity, i.e., loss of mechanical properties in the CFRPs due to the joule effect (i.e. Ohmic heating). Obviously, if CFRP aerostructures were multifunctional, i.e., if they possessed high electrical conductivities similar to metals while maintaining their excellent mechanical properties, the joule effect of the CFRPs would be eliminated. Moreover, it would be easier for the aircraft designer not only to install the electrical system, but also to handle the issues like Electromagnetic Interference (EMI), Electromagnetic Shielding (EMS) and Lightning Strike Protection (LSP) of the composites fuselage aircraft [2,3]. Therefore, research and development of structurally electrically conductive CFRPs is an attractive goal. However, achieving highly electrically conductivity of the state-of-the-art CFRPs without sacrificing structural performance via, e.g., interlaminar fracture toughness remains a technical challenge.



Aerostructures from CFRPs are typically laminated material system consisting of a number of carbon fibre plies, resulting in a significant anisotropy in electrical and mechanical properties, where the out-plane properties are particularly critical. These include the through-thickness electrical conductivity (TTEC), the interlaminar fracture toughness and Compression After Impact strength (CAI) [4–7]. Many methods have been studied for improving the overall toughness and electrical conductivities without paying special attention to the anisotropy of the laminate. One such way to enhance electrical conductivity is to blend conductive fillers into the matrix resins. The filler particles studied covers diverse conductive materials, and the particle sizes ranges from nano-scale to micro-scales [8–14]. As shown in Table 4-1, various levels of electrical conductivity improvements are achieved. However, it may be far away from the technical figures required for aircraft application in terms of the balanced electrical and mechanical properties.

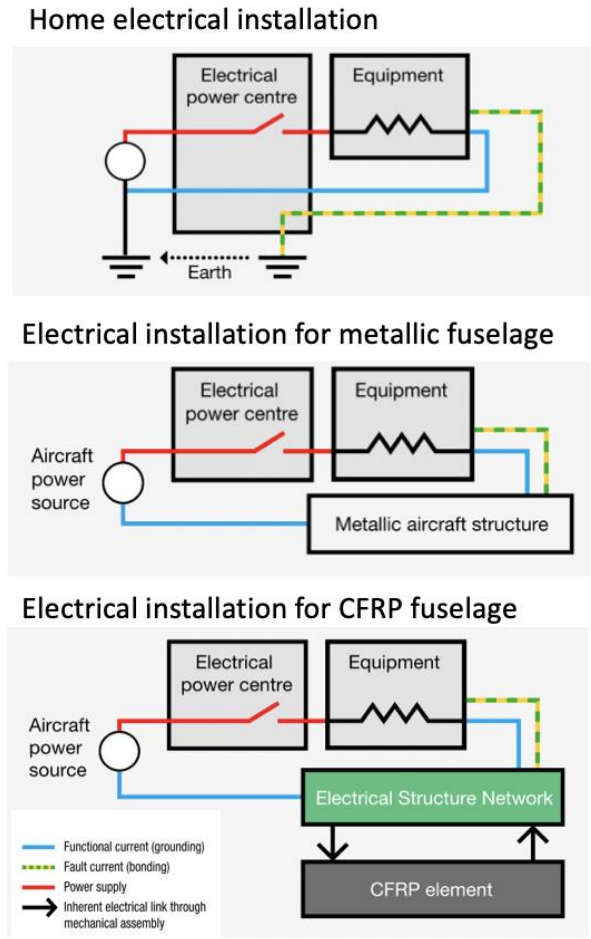


**Figure 4-1. Electrical installation principle of ENS applied to CFRP fuselage. [1]**

Focusing on the interlaminar region, selective toughening technology has also been investigated using different textiles as interleaf materials and a series of positive results have been achieved [15–22]. Yi et al. recently reported that not only the interlaminar fracture toughness were significantly improved by interleaving electrically functionalized polymer fibre veils, but also the electrical conductivities [23–26]. Thus, the technology is termed Functionalized Interlayer Technology (FIT) [27,28]. The intention of the present paper is to further explore the FIT concept to simultaneously increase the electrical conductivity, particularly the through-thickness electrical conductivity (TTEC), and the

interlaminar fracture toughness. Multifunctional CFRPs with high electrical conductivity and high interlaminar fracture toughness were produced by interleaving polyester veils plated with electroless copper and nickel. In order to investigate the electrical conductivity of the laminated system further, the conductive veils were also placed at the top and bottom surfaces to look at the effect of the electrical contact resistance, in comparison with control specimens.

Table 4-1. Electrical conductivity of composite specimens studied

Specimens	Electrical conductivity (S/cm)		Fibre volume fraction $V_{CF}$ (%)
	Through-thickness	In-plane	
Filled with 2 wt% SWNTs (0/90) [9]	0.018	142.85	-
3 wt% CB-CC (UD) [11]	0.556	X-19.61 Y-0.91	65.4
Interleaved with 2 vol% GNP (0/90) [12]	0.155	166.67	56.7
Filled with 2 vol% CNTs (Modelling) [8]	0.85	234.23	70
1 wt% CNTs on carbon fibre surface (0/90) [10]	0.01	-	-

Focusing on the interlaminar region, selective toughening technology has also been investigated using different textiles as interleaf materials and a series of positive results have been achieved[48,56,57,139–143]. Yi et, al. recently reported that not only the interlaminar fracture toughness were significantly improved by interleaving electrically functionalized polymer fibre veils, but also the electrical conductivities[136–138,144]. Thus, the technology is termed Functionalized Interlayer Technology (FIT) [89,145]. The

intention of the present paper is to further explore the FIT concept to simultaneously increase the electrical conductivity, particularly the through-thickness electrical conductivity (TTEC), and the interlaminar fracture toughness. Multifunctional CFRPs with high electrical conductivity and high interlaminar fracture toughness were produced by interleaving polyester veils plated with electroless copper and nickel. In order to investigate the electrical conductivity of the laminated system further, the conductive veils were also placed at the top and bottom surfaces to look at the effect of the electrical contact resistance, in comparison with control specimens.

## 4.3 Materials and methods

### 4.3.1 Materials

A commercial unidirectional carbon (UD) fibre/epoxy prepreg, designated as UD1500/180 was used in the study as the base material to fabricate the composite specimens. The prepreg comprised T700 carbon fibre and a 180°C cure epoxy resin of YPH-170, with 35 wt% resin content. The areal weight of the prepreg was 212 g/m<sup>2</sup> and nominal ply thickness was 0.15 mm.

A proprietary electroless copper-nickel plated polyester veil (CNPV) was used as the interleaf material, provided by M<sup>2</sup>IW Co Ltd, Beijing, China [27]. The areal weight and nominal thickness were 49 g/m<sup>2</sup> and 60 µm, respectively. The diameter of the polyester fibre was approximately 37 µm. The in-plane volume conductivity of the CNPV was approximately 5.2 × 10<sup>3</sup> S/cm, determined using the experimental procedure detailed below. Figure 4-2 shows microscopic images of the CNPV. It can be seen that the polyester fibres are randomly distributed and joined by bonded nodes, forming an electrically functionalized veil (Figure 4-2a). The shiny surface (Figure 4-2b) of each plated fibre can be easily observed. The coating thickness was approximately 3 µm (Figure 4-2c). The EDS images confirms the presence of nickel and copper elements in the coating (Figure 4-2d). It is also observable that the cross section of each polyester fibre is irregular and the coating thickness is nonuniform.

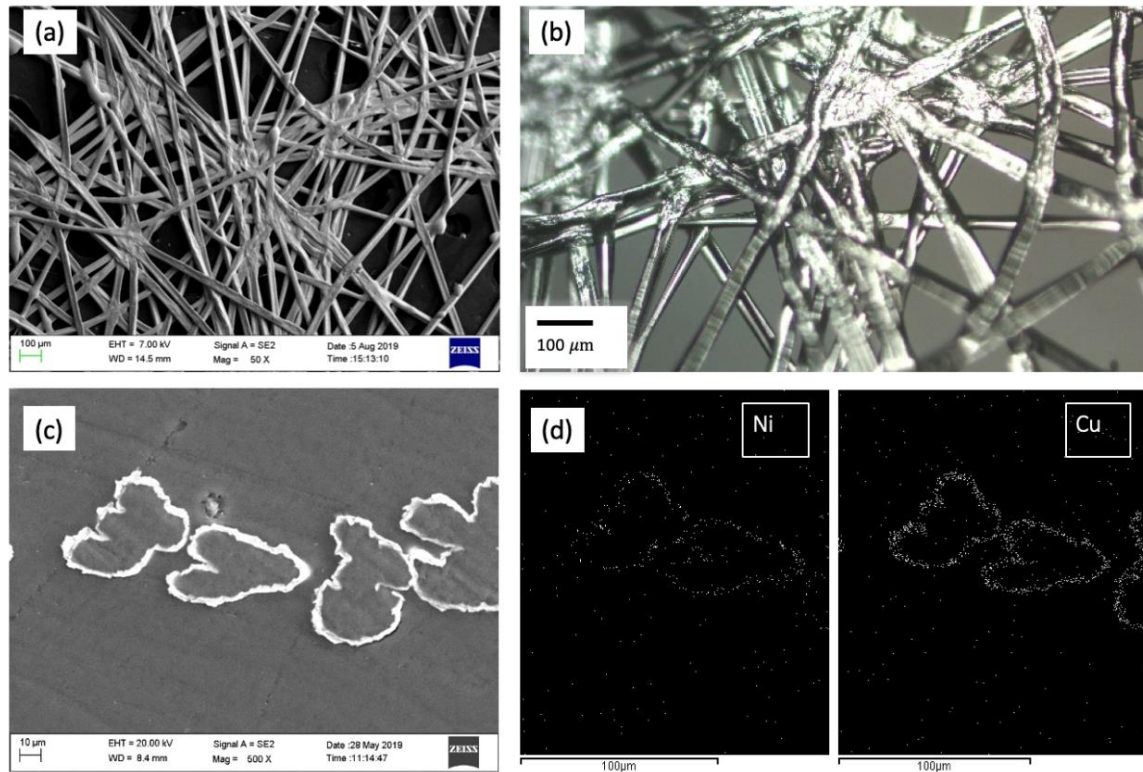


**Figure 4-2. Images of the copper-nickel plated polyester veil (CNPV). (a) Plane view of CNPV by SEM, (b) Plane view of CNPV by optical microscopy, (c) Section view of CNPV by SEM (d) EDS at the cross section of CNPV fibres**

### **4.3.2 Fabrication of composite laminates**

#### **4.3.2.1 Manufacturing**

All the composite laminates were manufactured by vacuum bag assisted compression moulding. The UD1500/180 prepregs and CNPVs were first cut to 290 mm×290 mm. The laminate preforms were then placed on the tool plates. Figure 4-3 shows the schematic of manufacturing set-up. A rigid hollow steel mould with 300 mm×300 mm inner area was used to hot press to the target thickness of the specimens (i.e. 4 mm for Mode I and II tests, 5 mm for electrical conductivity test). The laminate preforms were

degassed in a vacuum bag under room temperature. After the pressure reached 0.1 MPa, the preforms were transferred to the hot presser and dwelled at 70°C for 30 min. Then 5 MPa pressure was applied and the curing temperature was increased to 180°C in 30 minutes. Specimens were dwelled at 180°C for 120 minutes. Figure 4-4 gives the information of curing procedure. Cured composite laminates were removed from press and cooled to room temperature with vacuum applied throughout the cycle.

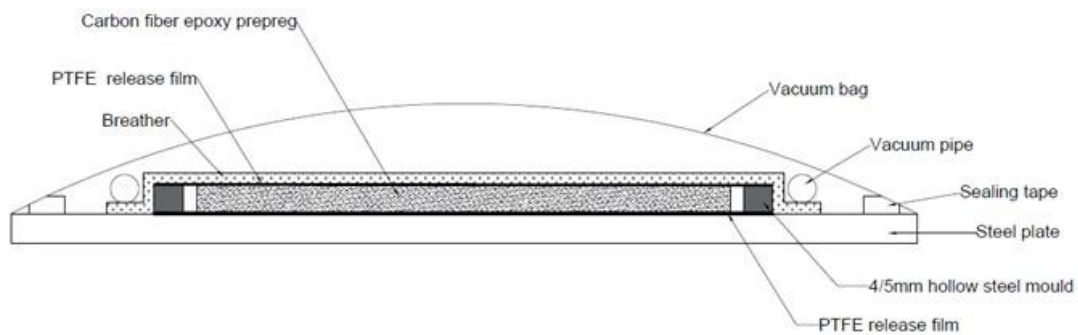


**Figure 4-3. Schematic diagrams of manufacturing set-up.**

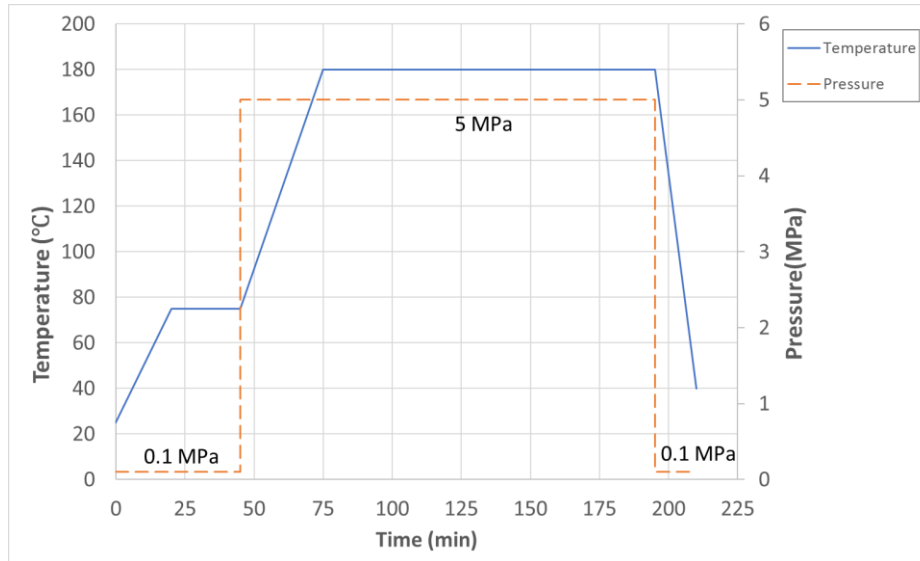


**Figure 4-4. Curing procedure of CFRP specimens**

#### 4.3.2.2 Fracture toughness specimens

Figure 4-5 shows the schematic diagram of FIT composite laminates for toughness study. 26 plies of UD1500/180 were hand-stacked in  $0^{\circ}$  orientation for Mode I and II interlaminar fracture toughness test specimens. Symmetrically at the central layer, i.e., between plies 13 and 14, a  $10\ \mu\text{m}$  thick release film (100 mm $\times$ 300 mm) was placed at one end to simulate an initial crack for manufacturing of the control specimen, designated as Control<sup>t</sup>. At another end of the symmetrically central layer, one single CNPV was additionally interleaved for manufacturing of the specimen according to the Functional Interlayer Technology (FIT), referred to FIT<sup>t</sup>. Table 4-2 gives the characteristics of specimens for toughening study.



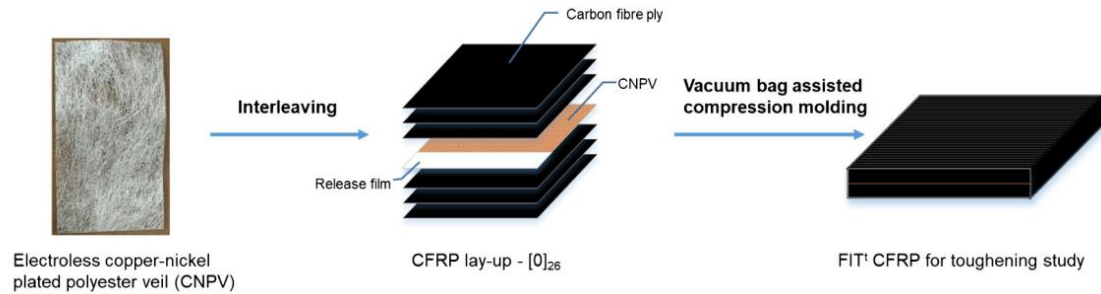


**Figure 4-5. Schematic diagram of FIT composite laminates for toughness study.**

**Table 4-2. Characteristics of test specimens for toughness study**

Specimen	Lay-up	Thickness (mm)	Carbon Fibre Volume Fraction %	Note
Control <sup>t</sup>	[0] <sub>26</sub>	3.8±0.1	54.64	No interleaf
FIT <sup>t</sup>	[0] <sub>26</sub>	3.8±0.1	54.36	Single CNPV between ply13 and ply 14

#### 4.3.2.3 Electrical conductivity specimens

Figure 4-6 shows the schematic diagram of FIT<sup>e</sup> composite laminates for electrical conductivity study. The stacking sequence of control laminate was [+45/0/-45/90]<sub>5s</sub>, designated as Control<sup>e</sup>. The interleaved laminates were designed as FIT<sup>e</sup>. In order to obtain a similar thickness to Control<sup>e</sup>, the stacking sequence of FIT<sup>e</sup> laminates was reduced to [+45/0/-45/90]<sub>4s</sub>, with CNPV veils putting in between each ply (i.e., FIT<sup>e</sup><sub>1</sub>). Two CNPVs were additionally placed at top and bottom surfaces to study the effect of surface electrical contact resistance, referred as FIT<sup>e</sup><sub>2</sub>. Table 4-3 gives the characteristics of specimens for the electrical conductivity study and Figure 4-7 shows the cured composite laminates as produced.

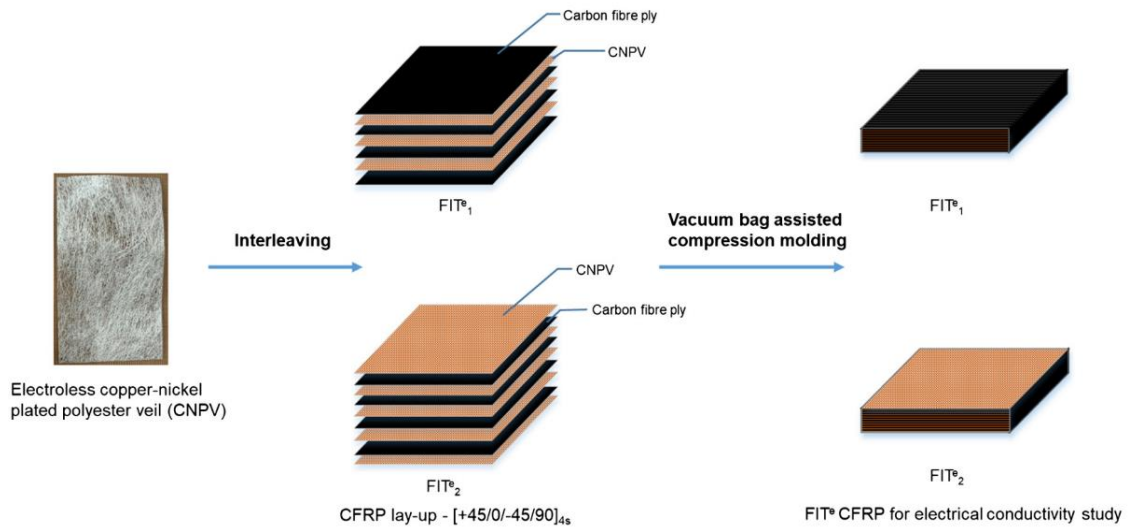


Figure 4-6. Schematic diagram of FIT<sup>o</sup> composite laminates for electrical conductivity study.



Figure 4-7. Cured composite laminates. (a)FIT<sup>o</sup><sub>2</sub>, (b) Control<sup>o</sup>

**Table 4-3. Characteristics of test specimens for electrical conductivity study**

<b>Specimen</b>	<b>Lay-up</b>	<b>Thickness (mm)</b>	<b>Carbon fibre volume fraction %</b>	<b>Note</b>
Control <sup>e</sup>	[+45/0/-45/90] <sub>5s</sub>	5.4±0.1	59.06	No interleaf
<i>FIT</i> <sup>e</sup> <sub>1</sub>	[+45/0/-45/90] <sub>4s</sub>	5.1±0.1	49.17	Fully interleaved with 31 CNPVs veils between each carbon fibre ply
<i>FIT</i> <sup>e</sup>				
<i>FIT</i> <sup>e</sup> <sub>2</sub>	[+45/0/-45/90] <sub>4s</sub>	5.1±0.1	49.10	Fully interleaved and additionally covering the top and bottom surfaces with the CNPVs

#### **4.3.3 Determination of interlaminar fracture toughness**

The interlaminar fracture toughness tests were conducted on an MTS E42 universal test machine with a 5KN load cell. Five specimens were tested for each group. The Mode I test followed ASTM D5228 [29]. Double Cantilever Beam (DCB) test specimens were prepared with dimensions: width  $b=25$  mm, length  $L=180$  mm and nominal thickness  $t=3.8\pm 0.1$  mm. The piano hinges were bonded by epoxy adhesive and the distance between load point and insert end was 50 mm, as the initial crack length  $a_0$ . In order to observe the crack propagation during the test, a thin layer of white water-based marking fluid was coated on one edge of the specimen. The first 5 mm from the insert end was marked with a 1 mm horizontal scale. For the remaining 55 mm, a 5 mm scale was used, as shown in Figure 4-8a. Specimens were loaded under a 1 mm/min constant crosshead rate. For unloading the specimens, the crosshead rate was set as 10

mm/min. The Mode-I energy release rate,  $G_{Ic}$  was obtained through modified beam theory (MBT) with the following governing equation (4-1):

$$G_{Ic} = \frac{3P\delta}{2b(a + |\Delta|)} \quad (4-1)$$

Where  $P$  is the load,  $\delta$  is the corresponding loading displacement,  $b$  is the specimen width,  $a$  is the delamination length and  $|\Delta|$  is a function of delamination length obtained by generating a least squares plot of the  $C^{1/3}$ . The initiation value  $G_{Ic-ini}$  was calculated from the maximum load point, and the propagation value  $G_{Ic-prop}$  was calculated from each recorded point during delamination process.

The Mode II test was conducted according to ASTM D7905 [30]. The 3-point End Notch Flexure (ENF) test specimens were prepared with the same specimen dimensions and the initial pre-crack length as DCB specimens. A thin layer of white water-based correction fluid was also coated one side of the ENF specimens. Three vertical compliance calibration lines were marked as 20, 30 and 40 mm from the tip of insert in initial cracked region, as shown in Figure 4-8b. The span length was 100 mm. The crosshead rate for loading and unloading process was 0.5 mm/min and 1 mm/min, respectively. The Mode-II interlaminar fracture toughness was determined by following equation (4-2):

$$G_{IIc} = G_Q = \frac{3mP_{Max}^2 a_0^2}{2B} \quad (4-2)$$

Where  $G_Q$  is the candidate toughness,  $P_{MAX}$  is the maximum force from fracture test,  $a_0$  is the initial crack length (30 mm),  $B$  is the specimen width and  $m$  is the slope CC coefficient which was obtained through linear least squares linear regression analysis.

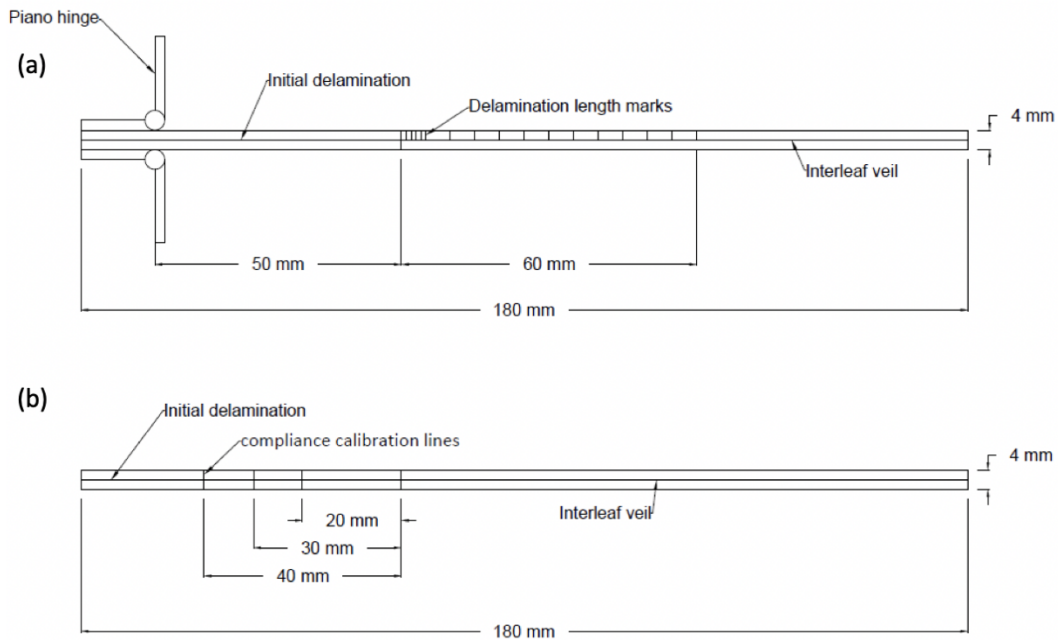


**Figure 4-8. Diagram of test specimens for interlaminar fracture toughness study. (a) DCB specimen, (b) ENF specimen.**

#### **4.3.4 Determination of volume electrical conductivity**

FIT<sup>e</sup> and Control<sup>e</sup> panels were cut into 20 mm×20 mm specimens for through-thickness (Z-direction) electric resistance measurement. In order to remove the surface epoxy layer, the top and bottom surfaces of specimens were polished using P1000 sandpaper and then cleaned by ultrasound for 1min. Cleaned surfaces were coated with conductive silver paste. For in-plane (X- and Y-direction) electrical resistance of

composite specimens, the specimens were cut into 100 mm×20 mm(length×width). Both ends were polished, cleaned and then coated with conductive silver paste.

The electrical resistance (R) of the specimen was measured through Tonghui TH2516 DC Resistance Meter with four input lines and 10 μΩ minimum resistance resolution, as shown in Figure 4-9b. The copper-nickel plated veils were cut into five 150 mm×20 mm (length×width) rectangles. For each piece, the two opposite ends were directly contacted with the fixtures of resistance meter to obtain the in-plane electrical resistance. For composite specimens, the two silver-coated surfaces were pressed with 0.1 mm thickness copper sheets as the electrodes. It is found that the measured resistance was reduced with the increase of the early stage pressure. The data became stable when the pressure was over 500N for the through-thickness direction and 200N for the in-plane direction, which was caused by the contact quality between copper sheets and silver-coated surfaces. Therefore, in order to unify the measurement, the thickness-through and in-plane electrical resistance were obtained under 500N and 200N pressure, respectively. Five specimens were measured for each test group. The volume conductivity  $\sigma$  was determined as follow (4-3):

$$\sigma = \frac{1}{\rho} = \frac{L}{RA} \quad (4-3)$$

where  $\rho$  is the volume resistivity, L is the distance between the two electrodes, R is the measured electric resistance of specimen and A is the area of coated surface,

respectively. Figure 4-9 shows the diagram of composite test specimens and electrical resistance measurement.

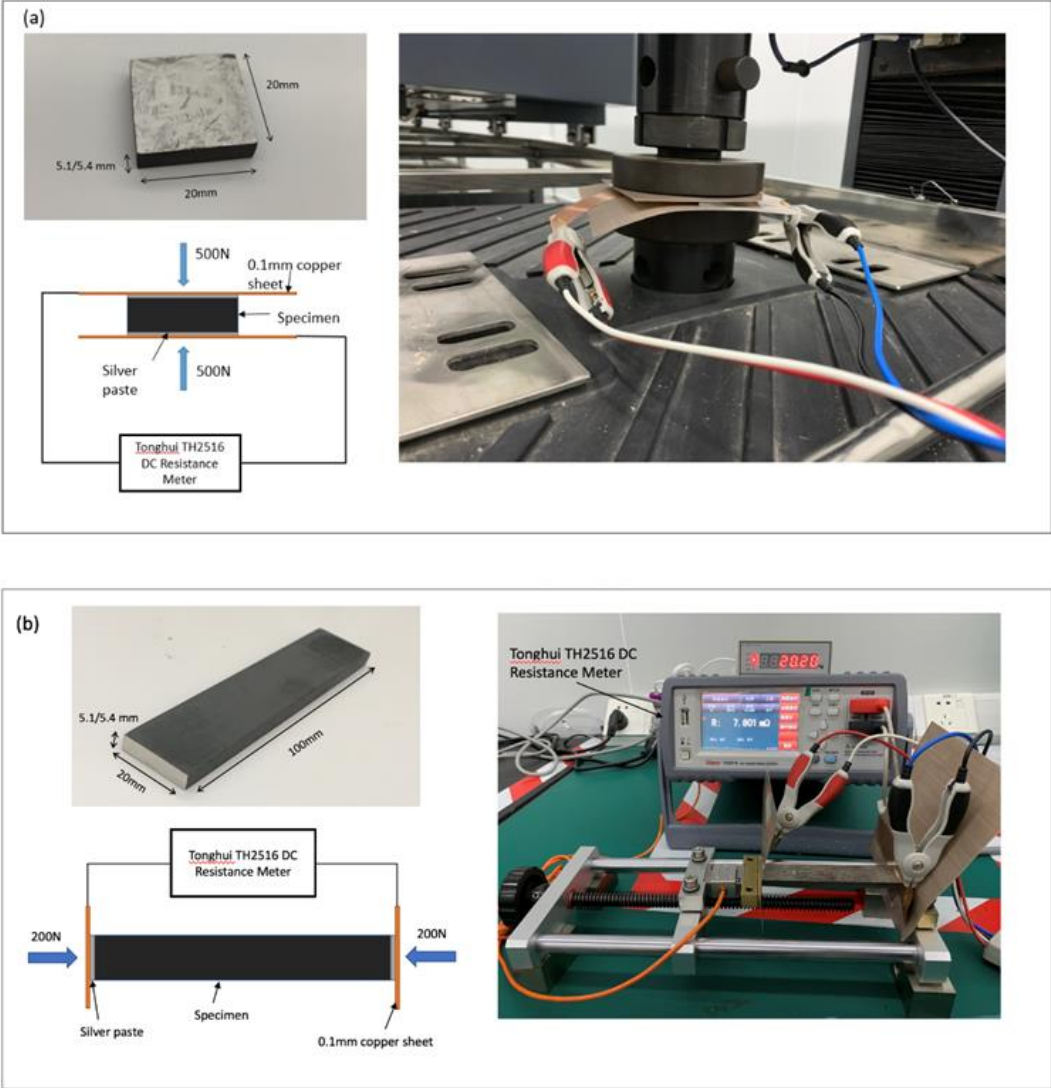


Figure 4-9. Diagram of test specimens and electrical resistance measurement. (a) through-thickness direction, (b) in-plane direction.

### **4.3.5 Scanning Electron Microscopy**

Scanning Electron Microscopy (SEM) was conducted on Zeiss Sigma VP SEM to investigate the fine microstructure. The Energy Dispersive Spectroscopy (EDS) was implemented by OXFORD INCA during SEM observation. Test specimens were coated with a 4  $\mu\text{m}$  thick gold layer through Leica EM SCD 500 Gold sputter before SEM observation.

## **4.4 Results and discussion**

### **4.4.1 Interlaminar fracture toughness of laminates**

The Mode I interlaminar fracture toughness of tested specimens are shown in Figure 4-10. Compared with Control<sup>t</sup>, the average  $G_{\text{IC-ini}}$  and  $G_{\text{IC-prop}}$  of FIT<sup>t</sup> are increased from 216.52 J/m<sup>2</sup> to 366.73 J/m<sup>2</sup> and 246.9 J/m<sup>2</sup> to 392.87 J/m<sup>2</sup>, respectively. The typical Mode I load-displacement curves are shown in Figure 4-11. During initial loading, the crack initiation was observed at higher loads and displacement for FIT<sup>t</sup> specimens. The addition of functionalized veil delayed the crack initiation and increased the load for further crack growth. Figure 4-12 shows the typical R-curves of the Mode I test specimens. Both curves show the stable crack propagation and the  $G_{\text{IC-prop}}$  values increase with the growth of delamination length. The  $G_{\text{IC-prop}}$  values of FIT<sup>t</sup> were higher than that of Control<sup>t</sup> at each recorded point.



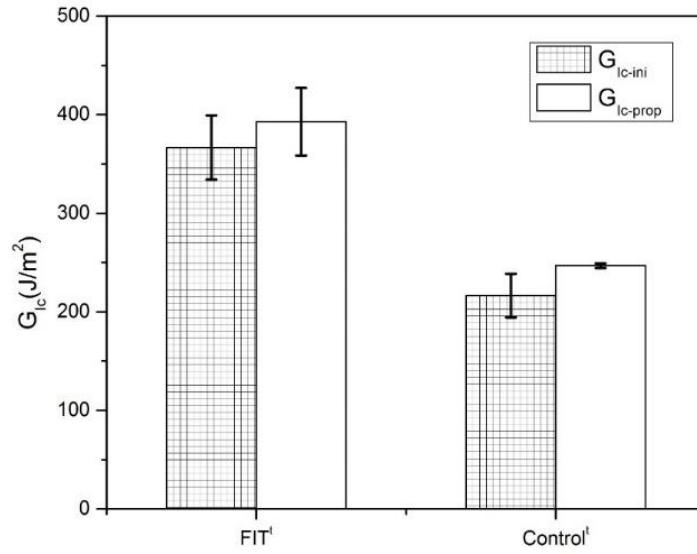


Figure 4-10. Mode I interlaminar fracture toughness for test specimens.

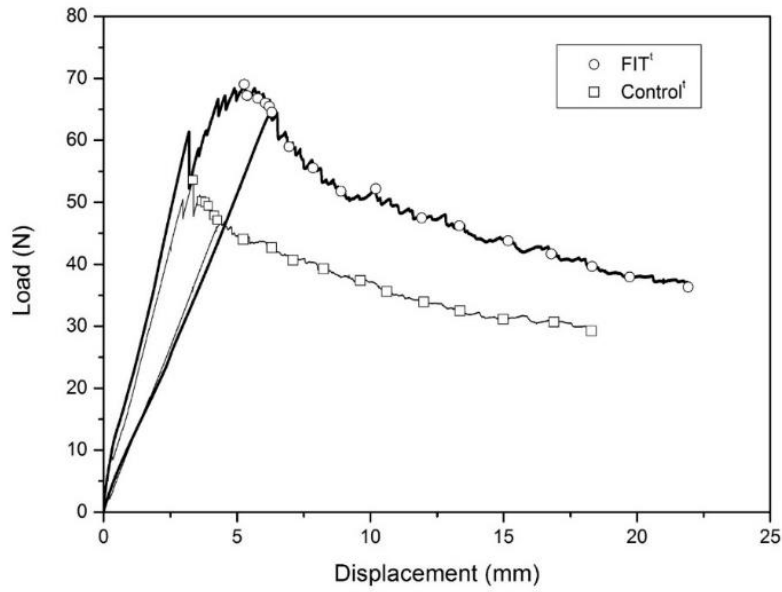
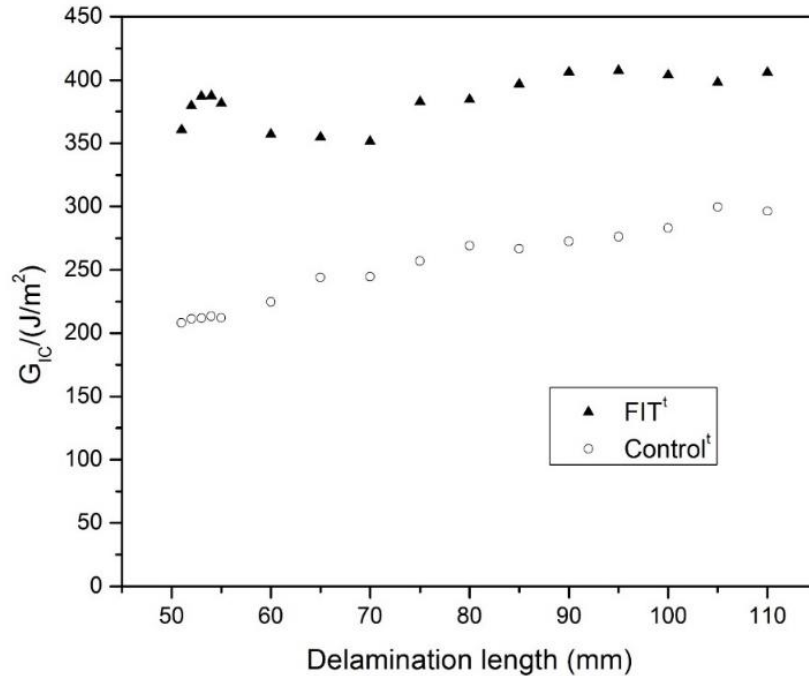


Figure 4-11. Typical DCB Load-displacement curves



**Figure 4-12. Typical R-curves for Mode I test**

The average  $G_{IIC}$  value of FIT<sup>t</sup> is also increased from 1155.76 J/m<sup>2</sup> to 1517.24 J/m<sup>2</sup>, as shown in Figure 4-13. According to Figure 4-14, the load displacement curve of Control<sup>t</sup> showed linear elastic behaviour up to the 1060 N maximum load, after which drops sharply to 520 N accompanied by a loud fracture. In contrast, FIT<sup>t</sup> demonstrated a ductile fracture at 3.4 mm displacement with maximum load of 1177 N, after which it dropped silently to 950 N. Similar to Mode I test, higher failure load with larger crosshead displacement for FIT<sup>t</sup> specimens implied that the initiation of cracks was delayed due to the existence of functional interlayers. In addition, higher resistance after failure indicated that more fracture energy is required for further crack propagation. It was also noted that both  $G_{Ic}$  and  $G_{IIC}$  values for FIT specimens presented relatively larger variations compared with controls. This phenomenon might be attributed to the

uneven distribution of interleaf fibres and the metallic coating. Detail discussions of Mode I and II toughening mechanisms will be provided in next section.

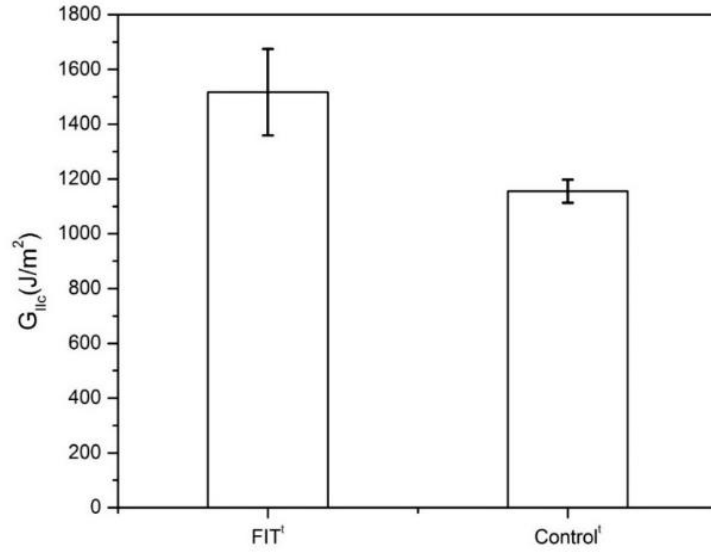


Figure 4-13. Mode II interlaminar fracture toughness for test specimens.

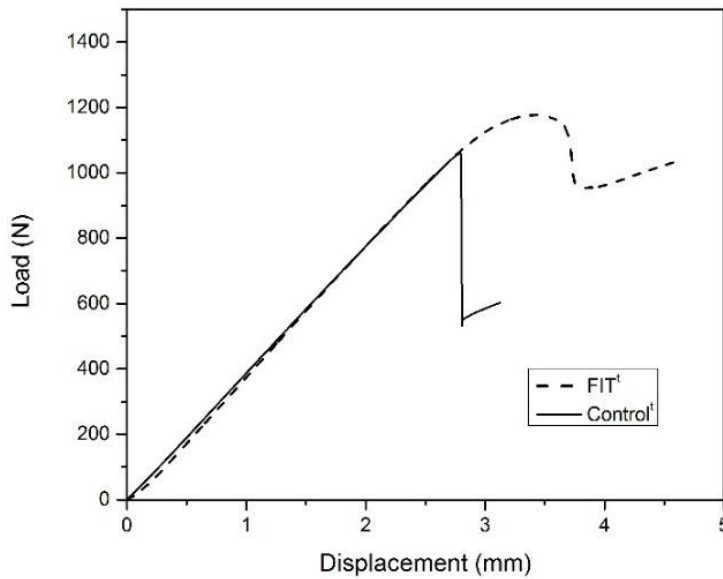


Figure 4-14. Typical Load-displacement curves for Mode II test.

#### **4.4.2 Morphology and toughening mechanisms**

Figure 4-15 shows the optical observations of FIT<sup>t</sup> during Mode I test, a Velcro-like connectivity was seen at both sides of fracture surfaces due to the co-continuity structure formed by epoxy resin and functionalized veils at interlaminar region. The functionalized fibres are gradually pulled out from the functional interlayer during crack propagation, with fibre directions changing from parallel to perpendicular to carbon fibre plies, which leads to fibre bridging and energy consumption when fibres break. Figure 4-15b shows the SEM images at the cracked section. Delamination clearly occurred in the functional interlayer. The overall optical observation also shows two fracture surfaces are covered with veil fibres completely (Figure 4-16a). It appeared that the bond strength between the functional interlayer and carbon fibre ply was higher than the out-plane strength of the functional interlayer itself, i.e. the Mode I delamination is dominated by cohesive failure. Referring to the further SEM images of Mode I fracture surface in Figure 4-16b, large numbers of fibre pull-out and fibre breakage were observed. The pull-out fibres result in the fibre bridging at the cracking region, the pinning mechanism and stress-shield effects at the crack tip work together to increase the applied load for further crack growth [22]. Therefore, the Mode I toughness improvement is attributed to fibre pull-out, bridging and fibre breakage.

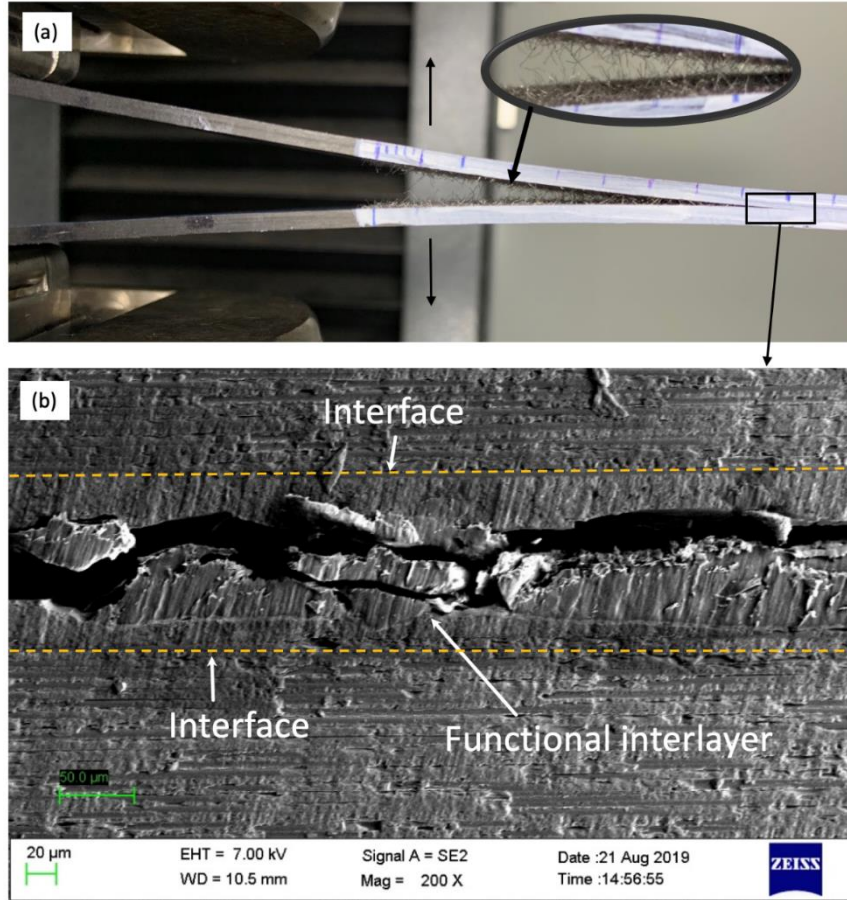
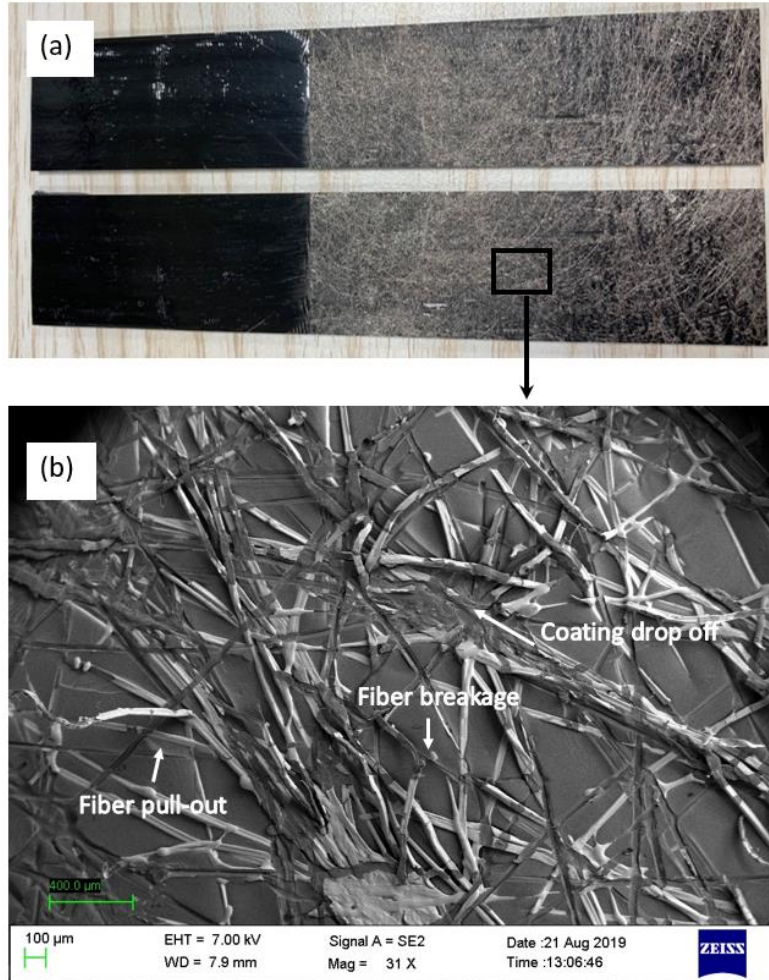


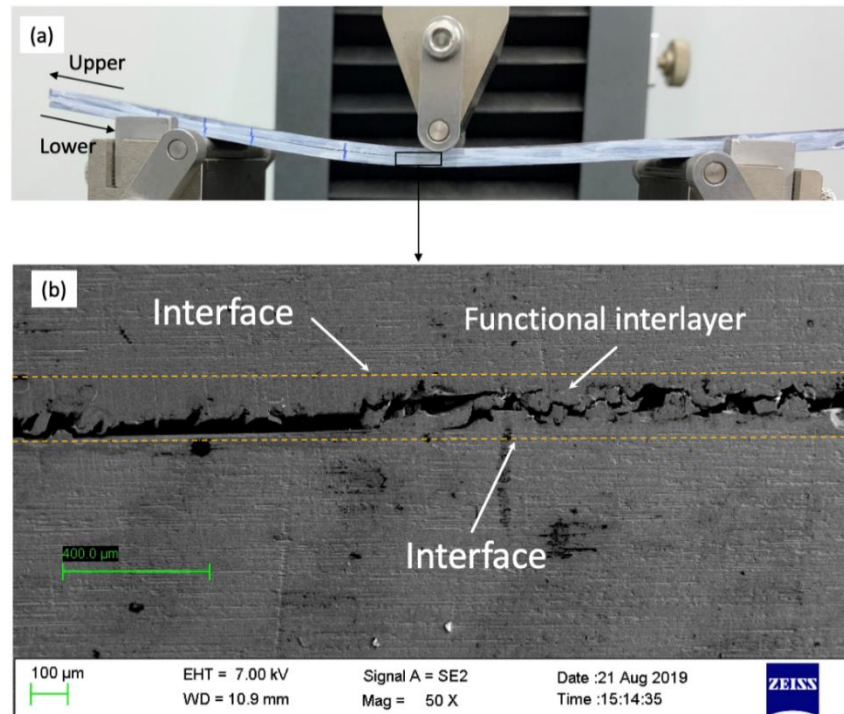
Figure 4-15. Typical side view of FIT<sup>t</sup> specimens for Mode I interlaminar fracture test. (a) Interlayer structure during Mode I test, (b) SEM image at crack region



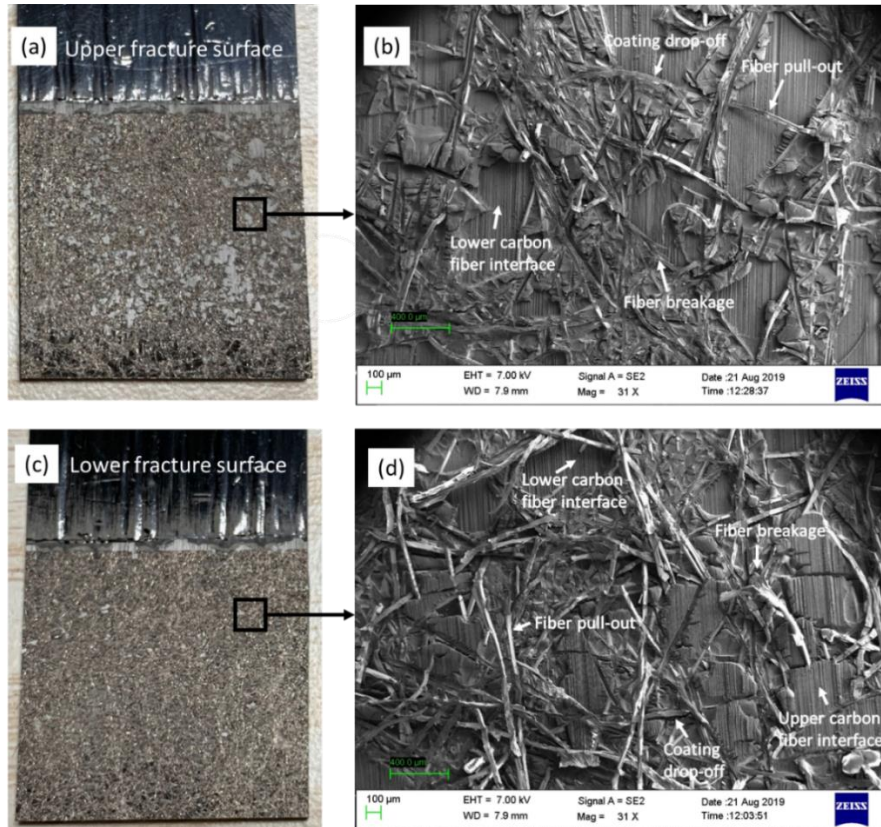
**Figure 4-16. Plane view of FIT<sup>t</sup> fracture surface after Mode I interlaminar fracture test. (a) Overall observation (b) SEM image**

Figure 4-17 shows the typical side observation of FIT<sup>t</sup> specimens for the Mode II test. According to the SEM image of the cross section at crack region (Figure 4-17b), cracks were seen at the CF/veils interface as well as the functional interlayer. Figure 4-18(a,c) shows the overall observation for upper and lower Mode II fracture surface of FIT<sup>t</sup>. Fracture mostly happened in the interlayer with small portion transferred into the interlayer/lamina interface. Therefore, it is suggested that the overall interfacial shear strength between functional interlayer and carbon fibre layer is slightly higher than the

in-plane shear strength of functional interlayer itself, i.e., the Mode II delamination is dominated by the combination effects of cohesive and adhesive failures. Figure 4-18(b,d) show the SEM images of Mode II fracture surface for FIT<sup>t</sup> specimens. Taking a closer inspection, large numbers of functionalized fibre pull-outs and breakages are also observed in the functional interlayer. The coexistence of typical cohesive failure and interfacial failure indicates that the crack is randomly deflected from one interface to another, with many micro-interfacial failure and material yielding, which is the major factor of Mode II toughening mechanism.



**Figure 4-17. Typical side view of FIT<sup>t</sup> specimens regarding to Mode II interlaminar fracture test. (a) Failure state of FIT<sup>t</sup> during Mode II test, (b) SEM images at crack region.**



**Figure 4-18. Plane view of FIT<sup>t</sup> fracture surface after Mode II interlaminar fracture test. (a) Overall observation of upper fracture surface (b) SEM image at upper fracture surface, (c) Overall observation of lower fracture surface, (d) SEM image at lower fracture**

Different from the general non-woven veil interleaving toughening technique, using metallic coated polyester veils as interleaves results in two inherent interfaces in the functional interlayer, i.e., the copper-nickel coating acts as a third component between the polyester fibre and epoxy matrix. Referring to the SEM images in Figure 4-16b and Figure 4-18(b, d), some of the metallic coating is stripped away from the polyester fibre after the Mode I and Mode II tests. This indicates that the interface between the polyester fibre and metallic coating is relatively weak, which may counter the overall toughening efficiency [25,26]. Moreover, less fibre pull-out and breakage was found



where the veil coverage is high, especially so for the Mode I fracture surfaces. According to the architecture of functionalized veil (Figure 4-2a), these regions could be defined as bonded nodes to fix the functionalized polyester fibres. Higher veil coverage results in a more complex interface in functional interlayers, which may be the dominant factor controlling the failure mechanism during fracture toughness test [31]. Potentially, the Mode I pre-cracking may be initiated first at the boundary of the high veil coverage areas (i.e. bonded nodes) and propagated in the functional interlayer. For Mode II delamination, the cohesive failure is more likely to occur at the nodes, which indicates that the pre-cracking may also occur at the nodes firstly and then traverse the functional interlayer randomly from one interface to another provoking large numbers of fibre pull-out and breakage. However, there is still no detail study regarding to the effects of metallic coating parameters and veil architectures on toughening performance for these composites. We will explore such relationships in further investigations.

#### **4.4.3 Volume electrical conductivity**

Figure 4-19 and Figure 4-20 provide the volume electrical conductivity for each test group. Logarithmic coordinates are used due to the nonlinear changes in conductivity for the FIT<sup>e</sup> specimens. Compared with Control<sup>e</sup>, the through-thickness electrical conductivity (TTEC) FIT<sup>e</sup><sub>1</sub> was increased from  $1.5 \times 10^{-3}$  S/cm to 3.25 S/cm (Figure 4-19). The significant improvement is attributed only to the existence of the functional interlayer. Numerous conductive units are formed as the connections form between stacked carbon fibre plies and functionalized fibres. These conductive units replace the conventional resin-rich interlaminar region so that the normal insulating barrier in

through-thickness direction is broken. In addition, the in-plane electrical conductivity of FIT<sup>e</sup><sub>1</sub> is also improved from 77.12 S/cm to 771.59 S/cm (Figure 4-20) due to the high conductivity and continuity of functional interlayers.

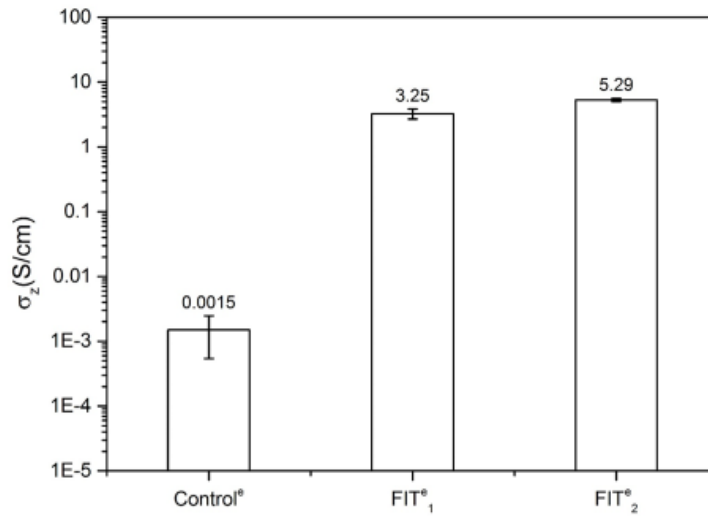


Figure 4-19. Through-thickness electrical conductivity of test specimens (TTEC)

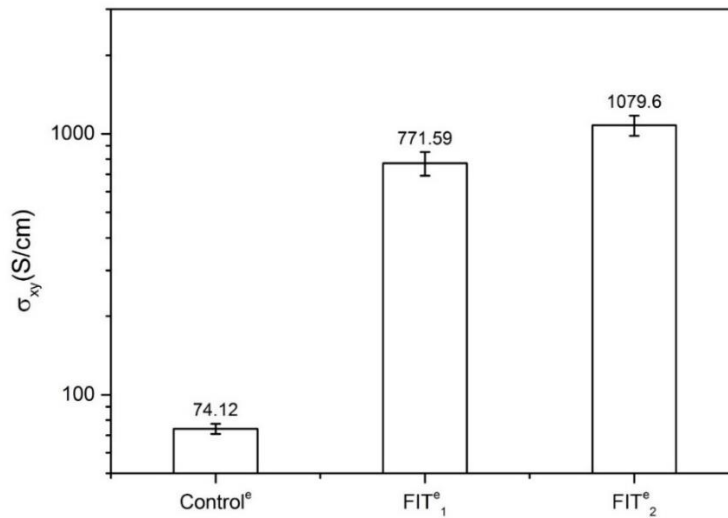


Figure 4-20. In-plane electrical conductivity of test specimens

Compared with FIT<sup>e1</sup>, the TTEC and the in-plane electrical conductivity of FIT<sup>e2</sup> are further improved from 3.23 S/cm to 5.29 S/cm and 771.59 S/cm to 1079.6 S/cm, respectively. Considering the conductive mechanism at the electrodes, the additional surface veil acts like a high electrically conductive medium between the silver layer and carbon ply for FIT<sup>e2</sup>, which actually increases the effective electric contact area of the electrodes. Therefore, for further application of FIT CFRPs, the issues of electrode contact resistance need to be addressed. Moreover, the improvement of FIT<sup>e2</sup> also indicates that the electrical conductivity efficiency is highly dependent on the electrical interface between functionalized fibres and carbon fibre plies which will lead to further study that might optimize the interleaf materials.

Figure 4-21 shows optical micrographs of the laminated structure of FIT<sup>e</sup> specimens. It can be seen that the carbon fibre layers and functional interlayers are well compacted with few voids and defects. The functional interlayers are regularly parallel to the carbon fibre plies and create a periodically laminated structure. The average thickness of carbon fibre layer and functional interlayer are about 130  $\mu\text{m}$  and 50  $\mu\text{m}$ , respectively. Inside the functional interlayer, many irregular circles which are the functionalized fibres are observed. The complete conductive surface can be easily recognized due to the metallic lustre under optical microscopy. These functionalized polyester fibres are compacted together and with carbon fibres plies to form the volume electrically conductive network.

It should be noted that the typical interlayer thickness is around 50  $\mu\text{m}$ , the carbon fibre volume fraction of FIT<sup>e</sup> is reduced from 59.06% to 49.1%, as mentioned in Table 4-1.

Although this paper focuses on toughening and electrical conductivity properties of FIT CFRPs, it is believed that the in-plane mechanical properties of FIT<sup>e</sup> will be reduced. The effects of in-plane mechanical properties remain under study and will not be discussed here.

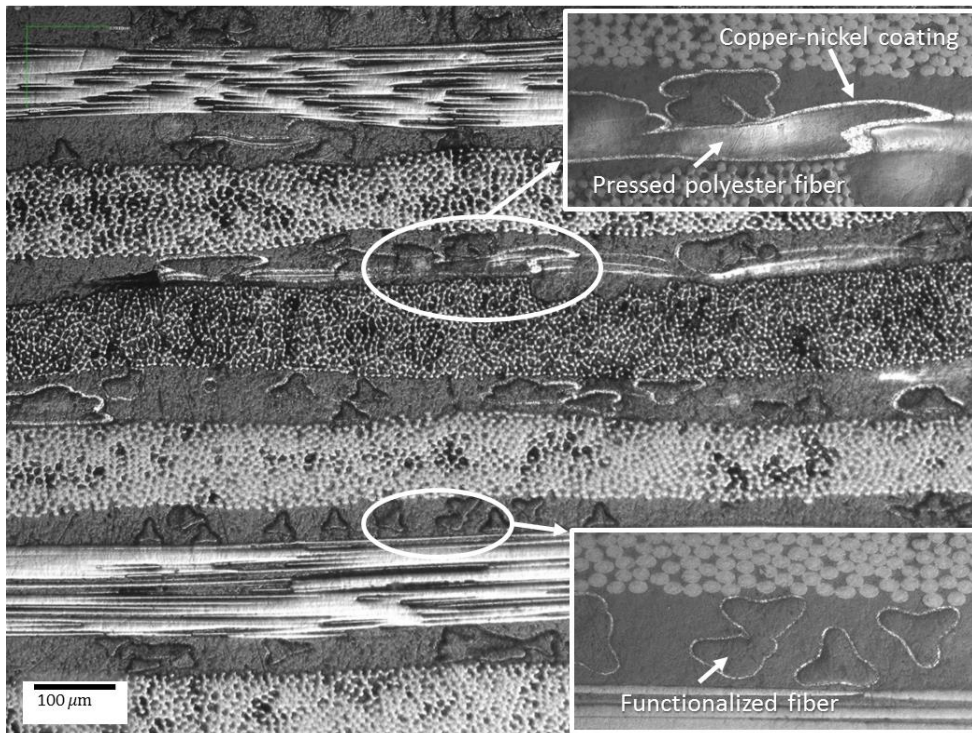


Figure 4-21. Typical cross section of FIT<sup>e</sup> specimens under optical microscope

## 4.5 Conclusion

Through the Functionalized Interleaf Technology, electrically functionalized veil provided the bi-functionality to simultaneously improve interlaminar fracture toughness and volume electrical conductivity of carbon fibre epoxy laminates. The bi-functional veils can be well infiltrated with epoxy resin to form a co-continuity structure at interlaminar regions. Through the toughening mechanism study, Mode I delamination occurred in the

bi-functional interlayer and the fracture energy was consumed by normal cohesive failure of the interlayer. Mode II toughness improvement was mainly contributed to by crack deflection, which was accompanied by in-plane shear failure of the interlayer. The interface between polyester fibre and metallic coating appeared to be weak and may negatively affect the overall toughening efficiency. The veil architecture is another factor to influence the failure mechanism for Mode I and II delamination process. Current results show that the in-plane cohesive strength of interlayer is relatively low at high veil coverage region. The large improvement in electrical conductivity of interleaved composites is also achieved due to the formation of high electrically conductive network, especially for the TTEC. In addition, higher electrical conductivity was obtained by additionally placing the functionalized veils at top and bottom surfaces, which shows the potential influence of electrical contact area for further investigation and application of FIT CFRPs.

## 4.6 References

- [1] C. Lochot, D. Slomianowski, A 350 XWB Electrical structure network, *Airbus Tech. Mag.* (2014) 20–25.
- [2] M. Gagné, D. Therriault, Lightning strike protection of composites, *Prog. Aerosp. Sci.* 64 (2014) 1–16. doi:10.1016/j.paerosci.2013.07.002.
- [3] F.S. Wang, X.S. Yu, S.Q. Jia, P. Li, Experimental and numerical study on residual strength of aircraft carbon / epoxy composite after lightning strike, *Aerosp. Sci. Technol.* 75 (2018) 304–314. doi:10.1016/j.ast.2018.01.029.
- [4] H. Park, C. Kong, Experimental study on barely visible impact damage and visible impact damage for repair of small aircraft composite structure, *Aerosp. Sci. Technol.* 29 (2013) 363–372. doi:10.1016/j.ast.2013.04.007.

- [5] N.H. Nash, T.M. Young, W.F. Stanley, The influence of a thermoplastic toughening interlayer and hydrothermal conditioning on the Mode-II interlaminar fracture toughness of Carbon / Benzoxazine composites, *Compos. Part A Appl. Sci. Manuf.* 81 (2016) 111–120.
- [6] P. Feraboli, M. Miller, Damage resistance and tolerance of carbon / epoxy composite coupons subjected to simulated lightning strike, *Compos. Part A Appl. Sci. Manuf.* 40 (2009) 954–967. doi:10.1016/j.compositesa.2009.04.025.
- [7] M.V. Mousavi, H. Khoramishad, The effect of hybridization on high-velocity impact response of carbon fiber-reinforced polymer composites using finite element modeling , Taguchi method and artificial neural network, *Aerosp. Sci. Technol.* 94 (2019) 105393. doi:10.1016/j.ast.2019.105393.
- [8] X. Ma, F. Scarpa, H. Peng, G. Allegri, J. Yuan, R. Ciobanu, Design of a hybrid carbon fibre / carbon nanotube composite for enhanced lightning strike resistance, *Aerosp. Sci. Technol.* 47 (2015) 367–377. doi:10.1016/j.ast.2015.10.002.
- [9] H.S. Kim, H.T. Hahn, Graphite fiber composites interlayered with single-walled carbon nanotubes, *J. Compos. Mater.* 45 (2011) 1109–1120. doi:10.1177/0021998311402726.
- [10] Y. Lin, M. Gigliotti, M.C. Lafarie-frenot, J. Bai, D. Marchand, D. Mellier, Experimental study to assess the effect of carbon nanotube addition on the through-thickness electrical conductivity of CFRP laminates for aircraft applications \*, *Compos. Part B.* 76 (2015) 31–37. doi:10.1016/j.compositesb.2015.02.015.
- [11] D. Zhang, L. Ye, S. Deng, J. Zhang, Y. Tang, Y. Chen, CF / EP composite laminates with carbon black and copper chloride for improved electrical conductivity and interlaminar fracture toughness, *Compos. Sci. Technol.* 72 (2012) 412–420. doi:10.1016/j.compscitech.2011.12.002.
- [12] H.S. Kim, Hahn, Graphite Nanoplatelets Interlayered Carbon/Epoxy Composites, *AIAA J.* 47 (2009) 2779–2784. doi:10.2514/1.39522.
- [13] B. Karami, D. Shahsavari, M. Janghorban, A comprehensive analytical study on functionally graded carbon nanotube-reinforced composite plates, *Aerosp. Sci. Technol.* 82–83 (2018) 499–512. doi:10.1016/j.ast.2018.10.001.

- [14] R.M. Rami, W. Karunasena, W. Lokuge, Free vibration of functionally graded-GPL reinforced composite plates with different boundary conditions, *Aerosp. Sci. Technol.* 78 (2018) 147–156. doi:10.1016/j.ast.2018.04.019.
- [15] M. Arai, Y. Noro, K. ichi Sugimoto, M. Endo, Mode I and mode II interlaminar fracture toughness of CFRP laminates toughened by carbon nanofiber interlayer, *Compos. Sci. Technol.* 68 (2008) 516–525. doi:10.1016/j.compscitech.2007.06.007.
- [16] W.X. Wang, Y. Takao, T. Matsubara, H.S. Kim, Improvement of the interlaminar fracture toughness of composite laminates by whisker reinforced interlamination, *Compos. Sci. Technol.* 62 (2002) 767–774. doi:10.1016/S0266-3538(02)00052-0.
- [17] Z. Wu, X. Yi, A. Wilkinson, Interlaminar fracture toughness of carbon fibre / RTM6-2 composites toughened with thermoplastic-coated fabric reinforcement, *Compos. Part B.* 130 (2017) 192–199. doi:10.1016/j.compositesb.2017.08.003.
- [18] G.W. Beckermann, K.L. Pickering, Mode I and Mode II interlaminar fracture toughness of composite laminates interleaved with electrospun nanofiber veils, *Compos. Part A Appl. Sci. Manuf.* 72 (2015) 11–21.
- [19] J.W. Kim, J.S. Lee, Influence of interleaved films on the mechanical properties of carbon fiber fabric/polypropylene thermoplastic composites, *Materials (Basel)*. 9 (2016). doi:10.3390/ma9050344.
- [20] L. Daelemans, S. Van Der Heijden, I. De Baere, H. Rahier, W. Van Paepegem, K. De Clerck, Improved fatigue delamination behaviour of composite laminates with electrospun thermoplastic nanofibrous interleaves using the Central Cut-Ply method, *Compos. Part A.* (2016). doi:10.1016/j.compositesa.2016.12.004.
- [21] M. Kuwata, P.J. Hogg, Interlaminar toughness of interleaved CFRP using non-woven veils: Part 2. Mode-II testing, *Compos. Part A Appl. Sci. Manuf.* 42 (2011) 1560–1570. doi:10.1016/j.compositesa.2011.07.017.
- [22] M. Kuwata, P.J. Hogg, Interlaminar toughness of interleaved CFRP using non-woven veils: Part 1. Mode-I testing, *Compos. Part A Appl. Sci. Manuf.* 42 (2011) 1551–1559. doi:10.1016/j.compositesa.2011.07.016.

- [23] M. Guo, X. Yi, Effect of paper or silver nanowires-loaded paper interleaves on the electrical conductivity and interlaminar fracture toughness of composites, *Aerospace*. 5 (2018) 1–15. doi:10.3390/aerospace5030077.
- [24] M. Guo, X. Yi, The production of tough, electrically conductive carbon fiber composite laminates for use in airframes, *Carbon N. Y.* 58 (2013) 241–244. doi:10.1016/j.carbon.2013.02.052.
- [25] M. Guo, X. Yi, G. Liu, L. Liu, Simultaneously increasing the electrical conductivity and fracture toughness of carbon-fiber composites by using silver nanowires-loaded interleaves, *Compos. Sci. Technol.* 97 (2014) 27–33. doi:10.1016/j.compscitech.2014.03.020.
- [26] M. Guo, X. Yi, C. Rudd, X. Liu, Preparation of highly electrically conductive carbon- fiber composites with high interlaminar fracture toughness by using silver-plated interleaves, *Compos. Sci. Technol.* 176 (2019) 29–36. doi:10.1016/j.compscitech.2019.03.014.
- [27] X. Yi, M. Guo, G. Liu, W. Zhao, L. Liu, H. Cui, Composite conductive sheet, fabricating method and application thereof, EP.2687364B1, 2015.
- [28] L. Ye, Functionalized interleaf technology in carbon-fibre-reinforced composites for aircraft, *Natl. Sci. Rev.* 1 (2014) 7–8. doi:10.1093/nsr/nwt007.
- [29] ASTM D5528-01 Standard Test Method for Mode I Interlaminar Fracture Toughness of Unidirectional Fiber-Reinforced Polymer Matrix Composites, ASTM Int. (n.d.).
- [30] ASTM D7905 Standard Test Method for Mode II Interlaminar Fracture Toughness of Unidirectional Fiber-Reinforced Polymer Matrix Composites, ASTM Int. (n.d.).
- [31] V.A. Ramirez, P.J. Hogg, W.W. Sampson, The influence of the nonwoven veil architectures on interlaminar fracture toughness of interleaved composites, *Compos. Sci. Technol.* 110 (2015) 103–110. doi:10.1016/j.compscitech.2015.01.016.



# **Chapter 5: The effects of compaction and interleaving on through-thickness electrical resistance and in-plane mechanical properties for CFRP laminates**

Status: Published in Composites Science and Technology

Authors: Dongyuan Hu, Xiaoling Liu, Weiping Liu, Guocai Li, Chris Rudd, Xiaosu Yi

In chapter 4, an electroless copper-nickel plated polyester veil was used as the bi-functional interleaf material to provide both toughening and electrical conductivity for CFRP laminates. The technology is termed Functional Interleave Technology (FIT). As the high through-thickness electrical conductivity is attributed to the volumetric conductive network formed by the effective contact between carbon fibres and conductive interleaf fibres. Thus, for better understand the mechanisms of FIT, the effects of compaction on through-thickness electrical conductivity and mechanical properties for so-called FIT composites must be considered and investigated deeply.

In this chapter, a similar electroless copper-nickel polyester veil was used as the interleaf material. Studies were conducted on dry carbon fibre fabrics as well as the cured laminates to further explore the through-thickness electrical conductivity behaviour under various compaction. Besides, the influences on mechanical properties were studied via flexural and short beam tests. Discussions on conductive mechanism and mechanical performance are presented, giving the optimization route for CFRP functionalization.



## The effects of compaction and interleaving on through-thickness electrical resistance and in-plane mechanical properties for CFRP laminates

Dongyuan Hu<sup>a</sup>, Xiaoling Liu<sup>a,\*</sup>, Weiping Liu<sup>b</sup>, Guocai Li<sup>b</sup>, Chris Rudd<sup>c</sup>, Xiaosu Yi<sup>a,\*</sup>

<sup>a</sup> New Material Institute, Faculty of Science and Engineering, University of Nottingham Ningbo China, 199 Taikang East Road, Ningbo, China

<sup>b</sup> Shanghai Aircraft Manufacturing Co. Ltd (SAMC), 3115, Chang Zhong Road, Shanghai, China

<sup>c</sup> James Cook University, Singapore, 149 Sims Drive, 387380, Singapore

### ARTICLE INFO

#### Keywords:

Carbon fibres  
Laminate  
Compaction  
Electrical properties  
Mechanical properties

### ABSTRACT

The electrical conductivity of carbon fibre reinforced polymer (CFRP) laminates has previously been shown to be significantly improved by using different electrically functionalized interleaves - Functional Interleave Technology (FIT), particularly in through-thickness direction. Here, the mechanism of FIT is explored via the influence of compaction and interleaving of nickel plated polyester non-woven veils (NPVs) on through-thickness electrical conductivity and in-plane mechanical properties for the CFRP laminates are investigated. The through-thickness electrical property is found to be dominated by the electrically conductive network elements (carbon fibres) and components (carbon fibre layers and NPV layers), which, in turn, is strongly affected by compaction. By using the highly conductive NPVs, the through-thickness resistivity for cured FIT laminates was consistently lowered from 9.3  $\Omega\cdot\text{m}$  to 0.48  $\Omega\cdot\text{m}$  and 1.54  $\Omega\cdot\text{m}$  to 0.016  $\Omega\cdot\text{m}$  for 56% and 64% carbon fibre volume fraction laminates, respectively. The conductive mechanism of FIT specimens follows the series-resistor model, providing the potential to predict the through-thickness electrical conductivity (TTEC) value by interleaving the desired number of NPV layers. Investigation of in-plane mechanical properties indicates the flexural properties and interlaminar shear strength (ILSS) are less affected by compaction. Meanwhile, a 20% reduction of ILSS for FIT laminates is detected because of the lower intra-ply shear resistance of NPV layers.

### 1. Introduction

Carbon fibre reinforced polymers (CFRPs) are extensively used in aircraft primary and secondary structures reduce to weight, CO<sub>2</sub> emissions and fuel costs. A growing number of studies have shown that future high-performance CFRPs can not only provide the load-bearing structures and lightweight, but also integrate additional functions such as the electrical conductivity to meet other functional requirements [1–3]. However, aeronautical CFRPs are typically laminated materials with relatively conductive carbon fibre (CF) layers alternated with insulating, resin rich layers, resulting in highly anisotropic electrical properties, where the through-thickness electrical conductivity (TTEC) is particularly low [4]. To improve the electrical, environmental and mechanical performance for CFRP structures, they are improved by different metallic conductors to deliver an electrically conductive network [5]. For example, an Electrical Structure Network (ESN), Metallic Bonding Network (MBN) and metal foils can be assembled within specific CFRP

structures to meet the requirements for lightning strike protection and electromagnetic interference [6]. Clearly, the lightweight benefits of CFRP structures are somewhat compromised by the incorporation of heavier metal components as well as the additional design and maintenance complexities.

The through thickness electric properties of CFRPs have been investigated in several earlier studies. Louis et al. [7] tested the effects of degree of cure, intra-ply interfaces, materials combinations and ply orientation on TTEC. Todoroki et al. [8] measured electrical conductivity in a commercial CFRP laminate at varying volume fractions, confirming a significant (positive) dependence on volume fraction. Wang and Chung [9] tested the electrical behaviour of continuous CF epoxy composites by measuring the contact resistance of the interlaminar interface. The results showed that the z-direction contact resistivity decreased as the consolidation pressure increased. In general, the TTEC of CFRP laminates are shown to be somewhat dependent on the contact geometry of adjacent tows. Logically, the compaction is a critical factor

\* Corresponding author.

\*\* Corresponding author.

E-mail addresses: [xiaoling.liu@nottingham.edu.cn](mailto:xiaoling.liu@nottingham.edu.cn) (X. Liu), [xiaosu.yi@nottingham.edu.cn](mailto:xiaosu.yi@nottingham.edu.cn) (X. Yi).

<https://doi.org/10.1016/j.compscitech.2022.109441>

Received 25 January 2022; Received in revised form 25 March 2022; Accepted 1 April 2022

Available online 5 April 2022

0266-3538/© 2022 Published by Elsevier Ltd.

**Blank page**

## 5.1 Abstract

The electrical conductivity of carbon fibre reinforced polymer (CFRP) laminates has previously been shown to be significantly improved by using different electrically functionalized interleaves - Functional Interleave Technology (FIT), particularly in through-thickness direction. Here, the mechanism of FIT is explored via the influence of compaction and interleaving of nickel plated polyester non-woven veils (NPVs) on through-thickness electrical conductivity and in-plane mechanical properties for the CFRP laminates are investigated. The through-thickness electrical property is found to be dominated by the electrically conductive network elements (carbon fibres) and components (carbon fibre layers and NPV layers), which, in turn, is strongly affected by compaction. By using the highly conductive NPVs, the through-thickness resistivity for cured FIT laminates was consistently lowered from  $9.3 \Omega \cdot m$  to  $0.48 \Omega \cdot m$  and  $1.54 \Omega \cdot m$  to  $0.016 \Omega \cdot m$  for 56% and 64% carbon fibre volume fraction laminates, respectively. The conductive mechanism of FIT specimens follows the series-resistor model, providing the potential to predict the through-thickness electrical conductivity (TTEC) value by interleaving the desired number of NPV layers. Investigation of in-plane mechanical properties indicates the flexural properties and interlaminar shear strength (ILSS) are less affected by compaction. Meanwhile, a 20% reduction of ILSS for FIT laminates is detected because of the lower intra-ply shear resistance of NPV layers.

Keywords: Carbon fibres; Laminate; Compaction; Electrical properties; Mechanical properties

## 5.2 Introduction

Carbon fibre reinforced polymers (CFRPs) are extensively used in aircraft primary and secondary structures reduce to weight, CO<sub>2</sub> emissions and fuel costs. Increasing research and development indicates CFRP not only to provide the load-bearing structures and lightweight in the future, but also integrate with additional functions such as the electrical conductivity to meet other functional requirements [1–3]. However, aeronautical CFRPs are typically laminated materials with relatively conductive carbon fibre (CF) layers alternated with insulating, resin rich layers, resulting in highly anisotropic electrical properties, where the through-thickness electrical conductivity (TTEC) is particularly low [4]. To improve the electrical, environmental and mechanical performance for CFRP structures, they are improved by different metallic conductors to deliver an electrically conductive network [5]. For example, an Electrical Structure Network (ESN), Metallic Bonding Network (MBN) and metal foils can be assembled within specific CFRP structures to meet the requirements for lightning strike protection and electromagnetic interference [6]. Clearly, the lightweight benefits of CFRP structures are somewhat compromised by the incorporation of heavier metal components as well as the additional design and maintenance complexities.

The through thickness electric properties of CFRPs have been investigated in several earlier studies. Louis et al. [7] tested the effects of degree of cure, intra-ply interfaces, materials combinations, and ply orientation on TTEC. Todoroki et al. [8] measured electrical conductivity in a commercial CFRP laminate at varying volume fractions, confirming a significant (positive) dependence on volume fraction. Wang and Chung [9]

tested the electrical behaviour of continuous CF epoxy composites by measuring the contact resistance of the interlaminar interface. The results showed that the z-direction contact resistivity decreased as the consolidation pressure increased. In general, the TTEC of CFRP laminates are shown to be somewhat dependent on the contact geometry of adjacent tows. Logically, the compaction is a critical factor that could determine the final TTEC by changing the fibre-fibre contact area and microstructure of the CFRP laminates [10].

Carbon fibre itself a modest conductor of heat and electrical current and generally 2 orders of magnitude lower than commonly used metal conductors ( $5.9 \times 10^4$  S/m to  $1.42 \times 10^5$ ) [11]. Clearly the epoxy matrix is an insulator. The through-thickness electrical resistivity ( $\rho_{tt}$ ) of a composite laminate should be high if every fibre were insulated by the resin matrix from its neighbours. In practice, conventional CFRP laminates remain a degree of z-direction electrical conductivity with large variability due to ply nesting effects etc. [11,12]. Thus, ply geometry and fabrication variables have potential to determine the availability of conductive paths in z-direction during laminate preparation.

Given that the electrical conductivity gap between conventional light metal alloys and even the most optimistic CFRP result many approaches have been taken to improve the TTEC by modifying the laminating materials. Introducing conductive nanoparticles such as graphene, CNTs and nano-scale silver wire are all potential methods to balance electrical conductivity improvements whilst retaining structural efficiency. Several experimental studies note accompanying TTEC improvements from  $6.4 \times 10^{-2}$  S/m to 20 S/m [13–19].

Our previous studies seeking to tackle the challenge represented by a structurally efficient but electrically conductive CFRP laminate have focussed on interleaving metallic functionalized thermoplastic non-woven veils, termed *Functionalized Interlayer Technology* (FIT) [20–23]. The volumetric, conductive network is formed via the contacts between the functionalized polymer fibres and adjacent carbon fibres. The non-woven veils also incorporate with the resin matrix in interlaminar region to form a continuous morphology, simultaneously improving interlaminar fracture toughness. Table 5-1 summarizes the recent attempts to improve the TTEC of carbon fibre-epoxy laminates. It can be seen that the TTEC of FIT modified specimens are significantly higher than that of other specimens.

**Table 5-1. Summary of different techniques to improve the through-thickness electrical conductivity for carbon fibre-epoxy laminates**

Technique	Conductive components	Initial TTEC (S/m)	Improved TTEC (S/m)	V <sub>CF</sub> %
	Graphene coated PA12 non-woven veil [24]	-	0.0025	54
Interleaving and	co-polyimide veils with 10 wt% CNT [25]	0.69	3.16	57
Nano-fillers modification	0.75 wt% CNT with PEI binder [26]	0.032	0.23	58
	0.4wt% DWCNT [27]	0.0066	0.53	67
	2.71 vol% GO [19]	5.43	18	57
Fibre surface modification	1wt% CNT coated Carbon fibre [5]	0.003	0.38	-
FIT	Nickel-copper plated polyester veil [23]	0.15	529	49
	Ag-plated nylon veil [22]	12.2	417	47

Since the fundamental mechanisms of conductivity enhancement rely upon the in-plane and z-direction networks of effective contacts of conductive elements in thickness direction, the improvement in conductivity of the FIT composites will reasonably be affected as the degree of compaction changes. The intention of this study is therefore to examine the compaction effect on TTEC and mechanical properties in the so-called FIT composites. Electrical conductivity studies were conducted on dry, cross-ply CF fabrics. The stacked fabrics were gradually compacted using a universal test machine and the real time relationship between compaction and through-thickness electrical resistance ( $R_{tt}$ ) was recorded. Carbon fibre epoxy composite laminates were then prepared using the same stacking sequences but with varying thicknesses. Electrical resistivity was



then compared with the dry counterparts to elucidate the conductivity mechanism. Finally, the compaction effect on in-plane mechanical properties was examined via flexural and short beam tests.

## **5.3 Material and methods**

### **5.3.1 Materials**

Unidirectional stitched carbon fabrics (12k, T700, Toray) with 300g/m<sup>2</sup> fibre areal weight were used as the reinforcement to study the compaction-electrical conductivity relationship in dry condition. The density of the CF was 1.78g/cm<sup>3</sup>.

A commercial unidirectional (UD) carbon fibre-epoxy prepreg (Easy Composites Ltd) was used to manufacture the composite laminates. The prepreg consisted of T700 grade fibre and 130°C cured epoxy resin of GXC120, with 200g/m<sup>2</sup> CF density and 35% resin content, designed as GXC120-T700. The nominal ply thickness was 0.2 mm.

The interleaf material was electroless nickel-plated polyester veil (NPV) with 42g/m<sup>2</sup> areal density and 52µm nominal thickness, provided by NIC, Ningbo, China. Figure 5-1 shows an SEM image of the veil. Continuous polyester fibres are randomly distributed and consolidated to form a flat and relatively dense veil architecture. Bonded nodes were evident with characteristics dimensions of 0.2 mm and 0.6 mm nodal spacing. The sheet resistance of the NPV was approximately 18 mΩ/sq measured by HELPASS 2523 sheet resistance meter.

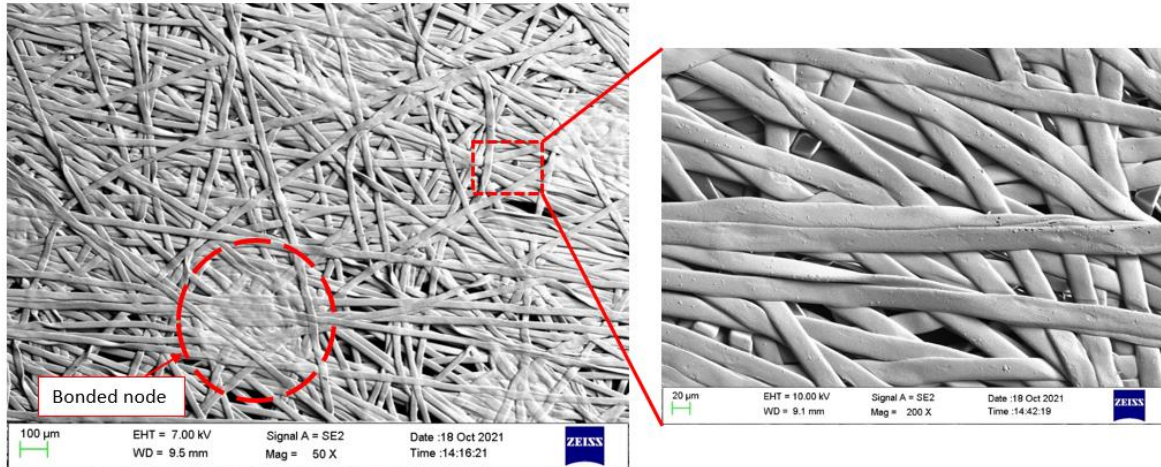


Figure 5-1. SEM image of nickel-plated polyester fibre veil

### 5.3.2 Design and fabrication of test specimens

#### 5.3.2.1 Design of the dry carbon fibre specimens

The unidirectional CF fabrics and the NPVs were cut into 70 mm×70 mm blanks. The CF blanks were hand-stacked in the following sequences:  $[0/90]_2$ ,  $[0/90]_4$  and  $[0/90]_8$ , designated as Control<sup>-D</sup>. In parallel, the CF stacks were additionally interleaved with the NPVs between each CF ply, designated as FIT<sup>-D</sup>. Veils were also placed at the upper and lower surfaces of all stacks to eliminate the contact resistance at electrodes. The NPVs were also  $[0/90]$  laid-up in the same stacking sequence, designated as NPV<sup>-D</sup>. In total, there were 3 specimen groups of Control<sup>-D</sup>, FIT<sup>-D</sup> and NPV<sup>-D</sup> for comparison, where superscript <sup>-D</sup> stands for the dry specimen condition.

#### 5.3.2.2 Design of the cured CFRP specimens

The cured laminated specimens were prepared for the through-thickness electrical conductivity (TTEC) study, designed as Control<sup>-E</sup> and FIT<sup>-E</sup>, with  $[0/90]_4$  stacking

sequence. A single NPV was placed at upper and lower surfaces, respectively. For FIT<sup>E</sup> laminates, the NPV was interleaved between each pair of CF plies. Different volume fractions ( $V_{CF}$ ) were prepared to link the variation of compaction, as shown in Table 5-2. To further understand the conductive mechanisms and the relationship between  $\rho_{tt}$  and the number of the NPVs inserted in the composites, 2 and 4 NPV veils were selectively interleaved from one side of the laminates. The thickness and  $V_{CF}$  for partially interleaved specimens were controlled at approximately 1.42 mm and 62.8%.

**Table 5-2. Characteristics of specimens for through thickness electrical conductivity (TTEC) study**

Specimen	Thickness (mm)	$V_{CF}$ (%)	Specimen	Thickness (mm)	$V_{CF}$ (%)	Lay-up
	1.58±0.01	57.1		1.61±0.01	56	
	1.54±0.02	58.5		1.55±0.02	58.1	
Control <sup>E</sup>	1.48±0.01	60.9	FIT <sup>E</sup>	1.5±0.01	60	[0/90] <sub>4</sub>
	1.40±0.01	63.7		1.46±0.01	62	
	1.34±0.01	67.1		1.4±0.01	64.2	

Table 5-3 gives the specimen information for the mechanical properties study. Similar to the specimen fabrication for electrical conductivity study, Control<sup>M</sup> and FIT<sup>M</sup> specimens were prepared with [0]<sub>12</sub> stacking sequence. Two different CF volume fractions were designed for each type of specimen, to evaluate the effect of compaction on in-plane mechanical test. Please refer the supplementary files for the schematic diagrams of specimen preparation.

**Table 5-3. Characteristics of specimens for mechanical properties study**

Specimen	Thickness (mm)	V <sub>CF</sub> (%)	Specimen	Thickness (mm)	V <sub>CF</sub> (%)	Lay-up
Control <sup>M</sup> -58.6%	2.29±0.01	58.6	FIT <sup>M</sup> -58.4%	2.31±0.01	58.4	[0] <sub>12</sub>
Control <sup>M</sup> -64.4%	2.09±0.02	64.4	FIT <sup>M</sup> -63.7%	2.12±0.01	63.7	

### **5.3.3 Manufacturing**

The cross-ply CFRP laminates were manufactured by compression moulding, as shown in Figure 5-2a. Prepregs and the interleaves were cut into 150 mm×150 mm blanks. A steel mould with 150 mm×150 mm inner area and 1.65 mm dam was used. Laminate preforms were assembled and placed into the steel mould at room temperature. Glass fibre reinforced PTFE (Polytetrafluorethylene) shims were used between preforms and the top steel plate to change the thickness of the specimens. The steel mould was transferred to the hot press and processed at 5 MPa pressure and 3°C/min heating rate. Preforms were heated from room temperature to 130°C then dwelled at 130°C for 90 minutes. Cured laminates were cooled on the press at 5°C /min cooling rate. Pressure was released when the temperature of the mould was below 60°C.

### **5.3.4 Test of compaction - through thickness electrical properties of dry cross-ply carbon fibre fabrics**

The dry CF fabrics preforms were placed between two 50 mm×50 mm×15 mm flat aluminium plates for compaction-TTEC studies. Figure 5-2b shows the schematic

diagram of experimental set-up. Two PNV veils with 0.1 mm thick copper sheets served as the electrodes. The set-up was loaded between the anvils of an MTS E42 universal test machine with a 5kN load cell. The loading rate was 0.5 mm/min. At the same time, the electrodes were connected to the TH2516 DC Resistance Meter to record the instantaneous through-thickness electrical resistance ( $R_t$ ) during the compaction process. The minimum resistance resolution of TH2516 was  $1\mu\Omega$ . The initial thickness of the stacked fabrics was measured by the crosshead position of the test machine at a nominal load of 10N. The CF volume fraction of the specimens is obtained through equation (1).

$$V_{CF} = \frac{mN}{\rho(t_0 - D) \times 10^3} \times 100\% \quad (5-1)$$

Where  $m=300\text{g/m}^2$  is the CF areal weight of the UD fabric,  $N$  is the number of plies,  $\rho=1.78\text{g/cm}^3$  is the density of the CF,  $t_0$  is the initial thickness of stacked dry fabrics measured by the test machine and  $D$  is the crosshead displacement.

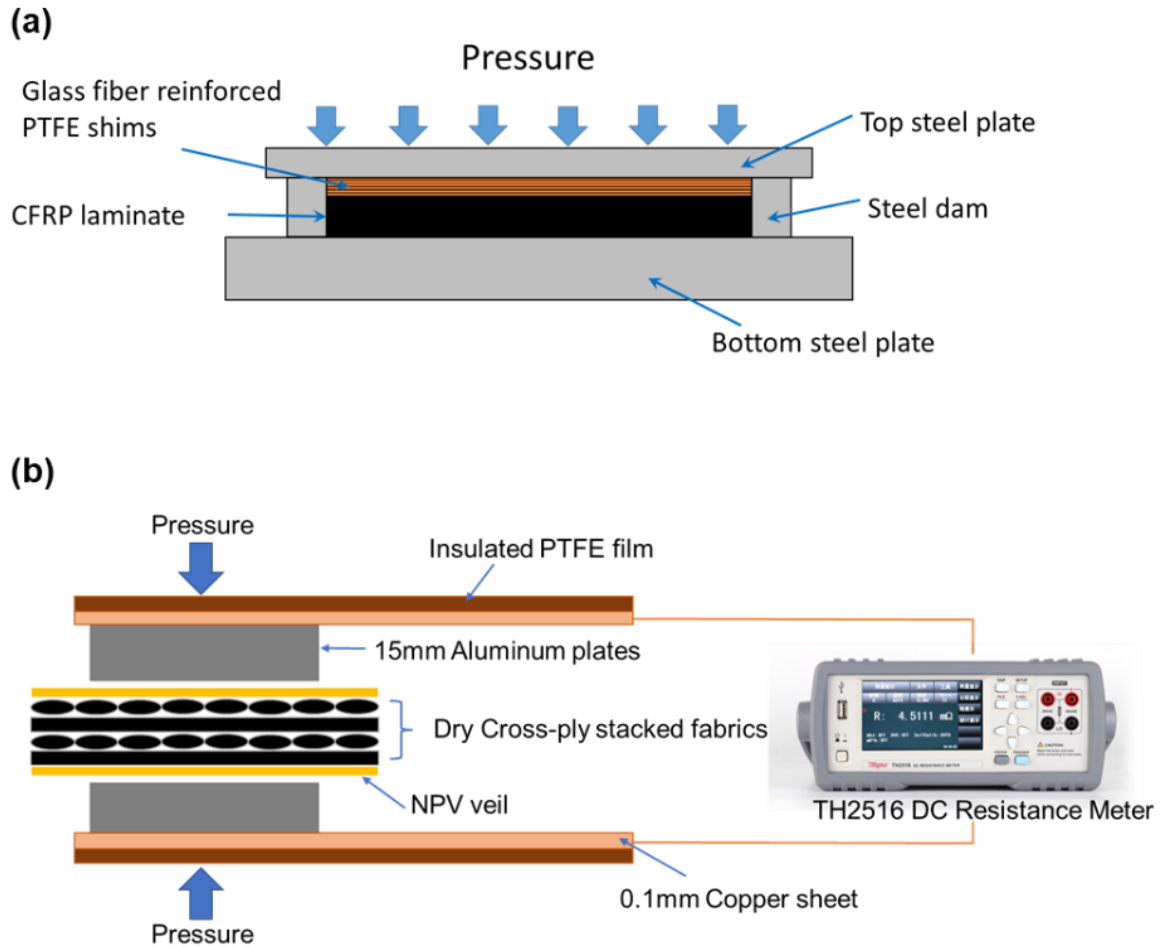


Figure 5-2. Schematic diagrams of experimental set-up. (a) compression moulding, (b) Real-time compaction-through thickness resistance recording.

### 5.3.5 Determination of through - thickness resistivity of cured CFRP laminates

Cured composite laminates were cut into 25 mm×25 mm specimens for through-thickness electric conductivity measurement. The upper and lower surfaces of the specimen were ground using P1500 sandpaper to expose the surface conductive veils. The specimens were cleaned by ultrasound for 1min and then dried at 80°C for 1 hour before the measurement.

The electrical resistance of the specimen was measured by using TH2516 DC Resistance Meter. Considering the great discrepancy between the longitudinal and the transverse resistance of the specimen, the highly conductive veil was assumed to be equi-potential [28]. The ground upper and lower surfaces were pressed with two 0.1 mm copper sheets under 500N to control contact resistance errors. Six specimens were measured for each test group. The through-thickness electric resistivity was determined by equation (2):

$$\rho_{tt} = \frac{RA}{t} \quad (5-2)$$

where  $\rho_{tt}$  is the specific resistivity,  $t$  is the specimen thickness,  $R$  is the measured electric resistance of specimen and  $A$  is the area of upper/lower surface.

### ***5.3.6 Determination of mechanical properties of CFRP specimens***

The flexural properties and interlaminar shear strength of the specimens were measured to study the interleaving effects on mechanical properties. Five specimens were tested for each experiment. The flexural strength and elasticity bending modulus ( $0^\circ$ ) was determined under 3-point bending following ASTM D790. The dimensions of the test specimens were width  $b=13$  mm and length  $L=140$  mm. The span-thickness ratio was 1:40. Specimens were tested using an MST E42 universal test machine under 6 mm/min crosshead rate. The flexural strength and modulus are calculated by equation (3) and equation (4), respectively.

$$\sigma_f = \frac{3PL}{2bd^2} \quad (5-3)$$

$$E = \frac{L^3 m}{4bd^3} \quad (5-4)$$

where  $\sigma_f$  is the flexural strength, E is the elasticity flexural modulus, P is the peak load, L is the support span, b is the width of specimen, d is the depth of specimen and m is the slope of tangent to the initial straight-line portion of load-displacement curve.

The interlaminar shear strength ( $0^\circ$ ) was determined by the short beam test according to ASTM D2344. The dimensions of the specimens were width b=4 mm and length L=12 mm. The span-thickness ratio was 1:4. Test specimens were loaded under 1mm/min crosshead rate. The interlaminar shear strength is determined as the short-beam strength in equation (5).

$$F^{sbs} = 0.75 \times \frac{P_m}{bh} \quad (5-5)$$

## 5.4 Results and discussion

### ***5.4.1 Compaction - through thickness electrical properties of dry cross-ply carbon fibre fabrics***

Whilst the compaction behaviour of dry CF fabrics has been comprehensively reported in terms of pressure- $V_{CF}$  relations relating to RTM technology [29], this study focusses



on load-thickness- $R_{tt}$  for the Control<sup>D</sup>, FIT<sup>D</sup> and NPV<sup>D</sup> specimens, where the Control<sup>D</sup> and FIT<sup>D</sup> always appear in pairs for comparison.

The compressive load-thickness curves of the test specimens are shown in Figure 5-3a. Each compaction curve has the similar shape and can be characterized using three different regions. At a constant compaction load, the thickness of the Control<sup>D</sup> is always lower than that of the FIT<sup>D</sup> due to the additional thickness of the NPVs inserted.

Figure 5-3b shows the variation of  $R_{tt}$  versus thickness. At any given thickness,  $R_{tt}$  for the FIT<sup>D</sup>s is always lower than that of the corresponding Control<sup>D</sup>s and the absolute thickness increases the larger the difference in  $R_{tt}$  between the Control<sup>D</sup>s and FIT<sup>D</sup>s. Eliminating the variable thickness in Figure 5-3a and Figure 5-3b yields the relationship of  $R_{tt}$  versus load, as shown in Figure 5-3c. It is obvious that all the curves tend to a minimum value which is slightly different only at lower compaction conditions. Figure 5-3d shows the relationship between the through-thickness electrical resistivity ( $\rho_{tt}$ ) and CF volume fractions ( $V_{CF}$ ) for the specimens tested. The  $V_{CF}$  and  $\rho_{tt}$  are obtained from equation 1 and 2. It is apparent that the FIT<sup>D</sup>s can achieve similar  $\rho_{tt}$  at a much lower  $V_{CF}$  than the Control<sup>D</sup>s. This confirms that the NPVs can significantly contribute to increase the laminate TTEC.

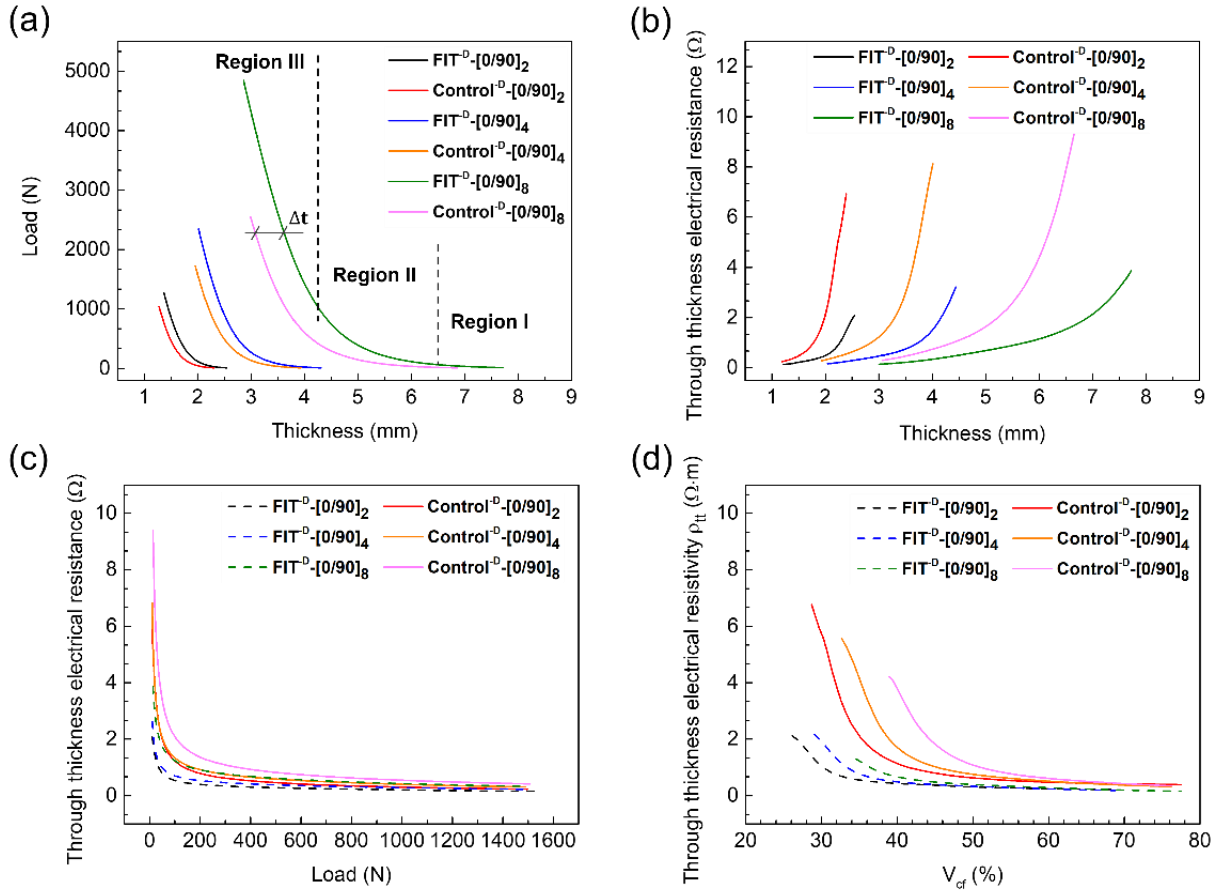


**Figure 5-3. Effects of compaction on different dry cross-stacked carbon fibre fabrics. (a) Compressive load-thickness curves, (b)  $R_{tt}$ -thickness curves, (c) Relationship between  $R_{tt}$  and compressive load, (d) Relationship between  $\rho_{tt}$  and  $V_{cf}$ .**

Considering the constant thickness of the CF plies used, further data processing from the experimental load-thickness- $R_{tt}$  curves shown in Figure 5-3 yields a relationship of  $R_{tt}$  against the number ( $n$ ) of the CF plies. Figure 5-4 shows the variation of the  $R_{tt}$  as a function of the number of the plies under constant compaction load of 250N, 500N and 1000N, respectively. According to the curves, there is a linear relationship between the  $R_{tt}$  and  $n$  for the Control<sup>-D</sup>, FIT<sup>-D</sup> and NPV<sup>-D</sup> specimens. The relationship can be described as follows:

$$R_{tt} = kn + R_0 \quad (5-6)$$

Where  $n$  is the number of plies,  $k$  is the slope and  $R_0$  is the intercept of the curve. The linearity of the curves suggests that the  $R_{tt}$ - $n$  relationship obeys a series-resistor model. Thus, the  $R_{tt}$  of the dry specimens can be easily understood as a sum of all the resistors in-series, where  $R_0$  can define the sum of interfacial contact resistance and  $k$  the resistance of each of the dry plies.

Taking a closer look and simply comparing the values of  $R_0$  and  $k$  indicated in the curves of Figure 5-4 for the respective Control<sup>-D</sup>, FIT<sup>-D</sup> and NPV<sup>-D</sup> specimens, it is obvious that the  $R_{tt}$  of each CF plies ( $k \approx 0.047, 0.032$  and  $0.021$ ) is approximately one order of magnitude lower than that of the interfacial contact resistance ( $R_0 \approx 0.46, 0.32$  and  $0.22$ ) for the Control<sup>-D</sup> group. This phenomenon is also applicable to the other two groups of FIT<sup>-D</sup> and NPV<sup>-D</sup>. The  $R_{tt}$  of the NPV<sup>-D</sup> group is particularly low and the values of  $k$  and  $R_0$  are about two orders of magnitude lower than that of Control<sup>-D</sup>s. The behaviour of FIT<sup>-D</sup>s is between the Control<sup>-D</sup> and NPV<sup>-D</sup> groups but more approaching the Control<sup>-D</sup>s. The finding reveals why inserting the NPV can improve the TTEC of the CF laminates. Self-evidently the higher the compaction, the lower is both  $k$  and  $R_0$ .

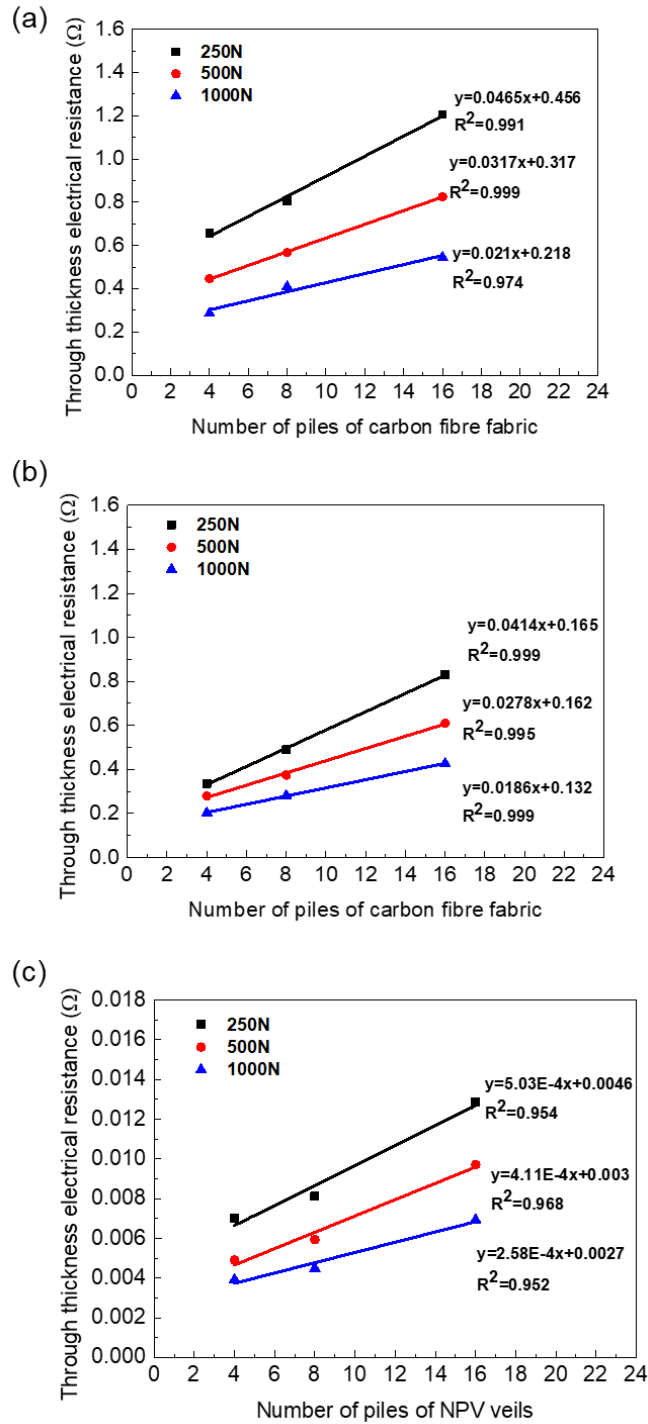
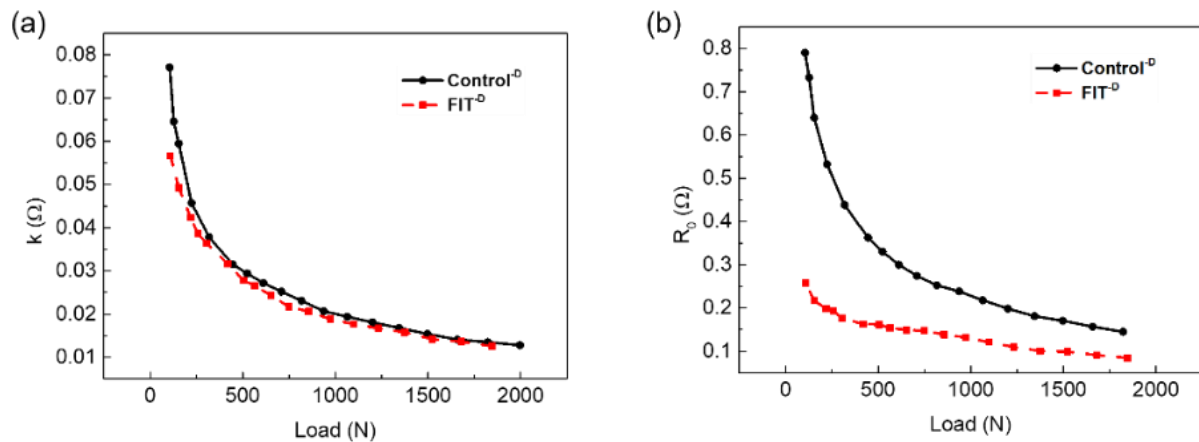


Figure 5-4. Relationship between  $R_{tt}$  and number of plies. (a) Control<sup>-D</sup>, (b) FIT<sup>-D</sup> and (c) NPV<sup>-D</sup>.

Figure 5-5 shows the variation of  $k$  and  $R_0$  versus load for Control<sup>D</sup> and FIT<sup>D</sup> groups within the range of 100N to 2000N . At any given load,  $R_0$  for the FIT<sup>D</sup>s is always lower than that of the corresponding Control<sup>D</sup>s and the difference in  $R_0$  increases with the decrease of load. It is known that the space architecture of the stacked CF fabrics consists of inter-ply and intra-ply structures, where the CF intra-ply is in-turn constructed by CF tows in terms of inter-tow and intra-tow structure. If a compaction load is applied, the inter-ply structure is mostly compressed, followed by the inter-tow. It is precisely because the NPVs fill the inter-ply space of the CF stackings so that the FIT<sup>D</sup>s exhibits a higher TTEC value than the Control<sup>D</sup>s.



**Figure 5-5. (a) Resistance of single dry ply ( $k$ ) and (b) interfacial contact resistance ( $R_0$ ) as a function of load.**

In this paper, the sum of the interfacial contact resistance is defined as an empirical constant  $R_0$  at given pressure. While the contact behaviours of multilayer dry carbon fibre fabric preform are very complicated due to ply nesting, inter-layer packing, number of plies and pressure etc. [30,31]. Further studies regarding the effects of these factors on interfacial contact resistance for dry carbon fibre fabric preforms remain ongoing.

### **5.4.2 Through-thickness electrical resistivity of cured cross-ply CFRP laminates**

The previous section provided an initial understanding of the resistance dependence on the spatial architecture and compaction, in which air represents the insulating phase. Figure 5-6 shows the relationship between the  $V_{CF}$  and  $\rho_{tt}$  for cured cross-ply laminates of Control<sup>E</sup> and FIT<sup>E</sup> specimens, in comparison with the dry cross-ply specimens of Control<sup>D</sup> and FIT<sup>D</sup> with [0/90]<sub>4</sub> lay-up, respectively. Similar to the dry counterparts, the  $\rho_{tt}$  of the Control<sup>E</sup> is always higher than that of the FIT<sup>E</sup>. With the increase of  $V_{CF}$ , the  $\rho_{tt}$  is non-linearly converged from 9.3  $\Omega \cdot m$  to 0.45  $\Omega \cdot m$  for the Control<sup>E</sup> and from 0.48  $\Omega \cdot m$  to 0.016  $\Omega \cdot m$  for the FIT<sup>E</sup>, respectively. Such variation looks similar to the dry counterparts of Control<sup>D</sup> and FIT<sup>D</sup>, but remarkably compressed into a narrow range of  $V_{CF}$  from 55% to 68%. Referred to a study of wetting and electrical conductivity of adhesive interfaces [32], it is evident that the epoxy resin will encapsulate the CFs leading to an electrical isolation between the adjacent CFs and thus significantly increase the interface resistance. Since the insulating phase shifts from air to epoxy resin matrix, the compaction density of Control<sup>E</sup>s and FIT<sup>E</sup>s must be much higher than that of the dry counterparts of Control<sup>D</sup>s and FIT<sup>D</sup>s to achieve a same  $\rho_{tt}$ .

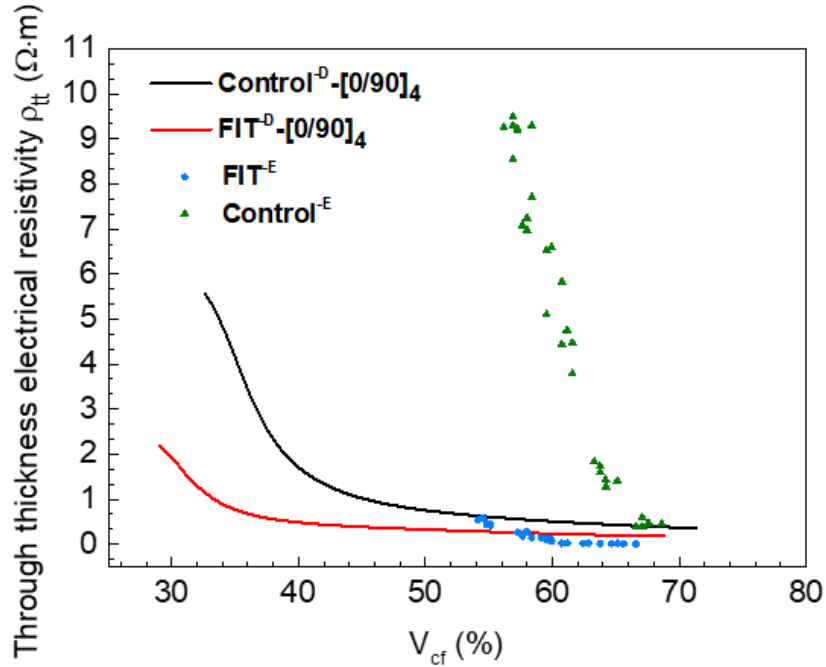


**Figure 5-6. Through-thickness electrical resistivity ( $\rho_{tt}$ ) versus carbon fibre volume fraction ( $V_{CF}$ ) for dry cross-stacked specimens (solid lines) and cured cross-ply specimens (scatters).**

It is very interesting to note that the difference of  $\rho_{tt}$  between the FIT<sup>E</sup> and FIT<sup>D</sup> is not significant. Moreover, the  $\rho_{tt}$  of the FIT<sup>E</sup> at higher compaction levels is even the lowest of all the specimens studied (Figure 5-6). To understand this phenomenon, the relationship between  $V_{CF}$  and effective resin content ( $\omega_{resin}$ ) was studied for the cured composites. The resin content is determined as the residual mass of the resin per square meter, as shown in equation (7):

$$\omega_{resin} = \frac{M_T}{A} - n_1 \times m_{CF} - n_2 \times m_{NPV} \quad (5-7)$$

Where  $m_{CF}$  and  $m_{NPV}$  are the areal mass of the CF (200 g/m<sup>2</sup>) and the NPV (42 g/m<sup>2</sup>), and  $n_1$  and  $n_2$  are the number of the CF plies and NPVs used, respectively.  $A$  is the

area of the specimen in square metres.  $M_T$  is the total mass of specimen measured via electronic balance.

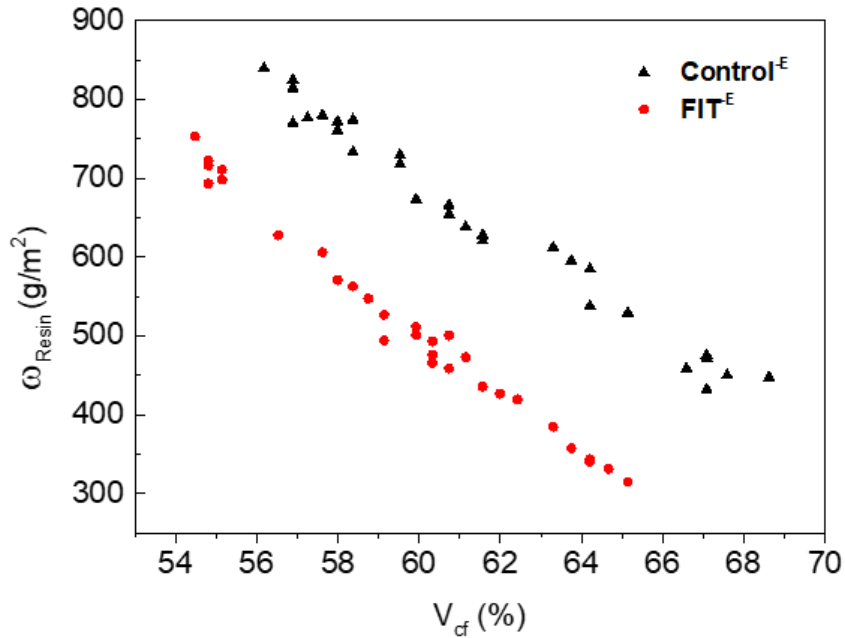
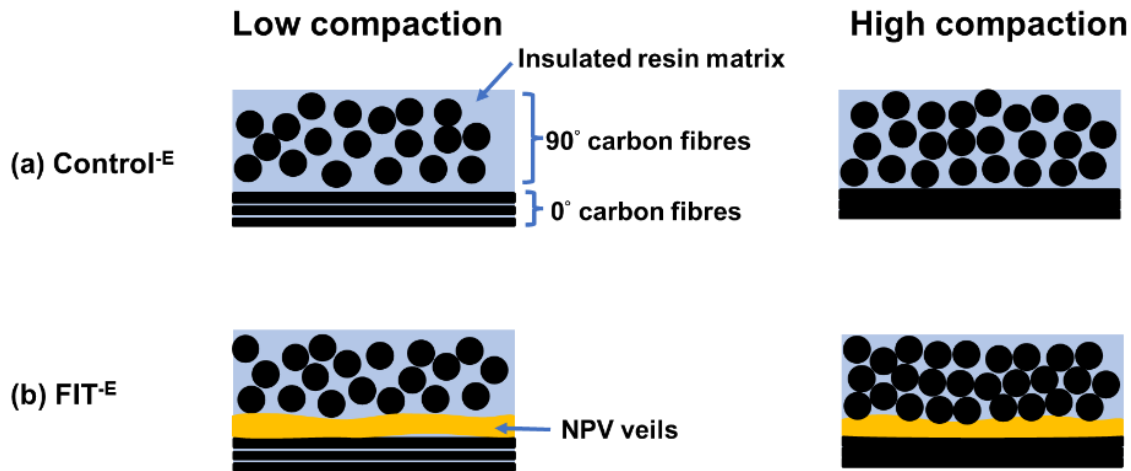


**Figure 5-7. The relationship between resin content ( $\omega_{resin}$ ) and carbon fibre volume fraction ( $V_{CF}$ ).**

As shown in Figure 5-7,  $\omega_{resin}$  is decreased linearly with the increase of  $V_{CF}$  and the two curves of Control<sup>E</sup> and FIT<sup>E</sup> are almost parallel. Specifically, the  $\omega_{resin}$  of the FIT<sup>E</sup> drops from about 700 g/m<sup>2</sup> to 300 g/m<sup>2</sup> corresponding an increase of  $V_{CF}$  from 55% to 65%. And it is about 100 g/m<sup>2</sup> to 150 g/m<sup>2</sup> lower than that of Control<sup>E</sup> at a same  $V_{CF}$ . This result shows that when the NPVs are interleaved, the resin matrix between the CF layers is squeezed out from the NPVs under the compaction pressure. Thus, the effective inter-ply  $\omega_{resin}$  is significantly reduced. In other words, the NPVs with the certain flexible compressibility occupy the most space of the electrically isolating resin in the originally resin-rich inter-ply region and provides hence more electrical connections between the adjacent CF layers.



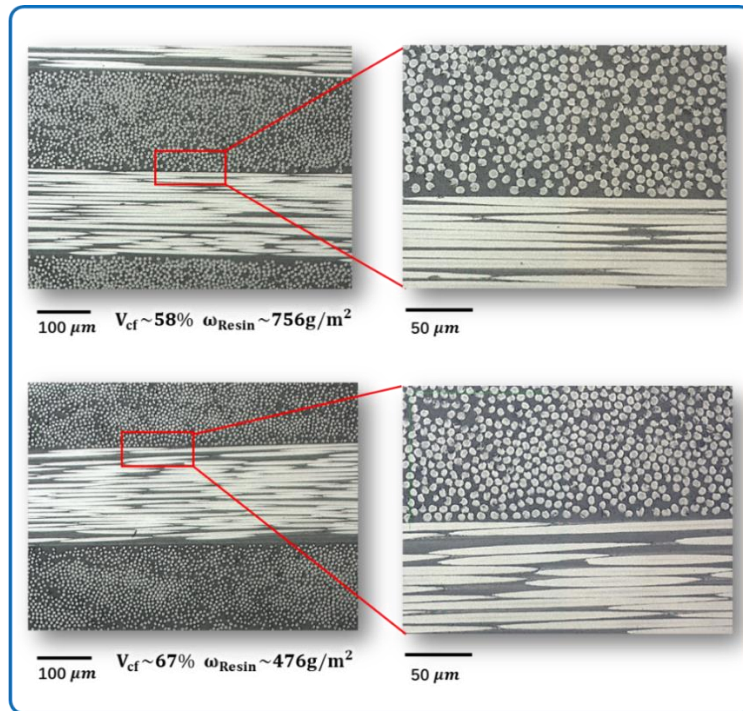
As the compaction increases, the inter-ply resin will bleed out, followed by the inter-tow resin to achieve denser contacts. At the highest  $V_{CF}$  about 68%, the  $\rho_{tt}$  of the different specimens, i.e., the FIT<sup>E</sup>, FIT<sup>D</sup>, Control<sup>E</sup> and Control<sup>D</sup>, tends to a very narrow range of about 0.016  $\Omega\cdot m$  to 0.4  $\Omega\cdot m$ , which defines the highest conductivity of the composite materials (Figure 5-6). This is the structural mechanism that the FIT composites possess the highest through-thickness electrical conductivity, which is schematically illustrated in Figure 5-8.



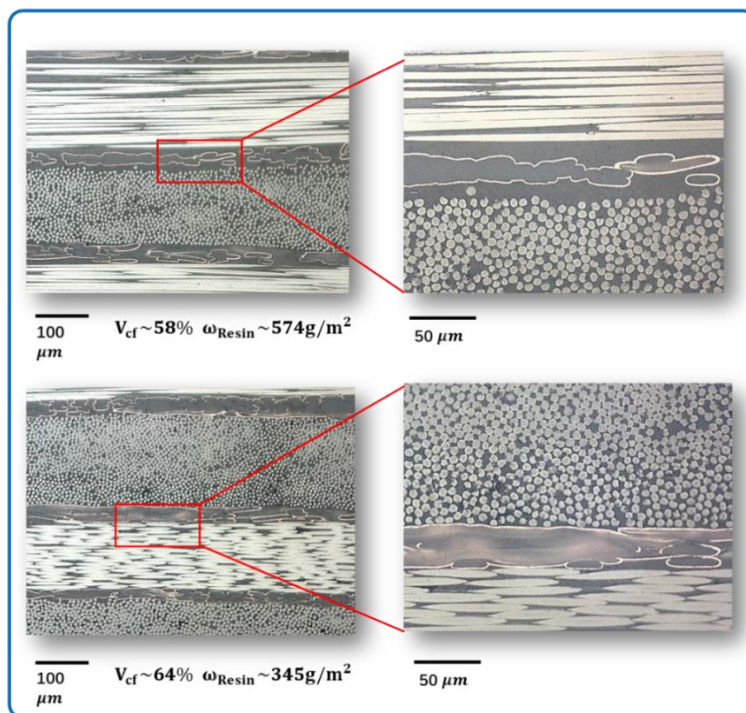
**Figure 5-8. Schematic illustration regarding the effects of electrical functionalized interleaves on through thickness conductive contacts, at low and high compaction. (a) Control<sup>E</sup> and (b) FIT<sup>E</sup>**

Figure 5-9 shows the sectional optical microscope images of test specimens. For the Control<sup>E</sup>s (Figure 5-9a), the CF plies are laminated layer by layer with fewer voids and defects. The adjacent CFs are in sporadic contact to construct a randomly distributed conductive network. The CF plies are maintained flat and parallel, with a clear and planar interface between the adjacent plies. There is no discernible difference of the interface morphology for the Control<sup>E</sup>s when the  $V_{CF}$  is increased from 58% to 67%.

The corresponding sections of the FIT<sup>E</sup>s specimens are displayed in Figure 5-9b, with different CF volume fractions and resin contents. The electrically conductive fibres of the NPV are apparent by their metallic lustre surface. There is evidently good wetting overall for the composite specimens. The resin-rich regions are easily observable between the layers of the CF and NPV, especially for the specimens with relatively low  $V_{CF}$ . The NPV layers are compacted between each CF plies, forming a periodic laminate structure. The nominal thickness of the NPV layer was approximately 40  $\mu\text{m}$ . At higher compaction levels, the NPVs become denser, and the electrically conductive fibres are contacted with the CFs in the through-thickness direction. The higher the compaction, the thinner the NPV layer, and the lower the residual resin content. Contrasting this with the rigid contact between the CF plies for the Control<sup>E</sup> shown in Figure 5-9a, the use of the NPVs with a relatively lower stiffness and a higher compressibility for the FIT<sup>E</sup> in Figure 5-9b provides a more dense contact area, which is obviously beneficial for continuity of electrically conductive paths across the laminate. See supplementary information for more pictures with different  $V_{CF}$ .



(a)



(b)

Figure 5-9. Sectional microscope observation for test specimens. (a) Control<sup>-E</sup>, (b) FIT<sup>-E</sup>

Given the demonstrated series-resistor conductive mechanism of the FIT composite, the TTEC can likely be varied by changing the disposition of the NPV layers. Figure 5-10 shows the relationship between the  $\rho_{tt}$  and the number of the NPVs selectively inserted in the composites under similar  $V_{CF}$ . Where  $n=2$  and  $n=4$  corresponding to the partially interleaved specimens,  $n=0$  and  $n=7$  corresponding to the Control<sup>E</sup> and FIT<sup>E</sup> with 63.7% and 62%  $V_{CF}$ . With the increasing NPV layers, the  $\rho_{tt}$  values of the composite gradually converge with a non-linear decrease. A deterministic  $\rho_{tt}$  value in the range between those achieved by the Control<sup>E</sup> and FIT<sup>E</sup> can be thus targeted by inserting the corresponding number of the NPV layers.

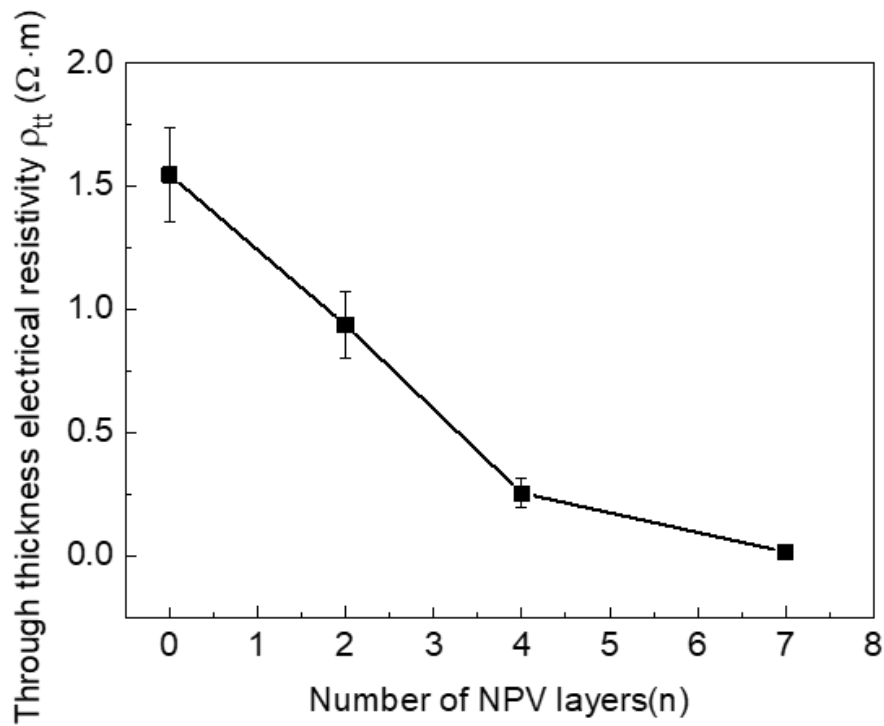


Figure 5-10. The effects of the number of NPV layers on  $\rho_{tt}$ .

### **5.4.3 Mechanical properties**

The flexural test results of the composite specimens are shown in Figure 5-11.

According to the load-displacement curves, a slight drop of the failure load is detected for control specimens with higher  $V_{CF}$ . The sharp load shedding obviously indicates the fracture and sudden loss of the flexural properties at the failure moment. No delamination occurred before the final failure for all interleaved specimens indicates the good interply bonding between the CF and NPV. Figure 5-11b summarises the flexural strength and modulus results.

There was no significant difference in the flexural strength and modulus between the Control<sup>M</sup> and FIT<sup>M</sup> specimens. At a  $V_{CF}$  of c.58%, the flexural strength was approximately 1400 MPa and the modulus about 115 GPa. Increasing the  $V_{CF}$  to c.64% raised the flexural strength and modulus to approximately 1600 MPa and 128 GPa, respectively.

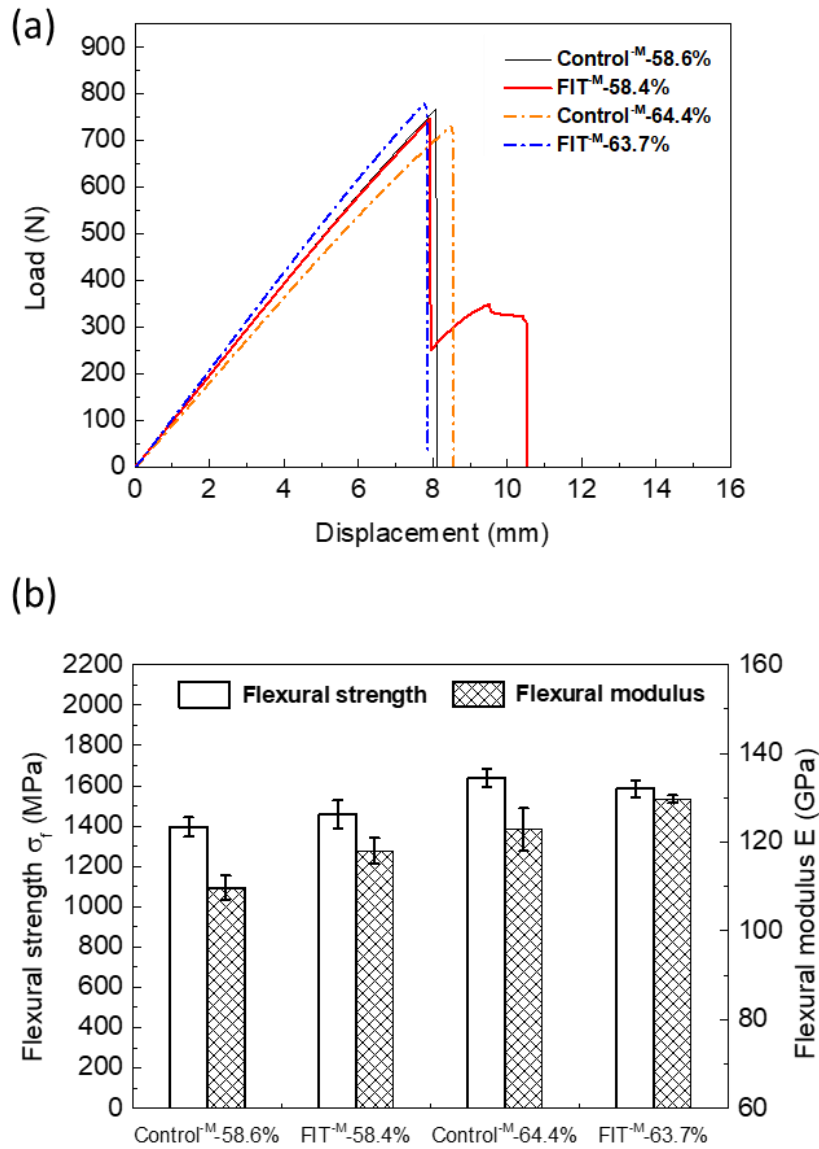


**Figure 5-11. Longitudinal flexural properties of test specimens. (a) Load-displacement curves, (b) flexural strength and modulus**

Figure 5-12 shows the interlaminar shear test results. Referring to the load-displacement curves in Figure 5-12a, lower peak load and displacement are detected for the FIT<sup>M</sup> specimens, in comparison with the Control<sup>M</sup>s. At a  $V_{CF}$  of about 58%, the interlaminar shear strength (ILSS) of the Control<sup>M</sup> was approximately 87 MPa, whereas

for the FIT<sup>M</sup>, it was about 67 MPa. At a higher  $V_{CF}$  of about 64%, the changes in ILSS were modest with 91 MPa for the Control<sup>M</sup> and 71 MPa for the FIT<sup>M</sup>, respectively.

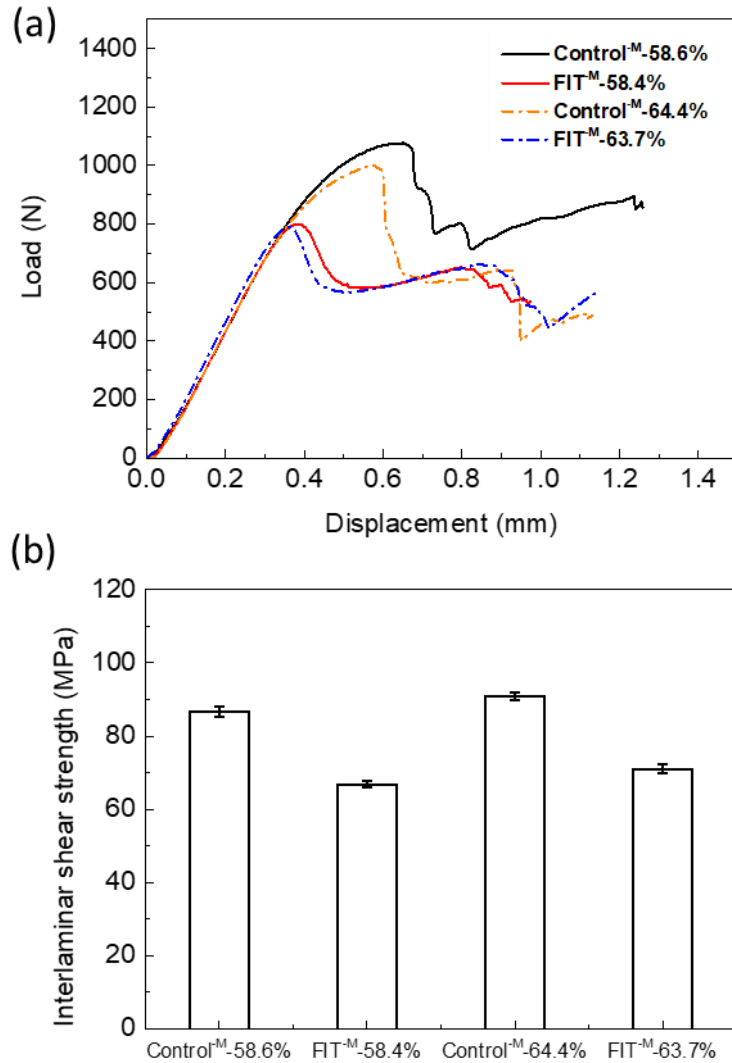


**Figure 5-12. Interlaminar shear properties of test specimens. (a) Load-displacement curves, (b) ILSS**

Noticeable differences in the crack morphology between the Control<sup>M</sup> and FIT<sup>M</sup> were observed via microscopy. For the Control<sup>M</sup>, multiple shear cracks were observed parallel to the carbon tows. In contrast, the cracks in the FIT<sup>M</sup> are concentrated within

the NPV layers and at the interface between the NPV and the resin, as shown in Figure 5-13. This suggests that the interfacial adhesion between the NPV and CF layers is higher than their intra-plane shear strength. The lower intra-plane shear resistance of the NPV layers and the poor interface between the metallized NPV fibres and the epoxy is likely responsible for the reduction of the ILSS for the FIT<sup>M</sup>.

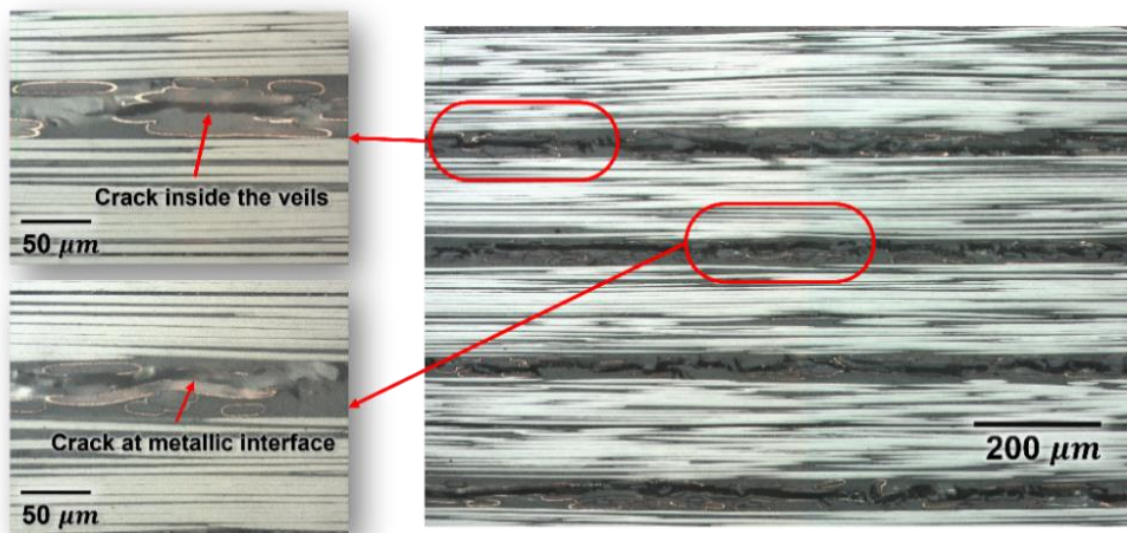


Figure 5-13. Sectional microscope images of FIT<sup>M</sup>-58.4% specimen after interlaminar shear test.

## 5.5 Conclusion

The through-thickness electrical resistance and conductivity in both preforms and laminates are primarily controlled by contact regions of the electrically conductive elements and components, i.e., the CFs, the CF layers and NPVs. This, in turn is strongly affected by the compaction. In the range of the experimental parameters in the present study, the  $R_{tt}$  of the FIT composites follows the conductive series-resistor



model, i.e., there is a linear relationship between the  $R_{tt}$  and the number of the electrically conductive plies or layers.

By interleaving the highly conductive NPV layers, the  $\rho_{tt}$  of the interleaved cross-ply laminate (FIT<sup>E</sup>) was reduced from 9.3  $\Omega\cdot m$  to 0.48  $\Omega\cdot m$  at  $V_{CF}$  of approximately 56%.

Transverse consolidation reduced this further; at 64%  $V_{CF}$ ,  $\rho_{tt}$  decreased to 1.54  $\Omega\cdot m$  for the Control<sup>E</sup>s and 0.016  $\Omega\cdot m$  for the FIT<sup>E</sup>s, respectively. Microscopy revealed that the densified laminate contained more electrical contacts with consequent improvement of the through-thickness electrical properties. Interpolating between the limiting Control<sup>E</sup> and FIT<sup>E</sup> values enabled prediction of  $\rho_{tt}$  based on the number of the NPV layers at a given  $V_{CF}$ .

Flexural and interlaminar shear properties were somewhat less impacted by the compaction. Increasing the  $V_{CF}$  from 58% to 64% increased the flexural strength from approximately 1400 MPa to 1600 MPa, and the flexural modulus from 115 GPa to 128 GPa for both composite groups. In the same  $V_{CF}$  range from 58% to 64%, the ILSS also increased slightly from 87 MPa to 91 MPa for the Controls<sup>M</sup> and from 67 MPa to 71 MPa for the FIT<sup>M</sup>, respectively. The further microscopic investigation indicates that the lower intra-ply shear resistance of the NPV layers is responsible for the c.20% reductions in the ILSS for FIT<sup>M</sup> specimens.

## 5.6 References

- [1] G. Gardiner, Aerocomposites: The move to multifunctionality, *Compos. World.* (2015) 42–48.
- [2] B. Zhang, S.R. Hallett, G. Allegri, Sensing delamination in composites reinforced by ferromagnetic Z-pins via electromagnetic induction, *Compos. Sci. Technol.* 217 (2022) 109113. doi:10.1016/j.compscitech.2021.109113.
- [3] Q. OuYang, X. Wang, L. Liu, High crack self-healing efficiency and enhanced free-edge delamination resistance of carbon fibrous composites with hierarchical interleaves, *Compos. Sci. Technol.* 217 (2022) 109115. doi:10.1016/j.compscitech.2021.109115.
- [4] Z.J. Zhao, G.J. Xian, J.G. Yu, J. Wang, J.F. Tong, J.H. Wei, C.C. Wang, P. Moreira, X.S. Yi, Development of electrically conductive structural BMI based CFRPs for lightning strike protection, *Compos. Sci. Technol.* 167 (2018) 555–562. doi:10.1016/j.compscitech.2018.08.026.
- [5] Y. Lin, M. Gigliotti, M.C. Lafarie-frenot, J. Bai, D. Marchand, D. Mellier, Experimental study to assess the effect of carbon nanotube addition on the through-thickness electrical conductivity of CFRP laminates for aircraft applications \*, *Compos. Part B.* 76 (2015) 31–37. doi:10.1016/j.compositesb.2015.02.015.
- [6] C. Lochot, D. Slomianowski, A 350 XWB Electrical structure network, *Airbus Tech. Mag.* (2014) 20–25.
- [7] M. Louis, S.P. Joshi, W. Brockmann, An experimental investigation of through-thickness electrical resistivity of CFRP laminates, *Compos. Sci. Technol.* 61 (2001) 911–919. doi:10.1016/S0266-3538(00)00177-9.
- [8] A. Todoroki, M. Tanaka, Y. Shimamura, Measurement of orthotropic electric conductance of CFRP laminates and analysis of the effect on delamination monitoring with an electric resistance change method, *Compos. Sci. Technol.* 62 (2002) 619–628. doi:10.1016/S0266-3538(02)00019-2.

- [9] S. Wang, D.D.L. Chung, Electrical behavior of carbon fiber polymer-matrix composites in the through-thickness direction, *J. Mater. Sci.* 35 (2000) 91–100.  
doi:10.1023/A:1004744600284.
- [10] H. Yu, J. Sun, D. Heider, S. Advani, Experimental investigation of through-thickness resistivity of unidirectional carbon fiber tows, *J. Compos. Mater.* 53 (2019) 2993–3003.  
doi:10.1177/0021998318809837.
- [11] L. Ye, Functionalized interleaf technology in carbon-fibre-reinforced composites for aircraft, *Natl. Sci. Rev.* 1 (2014) 7–8. doi:10.1093/nsr/nwt007.
- [12] S.C. Brown, C. Robert, V. Koutsos, D. Ray, Methods of modifying through-thickness electrical conductivity of CFRP for use in structural health monitoring, and its effect on mechanical properties – A review, *Compos. Part A Appl. Sci. Manuf.* 133 (2020) 105885.  
doi:10.1016/j.compositesa.2020.105885.
- [13] Z.J. Zhao, B.Y. Zhang, Y. Du, Y.W. Hei, X.S. Yi, F.H. Shi, G.J. Xian, MWCNT modified structure-conductive composite and its electromagnetic shielding behavior, *Compos. Part B Eng.* 130 (2017) 21–27. doi:10.1016/j.compositesb.2017.07.033.
- [14] I. Gaztelumendi, M. Chapartegui, R. Seddon, S. Flórez, F. Pons, J. Cinquin, Enhancement of electrical conductivity of composite structures by integration of carbon nanotubes via bulk resin and/or buckypaper films, *Compos. Part B Eng.* 122 (2017) 31–40.  
doi:10.1016/j.compositesb.2016.12.059.
- [15] X. Cheng, T. Yokozeke, L. Wu, H. Wang, J.M. Zhang, J. Koyanagi, Z. Weng, Q. Sun, Electrical conductivity and interlaminar shear strength enhancement of carbon fiber reinforced polymers through synergetic effect between graphene oxide and polyaniline, *Compos. Part A Appl. Sci. Manuf.* 90 (2016) 243–249. doi:10.1016/j.compositesa.2016.07.015.
- [16] E. Kandare, A.A. Khatibi, S. Yoo, R. Wang, J. Ma, P. Olivier, N. Gleizes, C.H. Wang, Improving the through-thickness thermal and electrical conductivity of carbon fibre/epoxy laminates by exploiting synergy between graphene and silver nano-inclusions, *Compos. Part A Appl. Sci. Manuf.* 69 (2015) 72–82. doi:10.1016/j.compositesa.2014.10.024.

- [17] Y. Li, H. Zhang, Z. Huang, E. Bilotti, T. Peijs, Graphite Nanoplatelet Modified Epoxy Resin for Carbon Fibre Reinforced Plastics with Enhanced Properties, *J. Nanomater.* 2017 (2017). doi:10.1155/2017/5194872.
- [18] G. Singer, G. Sinn, H. Rennhofer, R. Schuller, T.A. Grünewald, M.M. Unterlass, U. Windberger, H.C. Lichtenegger, High performance functional composites by in-situ orientation of carbon nanofillers, *Compos. Struct.* 215 (2019) 178–184. doi:10.1016/j.compstruct.2019.02.020.
- [19] E.C. Senis, I.O. Golosnoy, J.M. Dulieu-Barton, O.T. Thomsen, Enhancement of the electrical and thermal properties of unidirectional carbon fibre/epoxy laminates through the addition of graphene oxide, *J. Mater. Sci.* 54 (2019) 8955–8970. doi:10.1007/s10853-019-03522-8.
- [20] M. Guo, X. Yi, The production of tough, electrically conductive carbon fiber composite laminates for use in airframes, *Carbon N. Y.* 58 (2013) 241–244. doi:10.1016/j.carbon.2013.02.052.
- [21] M. Guo, X. Yi, G. Liu, L. Liu, Simultaneously increasing the electrical conductivity and fracture toughness of carbon-fiber composites by using silver nanowires-loaded interleaves, *Compos. Sci. Technol.* 97 (2014) 27–33. doi:10.1016/j.compscitech.2014.03.020.
- [22] M. Guo, X. Yi, C. Rudd, X. Liu, Preparation of highly electrically conductive carbon- fiber composites with high interlaminar fracture toughness by using silver-plated interleaves, *Compos. Sci. Technol.* 176 (2019) 29–36. doi:10.1016/j.compscitech.2019.03.014.
- [23] D. Hu, X. Yi, M. Jiang, G. Li, X. Cong, X. Liu, C. Rudd, Development of highly electrically conductive composites for aeronautical applications utilizing bi-functional composite interleaves, *Aerosp. Sci. Technol.* 98 (2020) 105669. doi:10.1016/j.ast.2019.105669.
- [24] E. Barjasteh, C. Sutanto, T. Reddy, J. Vinh, A graphene/graphite-based conductive polyamide 12 interlayer for increasing the fracture toughness and conductivity of carbon-fiber composites, *J. Compos. Mater.* 51 (2017) 2879–2887. doi:10.1177/0021998317705707.
- [25] K. Dydek, A. Boczkowska, P. Latko-Durałek, M. Wilk, K. Padykuła, R. Kozera, Effect of the areal weight of CNT-doped veils on CFRP electrical properties, *J. Compos. Mater.* 54 (2020) 2677–2685. doi:10.1177/0021998320902227.

- [26] C. Robert, W.B. Thitasiri, D. Mamalis, Z.E. Hussein, M. Waqas, D. Ray, N. Radacsi, V. Koutsos, Improving through-thickness conductivity of carbon fiber reinforced polymer using carbon nanotube/polyethylenimine at the interlaminar region, *J. Appl. Polym. Sci.* 138 (2021) 1–9. doi:10.1002/app.49749.
- [27] I. El Sawi, P.A. Olivier, P. Demont, H. Bougherara, Processing and electrical characterization of a unidirectional CFRP composite filled with double walled carbon nanotubes, *Compos. Sci. Technol.* 73 (2012) 19–26. doi:10.1016/j.compscitech.2012.08.016.
- [28] J.C. Abry, S. Bochard, A. Chateauminois, M. Salvia, G. Giraud, In situ detection of damage in CFRP laminates by electrical resistance measurements, *Compos. Sci. Technol.* 59 (1999) 925–935. doi:10.1016/S0266-3538(98)00132-8.
- [29] Y. Xiaosu, *Science and Technology of Aerospace Composites [Book in Chinese].*, Chinese Aviation Industry Press, Beijing, 2013.
- [30] Z.R. Chen, L. Ye, A micromechanical compaction model for woven fabric preforms. Part II: Multilayer, *Compos. Sci. Technol.* 66 (2006) 3263–3272. doi:10.1016/j.compscitech.2005.07.010.
- [31] Z. Yousaf, P. Potluri, P.J. Withers, Influence of Tow Architecture on Compaction and Nesting in Textile Preforms, *Appl. Compos. Mater.* 24 (2017) 337–350. doi:10.1007/s10443-016-9554-8.
- [32] Z. ZHAO, X. YI, G. XIAN, Fabricating structural adhesive bonds with high electrical conductivity, *Int. J. Adhes. Adhes.* 74 (2017) 70–76. doi:10.1016/j.ijadhadh.2017.01.002.

# Chapter 6: Conclusions and future work

## 6.1 Overall summary

This research aimed to develop a novel aeronautical carbon fibre composite with high electrical conductivity and fracture toughness using the bi-functional interleaves and elucidate its mechanisms. The project is divided into three main works, as shown in Figure 6-1.

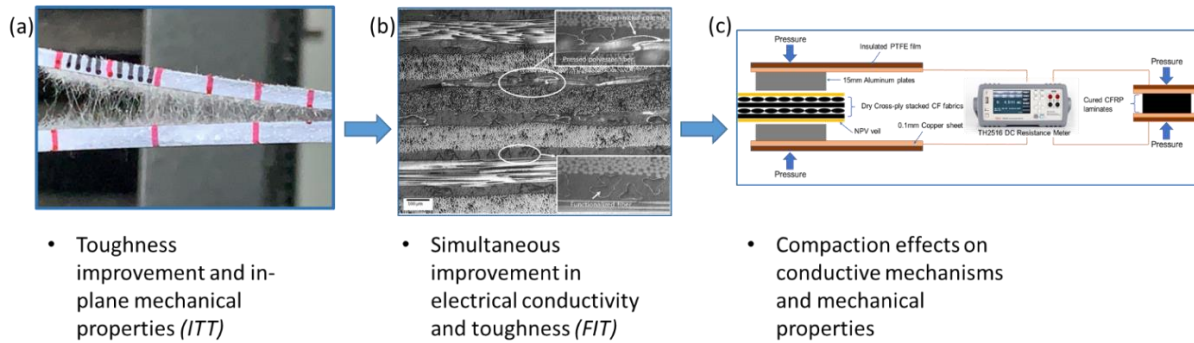


Figure 6-1. The three main studies of this thesis.

Firstly, a study of toughness improvement of green epoxy-based carbon fibre composites was conducted, in which a polyamide veil was used as the interleaf material. A significant toughening improvement with maintained in-plane mechanical properties provided a convincing proof-of-concept. Subsequently, a lightweight and functionalized polyester non-woven veil was developed to provide simultaneously the toughening effect and improved electrical conductivity for CFRP laminates. The technology is termed *Functional Interleave Technology* (FIT). The effects of veil architecture on electrical and mechanical properties of CFRPs were discussed. Finally,

the mechanisms of FIT based on the compaction and interleaving effects were further explored. The novel aspects of this research are listed below:

- Development of a thermoset-thermoplastic bi-continuous structure at interlaminar regions using a proprietary polyamide non-woven veil, achieving significant improvement in toughness as well as comparable in-plane mechanical properties to conventional materials.
- Incorporation of an electrically functionalized polyester non-woven veil. A three-dimensional conductive network was established through the effective carbon-carbon and carbon-interleave contacts to boost the volumetric electrical conductivity of interleaved CFRPs. Simultaneously, bi-continuous structures formed by the polyester veils and epoxy matrix at interlaminar regions improved the interlaminar toughness.
- The effects of compaction and interleaving on through-thickness electrical conductivity and in-plane mechanical properties for CFRP laminates, demonstrated the conductive series-resistor model and optimization route for this approach to CFRP functionalization.

## **6.2 Future works**

### ***6.2.1 Functionalized interleaves***

This work has established the potential of functionalized interleaves and their dependence on the properties of non-woven veils, specifically the veil structure and its electrical conductivity. The copper-nickel coatings used here ensure high sheet

conductivity around  $18\text{m}\Omega/\text{sq}$ , whereas the relative weak interface between metallic coating and polymers provoke negative effects on toughening and mechanical properties. Future improvement of electrical functionalization process might aim at better interfacial conditions between the interleaves and matrix as well as the high electrical conductivity.

The optimization of veil architecture to enhance the toughening performance and in-plane mechanical properties further is also a valuable objective. According to the current investigations it appears that a loose, compressible and continuous veil structure may not only enhance the toughening efficiency, but also increase the conductive contacts to boost the volumetric electrical conductivity potentially.

### ***6.2.2 Development of a hybrid inner network***

Conductive micro/nano fillers and surface electrical modification of carbon fibres continue to provide an intriguing opportunity for functionalised laminate design. Despite the different studies cited here it is clear that no uniquely successful approach has emerged as a “market leader”.

Referring to work reported in this thesis, we have demonstrated effective modifications of the interlaminar regions. Thus, the toughness and electrical conductivity of CFRP with acceptable mechanical properties have been enhanced. However, the technology does not alter the intra-ply properties of carbon fibre layers.

Modelling of these novel laminates has confirmed that the electrical characteristics follow a series-resistor circuit in terms of intralaminar resistance and interlaminar



resistance. To maximize the electrical conductivity, it is necessary to reduce all these resistors in the circuit as well as the interfacial contact resistance. Thus, further work in this field could concentrate on the development of current concept to propose a multi-structure carbon fibre laminate with ultra-high electrical conductivity and toughness. Potentially a three-dimensional bi-structure consisting of carbon fibre network and functionalized conductive network may be built into the composites in future investigations.